January 2011

The Advancement of Mass Spectrometry-based Hydroxyl Radical Protein Footprinting: Application of Novel Analysis Methods to Model Proteins and Apolipoprotein E

Brian Gau
Washington University in St. Louis

WASHINGTON UNIVERSITY IN ST. LOUIS

Department of Chemistry

Dissertation Examination Committee:
Michael Gross, Chair
Robert Blankenship
Carl Frieden
Jacob Schaefer
John Taylor
Reid Townsend

THE ADVANCEMENT OF MASS SPECTROMETRY-BASED HYDROXYL RADICAL PROTEIN FOOTPRINTING: APPLICATION OF NOVEL ANALYSIS METHODS TO MODEL PROTEINS AND APOLIPOPROTEIN E

by

Brian Craig Gau

A dissertation presented to the
Graduate School of Arts and Sciences
of Washington University in
partial fulfillment of the
requirements for the degree
of Doctor of Philosophy

August 2011

Saint Louis, Missouri

Abstract

Fast photochemical oxidation of proteins (FPOP) has shown great promise in the elucidation of the regions of a protein's structure that are changed upon interaction with other macromolecules, ligands, or by folding. The advantage of this protein footprinting method is that it utilizes the reactivity of hydroxyl radicals to stably modify solvent accessible residues non-specifically in a microsecond. The extent of •OH labeling at sites assays their solvent accessibility. We have corroborated the predicted profoundly short timescale of labeling empirically, by FPOP-labeling three oxidation-sensitive proteins and examining their global FPOP product outcomes. The novel test developed to validate conformational invariance during labeling can be applied generally to any footprinting methodology where perturbation to protein structure by the footprint labeling is suspected. The stable modifications can be detected and quantified by the same proteolysis, chromatography, and mass spectrometry techniques employed in proteomics studies; however, proteomics software does not automatically report the residue-resolved full-sequence-coverage footprint information found in proteomics-like FPOP data. Here we report the development of software tools to facilitate a comprehensive and efficient analysis of FPOP data, and demonstrate their use in a study of barstar in its unfolded and native states. We next show that SO_4^-• can serve as an alternative non-specific labeling agent that can be generated by the FPOP apparatus on the same fast timescale as •OH. This demonstrates the tunable nature of FPOP. We have used FPOP to characterize the oligomeric structures of three human apolipoprotein E (ApoE) isoforms and a monomeric

mutant in their lipid-free states. Only one isoform of ApoE is strongly associated with Alzheimer's disease; unfortunately, the structural reason for this association is not known, in part because no high resolution structure exists of any isoform. We find that the three common isoforms of ApoE are very similar in their solvent accessible footprint, that their oligomeric interactions involve several regions in the C-terminal domain, and that the N-terminal domain of each resembles the monomeric mutant's N-terminal domain, the truncated form of which has been characterized as a four-helix bundle. Finally, we find by FPOP that ApoE interacts with β-amyloid peptide 1-42 at a specific site in its N-terminal domain.

Acknowledgements

To my advisor, Dr. Michael Gross: thank you for allowing me to explore. Thank you for enriching the lab with erudite staff and thoughtful students (and nice equipment). It is a culture worth emulating.

To my parents, Dr. Gerald and Rita Gau: thank you for fostering my interest in science by, among many other things, watching Carl Sagan's Cosmos television series with me.

To my children, Alec and Anna: thank you for giving me perspective and for making science cool.

To my wife, Dr. Megan M. Gau: thank you for your patience and encouragement and patience.

Table of Contents

Table of Tables

Table of Figures

1 Mass Spectrometry-Based Protein Footprinting

1.1 Protein Structure Determination

1.1.1 High resolution determination.

The determination of tertiary and quaternary protein structure is the central issue in discovering the mechanisms of protein function. X-ray crystallography is the preeminent methodology capable of providing high resolution three-dimensional macromolecular structure. By this method, an electron density map is generated from the diffraction pattern created by X-rays diffracted by a protein crystal. The primary sequence of the protein is modeled to fit this electron density map, resulting in a structure with atomic-coordinate detail for most of its atom. At lower resolution the macromolecular shape can be determined. Of the 72,717 structures entered in the protein data bank (www.pdb.org)[1] as of April 2011, 63,322 were determined by X-ray crystallography.

The limitation of X-ray crystollography is primarily the limitation of protein crystallization. Some proteins cannot crystallize because their native structure is only stabilized by interaction with other biomolecules, which cannot be sequestered in an ordered crystal. Many transmembrane proteins fall in this category, though much progress has been made in their structural elucidation by crystallography[2]. Other proteins may not crystallize owing to the highly variable conformations parts of their sequence visit. The excision of such regions can give truncated protein variants that readily crystallize[3]. This strategy is one of several employed in crystallography that may perturb

the structure of the protein from its native conformation. Protein crystals are highly protein-concentrated. Due to this property, the determination of the monomer structure of proteins that have a propensity to oligomerize can be difficult or impossible.

The remaining fraction of high resolution structures in the protein data bank have been determined by NMR spectroscopy. This method utilizes the magnetic-spin properties of nuclei to determine distance constraints between the probed atoms of a macromolecule. These constraints and the primary sequence of the protein are used to construct a high resolution model. The NMR experiment is usually done on proteins in solution. This has enabled the study of proteins in a dynamic context, including protein folding[4], folding pathways[5], and enzyme dynamics[6]. The structural progression through such pathways can studied by NMR relaxation dispersion experiments that resolve short-lived intermediate states and conformations of low abundance relative to the dominant equilibrium conformation[7-8].

There are two primary limitations to NMR structural determination. The first is that, just as for X-ray crystallography, certain proteins are not well suited to study because their native conformation is not stable under the conditions of the experiment. NMR typically requires 100s of μg of material and operates on high protein-concentrated solutions. As well, very flexible proteins may present an ensemble of native conformations that thereby confounds resolved analysis. The second limitation is that proteins <40 kDa are not well assayed by NMR unless they are highly symmetric, such as seen with the 900 kDa GroES-GroEL complex[9]. Carbon-13, nitrogen-15, and fluorine-19 labeling of proteins permits NMR experiments that focus on these nuclei. For proteins

larger than 10 kDa, uniform ^{13}C and ^{15}N labeling is often employed to simplify the analysis without sacrificing structural resolution[10]. In conjunction with ^{13}C and ^{15}N labeling, solid state magic angle spinning NMR (MAS NMR)[11] can reveal the structure of proteins without the requiring their macroscopic alignment[12]; by this method the high resolution structures of membrane proteins have been determined[13-14]. In proteins that are intractable to high resolution elucidation by NMR, ^{19}F can be used to provide lower resolution information about domain and oligomeric properties[15].

1.1.2 Low resolution determination.

Other methodologies utilize the physical, nuclear, and electronic structure properties of the analyte protein to provide structural information about the protein by itself or in the context of an interaction. By themselves, such particle scattering, spectroscopic and physical methods cannot provide the detail afforded X-ray and NMR techniques. Cryo-electron microscopy (cryo-EM) is one method which, while it cannot determine individual protein structures at atomic resolution, is better suited for determining the gross structure of large biomolecular assemblies than either X-ray crystollography or NMR spectroscopy[16-17]. A common theme for low resolution techniques like cryo-EM is that the interpretation of the technique's data will coincide with the incorporation of X-ray or NMR high resolution structures, as components of the studied system or as a putative model of the system or part of the system[18].

Circular dichroism (CD) spectroscopy has a long history of use as a technique to characterize the secondary structure content of proteins in solution[19-20], wherein the allowed rotations between neighboring amide groups along the protein backbone are

probed. This spectroscopic method sees the average of all positions in a protein in its average conformation. For some protein systems, the ensemble of protein conformations may be broad. This may obscure important macromolecular interactions present in a subset of proteins in the ensemble if inherently averaged spectroscopic methods are used.

Fluorescence spectroscopy and Förster (fluorescence) resonant energy transfer (FRET) have been used to rescue such interactions by allowing for exquisite—even single molecule[21-22]—detection of proteins. FRET can provide quantitative distance information relating to the natural fluorophores tryptophan and tyrosine in their structural context, as well as strongly absorbing fluorophores like flouroscein and rhodamine when they are conjugated to the macromolecules or ligands. In fluorescence correlation spectroscopy (FCS), the size and shape of macromolecules can be inferred from the FCS-observed diffusion of a small number of such molecules in a very small volume. From this geometric model the stoichiometry and subunit orientations of protein complexes or oligomers can be determined[23].

Sedimentation and native gel electrophoresis techniques can distinguish protein complexes and oligomers from monomeric species. Though clearly of low resolution, such information is critical to the understanding of quaternary structure, which more resolved methods may not be able to probe. In addition, sedimentation experiments can be used to assay the shape of the macromolecule or complex[24].

1.2 Mass Spectrometry-Based Footprinting

1.2.1 General principles.

An intermediate level of structural information can be realized by mass spectrometry (MS)-based protein footprinting. Protein footprinting is an assay that monitors protein conformation by selectively labeling or cleaving residues. This selectivity is in part a function of the target solvent accessibility, thus an implicit picture of protein structure is afforded by footprinting. The ways of modifying residues are diverse and have been in practice for over forty years[25]. More recently, the advent of macro-biomolecular mass spectrometry using ESI and MALDI ionization sources has enabled the study of proteins in physiologic quantities—though the ionization by these methods cannot be said to be "physiologic" in most applications[26-27]. Certain modification strategies are well suited to mass spectrometric analysis as they can be employed under such physiologic conditions: aqueous neutral-buffered saline solution with dilute homogenous or mixed protein. As a result mass spectrometry is an important contributor to the elucidation of protein structure, and to the understanding of protein intermolecular interaction: identifying partner binding sites, stoichiometry, affinity, and dynamics[28].

The standard approach in protein footprinting is to determine which sites or regions on a protein exhibit a change in solvent accessibility between two or more states of the protein. This has been applied in thousands of studies that have variously examined protein folding[29], complexation[30], membrane orientation[31], and other contexts effecting change in protein structure. As long as the protein system is not perturbed by

the labeling, the extent of labeling will be attenuated in regions that have limited or no solvent accessibility. For example, to map the binding site of a protein with its ligand, one applies labeling conditions identically to both apo and holo states, digests the protein by proteolysis, and examines the extent of labeling visited on each peptide by mass spectrometry. Peptides or residues that have undergone more labeling in the apo state may comprise the ligand binding site, though they may instead be distal to it and are protected in the holo state by virtue of an allosteric response to binding. As with other methodologies, this strategy is empowered by *a priori* knowledge of the apo structure; mapping the protected regions onto the high resolution structure can help distinguish binding sites from other regions sensitive to allostery[32].

1.2.2 Global experiments.

When comparing states of a protein system, the overall level of labeling of each state's constituents is often informative of the presence of structural change, much like CD spectroscopy, and may provide important thermodynamic information. Hydrogen deuterium exchange (HDX) is a footprinting technique that probes the solvent accessible and hydrogen bonding environment of amide backbone hydrogens[33]. Commonly HDX experiments use pepsin proteolysis at low pH immediately after exchange labeling; the peptide products are then scanned by MS for peptide-resolved analysis. Alternatively, by skipping the proteolysis step the total protein deuterium uptake can be monitored. Such global analysis can detect whether protein rearrangement or binding is has occurred by comparison to a control state, for as few as 10 involved residues or fewer still, depending on experiment precision. This is an important tool sensitive to secondary, tertiary, and

quaternary structural change, whereas CD spectroscopy only assays changes in secondary structure. For example, by ligand titration the intermediate equilibria between apo and holo endpoint states scan be examined by HDX to elucidate the binding constant of the protein-ligand interaction[34].

1.2.3 Local experiments.

Ultimately mass spectrometry-based protein footprinting is used to examine changes in solvent accessibility at a peptide or residue-resolved level. As mentioned, HDX is a prominent choice for peptide-resolved footprinting. The advantage to this method is that it is non-residue specific in its amide labeling, except for proline. Moreover, the nature of HDX ensures that solvent-exposed amide hydrogens not involved in hydrogen bonding will be labeled with 100% efficiency for seconds-to-minutes exposures. A useful consequence of this is that determining the labeling yield for a peptide is done by measuring the change in mass of the peptide compared to its non-labeled theoretical mass. The more solvent-exposed residues a peptide possesses during the HDX exposure, the more its uptake mass will be increased. This makes HDX and MS natural partners, because the potential ionization biases affecting mass spectral intensity[35] are not shared by the m/z measurement.

Until recently, the goal for residue-resolved HDX footprinting could only be realized for those residues serendipitously overlapped by more than one pepsin proteolytic peptide[36]. The collision induced dissociation (CID) fragmentation experiment, conducted in ion trap mass spectrometers, is used to generate the characteristic fragment ion spectra of peptides to uniquely identify their sequences. This

experiment cannot be used to locate residue sites of HDX because of ^{1}H-^{2}H scrambling induced by the multiple collisions of CID[37]. A new method of fragmentation called electron-transfer dissociation (ETD)[38] has been demonstrated to solve this problem in the MS analysis of HDX-labeled peptides[39]. In ETD, scrambling is less probable due to the near vertical electronic transition a peptide undergoes with the addition an electron, from which state fragmentation directly proceeds.

If the labeling is stable, identification of the modification sites can be done using a proteomics-based "bottom-up" mass spectrometry methodology[40]. In this methodology, proteolytic peptides are chromatographically resolved and detected in a hybrid mass spectrometer capable of monitoring their accurate mass-to-charge ratios at high resolving power (ideally). The instrument's other spectrometer acquires the characteristic product ion spectra of peptide ions subjected to CID in an elution-dependent manner. The high-resolution LC-MS intensities provide a quantitative measure of each peptide, and their product ion spectra, acquired in this tandem MS/MS mode (MS^2), can indicate their identity and modification site(s). The yield of labeling at a residue or peptide is determined directly from levels of modified and unmodified peptides. An important aspect of stable (irreversible) covalent labeling is that, unlike HDX, protein conformation may be very sensitive to the labeling. If it is sensitive and its response occurs on the timescale of the labeling, the footprinting results will be biased by the sampling of these non-native structures. Sufficient care must be taken in the experiment and its analysis to avoid such bias.

1.3 Hydroxyl Radical Footprinting

1.3.1 Utility and chemistry

Hydroxyl radical labeling is a class of stable modification footprinting methods, each differentiated by the means of •OH generation. Hydroxyl radicals well probe solvent accessibility by virtue of their comparable size to water and high reactivity to several amino acid sidechains. The fundamental advantages to this strategy are twofold. (1) While modified protein is subjected to hours or days of handling and proteolysis before LC-MS/MS acquisition, the primary sequence of modified residues is preserved by virtue of the stability of the covalent modification. (2) The hydroxyl radical is a general reactant, affording a higher resolution footprint than covalent approaches which target single chemical groups, such as the acetylation of primary amines. Xu and Chance have shown in X-ray and γ-ray water radiolysis-initiated oxidation studies[41-43] that 14 of the 20 amino acid sidechains and the disulfide bond can be reliably modified when solvent exposed.

While there are many pathways for •OH-mediated labeling on residue sidechains, the most common net mass shift is the +15.9949 Da incorporation of oxygen in air-equilibrated solutions[40-41, 43-44]. The initial •OH reaction is different for aromatic and sulfur-containing residues than for aliphatic residues, but the involvement of molecular oxygen, the involvement of secondary radical reactions, and the similarity of the end products gives credence to examining one pathway; shown is reaction of •OH with leucine (Scheme 1.1). First, hydrogen is abstracted preferentially at the β- and γ- carbon

sites of the sidechain[45], followed quickly by reaction with O_2 to give a peroxy radical. The reaction with O_2 is diffusion controlled in oxygenated solutions[40, 46].

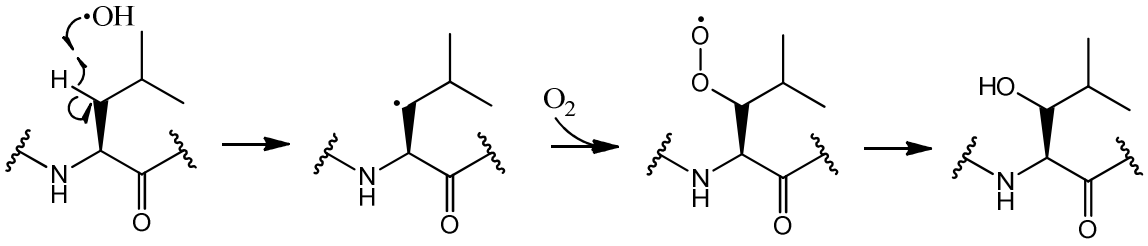

Scheme 1.1: The partial mechanism of leucine oxidation by hydroxyl radical to form a hydroxylated product.

There are several pathways by which the peroxy radical ultimately gives way to a hydroxyl modification; the other slightly less common product is a carbonyl modification[40]. In these pathways, reaction with radical species is required to return the protein to an even-electron molecule. The peroxy radical is capable of forming a dimer with other peroxy species such as HOO• and $O_2^{\bullet-}$, which through a cyclic transition state can give rise to carbonyl products[47]. Table 1.1 lists the common modifications we have observed in our •OH-mediated protein footprinting experiments[32, 48-51]; these are consistent with the contemporary and preceding work of others in the field[40].

Table 1.1: Initial •OH-amino acid sidechain reaction rates and common mass spectrometry-observed products of •OH-mediated protein footprinting

amino acid	$k_{\bullet OH}$ (M^{-1} sec^{-1})[52]	common modifications (Da)[40]				
Cys	3.5×10^{10}	–15.9772	+31.9898	+47.9847		
Trp	1.3×10^{10}	+3.9949	+15.9949	+31.9898	+47.9847	
Tyr	1.3×10^{10}	+15.9949	+31.9898	+47.9847		
Met	8.5×10^{9}	–32.0085	+15.9949	+31.9898		
Phe	6.9×10^{9}	+15.9949	+31.9898	+47.9847		
His	4.8×10^{9}	–23.0160	–22.0320	–10.0320	+4.9789	+15.9949
Arg	3.5×10^{9}	–43.0534	+13.9793	+15.9949		
Ile	1.8×10^{9}	+13.9793	+15.9949			
Leu	1.7×10^{9}	+13.9793	+15.9949			
Val	8.5×10^{8}	+13.9793	+15.9949			
Pro	6.5×10^{8}	+13.9793	+15.9949			
Gln	5.4×10^{8}	+13.9793	+15.9949			
Thr	5.1×10^{8}	–2.0157	+15.9949			
Lys	3.5×10^{8}	+13.9793	+15.9949			
Ser	3.2×10^{8}	–2.0157	+15.9949			
Glu	2.3×10^{8}	–30.0106	+13.9793	+15.9949		
Ala	7.7×10^{7}	+15.9949				
Asp	7.5×10^{7}	–30.0106	+15.9949			
Asn	4.9×10^{7}	+15.9949				
Gly	1.7×10^{7}	n.d.				

While hydroxyl radicals are non-specific reactants, they do not label sidechains with equal efficiency. The reaction rate of •OH with amino acid sidechains is 2000-fold higher for cysteine, the most reactive amino acid, than glycine, the least (Table 1.1). The second order rates in Table 1.1. pertain to amino acids free in solution, not residues in a protein. Even so, these rates reflect the inherent reactivity of residues in their fully exposed protein structural context: the MS-determined residue reactivity with •OH in unstructured peptides mirrors Table 1.1, with the exception that Met is second in the order[42].

Clearly another potential advantage to •OH-mediated footprinting is that it is so fast: the residue sidechain reactivity approaches the diffusion limit for Met, Trp, Tyr, and Cys residues. Recently Chen and colleagues[53] and Stocks and Konermann[29] were able to probe sub-millisecond protein folding using a methodology, described below, which takes advantage of inherent reactivity of •OH to make microsecond "snapshot" footprints of the proteins.

1.3.2 Methods of •OH-labeling

There are several hydroxyl radical footprinting approaches currently in use; a detailed review has been recently published[40]. Among the first DNA-protein and protein-ligand binding site footprinting studies have used hydroxyl radicals generated from catalytic Fenton chemistry[54] consuming hydrogen peroxide[55-56]. The Fe(II)-EDTA/H_2O_2/ascorbate Fenton system is currently a standard means for studying DNA and RNA interactions[57] because it allows for the stoichiometric generation of •OH from Fe(II) and H_2O_2 at neutral pH without risking Fe(III) precipitation as Fe_2O_3. The ascorbate is used to make the iron catalytic as it reduces Fe(III) back to Fe(II).

The synchrotron X-ray and ^{137}Cs γ-ray radiolysis methods generate hydroxyl radicals as the major reactive products from water radiolysis by high energy photons. The first step in •OH formation is the ejection of an electron from water. This high energy electron ionizes other water molecules, which ultimately generates hydroxyl radicals and other less reactive oxidants[58-59]. These methods have been successfully applied to footprinting DNA/protein interactions, RNA folding, and large proteins[60-62]. The synchrotron X-ray source produces a high intensity beam such that millisecond

exposures are sufficient to oxidize proteins[63]; longer times are typically needed for γ-ray radiolysis as the ^{137}Cs source is not as intense[64]. The benefit to the radiolysis method is that no additives are needed: water provides the source of •OH.

Ultraviolet light can homolytically cleave H_2O_2 to give •OH[65]. Sharp and colleagues first demonstrated this method of footprinting by their oxidative-labeling of myoglobin, with •OH generated from 5 M H_2O_2 irradiated by 254 nm light[66]. The quantum yield of UV H_2O_2 decomposition was first measured at 0.5[67], but a more recent measurement has $\Phi_{248}^{H_2O_2} = 0.80 \pm 0.1$[68].

1.3.3 Fast Photochemical Oxidation of Proteins (FPOP)

Hambly and Gross[50-51], and independently Aye and coworkers, have developed the method of fast photochemical oxidation of proteins (FPOP), which generates the radical from photolysis of hydrogen peroxide with pulsed 248 nm light[69]. At 248 nm the extinction coefficient is 24 $cm^{-1}M^{-1}$ [68]. The KrF excimer laser UV source provides a high flux of light, minimizing the exposure of protein to peroxide—the standard protocol uses 20 mM peroxide. Glutamine is included as a radical scavenger to limit the timescale of oxidation. The synchronization of the flow rate through the fused silica reaction cell with the excimer laser pulse frequency ensures all sample protein is irradiated once, but for a measurable exclusion fraction.

The primary advantage to FPOP is that the near mM •OH exposure of proteins is confined to a microsecond window, defined by the 17 ns laser pulse at its start and by the radical scavenging of glutamine. By one microsecond the free [•OH] is 50,000-fold less concentrated than at the outset under typical FPOP conditions, according to the pseudo-

first order analysis of its consumption[51]. This timescale of labeling predicts that the labeling-perturbed conformations of proteins aren't sampled by the labeling in cases where proteins are structurally sensitive to oxidation. Studies by Chung and coworkers[70-71] using 2D IR spectroscopy, dispersed vibrational echo spectroscopy, and MD simulation, showed that the fast-folding response of ubiquitin proceeds within 3 μs of an abrupt T-jump. Although such perturbation is wholly different than chemical modification, the timescale of ubiquitin response is suggestive of the earliest global changes we may expect for proteins conformationally sensitive to oxidative modification. In some cases, still faster ns motions in regions of flexibility give rise to larger-scale slower motions in the protein's exploration of conformation space[72]. It is possible that initial modifications to such regions of high flexibility may alter the attendant structural progression of larger regions. This should be kept in mind with all stable-modification footprinting methods, and is why FPOP, with its radical scavenger-tunable timescale, is an attractive footprinting method.

1.4 Dissertation Topics

1.4.1 Chapter 2 Validation of the FPOP timescale.

Like other chemical footprinting techniques, FPOP must ensure only the native conformation is labeled. Although oxidation via hydroxyl radical induces unfolding in proteins on a millisecond timescale, FPOP is designed to limit •OH exposure to 1 μs or less by employing a pulsed laser for initiation to produce the radicals and including a radical-scavenger to limit their lifetimes. We applied FPOP to three oxidation-sensitive proteins and found that the distribution of modification (oxidation) states is Poisson when

a scavenger is present, consistent with a single conformation protein modification model. This model breaks down when a scavenger is not used and/or hydrogen peroxide is not removed following photolysis. The outcome verifies that FPOP occurs on a time scale faster than global conformational changes in these proteins. This study has been published in *Analytical Chemistry*[73].

1.4.2 Chapter 3 Development of efficient and comprehensive footprinting analysis software.

Mass spectrometry-based protein footprinting is a powerful method for unveiling many kinds of protein interactions that cannot be studied by X-ray crystallography or NMR spectroscopy. To realize the maximum information a protein footprinting study can offer, residue-resolution of the footprinting label is needed for every residue sensitive to the labeling chemistry. Hydroxyl radical-mediated labeling has proven to be a very informative protein footprinting method, because of the number of solvent accessible residues that may be labeled by •OH. The paradox of such a method is that finding all •OH-labeling fates in the proteolyzed sample's LC-MS/MS acquisition data is daunting without the help of automated software. While the proteomics field has enjoyed the concomitant development and refinement of bioinformatics software, these software are not well suited to the task of assigning most LC-MS features from related sets of LC-MS/MS acquisitions to the modified and unmodified proteolytic peptides of one or a few proteins that have suffered a broad distribution of modifications. We present Excel-based tools developed to facilitate this task, providing a means for achieving a comprehensive residue-resolved analysis of footprinting data in an efficient manner. To demonstrate the

software and the utility of •OH-mediated labeling, we show that FPOP easily distinguishes the buried and exposed residues of barstar in its folded and unfolded states.

1.4.3 Chapter 4 Extension of the FPOP method to new reagents.

The focus of this work is to expand the original design of FPOP and introduce SO_4^{-}•, generated by 248 nm homolysis of low mM levels of persulfate, as a radical reactant in protein footprinting. A feature of FPOP is that its design accommodates other reagents, increasing its versatility. The new persulfate FPOP system is a potent, non-specific, and tunable footprinting method: 3-5 times less persulfate is needed to give the same global levels of modification seen with FPOP photolysis of hydrogen peroxide. Although solvent-exposed His and Tyr residues are more reactive with SO_4^{-}• than with •OH, a thorough LC/MS/MS and structural analysis of apomyoglobin and calmodulin labeled products, shows that •OH can probe smaller accessible areas than SO_4^{-}•, with the possible exception of when histidine is modified. This is consistent with the larger size of the SO_4^{-}• compared to •OH. We find that His64, an axial ligand in the heme-binding pocket of apomyoglobin, is substantially up-labeled by SO_4^{-}• relative to •OH. Finally, because the kinds of modification and residue selectivity for both FPOP methods are strikingly similar, we believe the choice for either method should be made considering first the physical properties of persulfate and hydrogen peroxide, especially their membrane permeability. This study has been published in *Analytical Chemistry*[48].

1.4.4 Chapter 5 Application of FPOP: apolipoprotein E oligomerization.

The three common isoforms of apolipoprotein E (ApoE) differ at two sites in their 299 amino-acid sequence but these differences modulate the structure of ApoE to affect

profoundly the isoform associations with disease. The ApoE ε4 allele in particular is strongly associated with Alzheimer's disease. The study of the structural effects of these mutation sites in aqueous media is hampered by the aggregation proclivity of each ApoE isoform. Hence, understanding the differences between isoforms must rely on lower resolution biophysical measurements, mutagenesis, homology studies, and the use of truncated ApoE variants. In this study, we report two comparative studies of the ApoE family by using the mass spectrometry-based protein footprinting methods of FPOP and glycine ethyl ester (GEE) labeling. The first experiment examines the three full-length WT isoforms in their tetrameric state and finds that the overall structures are similar with the exception of M108 in ApoE4, which is more solvent-accessible in this isoform than in ApoE2 and ApoE3. The second experiment provides clear evidence, from a comparison of the footprinting results of the wild-type proteins and a monomeric mutant, that several residues 183-205 and 232-251 are involved self-association.

1.4.5 Chapter 6 Application of FPOP: apolipoprotein E monomeric mutant structure prediction.

We validate the presumed four-helix bundle structure of the N-terminal domain of the full length Apolipoprotein E (ApoE) by means of protein footprinting using the method of FPOP in a new way. The validation of this structure is made by comparison of the extent of oxidative modifications at the amino-acid level with the calculated sidechain solvent-accessible surface area, taken from the most recent high resolution N-terminal domain structure of truncated Apolipoprotein E. We subjected a monomeric mutant of the Apolipoprotein E3 variant to FPOP footprinting to warrant conclusions

based on the monomeric structure of ApoE. This study highlights the applicability FPOP footprinting for structural hypothesis testing when high-resolution studies are not possible, and it points to immediate application towards unraveling the structural differences between the wild type variants of Apolipoprotein E in lipid-free and –bound states.

1.4.6 Chapter 7 Application of FPOP: apolipoprotein E-Aβ42 interaction.

The β-amyloid peptide 1-42 may be the most important biomolecule implicated in Alzheimer's disease pathogenesis. Cerebral plaques comprised of the insoluble fibrillar form of this peptide are found in all patients diagnosed with Alzheimer's disease. The soluble oligomers of β-amyloid 1-42 are neurotoxic. The amyloid hypothesis suggests that the clearance of this peptide in the brain is central to affecting the likelihood of Alzheimer's disease onset. One protein known to interact with this peptide in its fibrillar and soluble forms is apolipoprotein E. Strikingly, the apolipoprotein E4 isoform of this protein confers a 12-fold greater risk for Alzheimer's disease for people with two copies of this allele than for people with no copies. The molecular characterization of β-amyloid interaction with apolipoprotein E isoforms has thus been an important goal of many studies; owing to the oligomeric properties of both biomolecules, no high resolution structure of the complex or of ApoE exists. We have used the FPOP method of mass spectrometry-based protein footprinting to provide an intermediate-resolution picture of this interaction for lipid-free ApoE3 and ApoE4. We find that both proteins exhibit Aβ42 binding in their N-terminus domains, involving residues W34 and Y36. Arginine 167 also shows significant protection in the Aβ42-present state. It is not

contiguous in the N-terminus domain structures of ApoE, and we argue that this site is protected by a similar allosteric response by both proteins upon Aβ42 binding. Proline 293 is also involved in a C-terminal domain interaction in ApoE3, but the overall footprinting signals in the C-terminal domain suggest that this interaction is not as strong as the N-terminal domain. These results are consistent with several studies that have examined the domain interactions with Aβ independently.

1.5 References

1. Berman, H. M.; Westbrook, J.; Feng, Z.; Gilliland, G.; Bhat, T. N.; Weissig, H.; Shindyalov, I. N.; Bourne, P. E., The Protein Data Bank. *Nucleic Acids Research* **2000,** *28* (1), 235-242.
2. White, S. H., Biophysical dissection of membrane proteins. *Nature* **2009,** *459* (7245), 344-346.
3. Pantazatos, D.; Kim, J. S.; Klock, H. E.; Stevens, R. C.; Wilson, I. A.; Lesley, S. A.; Woods, V. L., Rapid refinement of crystallographic protein construct definition employing enhanced hydrogen/deuterium exchange MS. *Proc. Natl. Acad. Sci. U.S.A.* **2004,** *101* (3), 751-756.
4. Jane Dyson, H.; Ewright, P., Insights into the structure and dynamics of unfolded proteins from nuclear magnetic resonance. In *Advances in Protein Chemistry*, George, D. R., Ed. Academic Press: 2002; Vol. Volume 62, pp 311-340.
5. Dyson, H. J.; Wright, P. E., Unfolded Proteins and Protein Folding Studied by NMR. *Chemical Reviews* **2004,** *104* (8), 3607-3622.
6. Schnell, J. R.; Dyson, H. J.; Wright, P. E., Structure, Dynamics, and Catalytic Function of Dihydrofolate Reductase. *Annual Review of Biophysics and Biomolecular Structure* **2004,** *33* (1), 119-140.
7. Bouvignies, G.; Vallurupalli, P.; Cordes, M.; Hansen, D.; Kay, L., Measuring $^{1}H^{N}$ temperature coefficients in invisible protein states by relaxation dispersion NMR spectroscopy. *Journal of Biomolecular NMR* **2011,** *50* (1), 13-18.
8. Neudecker, P.; Lundström, P.; Kay, L. E., Relaxation Dispersion NMR Spectroscopy as a Tool for Detailed Studies of Protein Folding. *Biophysical journal* **2009,** *96* (6), 2045-2054.
9. Griswold, I. J.; Dahlquist, F. W., Bigger is better: megadalton protein NMR in solution. *Nat. Struct. Mol. Biol.* **2002,** *9* (8), 567-568.
10. Venters, R. A.; Calderone, T. L.; Spicer, L. D.; Fierke, C. A., Uniform carbon-13 isotope labeling of proteins with sodium acetate for NMR studies: application to human carbonic anhydrase II. *Biochemistry* **1991,** *30* (18), 4491-4494.
11. Andrew, E. R.; Bradbury, A.; Eades, R. G., Nuclear Magnetic Resonance Spectra from a Crystal rotated at High Speed. *Nature* **1958,** *182* (4650), 1659-1659.
12. Castellani, F.; van Rossum, B.; Diehl, A.; Schubert, M.; Rehbein, K.; Oschkinat, H., Structure of a protein determined by solid-state magic-angle-spinning NMR spectroscopy. *Nature* **2002,** *420* (6911), 98-102.

13. Li, Y.; Berthold, D. A.; Gennis, R. B.; Rienstra, C. M., Chemical shift assignment of the transmembrane helices of DsbB, a 20-kDa integral membrane enzyme, by 3D magic-angle spinning NMR spectroscopy. *Protein Sci.* **2008,** *17* (2), 199-204.
14. Andronesi, O. C.; Becker, S.; Seidel, K.; Heise, H.; Young, H. S.; Baldus, M., Determination of Membrane Protein Structure and Dynamics by Magic-Angle-Spinning Solid-State NMR Spectroscopy†. *J. Am. Chem. Soc.* **2005,** *127* (37), 12965-12974.
15. Garai, K.; Mustafi, S. M.; Baban, B.; Frieden, C., Structural differences between apolipoprotein E3 and E4 as measured by 19F NMR. *Protein Sci.* **2009,** *19* (1), 66-74.
16. Jomaa, A.; Stewart, G.; Martín-Benito, J.; Zielke, R.; Campbell, T. L.; Maddock, J. R.; Brown, E. D.; Ortega, J., Understanding ribosome assembly: the structure of in vivo assembled immature 30S subunits revealed by cryo-electron microscopy. *RNA* **2011,** *17* (4), 697-709.
17. Wulff, R. P.; Lundqvist, J.; Rutsdottir, G.; Hansson, A.; Stenbaek, A.; Elmlund, D.; Elmlund, H.; Jensen, P. E.; Hansson, M., The Activity of Barley NADPH-Dependent Thioredoxin Reductase C Is Independent of the Oligomeric State of the Protein: Tetrameric Structure Determined by Cryo-Electron Microscopy. *Biochemistry* **2011**, null-null.
18. Zheng, W., Accurate Flexible Fitting of High-Resolution Protein Structures into Cryo-Electron Microscopy Maps Using Coarse-Grained Pseudo-Energy Minimization. *Biophysical journal* **2011,** *100* (2), 478-488.
19. D'Anna, J. A.; Isenberg, I., Histone cross-complexing pattern. *Biochemistry* **1974,** *13* (24), 4992-4997.
20. Fasman, G. D., *Circular Dichroism and the Conformational Analysis of Biomolecules*. Plenum Press: New York, 1996.
21. Schuler, B.; Eaton, W. A., Protein folding studied by single-molecule FRET. *Current Opinion in Structural Biology* **2008,** *18* (1), 16-26.
22. Hofmann, H.; Hillger, F.; Pfeil, S. H.; Hoffmann, A.; Streich, D.; Haenni, D.; Nettels, D.; Lipman, E. A.; Schuler, B., Single-molecule spectroscopy of protein folding in a chaperonin cage. *Proc. Natl. Acad. Sci. U.S.A.* **2010,** *107* (26), 11793-11798.
23. Hess, S. T.; Huang, S.; Heikal, A. A.; Webb, W. W., Biological and Chemical Applications of Fluorescence Correlation Spectroscopy: A Review†. *Biochemistry* **2001,** *41* (3), 697-705.
24. Lebowitz, J.; Lewis, M. S.; Schuck, P., Modern analytical ultracentrifugation in protein science: A tutorial review. *Protein Sci.* **2002,** *11* (9), 2067-2079.
25. Hirs, C. H. W.; Di Sabato, G.; Ottesen, M.; Gold, A. M.; Gurd, F. R. N.; Horton, H. R.; Koshland, D. E.; Kimmel, J. R.; Klotz, I. M.; Ludwig, M. L.; Hunter, M. J.; Neumann, N. P.; Ray, W. J.; Riordan, J. F.; Vallee, B. L.; Sela, M.; Arnon, R.; Spande, T. F.; Witkop, B.; Stark, G. R.; Wilcox, P. E.; Wold, F., In *Methods in Enzymology*, Academic Press: 1967; Vol. 11, pp 485-748.
26. Fenn, J. B.; Mann, M.; Meng, C. K.; Wong, S. F.; Whitehouse, C. M., Electrospray ionization for mass spectrometry of large biomolecules. *Science* **1989,** *246* (4926), 64-71.
27. Karas, M.; Bachmann, D.; Hillenkamp, F., Influence of the wavelength in high-irradiance ultraviolet laser desorption mass spectrometry of organic molecules. *Anal. Chem.* **1985,** *57* (14), 2935-2939.
28. Konermann, L.; Tong, X.; Pan, Y., Protein structure and dynamics studied by mass spectrometry: H/D exchange, hydroxyl radical labeling, and related approaches. *J. Mass Spectrom.* **2008,** *43* (8), 1021-1036.

29. Stocks, B. B.; Konermann, L., Time-Dependent Changes in Side-Chain Solvent Accessibility during Cytochrome c Folding Probed by Pulsed Oxidative Labeling and Mass Spectrometry. *Journal of Molecular Biology* **2010,** *398* (2), 362-373.
30. Takamoto, K.; Chance, M. R., Radiolytic Protein Footprinting with Mass Spectrometry to Probe the Structure of Macromolecular Complexes. *Annual Review of Biophysics and Biomolecular Structure* **2006,** *35* (1), 251-276.
31. Wen, J.; Zhang, H.; Gross, M. L.; Blankenship, R. E., Membrane orientation of the FMO antenna protein from Chlorobaculum tepidum as determined by mass spectrometry-based footprinting. *Proc. Natl. Acad. Sci. U.S.A.* **2009,** *106* (15), 6134-6139.
32. Zhang, H.; Gau, B. C.; Jones, L. M.; Vidavsky, I.; Gross, M. L., Fast Photochemical Oxidation of Proteins for Comparing Structures of Protein-Ligand Complexes: The Calmodulin-Peptide Model System. *Anal. Chem.* **2010,** *83* (1), 311-318.
33. Chen, S.; Engen, J. R., Isotope Exchange and Covalent Modification Strategies for Studying Protein Structure and Function. *Cur. Anal. Chem.* **2009,** *5*, 205-212.
34. Zhu, M. M.; Rempel, D. L.; Du, Z.; Gross, M. L., Quantification of Protein-Ligand Interactions by Mass Spectrometry, Titration, and H/D Exchange: PLIMSTEX. *J. Am. Chem. Soc.* **2003,** *125* (18), 5252-5253.
35. Fenn, J. B., Ion formation from charged droplets: roles of geometry, energy, and time. *J. Am. Soc. Mass Spectrom.* **1993,** *4* (7), 524-535.
36. Althaus, E.; Canzar, S.; Ehrler, C.; Emmett, M.; Karrenbauer, A.; Marshall, A.; Meyer-Bäse, A.; Tipton, J.; Zhang, H.-M., Computing H/D-Exchange rates of single residues from data of proteolytic fragments. *BMC Bioinformatics* **2010,** *11* (1), 424.
37. Hoerner, J. K.; Xiao, H.; Dobo, A.; Kaltashov, I. A., Is There Hydrogen Scrambling in the Gas Phase? Energetic and Structural Determinants of Proton Mobility within Protein Ions. *J. Am. Chem. Soc.* **2004,** *126* (24), 7709-7717.
38. Syka, J. E. P.; Coon, J. J.; Schroeder, M. J.; Shabanowitz, J.; Hunt, D. F., Peptide and protein sequence analysis by electron transfer dissociation mass spectrometry. *Proc. Natl. Acad. Sci. U.S.A.* **2004,** *101* (26), 9528-9533.
39. Rand, K. D.; Zehl, M.; Jensen, O. N.; Jørgensen, T. J. D., Protein Hydrogen Exchange Measured at Single-Residue Resolution by Electron Transfer Dissociation Mass Spectrometry. *Anal. Chem.* **2009,** *81* (14), 5577-5584.
40. Xu, G.; Chance, M. R., Hydroxyl Radical-Mediated Modification of Proteins as Probes for Structural Proteomics. *Chem. Rev.* **2007,** *107* (8), 3514-3543.
41. Xu, G.; Chance, M. R., Radiolytic Modification of Acidic Amino Acid Residues in Peptides: Probes for Examining Protein-Protein Interactions. *Anal. Chem.* **2004,** *76* (5), 1213-1221.
42. Xu, G.; Chance, M. R., Radiolytic Modification and Reactivity of Amino Acid Residues Serving as Structural Probes for Protein Footprinting. *Anal. Chem.* **2005,** *77* (14), 4549-4555.
43. Xu, G.; Chance, M. R., Radiolytic Modification of Sulfur-Containing Amino Acid Residues in Model Peptides: Fundamental Studies for Protein Footprinting. *Anal. Chem.* **2005,** *77* (8), 2437-2449.
44. Xu, G.; Takamoto, K.; Chance, M. R., Radiolytic Modification of Basic Amino Acid Residues in Peptides: Probes for Examining Protein−Protein Interactions. *Anal. Chem.* **2003,** *75* (24), 6995-7007.

45. L. Hawkins, C.; J. Davies, M., EPR studies on the selectivity of hydroxyl radical attack on amino acids and peptides. *Journal of the Chemical Society, Perkin Transactions 2* **1998,** (12), 2617-2622.
46. Garrison, W. M., Reaction mechanisms in the radiolysis of peptides, polypeptides, and proteins. *Chem. Rev.* **1987,** *87* (2), 381-398.
47. Russell, G. A., Deuterium-isotope Effects in the Autoxidation of Aralkyl Hydrocarbons. Mechanism of the Interaction of PEroxy Radicals. *J. Am. Chem. Soc.* **1957,** *79* (14), 3871-3877.
48. Gau, B. C.; Chen, H.; Zhang, Y.; Gross, M. L., Sulfate Radical Anion as a New Reagent for Fast Photochemical Oxidation of Proteins. *Anal. Chem.* **2010,** *82* (18), 7821-7827.
49. Gau, B. C.; Sharp, J. S.; Rempel, D. L.; Gross, M. L., FPOP Labels Proteins Faster than They Unfold. In *Proceedings of the 56th ASMS Conference on Mass Spectrometry and Allied Topics*, Denver, Colorado, 2008.
50. Hambly, D.; Gross, M., Laser flash photochemical oxidation to locate heme binding and conformational changes in myoglobin. *Int. J. Mass Spectrom.* **2007,** *259* (1-3), 124-129.
51. Hambly, D. M.; Gross, M. L., Laser Flash Photolysis of Hydrogen Peroxide to Oxidize Protein Solvent-Accessible Residues on the Microsecond Timescale. *J. Am. Soc. Mass Spectrom.* **2005,** *16* (12), 2057-2063.
52. Buxton, G. V.; Greenstock, C. L.; Helman, W. P.; Ross, A. B., Critical Review of Rate Constants for Reactions of Hydrated Electrons, Hydrogen Atoms and Hydroxyl Radicals (*OH/*O-) in Aqueous Solution. *J. Phys. Chem. Ref. Data* **1988,** *17* (2), 513-886.
53. Chen, J.; Rempel, D. L.; Gross, M. L., Temperature Jump and Fast Photochemical Oxidation Probe Submillisecond Protein Folding. *J. Am. Chem. Soc.* **2010,** *132* (44), 15502-15504.
54. Fenton, H. J. H., The oxidation of tartaric acid in presence of iron. *J. Chem. Soc. Proc.* **1894,** *10*, 157-158.
55. Tullius, T. D.; Dombroski, B. A., Hydroxyl radical "footprinting": high-resolution information about DNA-protein contacts and application to lambda repressor and Cro protein. *Proc. Natl. Acad. Sci. U.S.A.* **1986,** *83* (15), 5469-5473.
56. Shanblatt, S. H.; Revzin, A., Interactions of the catabolite activator protein (CAP) at the galactose and lactose promoters of Escherichia coli probed by hydroxyl radical footprinting. The second CAP molecule which binds at gal and the one CAP at lac may act to stimulate transcription in the same way. *J. Biol. Chem.* **1987,** *262* (24), 11422-11427.
57. Tullius, T. D.; Greenbaum, J. A., Mapping nucleic acid structure by hydroxyl radical cleavage. *Current Opinion in Chemical Biology* **2005,** *9* (2), 127-134.
58. Hawkins, C. L.; Davies, M. J., Generation and propagation of radical reactions on proteins. *Biochim. Biophys. Acta Bioenergetics* **2001,** *1504* (2-3), 196-219.
59. Davies, M. J.; Dean, R. T., *Radical-Mediated Protein Oxidation: From Chemistry to Medicine*. Oxford University Press: 1997.
60. Maleknia, S. D.; Ralston, C. Y.; Brenowitz, M. D.; Downard, K. M.; Chance, M. R., Determination of Macromolecular Folding and Structure by Synchrotron X-Ray Radiolysis Techniques. *Anal. Biochem.* **2001,** *289* (2), 103-115.
61. Kiselar, J. G.; Maleknia, S. D.; Sullivan, M.; Downard, K. M.; Chance, M. R., Hydroxyl radical probe of protein surfaces using synchrotron X-ray radiolysis and mass spectrometry. *Int. J. Radiat. Biol.* **2002,** *78* (2), 101 - 114.
62. Guan, J. Q.; Takamoto, K.; Almo, S. C.; Reisler, E.; Chance, M. R., Structure and Dynamics of the Actin Filament. *Biochemistry* **2005,** *44* (9), 3166-3175.

63. Maleknia, S. D.; Brenowitz, M.; Chance, M. R., Millisecond Radiolytic Modification of Peptides by Synchrotron X-rays Identified by Mass Spectrometry. *Anal. Chem.* **1999,** *71* (18), 3965-3973.
64. Sharp, J. S.; Tomer, K. B., Analysis of the Oxidative Damage-Induced Conformational Changes of Apo- and Holocalmodulin by Dose-Dependent Protein Oxidative Surface Mapping. *Biophys. J.* **2007,** *92* (5), 1682-1692.
65. Schrank, S. G.; José, H. J.; Moreira, R. F. P. M.; Schröder, H. F., Applicability of Fenton and H2O2/UV reactions in the treatment of tannery wastewaters. *Chemosphere* **2005,** *60* (5), 644-655.
66. Sharp, J. S.; Becker, J. M.; Hettich, R. L., Analysis of Protein Solvent Accessible Surfaces by Photochemical Oxidation and Mass Spectrometry. *Anal. Chem.* **2003,** *76* (3), 672-683.
67. Weeks, J. L.; Matheson, M. S., The Primary Quantum Yield of Hydrogen Peroxide Decomposition. *J. Am. Chem. Soc.* **1956,** *78* (7), 1273-1278.
68. Schiffman, A.; Nelson, J. D. D.; Nesbitt, D. J., Quantum yields for OH production from 193 and 248 nm photolysis of HNO[sub 3] and H[sub 2]O[sub 2]. *The Journal of Chemical Physics* **1993,** *98* (9), 6935-6946.
69. Aye, T. T.; Low, T. Y.; Sze, S. K., Nanosecond Laser-Induced Photochemical Oxidation Method for Protein Surface Mapping with Mass Spectrometry. *Anal. Chem.* **2005,** *77* (18), 5814-5822.
70. Chung, H. S.; Ganim, Z.; Jones, K. C.; Tokmakoff, A., Transient 2D IR spectroscopy of ubiquitin unfolding dynamics. *Proc. Natl. Acad. Sci. U.S.A.* **2007,** *104* (36), 14237-14242.
71. Chung, H. S.; Khalil, M.; Smith, A. W.; Ganim, Z.; Tokmakoff, A., Conformational changes during the nanosecond-to-millisecond unfolding of ubiquitin. *Proc. Natl. Acad. Sci. U.S.A.* **2005,** *102* (3), 612-617.
72. Henzler-Wildman, K. A.; Lei, M.; Thai, V.; Kerns, S. J.; Karplus, M.; Kern, D., A hierarchy of timescales in protein dynamics is linked to enzyme catalysis. *Nature* **2007,** *450* (7171), 913-916.
73. Gau, B. C.; Sharp, J. S.; Rempel, D. L.; Gross, M. L., Fast Photochemical Oxidation of Protein Footprints Faster than Protein Unfolding. *Anal. Chem.* **2009,** *81* (16), 6563-6571.

2 Fast Photochemical Oxidation of Protein Footprints Faster than Protein Unfolding

2.1 Introduction

Protein footprinting is an assay that monitors protein conformation by selectively labeling or cleaving residues. This selectivity is, in part, a function of the target protein's solvent accessibility; thus, an implicit picture of protein structure is afforded by footprinting. Although the ways of modifying residues are diverse, and many have been in practice for over forty years,[1] the advent of biomolecular mass spectrometry, associated with ESI and MALDI ionization and interfaced to liquid chromatography, now makes possible highly specific, sensitive, and rapid analysis of modified peptides and proteins.[2-3] Thus, we are attempting to establish a marriage of mass spectrometry and chemical footprinting to afford a tool for the elucidation of protein structure and dynamics, and for the identification of partner binding sites, stoichiometry, and affinity.[4]

Protein oxidation by hydroxyl radicals is one class of footprinting methods; the various subclasses are differentiated by the means used to generate the •OH. Hydroxyl radicals probe solvent accessibility because they have comparable size to solvent water molecules and high reactivity with a significant fraction of amino acid side chains. The advantages of hydroxyl radical footprinting are twofold. First, the primary sequence of modified residues is preserved by virtue of the stability of the covalent modification even though a protein may be subjected to several hours and even days of handling and proteolysis following the chemical footprinting step. Second, the hydroxyl radical is a reactive reagent, modifying many amino acid residues and affording a higher coverage

footprint than those covalent approaches that target specific residues (e.g., the acetylation of primary amines). Xu and Chance[5-7] showed that in X-ray and γ-ray water radiolysis, up to 14 of the 20 sidechains and cys-cys disulfide bonds can be usefully modified for footprinting experiments.

As implied above, there are several hydroxyl radical footprinting approaches currently in use; a detailed review was recently published.[8] Among the first DNA:protein and protein:ligand binding site footprinting studies have used hydroxyl radicals generated from catalytic Fenton chemistry[9] consuming hydrogen peroxide.[10-11] The synchrotron X-ray and ^{137}Cs γ-ray methods generate hydroxyl radicals as the major reactive products from water radiolysis by high-energy photons. These methods were originally developed by Chance[12-14] and coworkers to footprint DNA/protein interactions, RNA folding, and large proteins. Recently Hambly and Gross, and independently Aye et al.,[15-17] reported a method of fast photochemical oxidation of proteins (FPOP) that generates •OH by photolysis of mM hydrogen peroxide with a pulsed laser (either 248-nm KrF excimer laser or 266-nm frequency quadrupled Nd YAG). The laser provides a spatially small, high flux of light, maximizing the exposure of a small volume of protein solution to radicals and ensuring all but a small exclusion fraction of the protein is irradiated only once (Figure 2.1). In the design by Hambly and Gross, a constituent radical scavenger limits the timescale of oxidation. During a short timescale of oxidation (~ μs), footprinting occurs at high yield.

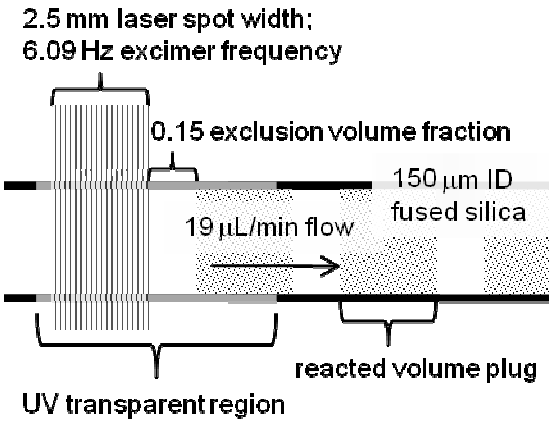

Figure 2.1: Schematic of the FPOP fused silica reaction region with normal flow, laser pulse frequency, and laser spot size settings.

Here we report the first experimental evaluation of FPOP to test the claim by Hambly and Gross that it labels a protein faster than its unfolding. Fast laser temperature-jump methods coupled with several spectroscopy techniques have measured timescales of folding for protein model systems.[18] Recent studies by Chung and coworkers[19-20] using 2D IR spectroscopy, dispersed vibrational echo spectroscopy, and MD simulation, showed that the fast-folding response of ubiquitin, of breaking native contacts in its β-sheet, proceeds within 3 μs of an abrupt T-jump. Although such perturbation is wholly different than chemical modification, the timescale of ubiquitin response is suggestive of the earliest changes we may expect for proteins conformationally sensitive to oxidative modification. Small in size and tractable for analysis, β-lactoglobulin (β-lg), apo-calmodulin (apo-CaM), and lysozyme (LysC) are not structurally similar, yet are representative of proteins exhibiting this sensitivity.[21-22] Therefore, we chose these proteins to test the hypothesis.

Venkatesh and coworkers[21] proposed a method of ascertaining whether hydroxyl radical reactions sample the native protein conformation or upset the structural equilibrium during the timescale of exposure. Their approach is appropriate for continuous-dose methods because they provide a near steady state hydroxyl radical concentration, allowing for a pseudo-first order kinetic model to be used.[22-23] The FPOP method, however, cannot be so evaluated because it is pulsed. A single laser pulse provides a well defined start, and chemical quenching provides the "shutter" for the reaction. The 17-nsec laser pulse generates an [•OH] of approximately 1 mM. We estimate that the presence of glutamine radical scavenger at 20 mM effectively quenches radical exposure by ~ 1 μs; thus, the [•OH] is not at steady state.[16] .

The desired test is one for change in conformation induced by FPOP, but only for change occurring on the labeling timescale. One means of monitoring protein conformational changes is to track their charge-state distribution.[24-29] This approach, however, has difficulty distinguishing fast and slow FPOP-induced conformation changes. One might follow Maleknia and coworkers[30-32], who developed a method of protein footprinting by generating reactive oxygen species in an ESI source, accommodating rapid mass spectrometry analysis, but this approach suffers from the uncertainty that protein conformation in a charge dense droplet in a high electric field is relevant to solution biology. The special experimental features of FPOP require an indirect evaluation method.

2.1.1 Test of Hypothesis that FPOP Oxidizes Protein Faster than its Unfolding.

If an effective radical exposure at 1 μs is shorter than a significant structural response to oxidative modification, and if the probability of modification at a site is a function of its solvent accessibility, it follows that the modification probability at each site is independent of other incurred modifications for such an exposure. It is also a function of the site's inherent chemical reactivity.[6, 33] The modification probabilities of the most sensitive sites can be approximated by an average probability. A binomial distribution models the outcomes of this approximation. The probability a protein will be modified k times is:

$$P(k; N, p) = \binom{N}{k} {p_{mod}}^{k} (1 - p_{mod})^{N-k} \quad (1)$$

for N potential modification sites, each with p_{mod} probability of modification. As N increases, this probability diminishes for any one site, yet the product Np_{mod} is invariant. For example, two proteins, one large and one small, undergoing controlled oxidative labeling will exhibit the same product distribution only if they are exposed at equal mass concentration other things being equal (i.e., the solvent accessibility/size ratio and average reactivity of each site). The limiting case of the binomial distribution as $N \to \infty$ is the Poisson distribution, with a probability mass function:

$$P(k; \lambda) = \frac{e^{-\lambda} \lambda^{k}}{k!} \quad (2)$$

Significantly, this is parameterized by only one factor, λ, which is the expected number of events $\langle k \rangle$ and their variance $\langle k^2 \rangle - \langle k \rangle^2$. In practice for $N > 50$ and $p < 0.02$, an optimal λ gives a Poisson distribution matching the binomial, per outcome, to within the

determination error (inclusive of experimental error and modeling uncertainty) of any •OH modification state of a protein.

The dominant product pathway for most residue sidechains reacting with •OH is the net addition of oxygen (+16 Da) as a hydroxyl group (as substitution of H for OH).[8, 34] Consequently, the distribution of modified products can be simplified as a 0, +16, +32. . . addition state distribution, wherein proteins are binned only by the number of increments in 16 Da they have gained. For a properly controlled FPOP experiment, we hypothesize that the distribution of 0, +16, +32… products should be very nearly Poisson if the footprinting reactions occur more rapidly than any significant protein unfolding. This hypothesis is the basis for our evaluation of the three aforementioned proteins subjected to varying oxidation conditions.

2.2 Experimental section

2.2.1 Reagents.

Bovine β-Lactoglobulin A, lysozyme from chicken egg white, 30% hydrogen peroxide, *L*-glutamine, *L*-methionine, catalase, urea, ethylene glycol-bis(2-aminoethylether)-*N*,*N*,*N*′,*N*′-tetraacetic acid (EGTA), acetonitrile, formic acid, and phosphate buffered saline (PBS) were purchased from the Sigma Aldrich Chemical Company (St. Louis, MO). Bovine CaM was purchased from Oceanbiologics (Corvallis, OR). The proteins were used without further purification. *tris*-(2-Carboxyethyl) phosphine hydrochloride (TCEP-HCl) was purchased from Pierce Biotechnology, Inc (Rockford, IL). Purified water (18 MΩ) was obtained from an in-house Milli-Q Synthesis system (Millipore, Billerica, MA).

2.2.2 Oxidative-modification labeling.

Each 50 μL sample was prepared in PBS (10 mM phosphate buffer, 138 mM NaCl, 2.7 mM KCl, pH 7.4 at 25 °C) with a final protein concentration of 10 □M. Apo-CaM samples included 100 μM EGTA for the chelation of adventitious calcium. Glutamine was added to a final concentration of 20 mM in normal FPOP samples. Hydrogen peroxide was added to a final concentration of 15 mM just before FPOP infusion. The flowing sample solution was collected in a 0.6 mL microcentrifuge tube containing an additional 20 μL of 100 nM catalase and 70 mM methionine in PBS, as per the normal FPOP procedure. The breakdown of peroxide by catalase was conducted by treating the sample for 10 min at room temperature before freezing the samples at -80°C.

FPOP was conducted as described previously, but with150 μm ID fused silica (Polymicro Technologies, Phoenix, AZ).[16] The 2.54 mm beam width was measured from a 30-shot burn pattern on label tape affixed to a temporary beam stop placed in the plane of the flow cell. Samples with an approximate 15% exclusion volume fraction (EVF) were infused at a rate of 19.00 ± 0.04 μL/min, and the excimer pulse frequency was set to 6.00 ± 0.02 Hz. 30% and 60% EVF samples were infused at the same rate but with 4.94 ± 0.02 and 2.82 ± 0.02 Hz pulse frequencies, respectively.

2.2.3 Mass spectrometry.

Each sample was thawed and Ziptip$_{C4}$-desalted (Millipore, Billerica, MA) before ESI MS acquisition on a Waters Ultima Global quadrupole time-of-flight (Milford, MA), operating in V mode at 12,000 FWHM resolving power at 838.8 m/z ($(CF_3COONa)_6Na^+$ calibrant ion). Some samples were subjected to a 1 h, 37 °C incubation in 8 M urea, 5

mM TCEP prior to de-salting. The 10 μL 50% acetonitrile 1% formic acid elution solution was diluted 3-fold with 50% acetonitrile prior to direct infusion. The capacity of the 0.6 μL bed $Ziptip_{C4}$ is approximately 3.3 μg, so that 180-230 pmol of protein was infused at a flow rate adjusted to insure accuracy in the time-to-digital conversion of the multi-channel plate detector, requiring 80-180 ion counts/scan base peak. Scans spanning the entire chromatogram were summed to improve the signal to noise, typically 60-150 scans depending on the flow rate.

2.2.4 Data analysis.

A 20-40 *m/z* spectrum window about the 15th charge state of β-lg and apo-CaM and 10th charge state of LysC was fit with a model FPOP product distribution (described below), for each protein replicate. The window range encompassed all detected product peaks and a 10 m/z region lower than the unmodified peak average m/z for baseline estimation.

2.3 Mathematical Modeling

The FPOP charge state spectrum model is the weighted sum of the set of N_{ox} non-zero oxygen-addition states $[M + O + z\cdot H]^{z+}$, $[M + 2\cdot O + z\cdot H]^{z+}$, …, $[M + N_{ox}\cdot O + z\cdot H]^{z+}$, together with the unmodified state $[M + z\cdot H]^{z+}$. The i^{th} state A_i is represented as an unresolved isotopic distribution centered on the $[M + i\cdot O + z\cdot H]^{z+}$ average m/z; its contribution is weighted by the coefficient a_i. The sum has the form:

$$Spectrum\ Model\left(m/z; a_0, a_1, \dots, a_{N_{ox}}\right) = \sum_{i=0}^{N_{ox}} a_i\, A_i(m/z) + E \qquad (1)$$

The baseline constant *E* is the average spectrum noise taken 5-7 *m/z* lower than the unmodified protein peak in the z^{th} charge state. There is no uncertainty in the form of the isotopic distribution as we know the elemental composition of each oxygen-addition product. A Mathcad 14 Minimize algorithm was used to fit the model to the spectrum to determine the coefficient values; these values convey the oxygen-addition state distribution and were tested for goodness-of-fit to a Poisson distribution. The solution convergence tolerance was 10^{-12}.

We further expand the spectrum model two ways. One motivation is to deal with the charge state spectrum that is complicated by low abundance starting material and electrospray adducts, and other FPOP oxidation products that do not correspond to +16, +32… We assume that these latter adducts are equally likely to be observed for each +16, +32… state, including the unmodified protein, with an important exception discussed below. ESI MS of control samples, wherein the protein is subjected to identical sample handling and peroxide exposure but not pulsed laser irradiation, provides spectra for determining the presence of adducts of the starting protein and other impurities, ESI-induced losses of ammonia and water, direct hydrogen peroxide oxidation, and salt complexation. A peak detection algorithm was employed to detect and pass the mass shifts and relative intensities of these peaks to the modeling algorithm.

The low abundance FPOP products that do not correspond to the substitution of H for OH or the simple addition of an oxygen atom (+16) fall into two categories: resolved and unresolved. Resolved peaks corresponding to losses of ammonia, water, and the -30 Da major product of acidic residue oxidation from the zero oxygen-addition state were

observable as they are shifted to lower m/z than the major oxygen-addition product series. Especially for apo-CaM (see Figure 2.4), these peaks were more conspicuous than in the control and must result from species produced in the FPOP treatment. Additional control experiments in which hydrogen peroxide was not added showed that the excimer laser did not contribute to these modifications (data not shown). Other FPOP products include but are not limited to +14 Da carbonyl incorporation at aliphatic residues, -23, -22, -10 and +5 Da shifted histidine oxidation products, and -43 Da deguanidination at arginine.[8] Their low abundance is obscured by the dominant 0, +16, +32… distribution and so are unresolved. The distribution of proteins undergoing such reactions and having *i*+16 Da additions, was modeled as a normal distribution, whose amplitude, variance, and centroid displacement from the i^{th} oxygen-addition state were set by the algorithm. All of the parameters that model the complexity of each population of proteins having 0, +16, +32… mass increments were determined by preliminary empirical modeling, in the case of resolved and control adducts, or for the unresolved adducts, by the same Minimize algorithm that determines the state coefficients. It is important to note that these parameters are state-invariant, unlike the state coefficients.

The second spectrum model expansion is crucial for determining the distribution of 0, +16, +32, . . . for its Poisson goodness-of-fit evaluation. Owing to the EVF, only a fraction of the full contribution of the 0^{th} state (i.e., the signal for the unoxidized protein) should be included in the FPOP product distribution analysis. This fraction represents the proteins in the irradiated volume that undergo no additions of 16, 32… Furthermore this

fraction contributes FPOP adducts other than those in the series corresponding to +16, +32…, whereas the EVF does not. The model is rewritten as:

$$Spectrum\ Model = (1-f)a_0A'_0 + fa_0A_0 + \sum_{i=1}^{N_{ox}} a_i\,A_i + E \qquad (2)$$

Here the 0^{th} state is split between the exclusion volume portion $(1-f)a_0A'_0$, which has the form of a simple isotopic distribution convolved with those adduct peaks seen in the control experiments, and the irradiated volume portion, fa_0A_0, which has a form identical to all other oxygen-addition states and so contains all complicating terms. The parameter *f* is not the irradiation fraction of the 0^{th} state; rather, the adjusted coefficient fa_0, is proportional to the 0^{th} state peak area attributed to this fraction by definition (eq 2). The other a_i coefficients are likewise proportional to their +16, +32… state peak areas. The parameter f is fixed in the modeling algorithm by its relation to the independently measured EVF:

$$f(EVF) = 1 - \frac{EVF\cdot\sum_{i=0}^{N_{ox}}\underline{A_i}}{\underline{A_0}'+EVF\cdot(\underline{A_0}-\underline{A_0}')} \qquad (3)$$

The underscored state variables denote integration over the entire m/z spectrum encompassing the charge-state product distribution.

A Mathcad 14 Minimize algorithm was also used to fit a Poisson distribution to the set of 0, +16, +32… state peak areas $\{f\underline{A}_0, \underline{A_i} \mid i = 1, \ldots, N_{ox}\}$. The Poisson characteristic parameter λ determined by this minimization gives the Poisson +16, +32… addition state expectation value. A second modeling approach was also examined, in which *f* was varied to optimize a Poisson fit, thereby determining the EVF. This tests the corollary of our hypothesis: that an FPOP protein-product distribution well modeled by a

Poisson should provide an EVF corroborating its independent measure—although a match doesn't prove the converse. The reader is referred to Supporting Information for a more detailed discussion of the modeling and Poisson-fitting algorithms.

2.4 Results and Discussion

2.4.2 Argument for Poisson.

Taking that a single conformation protein invariant to FPOP has a large number of independent sites of low modification probability, the distribution of species for which the molecular weight has increased by 0, +16, +32… should be well modeled by a Poisson distribution. The low specificity of hydroxyl radical footprinting means up to 85 residue sidechains in a 100-residue protein may be modified, depending on •OH exposure. The frequency of a residue's modification can be further split among the atomic sites of the residue (e.g., phenylalanine can be modified at *o*, *m*, *p* sites). It follows that there are more than 100 oxidative-modification sites, even for a small 100-residue protein. The probability of reaction is site-specific, and is determined by the site's inherent reactivity and solvent accessibility. Xu and Chance[6] showed in γ-ray radiolysis dose experiments that among 10 of the 12 most reactive amino acids, oxidation by hydroxyl radicals spans a 30-fold range of first-order product formation rates..

While the reactivity at any site is unique, it is well approximated as having an average modification probability p_{mod}. We designed the FPOP experiment so that the OH radicals have a short lifetime in a properly quenched experiment. Shortening the radical exposure time reduces the set of reactive sites, thereby improving the representation of each site as the average—though if too short the semi-residue resolution

of the footprint experiment is lost. Replacing 20 mM Gln with 20 mM Phe depletes [•OH] at a 10-fold faster rate[16]; we observed that >90% of oxidative-modification products for several proteins are abolished with this change (data not shown).

In the event that the protein partially contorts from its native conformation on the timescale of radical exposure, the distribution of products from oxygen addition will change if one or more oxidation targets has a substantially different solvent accessibility. In this case, the resultant distribution cannot be Poisson for two reasons. First, the site probabilities are no longer independent. Second, the native state p_{mod} cannot describe the average modification probability for newly exposed sites because their exposure time is shorter. For the simplest example, consider the oxidative modification of a mixture of two protein conformations, each insensitive to oxidation-induced perturbation and each with its own p_{mod}. The oxygen-addition state distribution for each population is ideally Poisson, but the overall protein population is not; that is, the distribution from the sum of two Poisson distributions having different means is not itself Poisson.

Although we have not tested that a protein with an invariant conformation exhibits a Poisson-like oxygen-addition distribution following FPOP, this is a reasonable assumption. Rather, if we find the distribution of products is Poisson or nearly so, we may conclude the conformation was unaffected during labeling. Thus, the test for induced FPOP-timescale conformation change requires (1) determining the distribution of products corresponding to substitution of H by OH or by addition of an oxygen atom, (2) determining its best-fitting Poisson distribution, and (3) evaluating the goodness-of-fit.

We also tested whether changes to the FPOP procedure and to post-labeling conditions and sample handling affect the product distribution. When the Gln radical scavenger normally constituent with the sample is removed, the radical lifetime is determined principally by its self-reaction rate and is 100-times longer.[16, 33] Consequently, we expect that oxidation-sensitive proteins will adopt significantly different product distributions from a best fitting Poisson because there will likely be a structural response on this timescale. Furthermore, given that covalent modification footprinting can involve days of sample handling, millimolar levels of hydrogen peroxide may slowly oxidize proteins especially at exposed Met and Cys.[35] Intentionally or otherwise, buried residues often experience solvent exposure with such handling, so that all peroxide-reactive residues are vulnerable. By omitting catalase and allowing hydrogen peroxide to persist following FPOP treatment, we can test the sensitivity of FPOP-treated protein to further peroxide oxidation and long-time (minute-hour) conformational change.

2.4.2 Data Acquisition and Analysis.

We chose not to model a deconvoluted or de-charged mass spectrum of each sample, owing to uncertainties in fitting to the output of the Waters MaxEnt1 maximum entropy algorithm supplied with the mass spectrometer data system. We selected single charge states instead: the 15^{th} charge state of β-lg and 10^{th} charge state of LysC. These choices are justified by their match to the charge state-invariant product distribution of the FPOP-treated protein, determined in an experiment wherein the protein was denatured by urea prior to ESI-MS (data not shown).

This integrity of a distribution determined for a charge state is of concern because ESI affords different responses (different charge-state distributions) to different conformers of a protein. A partially unfolded protein can accommodate more protons and will have a charge state distribution shifted to higher charge. In fact, two proteins (β-lg and LysC) exhibited product distributions that were charge-state dependent; that is, at higher charge states, the unmodified peak is significantly diminished, and the higher +16, +32… states are relatively more populated than at lower charge states. Denaturing and reducing (β-lg has 2 and LysC 4 disulfide linkages) a portion of each protein following FPOP treatment just prior to desalting and direct infusion, we could minimize any dependence of the relative product distribution on charge state. This charge-state dependence indicates that the protein ultimately infused for ESI analysis existed as a mixture of conformers in the un-denatured treatment (an acidic 50% acetonitrile solution does not fully denature β-lg and LysC although this may be a function of their intact disulfide bonds). Venkatesh, Sharp and coworkers[21-22] showed that the proteins selected for this study are susceptible to partial unfolding upon oxidation. Our finding that proteins undergoing multiple +16, +32…additions dominate the higher charge states corroborates their finding. Although the 8 M urea denaturing solution was freshly prepared, significant carbamylation (+43 Da) of primary amines was observed in the unoxidized control sample for both proteins. On this basis, we chose to analyze single charge states to obtain the distribution of 0, +16, +32… states and eschewed the analysis of post-FPOP urea-denatured samples.

On the other hand, apo-CaM, a 16.8 kDa dumbbell-shaped protein with no disulfide bonds, showed a relative distribution of FPOP products that were invariant of charge state. Its 15^{th} charge state was analyzed because its peaks were the most intense in the mass spectrum.

2.4.3 Agreement with a Poisson Distribution.

The optimum model fit to the 15th charge state of β-lg sample oxidized under normal FPOP conditions (Figure 2.2) typifies the fit observed for all three proteins under the same conditions. The spectrum/model relative residuals (normalized to the spectrum intensity) at each data point are generally in good agreement. The model fit, however, is poorer at higher *m/z*: the average |relative residual| doubles from 0.042 at to 0.082 at *m/z* > 1235 (Figure 2.2a). The higher +16, +32… addition states are more resolved in the calculated (model) spectrum than in the experimental spectrum. This may be a consequence of an underestimation of the background contribution in this region. Given this uncertainty, the states analyzed for Poisson likeness were restricted to the first states, accounting for at least 95% of the signal.

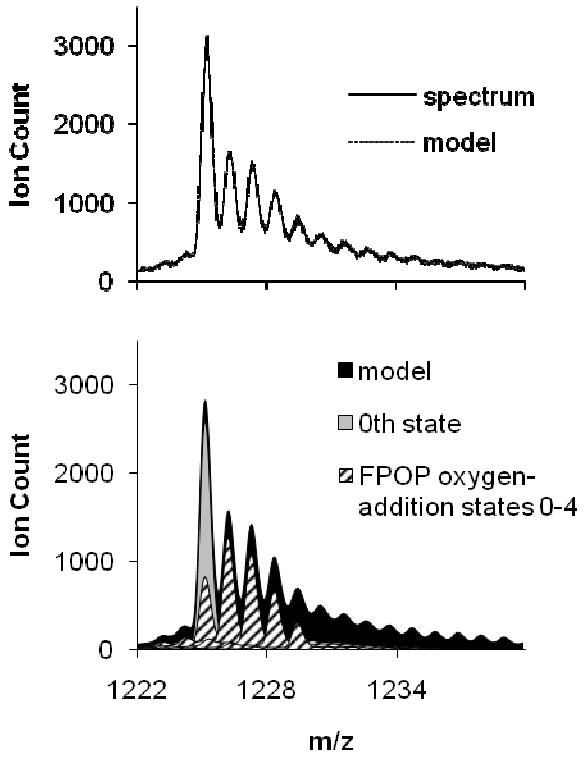

Figure 2.2: Mass spectrum and model of protein FPOP products. Graph (a) is of the ESI-QTOF mass spectrum of the 15th charge state of FPOP-treated β-lactoglobulin and its composite model. Graph (b) is of the background-subtracted model and its first five oxygen-addition state components (hashed fill). The 0^{th} state (gray) has a 53% contribution from the exclusion volume fraction (not shown) and a 47% contribution from the irradiated portion of the sample.

Each 0, +16, +32…state contribution in 2b has two dominant features: a major isotopic distribution peak with a centroid at $[M_r + O + 15H]^{15+}$, and a broad normal distribution with an intensity 1.0 ± 0.3% that of the major peak; this was seen for all proteins and FPOP treatments. The portion of the 0^{th} state owing to zero oxygen additions in the irradiated volume is fixed in the spectrum modeling by the measured EVF (eq 3).

The distribution is affected by changes in EVF, radical scavenger, and post-FPOP oxidation protection: Figure 2.3 shows spectra of β-lg treated with these variations and again typifies the CaM and LysC spectra (Figure 2.4). Intensity is plotted relative to each spectrum's maximum. Exposure for 5 min to 15 mM H_2O_2 does not oxidize the proteins (Figures 2.3a, 2.4a, 2.4d). In the "normal" FPOP treatment, radical exposure is controlled with constituent Gln scavenger. Post-FPOP oxidation is minimized by removing any left over H_2O_2 with catalase and adding millimolar levels of Met.[36] Methionine, a competitive oxidation reagent, was used because the samples were not analyzed immediately after their treatment. Tuning the EVF from 60 to 15% by increasing the laser frequency for samples submitted to a properly controlled FPOP procedure (Figure 2.3b-d) increases the levels of oxidation. Without radical control (no Gln scavenger) and/or removal of peroxide post-FPOP (Figure 2.3e-f), the product distributions skew significantly to higher oxidation levels. The S/N is also worse, as an equivalent amount of protein is spread over more states, relative to the other spectra.

The Poisson fitting to the modeled distribution of β-lg samples is shown in Figure 2.5. The state coefficients $\{fa_0, a_i | \, i = 1, \ldots, N_{ox}\}$ determined by the spectrum modeling are proportional to the ion counts comprising the peak area of each state; these values are normalized to give probability values in the figure. In all cases, the f factor was fixed by the measured EVF, except for the FPOP experiments without the glutamine scavenger. The standard error bars are in general small except for the 0^{th} state. This stems from the sensitivity of the 0^{th} state to the f factor calculation—small changes in the set of

coefficients can compensate a larger change in without unduly worsening the spectrum model fit.

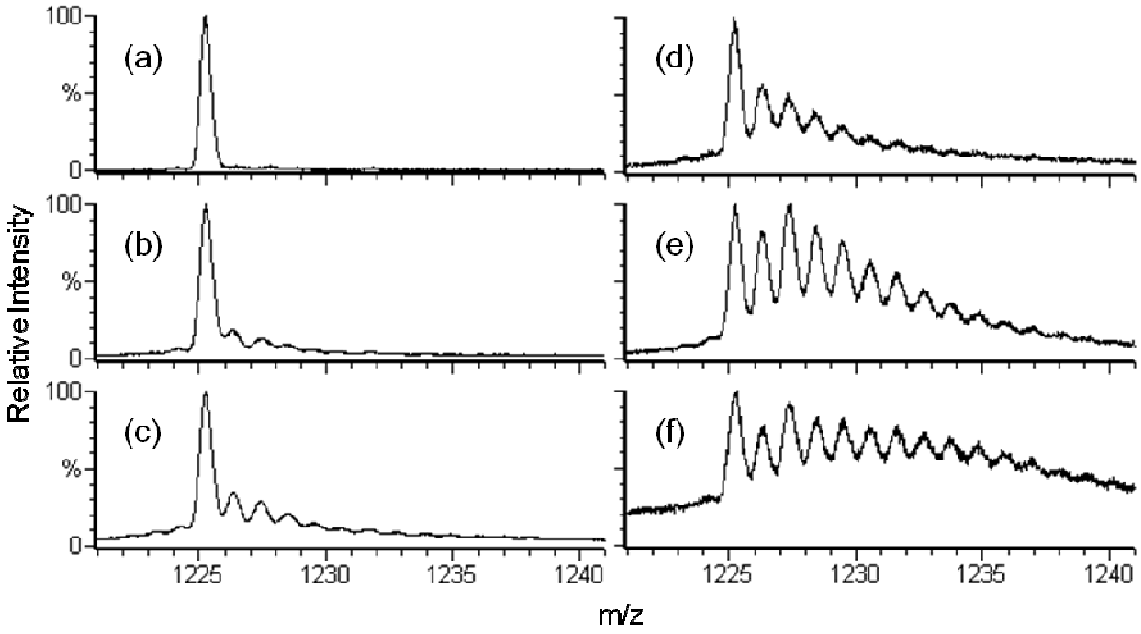

Figure 2.3: ESI-QTOF mass spectra of the 15th charge state of six *β*-lactoglobulin samples subjected to varying FPOP conditions. Spectrum (a) is of the control, absent only laser irradiation; (b) is of a normal FPOP treatment with an EVF 60%; (c) is of a normal treatment with an EVF 30%; (d-f) are of samples with an EVF of 15%; (d) is of a normal treatment (all controls); (e) is of a treatment absent 20 mM Gln; and (f) is of a treatment without use of scavenger (Gln), removal of peroxide (by catalase) and control of post FPOP oxidation (addition of Met).

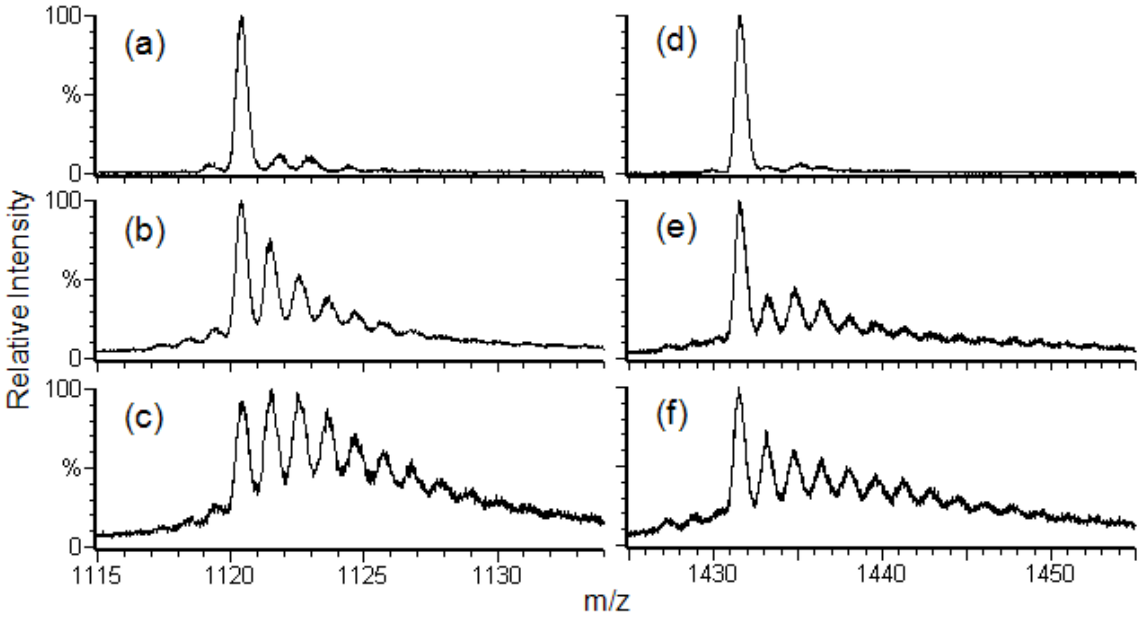

Figure 2.4: ESI-QTOF mass spectra (a-c) are of the 15th charge state apo-calmodulin; spectra (e-g) are of the 10th charge state of lysozyme. Spectra (a) and (d) are of the controls, absent only laser irradiation; (b) and (e) are of samples after normal FPOP treatment (i.e., with scavenger and removal of peroxide post FPOP); (c) and (f) are of samples after FPOP treatment absent the scavenger (20 mM Gln).

Qualitatively, the Poisson distribution fitting to the sample distributions obtained by appropriately controlled FPOP at all experimental EVF levels is much better than for samples submitted to FPOP but without scavenger (Gln) or post-FPOP removal of peroxide by catalase. This is also realized for the other two proteins, apo-CaM and LysC. Table 1 summarizes the Student's-t goodness-of-fit evaluation for each 0,+16, +32,…oxidation state. The chi-Squared goodness-of-fit test was not employed because of the modeling uncertainty in binning large ion counts among oxidation states, and it does not convey per state residual statistics.

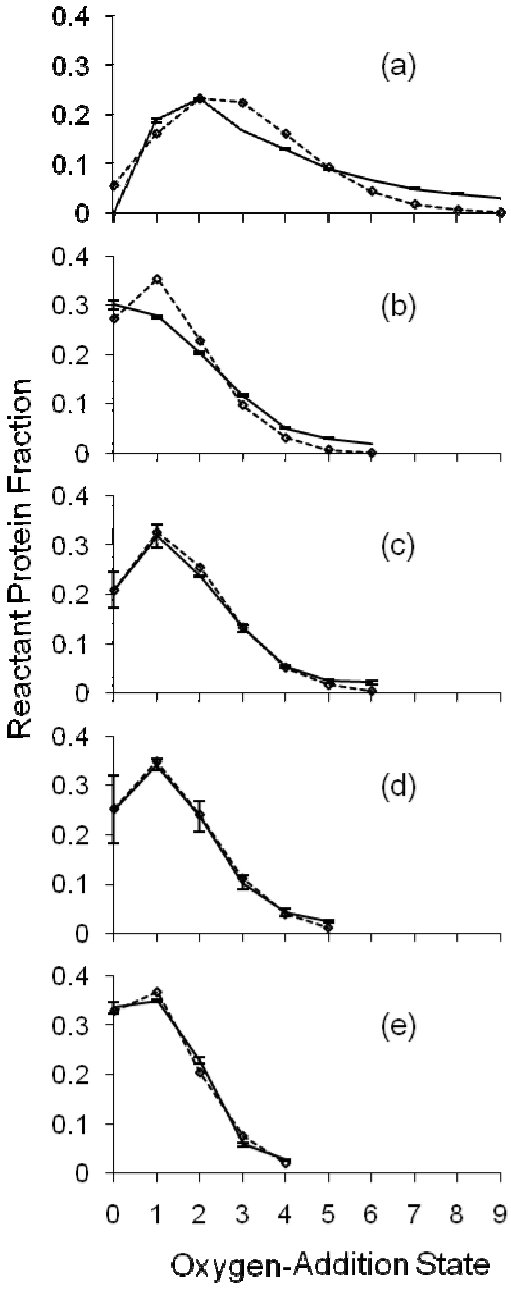

Figure 2.5: The irradiation volume oxygen-addition state ion counts are modeled for the spectrum of each bovine β-lactoglobulin sample. The modeling was constrained such that the calculated EVF matched the independently measured EVF. Per condition, shown with standard error bars along a solid line, are the averages of the normalized ion counts of 4 replicates (a-c) and 2 replicates (d-e). The diamonds along a dotted line show the non-linear regression best fit Poisson distribution to the average oxygen-addition state

distribution. The number of states per sample distribution fit to a Poisson was chosen to account for at least 95% of protein signal. Plot (a) is for sample submitted to FPOP but without the glutamine radical scavenger. When all zero oxygen-addition protein is assigned to the EVF, its value is 9%, short of the measured 15%. Plot (b) is for sample submitted to FPOP but without removal of peroxide post-FPOP, with a 15% EVF. Plot (c) is for sample FPOP-treated with a 15% EVF. Plot (d) is for sample FPOP-treated with a 30% EVF. Plot (e) is for sample FPOP-treated with a 60% EVF.

Table 2.1: Student's t Goodness-of-Fit Statistics of the Poisson Fit to the FPOP 16 Da-Increment State Distribution[a]

Protein	β-Lactoglobulin					Apo-Calmodulin		Lysozyme	
FPOP Condition	Normal	Absent Gln	Absent Catalase	Normal[d]	Normal[d]	Normal	Absent Gln	Normal[d]	Absent Gln[d]
EVF	15%	15%	15%	30%	60%	15%	15%	15%	15%
Poisson Mean	1.6	2.9	1.3	1.4	1.1	1.6	2.7	2.5	3
No. of States Fit[b]	7	10	7	6	5	6	10	7	10
No. of States, p-value > 0.05[c]	6	2	2	6	5	5	0	5	4
Student's t p(state)-values									
p(0)	0.9	[e]	0.1	0.9	1.0	0.04	[e]	0.7	[e]
p(1)	0.6	0.007	0.00001	0.2	0.3	1.0	0.01	0.02	0.3
p(2)	0.003	0.1	0.001	0.8	0.5	0.01	0.006	0.5	0.01
p(3)	0.9	0.0001	0.1	0.4	0.2	0.8	0.0002	0.5	0.01
p(4)	0.1	0.002	0.001	0.6	0.4	0.03	0.003	0.5	0.1
p(5)	0.9	0.4	0.0004	0.2		0.2	0.03	0.2	0.1
p(6)	0.3	0.00005	0.0001			0.3	0.002	0.005	0.0009
p(7)		0.00002				0.2	0.001		0.0003
p(8)		0.0002					0.002		0.1
p(9)		0.0004					0.004		0.01

[a] Each Poisson distribution was fit to the exclusion volume fraction constrained model of a single charge state Q-TOF spectrum of the FPOP-treated sample spectrum.

[b] The number of states is inclusive of ≥ 95% of protein signal

[c] The null hypothesis for each state is that its observed normalized frequency = Poisson distribution probability for that outcome.

[d] These treatments were analyzed in duplicate; all others in quadruplicate.

For the FPOP experiment in which the EVF was 15% and no scavenger (Gln) was present, the EVF could not be correctly calculated (Figure 2.5a). Setting the f factor to zero (i.e., the protein in the exclusion volume accounts for all of the zero-addition state) forces the model to give an EVF of 9%. The fraction of unoxidized protein is significantly less than the measured EVF. A reasonable interpretation of the result in Figure 2.3e is that there is some zero oxygen-addition state contribution from the irradiated volume; this further depresses the calculated EVF from the expected value. In fact, uncoupling the calculated EVF from its measured value by using the Poisson-dependent modeling approach shows that for the FPOP-treated sample without scavenger, the EVF is less than half 15% (Table 2). This is illustrated for β-lg in Figure 2.6. Each normalized distribution is for sample submitted to FPOP with a 15% EVF; plots a and b clearly show poorer fitting than the plot obtained when the sample is submitted to FPOP with the correct controls in place (plot c).

Table 2.2: Exclusion Volume Fraction (EVF) Determination From the Poisson-Parameterized Modeling of Spectra

Protein	β-Lactoglobulin						Apo-Calmodulin			Lysozyme	
FPOP Condition	Normal	Absent Gln	Absent Cat	Absent All	Normal	Normal	Normal	Absent Gln	Absent Cat	Normal	Absent Gln
EVF	15%	15%	15%	15%	30%	60%	15%	15%	15%	15%	15%
Modeled EVF	0.17 ±0.02	0.070 ±0.004	0.211 ±0.003	0.066	0.30 ±0.03	0.54 ±0.01	0.11 ±0.01	0.060 ±0.005	0.031 ±0.006	0.11 ±0.01	0.048 ±0.001

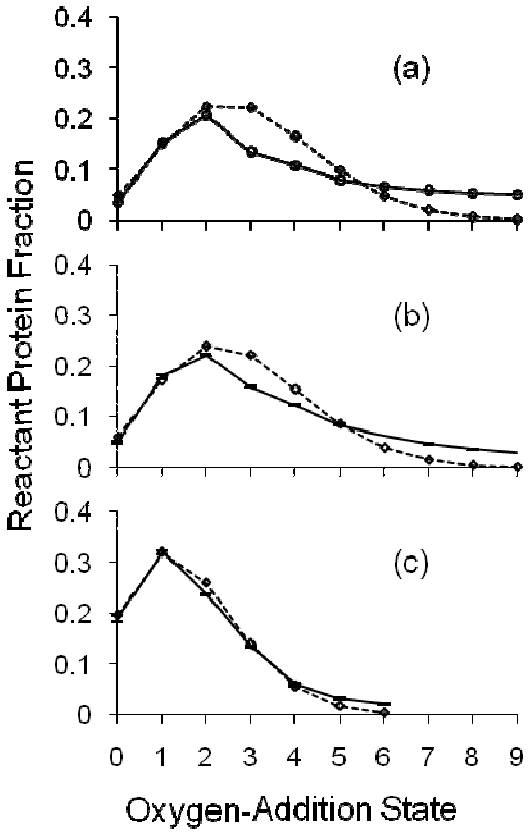

Figure 2.6: The irradiation volume oxygen-addition state ion counts are modeled for the spectrum of each β-lactoglobulin sample. A non-linear regression best fit Poisson distribution was simultaneously determined; the EVF was varied to optimize the fit. Per condition, shown with standard error bars along a solid line, are the averages of the normalized ion counts of 4 replicates (b and c); case (a) is singlicate. The number of states per sample distribution plotted account for at least 95% of protein signal. The diamonds along a dotted line show the Poisson distribution. Plot (a) is for sample FPOP-treated without glutamine radical scavenger, post-FPOP catalase, or post-FPOP methionine. The best fit exclusion volume was calculated at 6.6%. Plot (b) is for sample FPOP-treated without glutamine, with a calculated EVF of 7.0 ± 0.4%. Plot (c) is for sample FPOP-treated with a calculated EVF of 17 ± 2%. In all cases the measured EVF was 15%.

Thus, contrary to the controlled FPOP treatment, some of the protein in the EVF is oxidized when the radical scavenger is absent. This may occur for three reasons: (1) the radical and protein diffuse from the irradiated volume, (2) oxidation is initiated by

diffuse 248 nm light outside the considered reaction volume, and/or (3) one protein is oxidized by another following laser irradiation. The first mechanism is unlikely. Even without considering the hydroxyl radical recombination rate of $5.5x10^{-9}$ $M^{-1}s^{-1}$, the concentration of hydroxyl radical 5 microns into the exclusion volume after 100 μsec is only 0.15% the 1 mM theoretical maximum instantaneous [•OH] in the irradiated volume[16, 33] The •OH diffusion coefficient was estimated by molecular dynamics simulation to be $7.1x10^{-9}$ m^2 s^{-1}.[37-38] Without any scavenger, protein oxidation in the excluded volume may be due to lingering radicals created at low levels from H_2O_2 photolysis. Although highly collimated, the incident laser beam edges may extend >10 microns beyond the observed irradiation width. Finally, the oxidation by hydroxyl radicals is not a one-step process. In some protein-hydroxyl radical reactions, superoxide is created. Superoxide has a longer half-life than hydroxyl radical; sulfur-containing residues are sensitive to this ROS, although their reaction with O_2^-• is much slower than with •OH.[7, 36] Additionally, some protein-hydroperoxide intermediates may react intermolecularly instead of following the usual pathways to modification.[39] These peroxides are formed predominantly at aliphatic residues where a carbon-centered radical from hydrogen abstraction by an hydroxyl radical is stabilized by aqueous molecular oxygen.[34]

The last mechanism of intermolecular oxidation is potentially a problem for all oxidative-modification footprinting strategies. Yet evidence thus far from proteolysis and MS/MS analysis of constituent peptides shows that the sites of oxidation are consistent with the residue sidechain solvent accessibilities calculated from x-ray

crystallography and NMR structures of several proteins.[13, 15-16, 22] States higher than +8 oxygens are of very low abundance when FPOP is correctly controlled, but they are significantly more populated when a radical scavenger is not included. Latent protein-peroxide oxidation of newly accessible residues may be a millisecond-minute pathway capable of enriching these higher states without the presence of large excesses of Gln.

2.5 Conclusion

FPOP conducted properly by including control on radical lifetime and minimizing exposure to peroxide post FPOP provides a means of footprinting proteins without perturbing unduly their conformation during labeling. Although some proteins undergoing several oxidations do unfold at longer times (by the time of ESI-MS), this unfolding occurs post-FPOP, as established by finding a good fit of the +0, +16, +32… state product distribution to a Poisson distribution under proper conditions. The underlying assumption is that the Poisson model is applicable to footprinting a protein population sharing an invariant conformation and having many non-cooperative oxidation sites. In cases where radical and peroxide controls are not sufficient, the product distribution is shifted to higher states of modification, as expected, and is not well described by a Poisson distribution. The implication that partial unfolding occurs during the timescale of modification is consistent with the Poisson model. This test is not ad-hoc as it holds for three proteins. Moreover, we suggest that the approach is an appropriate validation of any oxidative-modification footprinting. The global modification distribution of •OH-treated proteins larger than 20 kDa can also be examined for concordance with a Poisson distribution—in fact the Poisson approximation

of the binomial distribution is improved with more labeling sites. Accurate modeling requires approximately half-height resolution of distinct +16 Da states; FTMS resolution is needed for proteins as large as BSA (66 kDa). The modification distribution should be only a function of the native conformation state of a protein. If the native state is an equilibrium mixture of conformations, the distribution will not necessarily be Poisson. If this non-Poisson distribution is the product of properly controlled FPOP, then it serves as the model distribution for testing conformation change with additional perturbations (such as denaturant) to the native equilibrium.

2.6 Supplemental Section: Mathematical Modeling

A model of the control spectrum was first determined, providing a set of model peaks which were overlaid with each 0, +16, +32… peak of the oxidized protein sample spectrum. This reasonably assumes that the adduct peaks owing to inherent protein modification, ESI losses of ammonia and water, hydrogen peroxide oxidation, and salt complexation were equally likely for any major 0, +16, +32… protein state. These peaks never comprised more than 5% of the unmodified protein signal in the control spectrum (see Figures 3a, 4a). Peak detection made use of a filter matched to the natural isotopic profile component orthogonal to the class of linear functions, first, to identify the spectrum points that had a filter response that was a fraction of the difference between the local maximum and minimum as noise, second, to mark the peaks at the local maxima of the filter response that were above the filter response to the noise points, and third, to provide the basis for finding the peak edges via mass shifted versions of the filter followed by peak centroid and area calculation. The parameters passed for subsequent

modeling are a set of mass shifts $\left\{\Delta x_{control_j} | \, j = 1 \ldots N_{control}\right\}$, each with an according fraction b_j, relative to $b_l = 1$ for the base l^{th} peak at $\Delta x_{control_l} = 0$.

The FPOP charge state spectrum model is the weighted sum of the set of N_{ox} 0, +16, +32… states $\left\{A_0^{total}(x), A_1(x), \ldots \, A_{N_{ox}}(x)\right\}$; the set of a_i contribution coefficients are determined by a non-linear regression fitting to the spectrum (eq 3).

$$S(x; f) = a_0 A_0^{total}(x; f) + \sum_{i=1}^{N_{ox}} a_i \, A_i(x) + E \tag{3}$$

The independent variable x is the spectrum m/z; the model is parameterized by $0 \leq f \leq 1$. The baseline constant E is the average noise 5-7 m/z lower than the unmodified protein peak of the spectrum about the charge state cs. The contribution of proteins suffering zero +16 Da additions to the spectrum can be split between the fraction excluded from the reaction volume and the fraction in the irradiated volume escaping +16 Da chemistry (eq 4).

$$A_0^{total}(x; f) = (1 - f) A_0^{excl}(x) + f A_0(x) \tag{4}$$

The exclusion volume component absent the factor $(1 - f)$ is the sum over control spectrum peaks, of which the base peak at M_r/cs is dominant.

$$A_0^{excl}(x) = \sum_{j=1}^{N_{control}} b_j \, I\left(cs \cdot x \, ; \, \hat{x}_{0j}\right) \tag{5}$$

$I(y; \hat{y})$ is the isotopic distribution interpolation function with its centroid at $\hat{y}$ Da; the argument y is supplied as a de-charged mass in Da. The isotopic distribution for a

protein of known composition is approximated by binning in one Da increments its isotopes, considering the natural isotope abundances of carbon, hydrogen, nitrogen, oxygen, and sulfur. The mass difference $y - \hat{y}$ determines the interpolation from M_r; the normalized values of the closest bin nearer M_r and closest bin further M_r define a straight line whose intersection with $y - \hat{y}$ provides the function value. The centroid (eq 6) is a de-charged mass centered about the i^{th} +16 Da state, shifted by the j^{th} control mass shift.

$$\hat{x}_{ij} = M_r + cs \cdot \Delta x_{control_j} + i \cdot 16 \tag{6}$$

The i^{th} +16 Da state (eq 7) has an additional compound component $D_{ij}(x)$ (eq 8) which accounts for low abundance resolved and unresolved FPOP products.

$$A_i(x) = \sum_{j=1}^{N_{control}} b_j \left[I\left(cs \cdot x\,;\, \hat{x}_{ij}\right) + D_{ij}(x) \right] \tag{7}$$

$$\begin{aligned} D_{ij}(x) = \alpha \exp\left\{ \frac{\left[x - \left(\hat{x}_{ij} + \beta\right)\right]^2}{2\gamma^2} \right\} \\ + \sum_{k=1}^{N_{aux}} c_k \left(I\left(cs \cdot x\,;\, \hat{x}_{ij} + cs \cdot \Delta x_{aux_k}\right) \right. \\ \left. + \alpha \exp\left\{ \frac{\left[x - \left(\hat{x}_{ij} + \beta + cs \cdot \Delta x_{aux_k}\right)\right]^2}{2\gamma^2} \right\} \right) \end{aligned} \tag{8}$$

Losses of ammonia, water, and the -30 Da acidic residue FPOP product from the 0 state are resolved from the major 0, +16, +32… states by virtue of a negative m/z shift. A preliminary peak detection algorithm is employed to detect and pass the mass shifts Δx_{aux_k} and relative intensities c_k of $N_{aux} \leq 2$ "auxiliary" resolved peaks to the iterative modeling algorithm. We model proteins suffering unresolved non +16 Da chemistry and having i +16 Da additions as a normal distribution with an amplitude α, standard deviation γ, and with a centroid shifted from the i^{th} +16 Da state by β.

As there are many atomics sites for dominant 0, +16, +32… chemistry, so there are many for the low yield pathways. We presume the likelihood of dominant chemistry at any site is independent of the fates at other sites, as long as the protein conformation is in stasis; it follows that the low abundance non +16 Da chemistry is also independent of additional FPOP modification. Consequently the distribution of proteins suffering any such resolved or unresolved non +16 Da pathway and having i +16 Da additions, but for the centroid shift $\hat{x}_{ij}$ and amplitude a_i of the state, is otherwise the same. We further suppose that any resolved modification has its own set of additional unresolved "daughter" products with the same normal distribution (we do not imply a lineage of products).

Substituting equations 5 and 7 into 4 gives equation 9.

$$A_0^{total}(x; f) = \sum_{j=1}^{N_{control}} b_j \, I\left(cs \cdot x \, ; \, \hat{x}_{0j}\right) + f \cdot \sum_{j=1}^{N_{control}} b_j \, D_{0j}(x) \qquad (9)$$

The parameter f isn't determined at *a priori* but rather is constrained by the independent measure of the EVF (eq 10).

$$EVF(f) = \frac{(1-f)\underline{A}_0^{excl}}{(1-f)\underline{A}_0^{excl} + f\underline{A}_0 + \sum_{i=1}^{N_{ox}} \underline{A}_i} \tag{10}$$

The integrated 0, +16, +32… spectrum contributions absent f coefficients are given equations 11 and 12. The numerical integration range $m/z_1 - m/z_0$ spans the entire charge state and its return to baseline noise.

$$\underline{A}_i = \int_{m/z_0}^{m/z_1} a_i A_i(x)dx \tag{11}$$

$$\underline{A}_0^{excl} = \int_{m/z_0}^{m/z_1} a_0 A_0^{excl}(x)dx \tag{12}$$

The EVF is independently determined from the ID of the fused silica tubing and the measured flow rate of the infusion, pulse frequency of the excimer laser, and irradiation cross-section width of the beam (see Figure 1). Equation 10 can be rearranged to give the explicit constraint on f (eq 13).

$$f(EVF) = 1 - \frac{EVF \cdot \sum_{i=0}^{N_{ox}} \underline{A}_i}{\underline{A}_0^{excl} + EVF \cdot \left(\underline{A}_0 - \underline{A}_0^{excl}\right)} \tag{13}$$

The model is fit to the real spectrum in Mathcad 14 by the "Minimize" algorithm, which uses a quasi-Newton nonlinear regression process to determine the set AA of parameters $\{\alpha, \beta, \gamma, a_i \mid i = 0,1, \dots, N_{ox}\}$ minimizing the RMSD function (eq 14).

$$RMSD(AA) = \sqrt{\frac{\sum_x [S(x;f) - R(x)]^2}{N_x}} \tag{14}$$

The sum is over all N_x data/model pairs; tolerance for RMSD convergence was 10^{-12} in all cases. The minimization algorithm is invoked iteratively; each iteration is parameterized by f, determined in the previous step by eq 13 or by an estimate at the outset. The modeling is completed when f converges to within ± 0.0005 of the previous value.

The same Mathcad 14 Minimize algorithm can be used to fit a Poisson distribution to the set of 0, +16, +32… state abundances $\{f\underline{A}_0, \underline{A}_i | \ i = 1, \ldots, N_{ox}\}$. The Poisson characteristic parameter λ can be determined by this minimization of the root squared deviation function (eq 15).

$$RSD(\lambda) = \sqrt{\left[f\underline{A}_0 - \left(f\underline{A}_0 + \sum_{m=1}^{N_{ox}} \underline{A}_m\right)e^{-\lambda}\right]^2 + \sum_{i=1}^{N_{ox}} \left[\underline{A}_i - \left(f\underline{A}_0 + \sum_{m=1}^{N_{ox}} \underline{A}_m\right)\frac{e^{-\lambda}\lambda^i}{i!}\right]^2} \tag{15}$$

As long as the centroid for each peak in each +16 Da state is well within the domain of integration, the integrated states absent their contribution coefficients is constant (eq 16). This simplifies the RSD to the form used for our fitting (eq 17).

$$\int_{m/z_0}^{m/z_1} A_i(x)dx = G, \qquad i = 0, \ldots, N_{ox}; \quad m/z_0 \ll \hat{x}_{ij} \ll m/z_1 \tag{16}$$

$$RSD = G \cdot \sqrt{\left[fa_0 - \left(fa_0 + \sum_{m=1}^{N_{ox}} a_m\right)e^{-\lambda}\right]^2 + \sum_{i=1}^{N_{ox}} \left[a_i - \left(fa_0 + \sum_{m=1}^{N_{ox}} a_m\right)\frac{e^{-\lambda}\lambda^i}{i!}\right]^2} \tag{17}$$

Thus the Poisson fitting determines the set of state coefficients $\{fa_0, a_i | \, i = 1, \ldots, N_{ox}\}$; it is useful to consider the value each takes on as a scaled ion count. The fit is to the first N_{ox} states which comprise ≥ 95% of protein signal.

In the second modeling approach $S(x; f)$ is constructed as described above. At each iteration, the model is fit to the spectrum, parameterized by the preceding step f value. The next f is determined by the Minimize algorithm on the Poisson fitting function $RSD(\lambda, f)$ (eq 15). Unlike the first modeling procedure, here a Poisson fitting is accomplished in tandem with each model fitting until convergence in f is met, as defined above.

2.7 References

1. Hirs, C. H. W.; Di Sabato, G.; Ottesen, M.; Gold, A. M.; Gurd, F. R. N.; Horton, H. R.; Koshland, D. E.; Kimmel, J. R.; Klotz, I. M.; Ludwig, M. L.; Hunter, M. J.; Neumann, N. P.; Ray, W. J.; Riordan, J. F.; Vallee, B. L.; Sela, M.; Arnon, R.; Spande, T. F.; Witkop, B.; Stark, G. R.; Wilcox, P. E.; Wold, F., In *Methods in Enzymology*, Academic Press: 1967; Vol. 11, pp 485-748.
2. Fenn, J. B.; Mann, M.; Meng, C. K.; Wong, S. F.; Whitehouse, C. M., Electrospray ionization for mass spectrometry of large biomolecules. *Science* **1989,** *246* (4926), 64-71.
3. Karas, M.; Bachmann, D.; Hillenkamp, F., Influence of the wavelength in high-irradiance ultraviolet laser desorption mass spectrometry of organic molecules. *Anal. Chem.* **1985,** *57* (14), 2935-2939.
4. Konermann, L.; Tong, X.; Pan, Y., Protein structure and dynamics studied by mass spectrometry: H/D exchange, hydroxyl radical labeling, and related approaches. *J. Mass Spectrom.* **2008,** *43* (8), 1021-1036.
5. Xu, G.; Chance, M. R., Radiolytic Modification of Acidic Amino Acid Residues in Peptides: Probes for Examining Protein-Protein Interactions. *Anal. Chem.* **2004,** *76* (5), 1213-1221.
6. Xu, G.; Chance, M. R., Radiolytic Modification and Reactivity of Amino Acid Residues Serving as Structural Probes for Protein Footprinting. *Anal. Chem.* **2005,** *77* (14), 4549-4555.
7. Xu, G.; Chance, M. R., Radiolytic Modification of Sulfur-Containing Amino Acid Residues in Model Peptides: Fundamental Studies for Protein Footprinting. *Anal. Chem.* **2005,** *77* (8), 2437-2449.
8. Xu, G.; Chance, M. R., Hydroxyl Radical-Mediated Modification of Proteins as Probes for Structural Proteomics. *Chem. Rev.* **2007,** *107* (8), 3514-3543.

9. Fenton, H. J. H., The oxidation of tartaric acid in presence of iron. *J. Chem. Soc. Proc.* **1894,** *10*, 157-158.
10. Tullius, T. D.; Dombroski, B. A., Hydroxyl radical "footprinting": high-resolution information about DNA-protein contacts and application to lambda repressor and Cro protein. *Proc. Natl. Acad. Sci. U.S.A.* **1986,** *83* (15), 5469-5473.
11. Shanblatt, S. H.; Revzin, A., Interactions of the catabolite activator protein (CAP) at the galactose and lactose promoters of Escherichia coli probed by hydroxyl radical footprinting. The second CAP molecule which binds at gal and the one CAP at lac may act to stimulate transcription in the same way. *J. Biol. Chem.* **1987,** *262* (24), 11422-11427.
12. Maleknia, S. D.; Ralston, C. Y.; Brenowitz, M. D.; Downard, K. M.; Chance, M. R., Determination of Macromolecular Folding and Structure by Synchrotron X-Ray Radiolysis Techniques. *Anal. Biochem.* **2001,** *289* (2), 103-115.
13. Kiselar, J. G.; Maleknia, S. D.; Sullivan, M.; Downard, K. M.; Chance, M. R., Hydroxyl radical probe of protein surfaces using synchrotron X-ray radiolysis and mass spectrometry. *Int. J. Radiat. Biol.* **2002,** *78* (2), 101 - 114.
14. Guan, J. Q.; Takamoto, K.; Almo, S. C.; Reisler, E.; Chance, M. R., Structure and Dynamics of the Actin Filament. *Biochemistry* **2005,** *44* (9), 3166-3175.
15. Hambly, D.; Gross, M., Laser flash photochemical oxidation to locate heme binding and conformational changes in myoglobin. *Int. J. Mass Spectrom.* **2007,** *259* (1-3), 124-129.
16. Hambly, D. M.; Gross, M. L., Laser Flash Photolysis of Hydrogen Peroxide to Oxidize Protein Solvent-Accessible Residues on the Microsecond Timescale. *J. Am. Soc. Mass Spectrom.* **2005,** *16* (12), 2057-2063.
17. Aye, T. T.; Low, T. Y.; Sze, S. K., Nanosecond Laser-Induced Photochemical Oxidation Method for Protein Surface Mapping with Mass Spectrometry. *Anal. Chem.* **2005,** *77* (18), 5814-5822.
18. Dill, K. A.; Ozkan, S. B.; Shell, M. S.; Weikl, T. R., The Protein Folding Problem. *Annu. Rev. Biophys.* **2008,** *37* (1), 289-316.
19. Chung, H. S.; Ganim, Z.; Jones, K. C.; Tokmakoff, A., Transient 2D IR spectroscopy of ubiquitin unfolding dynamics. *Proc. Natl. Acad. Sci. U.S.A.* **2007,** *104* (36), 14237-14242.
20. Chung, H. S.; Khalil, M.; Smith, A. W.; Ganim, Z.; Tokmakoff, A., Conformational changes during the nanosecond-to-millisecond unfolding of ubiquitin. *Proc. Natl. Acad. Sci. U.S.A.* **2005,** *102* (3), 612-617.
21. Venkatesh, S.; Tomer, K. B.; Sharp, J. S., Rapid identification of oxidation-induced conformational changes by kinetic analysis. *Rapid Commun. Mass Spectrom.* **2007,** *21* (23), 3927-3936.
22. Sharp, J. S.; Tomer, K. B., Analysis of the Oxidative Damage-Induced Conformational Changes of Apo- and Holocalmodulin by Dose-Dependent Protein Oxidative Surface Mapping. *Biophys. J.* **2007,** *92* (5), 1682-1692.
23. Sclavi, B.; Woodson, S.; Sullivan, M.; Chance, M.; Brenowitz, M.; Gary, K. A.; Michael, L. J., [19] Following the folding of RNA with time-resolved synchrotron X-ray footprinting. In *Methods in Enzymology*, Academic Press: 1998; Vol. Volume 295, pp 379-402.
24. Meng, C. K.; Mann, M.; Fenn, J. B., Of protons or proteins. *Z. Phys. D: At., Mol. Clusters* **1988,** *10* (2), 361-368.
25. Chowdhury, S. K.; Katta, V.; Chait, B. T., Probing conformational changes in proteins by mass spectrometry. *J. Am. Chem. Soc.* **1990,** *112* (24), 9012-9013.

26. Mirza, U. A.; Cohen, S. L.; Chait, B. T., Heat-induced conformational changes in proteins studied by electrospray ionization mass spectrometry. *Anal. Chem.* **1993,** *65* (1), 1-6.
27. Robinson, C. V.; Radford, S. E., Weighing the evidence for structure: electrospray ionization mass spectrometry of proteins. *Structure* **1995,** *3* (9), 861-865.
28. Kaltashov, I. A.; Abzalimov, R. R., Do Ionic Charges in ESI MS Provide Useful Information on Macromolecular Structure? *J. Am. Soc. Mass Spectrom.* **2008,** *19* (9), 1239-1246.
29. Liu, J.; Konermann, L., Irreversible Thermal Denaturation of Cytochrome c Studied by Electrospray Mass Spectrometry. *J. Am. Soc. Mass Spectrom.* **2009,** *20* (5), 819-828.
30. Simin D. Maleknia, M. R. C. K. M. D., Electrospray-assisted modification of proteins: a radical probe of protein structure. *Rapid Commun. Mass Spectrom.* **1999,** *13* (23), 2352-2358.
31. Wong, J. W. H.; Maleknia, S. D.; Downard, K. M., Study of the Ribonuclease-S-Protein-Peptide Complex Using a Radical Probe and Electrospray Ionization Mass Spectrometry. *Anal. Chem.* **2003,** *75* (7), 1557-1563.
32. Maleknia, S. D.; Wong, J. W. H.; Downard, K. M., Photochemical and electrophysical production of radicals on millisecond timescales to probe the structure, dynamics and interactions of proteins. *Photochem. & Photobiol. Sci.* **2004,** *3*, 741-748.
33. Buxton, G. V.; Greenstock, C. L.; Helman, W. P.; Ross, A. B.; Tsang, W., Critical Review of rate constants for reactions of hydrated electronsChemical Kinetic Data Base for Combustion Chemistry. Part 3: Propane. *J. Phys. Chem. Ref. Data* **1988,** *17* (2), 513-886.
34. Garrison, W. M., Reaction mechanisms in the radiolysis of peptides, polypeptides, and proteins. *Chem. Rev.* **1987,** *87* (2), 381-398.
35. Shechter, Y.; Burstein, Y.; Patchornik, A., Selective oxidation of methionine residues in proteins. *Biochemistry* **1975,** *14* (20), 4497-4503.
36. Xu, G.; Kiselar, J.; He, Q.; Chance, M. R., Secondary Reactions and Strategies To Improve Quantitative Protein Footprinting. *Anal. Chem.* **2005,** *77* (10), 3029-3037.
37. Van Holde, K. E.; Johnson, C.; Ho, P. S., *Principles of Physical Biochemistry*. 2 ed.; Prentice Hall: Upper Saddle River, NJ, 2005.
38. Campo, M. G.; Grigera, J. R., Classical molecular-dynamics simulation of the hydroxyl radical in water. *The Journal of Chemical Physics* **2005,** *123* (8), 084507-6.
39. Saladino, J.; Liu, M.; Live, D.; Sharp, J. S., Aliphatic Peptidyl Hydroperoxides as a Source of Secondary Oxidation in Hydroxyl Radical Protein Footprinting. *J. Am. Soc. Mass Spectrom.* **2009,** *20* (6), 1123-1126.

3 Characterization of the Mass Spectrometry-Observed Hydroxyl Radical Footprint of Barstar in its Native and Cold-Denatured States, Using a Novel Excel-based Data Analysis Platform, Commercial LC-MS Peak Detection Software, and Error-Tolerant Database Search.

3.1 Introduction

The promise of mass spectrometry-based (MS-based) protein footprinting is that residue-resolved structural information may be realized for proteins in states inaccessible to study by NMR spectroscopy and X-ray crystallography[1-2]. Hydroxyl radical-mediated footprinting[3] is one such method that has come to prominence in the last decade for several reasons. First, all residue sidechains except glycine are reactive with •OH[4], though at differing rates[5]. Secondly, most of the •OH-mediated products are stable modifications detectable by MS[6-8]. Finally, the size of •OH is comparable to water. Thus with proper radical control, the extent of labeling of protein sidechains by •OH is a function of their solvent accessibilities. The protein footprinting goal is usually to determine which sites exhibit changes in their solvent accessible surface areas (SASAs) upon the protein's interaction with a ligand, another protein, or folding induction. Where there is direct interaction, so must the labeling be attenuated[9]. Thus, the accurate determination of the labeling yield at each residue is the central analytic challenge of •OH-mediated protein footprinting.

The MS-based detection of footprinting modifications is often done in a "bottom-up" approach, where the protein(s) of interest are isolated and proteolyzed prior to

chromatographic (LC) separation and MS detection. This methodology is also employed in proteomics[10]. Owing to its non-specificity and reactivity, •OH-mediated footprinting in particular complicates the LC-MS pattern of a single proteolyzed protein, so as to resemble the information content from a more complex biological sample in a proteomics study (Figure 3.1). In such studies, the inference of proteins in the sample is based on the detection of their proteolytic peptides. One means of detecting these peptides is to couple the LC to a hybrid mass spectrometer, capable of determining with ppm resolution peptide "precursor" masses eluting in time, while in tandem performing fragmentation, or MS^2, experiments on a subset of these peptides to generate their characteristic fragmentation spectra. These MS^2 spectra, together with their precise precursor masses, can be identified with a high degree of confidence using such algorithms such as Mascot[11] and the appropriate protein database. Automated matching can also determine the location of modifications, if the appropriate variable modifications are considered in the search algorithm.

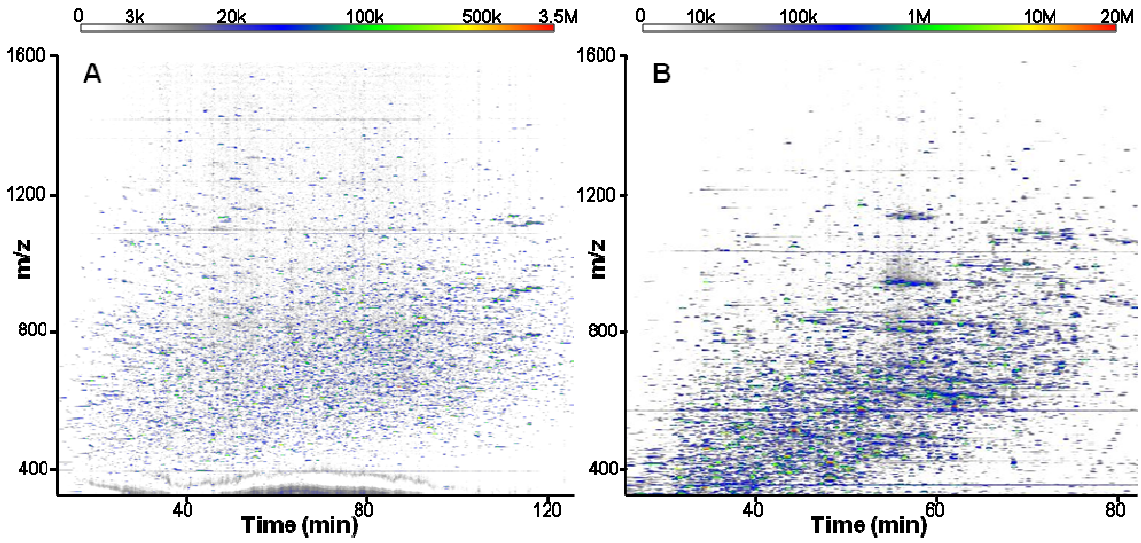

Figure 3.1: The LC vs. high resolution MS plots for the LC-MS/MS acquisitions of two complex samples. Plot A shows a 130 min acquisition for a proteomics sample from a biological source (unpublished data)[12]. Plot B shows an 85 min acquisition for a protein-footprinting sample, of FPOP-treated purified human apolipoprotein E3.

The quantitative analyses of LC-MS data from proteomics and footprinting studies are similar. In either case the intensities of the same or related precursor ions shared by the samples are used in the fold change metric, unless an MS^2 spectral counting method is employed. This usually requires high resolution LC-MS monitoring, so that two or more species with the same nominal mass and charge state can be distinguished in their elution. Typically the peak area from an extracted ion chromatogram (EIC) with a stated m/z +/-5 ppm can be attributed to a single ion, though MS^2 experimentation is needed for its confirmation or identification. In quantitative proteomics, a comparison is made between two or more samples, either by a method of stable-isotope labeling or by side-by-side label-free quantitation with normalization[13]. If the stable-isotope-labeled

sample is labeled perfectly—that is, at a precisely known frequency—and if the labeled sample is mixed with the basis sample perfectly, then the only bias remaining between samples is biological. The peptides that exhibit a significant difference in abundance between samples are attributed to the up or down regulation of their associated protein. More care must be taken in the normalization of label-free proteomics samples, to correct for biases in overall protein expression, loss, and column loading. One large potential source of bias is chromatographic variation—EIC peak alignment is crucial to ensure that the same peptide abundances are compared between samples.

While mass spectrometry-based protein footprinting uses the same analytical tools and protocols as proteome studies, there are several important distinctions that ultimately have motivated the work presented in this study. The first is that the analyte protein(s) is known, is often highly purified, and often is not in a biologically complex milieu. In our footprinting studies, the quantities needed for LC-MS/MS analysis has not exceeded a picomole[9, 14-16], allowing study of protein at sub-micromolar levels if an absence of interaction is required. This is still very much more than some proteins detected in complex biological mixtures. The second distinction is that, whereas the detection of only two unique peptides belonging to a protein are required to declare its presence in a typical proteomics experiment[10], the goal of footprinting analysis is to detect all proteolytic peptides of the analyte protein at levels that enable the detection of their footprinting-modified sibling peptides.

The final distinction between proteomics and footprinting LC-MS/MS: the comparison is not of the abundances of a single peptide shared by two samples. Rather

the comparison is inherently normalized, in that per-residue labeling yields are compared. Biases in proteolysis and column loading are unimportant because these should not affect yield—what happens to the unmodified peptide happens equally to modified peptide. Biases in ionization efficiency may not be shared equally between modified and unmodified peptides, but they should be shared equally among different samples, as long as the same column and MS source conditions are used within a contiguous time frame. Biases in labeling are obviated by doing same-day labeling.

These distinctions have several consequences. Full "analytic" coverage is a more stringent criterion than full sequence coverage, because regions of the protein that have too few or many intervening sites of proteolysis may give rise to peptides that are detected only at low abundance. Detecting the modified sibling of such peptides can be problematic. Compensating this drawback is the *a priori* knowledge of protein sequence and possible modification fates. This can be used to program the spectrometer on which peptides to perform MS^2 experiments. Low abundant eluting peaks having the right precursor mass may thus be selected when they would have otherwise been ignored by the normal decision algorithm. More importantly, knowing all probable outcomes of a labeling experiment should empower the data analysis to greatly enhance analytic coverage.

The software packages now available to analyze quantitative proteomic data is extensive[13]. These software are tasked, as a first step, with identifying and measuring peptide levels in a biological samples from the LC-MS/MS raw data. Such programs could be used to analyze the same kind of data from a protein-footprinting study.

Generating a concise and single-protein-centric output, amenable to addressing the questions of structural change, is not easily accomplished by these large packages yet. The goal of analytic coverage, and the providence of *a priori* knowledge of sample composition, demands that the highest level of scrutiny be used in indentifying modified and unmodified peptides. Ultimately this requires the scientist's inspection of spectra. This also falls out of the normal purview of proteomics studies. We have written Excel-based protein-footprinting software with these considerations in mind. Automated LC-MS peak detection and alignment must still be performed by external software, and MS^2 database searching also done by Mascot (forthcoming versions will allow for Sequest[17] and OMSSA[18] searching). Our software accomplishes four things. (1) All LC-MS species within a certain mass tolerance of putative modified or unmodified peptides of the analyte protein or proteins are found, and when possible, annotated with their associated MS^2 Mascot call, in a protein-centric output. (2) Chromatographically unresolved peptide isomers and discrepant calls are identified and ranked for validation decisions. (3) Validation can be done systematically and efficiently with the MS^2 testing tools, and by virtue of the organized protein-centric output. (4) The final per-residue output necessary for hypothesis testing is generated.

As a demonstration of the software and the value of •OH-mediated protein footprinting, we present the footprinting results of barstar in its folded and unfolded states. Barstar is a 10.2 kDa protein, whose function is to inhibit the ribonuclease activity of barnase in *Bacillus amyloliquefaciens*[19-20]. We have chosen this protein due to its peculiar thermal stability: it adopts its native structure at room temperature but is

unfolded at 0 °C [21-22]. The footprinting method we employed is fast photochemical oxidation of proteins (FPOP) [16, 23], which creates •OH at sub mM levels with the homolytic cleavage of H_2O_2 by a 17 ns pulse of 248 nm from a KrF excimer laser source. The protein exposure to •OH is kinetically limited to a microsecond by the inclusion of a radical scavenger, such that only the equilibrium state of the protein is sampled[24].

3.2 Experimental Procedures

3.2.1 Reagents.

E. coli-expressed and purified barstar C82A variant was kindly provided by Drs. C. Frieden and G. DeKoster. HPLC-grade water, 30% H_2O_2, *L*-glutamine, *L*-methionine, catalase, guanidinium chloride (GdnCl), and phosphate buffered saline (PBS) were purchased from the Sigma Aldrich Chemical Company (St. Louis, MO).

3.2.2 Equilibration and FPOP labeling.

Each sample was composed of 10 μM barstar, 1.5 M GdnCl, and 15 mM glutamine in PBS buffer. The "cold" equilibration solution was incubated at 0 °C and the "warm" solution at 22 °C room temperature two hours prior to labeling. Cold and warm sample replicates were drawn from these solutions; to each replicate H_2O_2 was added by 10-fold dilution to a 20 mM final concentration, two min prior to its infusion through the FPOP apparatus. The FPOP apparatus was used as previously described [16] but with 150 μm i.d. fused silica (Polymicro Technologies, Phoenix, AZ). In addition, for cold samples, a thermally insulated box with two chambers abutted the FPOP apparatus. The 1st chamber contained an ice batch and copper tubing connected to a compressed air supply. The 2nd adjacent chamber, into which the copper tubing emptied, was

constructed to enclose the syringe pump, optics stand, and intervening fused silica, with a 2 cm^2 window for laser transmission. The 2nd chamber temperature was kept to less than 3°C by adjusting the compressed air flow through the ice bath.

The KrF excimer laser power (GAM Laser Inc., Orlando, FL) was adjusted to 45 mJ/pulse, and its pulse frequency was set to 5 Hz. The flow rate was adjusted to ensure a 25% exclusion volume to avoid repeat •OH exposure[24]. Excess H_2O_2 was removed immediately following FPOP labeling by collecting samples in microcentrifuge tubes containing 10 μL of 200 fM catalase. This catalase solution also contained methionine to give a final concentration of 20 mM following collection. $O_2(g)$ was removed from the samples by centrifugation, and samples were subsequently frozen in $N_2(l)$ and stored at -80°C prior to proteolysis. A control sample was drawn from the same equilibration solutions and handled identically except that the laser was not used.

3.2.3 Proteolysis.

All samples were proteolyzed with 10:1 protein:trypsin (by weight) at 37 °C for 3 h, then de-salted by $Ziptip_{C18}$ (Millipore, Billerica, MA) with elution into 10 uL of 50% acetonitrile 1% formic acid solution. A portion of this was diluted 25-fold with water and 0.1% formic acid for autosampler loading.

3.2.3 LC-MS/MS acquisition.

Five microliters of each replicate was loaded by autosampler onto a 20 cm column with a PicoFrit tip (New Objective, Inc, Woburn, MA), bomb-packed with C18 reverse phase material (Magic, 0.075 mm × 200 mm, 5 μm, 300 Å, Michrom, Auburn, CA). Peptides were eluted by a 70 min, 260 nL/min gradient coupled to the nanospray

source of an LTQ-Orbitrap mass spectrometer (Thermo Fisher, Waltham, MA). Mass spectra were obtained at high mass resolving power (100,000 for ions of *m*/*z* 400) on the Orbitrap component, and the six most abundant ions eluting per scan were each subjected to CID MS^2 experiment in the LTQ component, using a collision energy 35% of the maximum, a 2 Da isolation width, and wideband activation. Precursor ions were added to a dynamic exclusion list for 8 s to ensure good sampling of the apex of their elution peaks. Blanks were run between every sample acquisition.

3.3 Data Analysis

3.3.1 Overview.

The general approach for data analysis is diagramed in Figure 3.2. Sample replicates are drawn from a stock solution of the equilibrium conditions. Analytic replicates can also created at the time of LC-MS/MS acquisition as typically more than five-fold of material is present in the de-salted peptide eluent than is needed. We note that creating analytic replicates may treble again the instrument time, already long because of the replicate no-laser controls needed for FPOP. The inclusion of replicates serves more than the purpose of providing statistics. Just as replicate LC-MS/MS analyses expands the number of identified proteins in a proteomics experiment[25-26], so with replicates does the probability of selection for MS^2 and subsequent identification improve for low-abundance modified peptides.

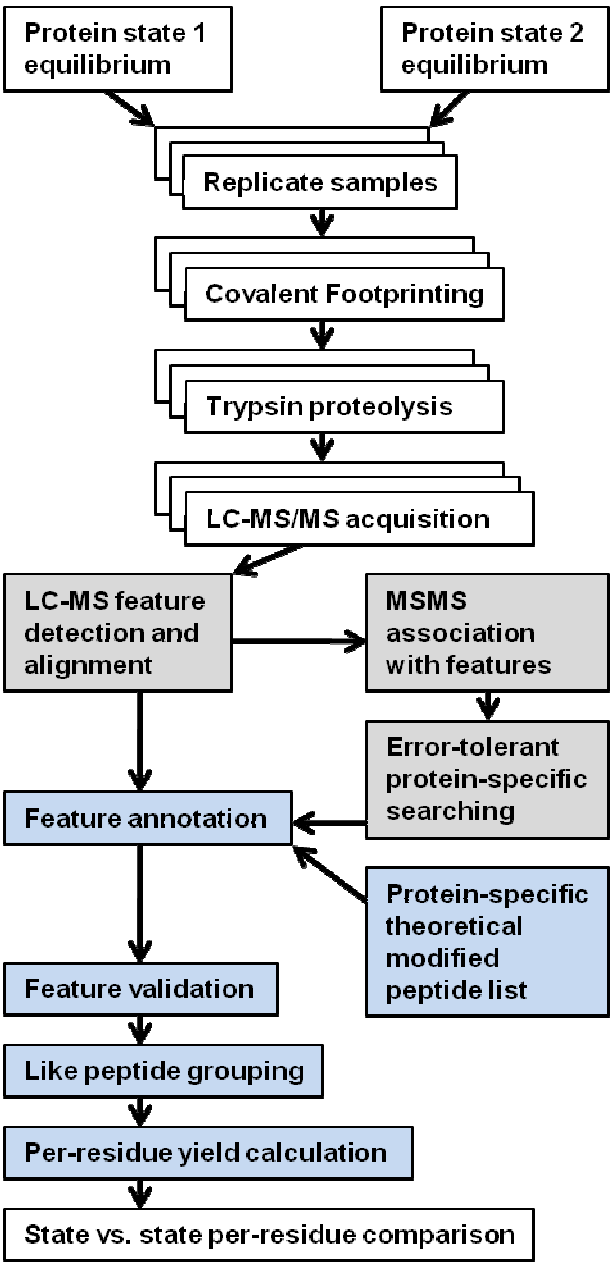

Figure 3.2: The workflow for protein footprinting, LC-MS/MS acquisition, and analysis. Gray boxes signify external software used in this study; blue boxes signify software developed for protein footprinting.

Good peak sampling is important in both the MS and MS^2 domains. The abundance of an ion is determined from its integrated EIC peak area in the high resolution MS domain (Figure 3.3). Automatic gain control, maximum trap fill times, lock-mass selection, m/z resolution, and number of MS^2 experiments are all parameters that affect the frequency of the Orbitrap scans; we have striven for a 0.3 Hz frequency to well represent 10-20 sec peak widths. For data-dependent MS^2 selection, precursor ions were added to a dynamic exclusion list on their first occurrence for 8 s to ensure good MS^2 sampling of the apex of their elution peaks.

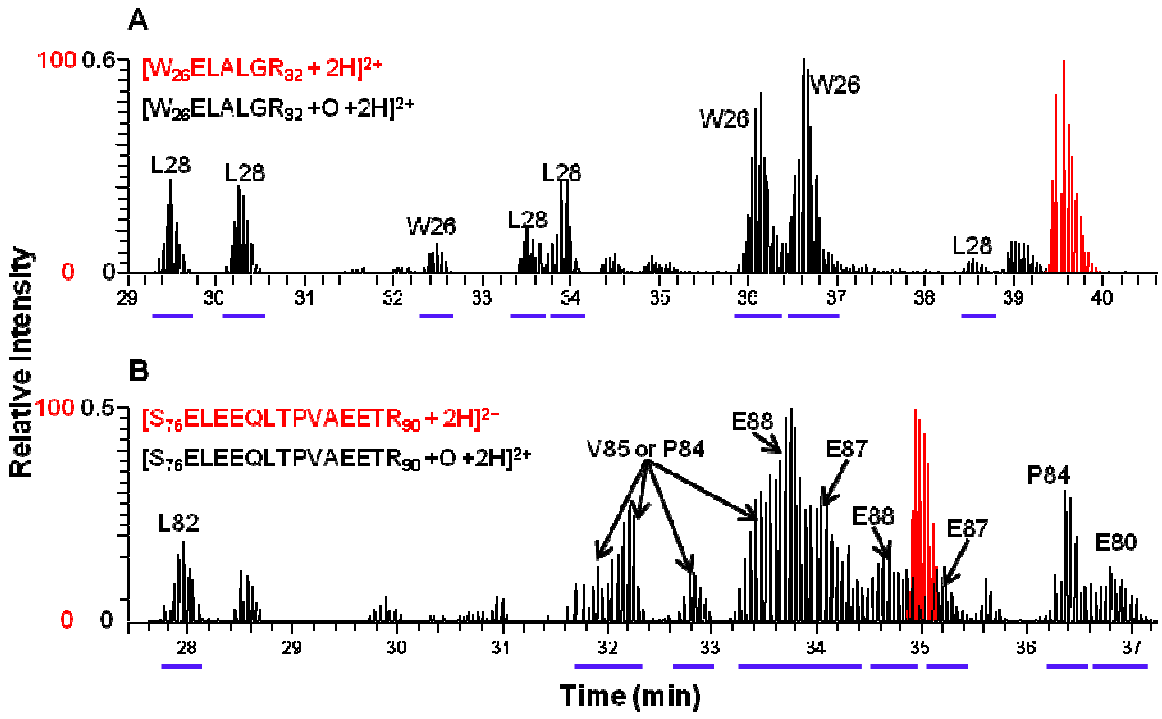

Figure 3.3: Four high MS resolution extraction ion chromatograms of FPOP-modified and unmodified tryptic peptides of Apolipoprotein E3 (unpublished data). Plot A shows in red the EIC at 422.7374 +/- 0.0021 m/z, and in black 430.7349 +/- 0.0021 m/z. These correspond respectively to the unmodified and oxygen-modified doubly-protonated WELALGR peptide. Plot B shows in red the EIC at 865.9258 +/- 0.0043 m/z, and in black 873.9232 +/- 0.0043 m/z. These correspond respectively to the unmodified and oxygen-modified doubly-protonated SELEEQLTPVAEETR peptide. In both plots the relative intensity is determined relative to the unmodified peptides' maximum intensities; the modified peptides are shown on a magnified scale. The LC-MS acquisition in the LTQ-Orbitrap cannot continuously monitor each m/z; rather are shown the discrete scans' intensities at each m/z. The MS2 spectra associated with each peak have been matched by Mascot database searching and been validated by manual inspection; the residue-resolved +15.9949 Da modifications are indicated for each black EIC where possible. The blue underlines convey the LC-MS peaks tabulated by the Rosetta Elucidator feature detection and alignment system.

3.3.2 Feature detection and alignment.

Accurate LC-MS peak software must be used to automate the accounting of 1000s of EIC peaks. A feature is tabulated as the sum of all EIC peaks of ions with the same elution time and same (+/- 5 ppm) de-charged monoisotopic mass. Abundant tryptic peptide features are often the sums of ten or more ion isotopomer intensities split among two or more charge states. The features must be listed with their de-charged monoisotopic mass centroids. The fidelity of peak alignment software is extremely important in footprinting analysis, as it is in label-free proteomics. If the chromatographic reproducibility is poor, we recommend individually processing each data set; this significantly increases the analysis time because the validation step must be repeated for each occurrence. We have used Rosetta Elucidator (Microsoft, Bellevue, WA) in our work, though several other free and commercial packages are available[13, 27].

Usually oxidative modifications make a peptide more hydrophobic than its unmodified root, such that it will elute earlier in reverse phase chromatography. A solvent-exposed region of a protein may undergo modifications at several neighboring sites in the protein population. Often the resulting set of peptide isomers perfectly resolve, as is seen in Figure 3.3A for a peptide of FPOP-treated apolipoprotein E3 (unpublished data). Modified residues that exhibit more than one EIC peak are the result of the non-specificity of •OH in hydrogen abstraction or direct addition[4]. Sometimes these modifications are not well chromatographically resolved (Figure 3.3B), and some peak detection programs such as Elucidator may tabulate these as a single broad peak.

The methodology and software presented here helps the user to make consistent, systematic decisions about such data.

3.3.3 Mascot database searching.

The searching must be done on the .dta files created by the feature detection and alignment software, which has been parameterized to associate one .dta file per MS^2 spectrum. The IDs assigned by the LC-MS peak software connect the MS^2 spectra to their parent MS features; each unique feature ID is linked to the exact .dta filenames created by the same LC-MS peak software for the feature's MS^2 spectra. Other programs which also extract MS^2 spectra from .raw files as .dta files, should not be used because they will not follow the precise naming convention of the LC-MS peak software alignment software.

Currently the software supports the comma separated values (.csv) output of Mascot[11]. For •OH-mediated footprinting, all commonly observed modifications for residues should be input into the Mascot variable modification database; redundant entries do not confuse the algorithm. A recent review lists these and their likely mechanisms of formation[3]. The set of .dtas created by the LC-MS peak software must be merged into a Mascot generic file (.mgf) prior to search submission. If .mgf file is smaller than 50 Mb, a single search against a restricted database and specifying the most likely •OH modifications, such as the single and double net oxygen additions to Met, Trp, Tyr, Phe, and His, and single net oxygen additions to Leu, Ile, Val, Gln, Glu, Lys, and Arg, may be attempted.

An approach less prone to crashing and more comprehensive in its output, is to do an "error-tolerant" search[28] of the analyte protein after a preliminary search is done without specifying variable modifications. In this approach the error-tolerant .csv output is used as it contains a large set of modified peptide identifications, many of which will indicate •OH-mediated product chemistry. The error-tolerant search will also contain incorrect assignments in part because the MS^2-matched putative peptide is no longer required to have a precursor mass within the specified instrument tolerance of the observed ion. We recommend also using the .csv output of the preliminary search in the feature-matching program, as some spectra erroneously matched by the error tolerant search will have their true match in the preliminary search. The benefit to doing error tolerant searching is that many more MS^2 spectra are discovered, which may be associated with modified and unmodified peptides of the analyte protein. Then more features of LC-MS low intensity may be considered. The tradeoff is that more manual validation is required to accept these calls in the quest for accurate and full analytic coverage. If two or more proteins are labeled in the experiment, error tolerant searching should be done for each independently. Any number of .csv reports can be used by our software.

3.3.4 Protein-specific theoretical modified peptide list.

To augment the MS^2-Mascot-matched list of LC-MS features associated the analyte protein, a list of proteolytic peptides of the protein together with any combination of anticipated residue modifications is needed for accurate LC-MS mass matching. The Excel spreadsheet tool "Unmodified and modified peptide masses from proteolysis of

protein" generates such a list. This tool uses the input sequence of the analyte protein, and may also use optional inputs: user-defined variable and fixed modifications per amino acid type or per specific residue, sites of known sequence breaks, and proteolytic sites masked from cleavage. Execution of the "Get_Peptides" macro will guide the user through choices in proteolytic enzyme, number of modifications to allow, and which •OH-mediated products to consider, if desired. The output provides the list of putative peptides for accurate mass matching and a list of protonated ion m/z values for manual EIC lookup or inclusion list building. For two or more proteins in a single study, specify an abbreviation to append to each peptide corresponding to its protein source.

3.3.5 Feature annotation.

The Excel spreadsheet "Match LCMS features with acc mass and Mascot calls" marries the MS^2-Mascot-matched calls with their LC-MS peak software-derived feature list, and augments these with accurate mass matches from the "Unmodified and modified peptide masses from proteolysis of protein"-generated theoretical modified peptide list. There are four input worksheets that must be completed before the "Match_peaks_to_peptides" macro can be run. The "input LCMS features" worksheet of the spreadsheet requires as input, a list of the feature IDs determined by the LC-MS peak software. Their mass and time centroids can also be included, as well as the feature intensities for each sample by column; this option allows for other kinds of LC-MS peak software outputs. In the "input dta list" worksheet the list of all .dta filenames and their associated feature IDs and .raw file sources should be provided. The LC-MS peak software should create .dta filenames for the MS^2 spectra by including in them the name

of the .raw file from which each MS^2 spectrum originated. The spreadsheet uses this information to group spectra with their original acquisition names, thereby allowing acquisition-specific spectral counting per feature. Into the "input exact mass list" worksheet the theoretical modified peptide list is put.

The "input proteins" worksheet, the fourth and final input worksheet of the spreadsheet, specifies the precedent order of proteins by the position of their sequence entry. These sequences are used as the organizing directory for outputting annotated features. They should be the same sequences used to generate the exact mass list, if a list is to be used, and they must be the same sequences used by Mascot to generate the .CSV report(s). The protein list is prioritized: a feature having a Mascot annotation exactly matching a sequence from the first protein will be described as a peptide originating from the first protein, even if a homologous protein lower on the list shares the same sequence. This is intended. Same sequence peptides from two protein sources share the same LC-MS properties, so their intensities should be compared in a single output line having one annotation. The output columns differentiate the peptides' sources by passing along their acquisition names.

Execution of the "Match_peaks_to_peptides" macro initiates the dialog for looking up aligned data files specific to each LC-MS acquisition, if this sample intensity information was not provided in the 1st worksheet. A second dialog will ask for the .csv report(s); these should be placed in the same folder. A threshold can optionally be employed to filter low intensity data, though this is not recommended for beginning experiments. We do recommend using a Mascot score threshold of 30 or better, as

validating matches deemed poor by Mascot is likely to be challenging or impossible. Finally, the macro will ask for an accurate mass match tolerance; for Fourier transform spectrometers we have used 8-10 ppm.

After execution the two outputs are provided. The “condensed Mascot output” worksheet is a report of the Mascot-matched spectra exceeding the threshold and matched to the proteins on the list. The first eight columns are the same fields found in the Mascot .csv report(s), where each row pertains to a unique Mascot call. Rather than repeat the same entry lower on the list for other matching MS^2 spectra, all spectra that match this entry are listed to the right of the annotation columns, and the best scoring peptide of these is listed in column 19. Instead of relying on Mascot for the proper protein annotation, the matched peptide sequence is tested against the protein list provided in the “input proteins” worksheet. In this way redundant entries in the search database do not confuse the output annotation. The protein-centric peptide annotation and associated LC-MS feature ID are provided in columns 9-18. These fields are shared in the second output described next.

The “annotate LCMS output” worksheet lists the LC-MS features matched by Mascot searching or accurate mass matching first by protein, then N-terminus to C-terminus peptide order, then by elution time. The first 15 columns in the output worksheet annotate the LC-MS feature; the subsequent columns provide the intensities, relative intensities, and spectral counts per feature for each sample acquisition. A feature's relative intensity per sample acquisition is its absolute intensity divided by the average of all absolute intensities, at least 0.1% as large as the acquisition’s maximum

intensity, in the subset of LC-MS peak software features putatively matched to the analyte protein(s) in the "input proteins" worksheet. Table 3.1 shows the annotation columns for one tryptic peptide of barstar. The theoretical mass is based on the Mascot-matched call or accurate mass match, and the ppm error is based on the observed mass difference with the putative theoretical peptide. The "net modified mass change" is determined as the difference between the observed mass centroid and the theoretical unmodified peptide. Features with the "# supporting MS2 spectra" field blank are present owing to an accurate mass match with the theoretical modified peptide list. The "potential modification(s)" field reflects one potential combination of modifications giving rise to the net-modified-mass change for these entries.

3.3.6 Ranked calls.

Sometimes when more than one spectra are associated with a single LC-MS feature, Mascot-matching will determine that some of the spectra are indicative of one peptide, while the other spectra are indicative something else. These discrepancies arise for two reasons. The first is the occasional nearly-coincident elution of modified peptide isomers. In Figure 3.3B, a single LC-MS feature between 33.3 and 34.3 min is clearly a mixture of three modified peptide isomers that are not resolved to half height. The second reason is mistakes are sometimes made by error-tolerant Mascot-matching, particularly when an MS^2 spectrum is sparse, the modification is in a peptide region insensitive to CID fragmentation, or multiple modifications are present on the peptide. It has been beyond our scope to construct an algorithm that could resolve these

discrepancies with high fidelity. Rather a ranking is made of all discrepant calls to allow for systematic decisions as to which calls deserve validation or correction, and which are

Table 3.1: Annotation output for barstar tryptic peptide 3-11, from the "Match LCMS features with acc mass and Mascot calls" spreadsheet.

peptide	sequence	theoretical mass	observed mass	error (ppm)	net modified mass change	potential modification(s)	MS2 ID'd modification	call rank	# calls per feature	# supporting MS2 spectra	call spectra/all spectra per feature	max score	peak centroid time (min)	unique ID
3-11_bs	AVINGEQIR	1014.54580	1014.5444	-1.4	15.994		I10	1	2	10	0.67	51.2	27.60	44682884_1
3-11_bs	AVINGEQIR	1014.54580	1014.5444	-1.4	15.994		I5	2	2	5	0.33	43.4	27.60	44682884_2
3-11_bs	AVINGEQIR	1012.53016	1012.5289	-1.2	13.979	_14		1	1				27.68	44682976_1
3-11_bs	AVINGEQIR	1014.54580	1014.5437	-2.1	15.993		I10	1	1	5	1.00	56.8	28.59	44682694_1
3-11_bs	AVINGEQIR	1028.56140	1028.5590	-2.3	30.008		N6	1	2	6	0.75	49.1	28.78	44682198_1
3-11_bs	AVINGEQIR	1028.56140	1028.5590	-2.3	30.008		G7	2	2	2	0.25	39.9	28.78	44682198_2
3-11_bs	AVINGEQIR	1012.53016	1012.5284	-1.7	13.979	_14		1	1				28.83	44683820_1
3-11_bs	AVINGEQIR	1014.54580	1014.5442	-1.6	15.993		I5	1	2	5	0.63	52.1	29.90	44683417_1
3-11_bs	AVINGEQIR	1014.54580	1014.5442	-1.6	15.993		V4	2	2	3	0.38	41.6	29.90	44683417_2
3-11_bs	AVINGEQIR	1012.53016	1012.5287	-1.4	13.979	_14		1	1				31.23	44684712_1
3-11_bs	AVINGEQIR	1028.56140	1028.5593	-2.0	30.008		G7	1	1	1	1.00	45.7	31.26	44683899_1
3-11_bs	AVINGEQIR	970.54470	970.5429	-1.9	-28.008		R11	1	1	14	1.00	65.6	31.44	44681013_1
3-11_bs	AVINGEQIR	998.55089	998.5508	-0.1	0.000			1	1				31.81	44682389_1
3-11_bs	AVINGEQIR	998.55090	998.5482	-2.7	-0.003			1	1	46	1.00	62.2	31.82	44681205_1
3-11_bs	AVINGEQIR	1001.56290	1002.5631	997	4.012		N6	1	1	10	1.00	44.2	31.83	44681370_1
3-11_bs	AVINGEQIR	998.58730	998.5865	-0.8	0.036		Q9	1	1	33	1.00	62.2	31.86	44681624_1
3-11_bs	AVINGEQIR	999.53490	999.5318	-3.1	0.981		N6	1	2	50	0.96	70.7	32.24	44681006_1
3-11_bs	AVINGEQIR	999.53490	999.5318	-3.1	0.981		Q9	2	2	2	0.04	37.4	32.24	44681006_2
3-11_bs	AVINGEQIR	999.53490	999.5319	-3.0	0.981		N6	1	2	50	0.88	70.7	33.18	44681251_1
3-11_bs	AVINGEQIR	999.53490	999.5319	-3.0	0.981		Q9	2	2	7	0.12	43.0	33.18	44681251_2
3-11_bs	AVINGEQIR	1012.56650	1012.5649	-1.6	14.014		V4	1	2	8	0.62	55.1	34.00	44681184_1
3-11_bs	AVINGEQIR	1012.56650	1012.5649	-1.6	14.014		A3	2	2	5	0.38	47.9	34.00	44681184_2

worth deleting. The ranking rule preferences first the number of MS^2 spectral counts among all samples that match a call above the specified threshold. Ties in spectral counts are rank-resolved by the maximum score. The feature entries possessing discrepant calls are listed contiguously in the "annotate LCMS output" worksheet with the best (lowest) rank listed first, and so on. At this stage the sample intensity information is preserved among each repeated entry. The "call spectra/all spectra per feature" field is also based

on the spectral counts associated with calls, and can be used for quick filtering, using the "Rank_Filter_Output" macro or Excel filtering capability.

3.3.7 Validation.

Depending on the protein system, footprinting chemistry, Mascot search parameters, and desired level of quantitative resolution, the validation step in data processing (Figure 3.2) can be nearly a "rubber stamp" step or can require a several-day endeavor. This is an intimate step: no computer algorithm is employed to make decisions. The first step is usually one of filtering. The features important to the footprinting experiment should be scrutinized while superfluous features can be ignored by deletion. The organization of the data in Excel allows the use of several Excel capabilities including filtering and formula entry to assist in this filtering.

For FPOP footprinting, where analytic coverage requires finding low abundant modifications, the filtering is often as follows. (1) Features with a maximum relative intensity, among all samples, of less than 2% are marked for exclusion. Very often these features did not trigger any MS^2 experiments in any of the acquisitions. (2) Features with |accurate mass errors| > 10 ppm and features with spurious modifications are corrected, where possible, using the "Unmodified peptide accurate mass comparison" Excel tool. This spreadsheet is not macro-enabled. Its function is to allow the user to hypothesize correct modification calls when Mascot has made a mistake, or fill in missing sequence when a non proteolytic peptide is suggested with a large N- or C-terminal modification. (3) Modification calls associated with deamidation, water loss, ammonia loss, and other chemistries that show as much abundance in control samples as FPOP samples are

marked for exclusion. (4) Non-tryptic peptides are marked for exclusion, though some of the time these are born from radical labeling chemistry. (5) The .dta filename/feature ID list prepared for the "Match LCMS features with acc mass and Mascot calls" spreadsheet is used to determine which accurate mass-matched features lack MS^2 spectra; these are marked for exclusion. The final inclusion list is ready for validation decisions.

Without automated software and in the interest of expeditious analysis, a further filtering step based on relative intensity may be necessary for validating and completing the modification annotation of accurate mass-matched features. We have used a custom Perl-based correlation program to facilitate this analysis[29], and are working to make this software available and easier to use. Manual accurate mass-matching validation and annotation completion requires using the .raw data browser and any tools for peptide hypothesis testing or de novo sequencing the user may already have.

The majority of features useful for footprinting should have a putatively assigned Mascot-derived identity. The final decision in the validation step rests with which features to accept as correct without further validation. This requires a familiarity with the expected sites and yields of modification. For FPOP, a good starting place is the excellent review of •OH-mediated footprinting by Xu and Chance[3] as well as the bottom-up FPOP-analyses published by the Gross lab[9, 14-16].

Features selected for validation can be processed in two ways. Clearly one way is by manual inspection. This may be necessary for LC-MS features with more than 5-10 associated spectra and having more than one probable call, as determined from each call's fraction of feature spectra—if such a feature provides information other

chromatographically resolved features do not (a new modified residue, perhaps). Alternatively, two Excel macro-enabled tools can expedite validation and correction before undertaking manual inspection. The "UniqueID MS2 spectra extractor" spreadsheet takes as input the first 15 annotation columns as shown in Table 3.1 for all selected features needing validation, and uses the "condensed Mascot output" worksheet of the "Match LCMS features with acc mass and Mascot calls" spreadsheet to determine the best Mascot-matched MS^2 spectra supporting each uncertain feature's annotation. These spectra are found either in the folder containing all .dta files from the experiment or from the merged .mgf file(s) submitted to Mascot. Keeping the latter on one's hard drive is preferable from a file management standpoint. The x-y data of each spectra is output to a worksheet together with the pertinent annotation hypothesis needing testing. The "MS2 call checker" spreadsheet is used to examine each of the spectra one-by-one by copying and pasting the desired spectrum and its hypothesis information into the first worksheet and executing the "compare_to_MS2_spectrum" macro. An overlay of the theoretical and observed spectrum can provide definitive validation (Figure 3.4) of the call, or the user may inspect the "matches" and "missed" worksheets for numerical checking. If the hypothesis is wrong, a new one can be made by altering the sequence, modification location(s), or modification mass in the first worksheet. With each change or confirmation, update the final footprinting annotations accordingly.

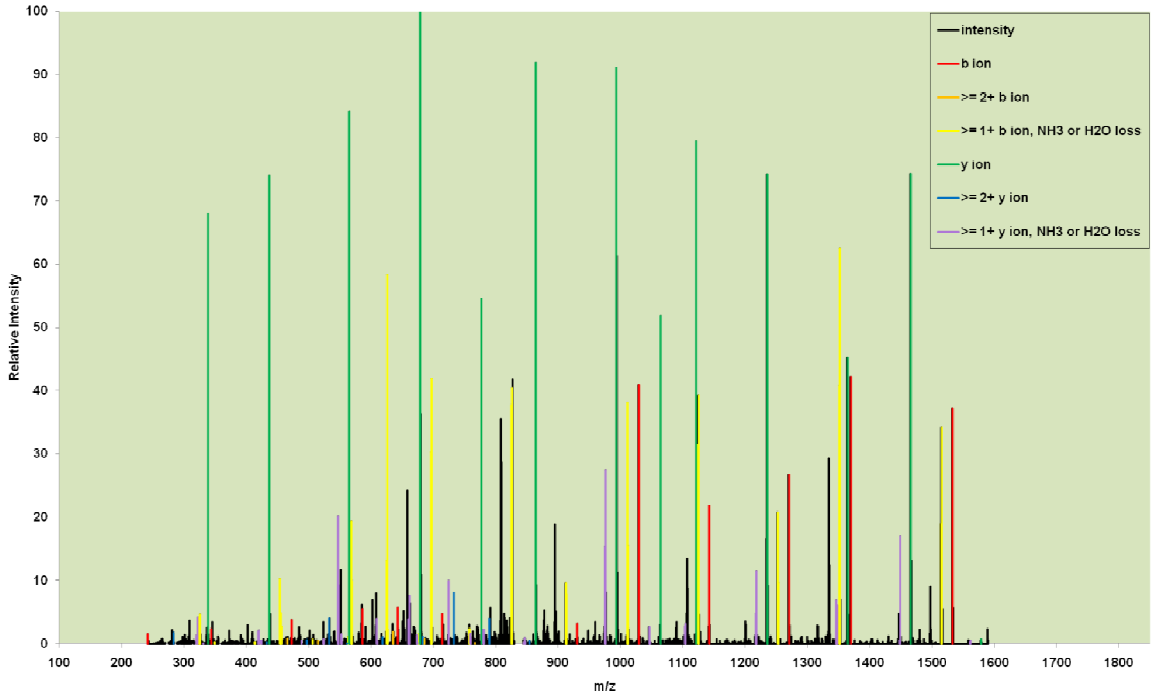

Figure 3.4: An output match spectrum of the "MS2 call checker" spreadsheet. The theoretical spectrum of barstar peptide Q_{61}LTENGAESVLQVFR$_{75}$, modified by 16 Da at F74, is mapped onto the best Mascot-scoring MS2 spectrum associated with this call. In this case manual validation clearly confirms the Mascot peptide call, as nearly all observed black peak ions are obscured by colored peaks signifying y- and b- and related ions. The modification location is also confirmed because the observed ion at 1369.4 m/z matches the expected unmodified b13 ion and the ion at 1532.4 matches the expected modified b14 ion.

3.3.8 Per-peptide data processing.

Once the heavy lifting of validation is complete, the next steps can be completed in minutes. The "Annotated Features Combiner" spreadsheet uses the final array of validated features and intensities; the format should be preserved from the longer output list from the "Match LCMS features with acc mass and Mascot calls" spreadsheet. Execution of the "Average_Like_Samples" macro initiates several dialogs. The user specifies which samples are replicates for each entered treatment (protein state, labeling

condition, etc.). For •OH-mediated footprinting samples, a time window can be set about the major unmodified elution time for each proteolytic peptide. Typically oxidative modifications make peptides more hydrophilic such that they elute up to 10-15 min earlier than their unmodified analog in an 80 min gradient (Figure 3.3). The fellow modified peptides eluting in this time window will be grouped with the unmodified to determine the "root" or total measured abundance (sum of intensities) of each proteolytic peptide. From these values the fractions of modified and unmodified peptides are determined. The last dialog asks the user to decide how to treat features still having more than call. The two most-used treatments are to either (1) ignore all such features, or (2) include them but multiply their intensities by the fraction of spectral counts indicative of each discrepant call. In this latter way important mixture peaks can be included without overestimating their contributions.

The Combiner spreadsheet's "output" worksheet conveys these per-peptide footprinting results for each replicate and reports their averages and standard errors, in addition to each feature's fractional contribution to its root. The second output worksheet of the Combiner spreadsheet, "per sample absolute data", carries through the list of all absolute intensities for each feature from the input, and reports each feature's associated peptide's total intensity. This output worksheet is needed for the final Excel data processing spreadsheet. The coloring of peptides by their root group in the output worksheets does not convey meaning but is meant to allow easier inspection.

3.3.9 Per-residue data processing.

Often for radical-based modification strategies, multiple features are observed that indicate modification at a single residue, due to five reasons. (1) Multiple atomic sites of a residue may be vulnerable to modification, such as the indole ring of tryptophan to •OH attack[3, 30], and these isomers separate in chromatography. (2) The product chemistry may be varied at a single site. For example, methionine is easily oxidized to a +16 Da sulfoxide, and will readily further oxidize to a +32 Da sulfone[3]. (3) More than one set of modified and unmodified proteolytic peptides spanning the residue are used in the analysis, due to a frequent missed cleavage. Sometimes missed cleavages are desirable as they expand the region of analytic coverage into sequence regions having proteolytic substrate sites every 3-6 residues. (4) The LC-MS peak software has split an LC-MS feature into two co-eluting features of the same mass centroid. Sometimes the peak software is conservative in its de-charging, such that it does not group these LC-MS isobaric and co-eluting component EIC peaks together as one feature. As long as these entries were not deleted in the validation step, their proper inclusion in the per-peptide and per-residue analysis is guaranteed. (5) Oxidations at the ESI source give rise to post-chromatography modifications of eluted unmodified species. These features can be filtered in the validation step by inspection of their elution times and control levels, unless one is employing the method of •OH footprinting that utilizes the oxidative electrochemistry possible at the ESI source[31-33].

The signals from all same-residue modifications should be incorporated in its modification yield calculation, according to equation 1.

$$residue_i\ yield = \frac{\sum peptide\ intensities\ modified\ at\ residue_i}{\sum peptide\ intensities\ with\ same\ 1^\circ\ sequence\ as\ numerator\ peptides} \quad (1)$$

Note that this equation will not sum missed cleavage peptides spanning *residue*$_i$ in the denominator if no modifications at *residue*$_i$ are detected for a peptide having the same missed cleavage sequence. The argument is as follows: The protein modification yield at a residue should be recapitulated at the peptide level. Unless there is a modification bias with proteolysis, the missed-cleavage peptide will also be modified at the residue in the same yield. The lack of detection of the modified missed-cleavage peptide does not mean the missed-cleavage peptide isn't modified; rather it is an analytic failure usually owing to a low frequency of missed cleavages. Therefore the unmodified missed-cleavage peptide should not be included in the yield denominator in this instance. With trypsin proteolysis and •OH footprinting, an exception to this rule should be made for features showing deguanidination (-43 Da) at arginine[34]. In this case the root total should be adjusted to include the root total of the shorter proteolytic peptide that shares the most number of residues with the deguanidination missed-cleavage peptide.

The "per-residue fraction modified analysis" spreadsheet performs the per-residue yield calculations on the "per sample absolute data" output from the Combiner spreadsheet with the execution of the "calculate_ratios" macro. If uncertain modifications annotations were altered to include "or", such as "M64 or M68" in the "MS2 ID'd modification" field, these uncertain calls should be resolved before final per-residue calculation by their omission. Alternatively the "read_in_modifications" macro will direct the user to fix these entries before the "calculate_ratios" macro is executed; the "calculate_ratios" cannot interpret any modification entries that do not follow the 1-letter amino acid residue number

format with comma separations for multiply modified features. The set of features used in the per-residue analysis may be smaller than used in the per-peptide analysis, because uncertain modification features still accurately convey labeling at the peptide level but should not be used at the residue level.

With the per-residue yields in hand, the analysis of SASA and structure(s) can begin. For footprinting strategies like FPOP, in which labeling yield depends on the inherent reactivity of a residue as well as its SASA, state vs. state comparisons at the per-residue level will be more discriminating than at the per-peptide level. At the per-peptide level, small changes in yield at some sites may be masked by invariant yields at neighboring residues that are more sensitive to •OH, like methionine.

3.4 Results and Discussion

3.4.1 LC-MS feature coverage.

Of the 19,280 LC-MS EIC ion peaks detected among the cold, warm and control samples, 1,116 are the isotope and charge state contributors to 367 features associated with barstar or catalase. The total peak area intensities of these 1,116 ion EICs is 69% of all EIC peaks. The remaining 18,164 ions are predominantly singly charged or do not have a discernable charge state, and are very low in abundance. Of the 367 features, 76 were used in the final per-residue analysis of cold and warm barstar states. Seventy-eight features were excluded because their relative intensities were less than 2% the average intensity for putative barstar features. Eighty-seven features were omitted because they were not tryptic peptides of barstar. Most of these features were also present in the control, indicating a chymotryptic or non-specific enzymatic origin, and 95% were less

than half the average intensity for each sample. This may be more than expected; shortening the trypsin proteolysis may diminish the occurrence of these cleavages. It is not clear how frequently non-specific cleavage products should be expected, as the discovery by error-tolerant searching of non-tryptic peptides is not typically disseminated in proteomics studies. The remaining exclusions were for features indicated as mixtures of modified peptide isomers that could not be accurately split, features whose MS^2 spectra cannot definitively locate the modification, peptide features bearing known sample handling and ESI modifications (e.g. water loss, ammonia loss, deamidation), peptide features bearing unexpected modifications shared by control and FPOP samples alike (and thus are not FPOP signal), and catalase peptide features.

3.4.2 Analytic sequence coverage.

The sequence coverage of barstar in this study was 100%. All 89 residues were spanned among the detected unmodified tryptic and non-tryptic peptides of barstar. The analytic sequence coverage of barstar was 63%. The first two lysine residues are invisible by virtue of trypsin proteolysis. The tryptic peptide E_{23}LALPEYYGENLDALWDCLTGWVEYPLVLEWR_{54} was not detected, but several low abundance unmodified semi-tryptic peptides spanning this region were detected. Unfortunately none were of sufficient abundance to warrant looking for their modified siblings; consequently barstar 23-54 is silent in this study. This illustrates the need for more than one proteolysis method when the footprinting study goal is complete analytic coverage. Nevertheless, the N- and C- terminal regions of barstar are well represented,

and we are confident in the structural conclusions drawn from the yield data for these regions.

3.4.3 Barstar folding.

The FPOP data indicates Barstar is folded at 22°C and partially or completely unfolded at 0 °C. Nineteen residues were detected as modified (Table 3.2); of these, I5, I10, L16, L20, T63, V70, L71, V73, F74, I84 are significantly more labeled and hence solvent accessible in the cold state. E8 and E68 are significantly more protected in the warm state. Significance is determined by the Student's t-test at 95% confidence. We cannot yet make any statistical conclusions for R11 and R75 (they're both higher in the cold state) because their modification signals stem solely from -43 Da deguanidination missed-cleavage peptides. It is not yet clear if the denominator treatment described in the Data Analysis section is appropriate for these modifications since these arginines are positioned in the middle of their missed-cleavage peptides.

Statistical significance does not necessarily convey a large change in SASA. To approximate the physical change in SASA per residue, we have normalized the cold-warm yield difference by the maximum yield measured for residues of the same amino acid class in Figure 3.5. The maximum yields observed for each amino acid-kind of residue approximates the inherent reactivity of each residue type to •OH in the FPOP experiment, because these residues are expected to be the least sterically obscured in their respective classes. Then for a relative change approaching 100% of this maximum, as seen for L16, L20, T63, V73, F74, and I84, signifies a large change in SASA, and thus

Table 3.2: FPOP yields per residue for barstar in two states.

residue	0 °C	22 °C
I5	0.45 +/- 0.01%	0.14 +/- 0.01%
E8	0.005 +/- 0.002%	0.053 +/- 0.004%
I10	0.177 +/- 0.003%	0.0354 +/- 0.0008%
R11	0.056 +/- 0.007%	0.022 +/- 0.003%
L16	0.27 +/- 0.01%	0.066 +/- 0.004%
H17	0.42 +/- 0.04%	0.24 +/- 0.06%
T19	0.0025 +/- 0.0005%	0.07 +/- 0.03%
L20	0.204 +/- 0.004%	0.022 +/- 0.002%
E57	0.64 +/- 0.02%	0.65 +/- 0.03%
L62	0.16 +/- 0.03%	0.110 +/- 0.006%
T63	0.11 +/- 0.02%	0.021 +/- 0.003%
E68	0.010 +/- 0.002%	0.047 +/- 0.005%
V70	0.013 +/- 0.001%	0.0033 +/- 0.0002%
L71	0.013 +/- 0.001%	0.0033 +/- 0.0002%
V73	0.10 +/- 0.02%	0.030 +/- 0.002%
F74	2.9 +/- 0.2%	0.86 +/- 0.08%
R75	0.066 +/- 0.007%	0.045 +/- 0.004%
I84	1.8 +/- 0.8%	0.3 +/- 0.2%
I86	0.6 +/- 0.3%	0.011 +/- 0.004%

may convey complete exposure in the cold state. A clear picture of structural differences between states is afforded by mapping the labeled residues onto the monomeric structure of WT barstar (we have used barstar C82A in this study) (Figure 3.6). Residues determined by FPOP to be buried in the warm state relative to the cold state are also clearly buried in the native NMR structure (red residues). E8 and E68 are very exposed in the native structure (green residues), and our data suggests they are less so in the cold state when. Residues approximately half-exposed in the native structure are also deemed statistically equivalent in our analysis (blue residues). Significantly, the majority of

residues assayed as protected in the native state are hydrophobic, whereas residues which show little change or the opposite trend are hydrophilic. This segregation in exposure is consistent with the essential role hydrophobic residues play in the phenomenon of cold denaturation of proteins, in which the loss of van der Waals interactions between such residues in the denatured state is compensated by their hydration at low temperature[35].

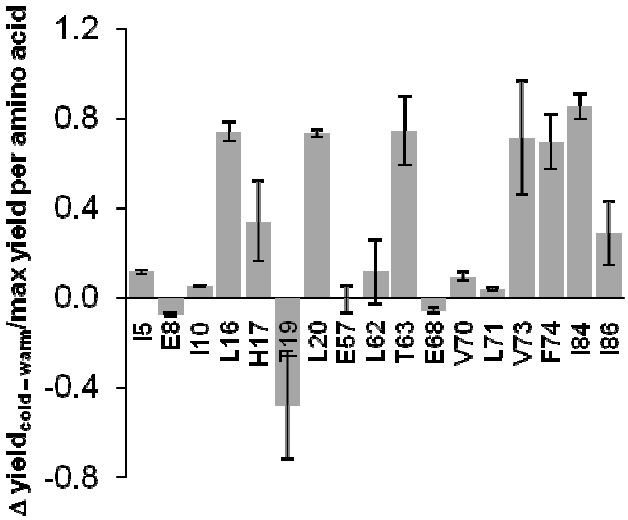

Figure 3.5: The difference plot of all modified residues except R11 and R75. Each cold – warm yield difference is divided by the maximum yield for each kind of residue. Residues with values above the x-axis exhibit more labeling in the cold state. Error bars shown are propagated from the replicate-derived standard errors for each state.

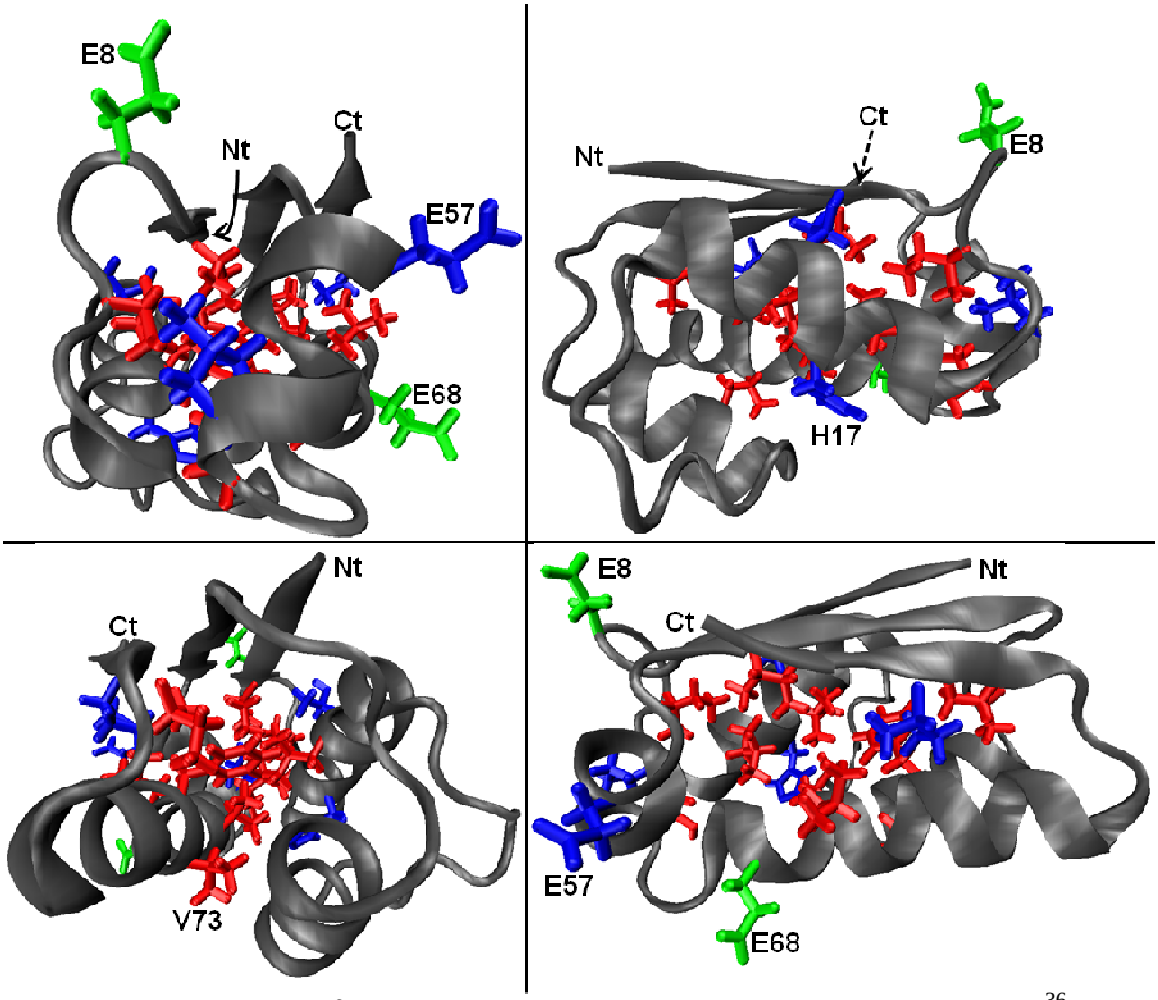

Figure 3.6: Four views of the native monomer barstar NMR structure 1BTA.pdb[36], with 17 residue sidechains shown in bond depiction. Red residues are significantly more labeled in the cold state. Green residues are significantly more labeled in the warm state. Blue residues are labeled in both states, but do not show a statistical difference.

3.5 Conclusion

In this study we have introduced a comprehensive protein-footprinting data analysis method that can deliver residue-resolved labeling yields for the full complement of label-sensitive residues in a protein or protein complex. This methodology is best served by using high resolution MS hybrid instruments, nano-flow chromatography, automated LC-MS peak detection and alignment software, and Mascot error-tolerant

search capabilities. Each of these things is a prime component of many proteomics centers (help with reference). The methodology is applicable to targeted PTM analysis and any protein-footprinting strategy that imparts stable covalent modifications. In particular, this analysis method well serves •OH-mediated footprinting studies.

The application of this method to the FPOP study of cold-denatured and room temperature-folded barstar protein shows the utility of •OH-labeling in identifying sites sensitive to changes in SASA between protein states. In doing so, we have highlighted the means of implementing the data analysis tools, paying particular attention to aspects of data validation important to generating high-fidelity residue-resolved labeling yields.

Six of the seven Excel application tools presented here utilize macros written in visual basic for applications (VBA); the seventh is code-free. We feel the relative transparency of the VBA and capabilities of Excel make these tools excellent resources for the skeptical protein-footprint scientist, as the data flow from one tool to the next is eminently not "black-box" but user-guided. As of now, these tools will be available on request; we intend to make them freely available online in the coming months. Finally, we acknowledge that the pioneers in •OH-mediated protein footprinting have also developed a software platform for the analysis of such data[37]; we have not yet compared analysis strategies.

3.6 References

1. Hambly, D. M.; Gross, M. L., In *The Encyclopedia of Mass Spectrometry: Ionization Methods*, Gross, M. L.; Caprioli, R. M., Eds. 2006; Vol. 6.
2. Guan, J.-Q.; Chance, M. R., Structural proteomics of macromolecular assemblies using oxidative footprinting and mass spectrometry. *Trends Biochem. Sci* **2005,** *10*, 583-592.
3. Xu, G.; Chance, M. R., Hydroxyl Radical-Mediated Modification of Proteins as Probes for Structural Proteomics. *Chem. Rev.* **2007,** *107* (8), 3514-3543.
4. Garrison, W. M., Reaction mechanisms in the radiolysis of peptides, polypeptides, and proteins. *Chem. Rev.* **1987,** *87* (2), 381-398.
5. Buxton, G. V.; Greenstock, C. L.; Helman, W. P.; Ross, A. B., Critical Review of Rate Constants for Reactions of Hydrated Electrons, Hydrogen Atoms and Hydroxyl Radicals (*OH/*O-) in Aqueous Solution. *J. Phys. Chem. Ref. Data* **1988,** *17* (2), 513-886.
6. Xu, G.; Chance, M. R., Radiolytic Modification of Sulfur-Containing Amino Acid Residues in Model Peptides: Fundamental Studies for Protein Footprinting. *Anal. Chem.* **2005,** *77* (8), 2437-2449.
7. Xu, G.; Chance, M. R., Radiolytic Modification and Reactivity of Amino Acid Residues Serving as Structural Probes for Protein Footprinting. *Anal. Chem.* **2005,** *77* (14), 4549-4555.
8. Xu, G.; Chance, M. R., Radiolytic Modification of Acidic Amino Acid Residues in Peptides: Probes for Examining Protein-Protein Interactions. *Anal. Chem.* **2004,** *76* (5), 1213-1221.
9. Zhang, H.; Gau, B. C.; Jones, L. M.; Vidavsky, I.; Gross, M. L., Fast Photochemical Oxidation of Proteins for Comparing Structures of Protein-Ligand Complexes: The Calmodulin-Peptide Model System. *Anal. Chem.* **2010,** *83* (1), 311-318.
10. Cutillas, P. R.; Timms, J. F., *LC-MS/MS in Proteomics Methods and Applications*. Humana Press: 2010; Vol. 658.
11. Perkins, D. N.; Pappin, D. J. C.; Creasy, D. M.; Cottrell, J. S., Probability-based protein identification by searching sequence databases using mass spectrometry data. *ELECTROPHORESIS* **1999,** *20* (18), 3551-3567.
12. Lichti, C.; Townsend, R. R., 2011.
13. America, A. H. P.; Cordewener, J. H. G., Comparative LC-MS: A landscape of peaks and valleys. *PROTEOMICS* **2008,** *8* (4), 731-749.
14. Gau, B. C.; Chen, H.; Zhang, Y.; Gross, M. L., Sulfate Radical Anion as a New Reagent for Fast Photochemical Oxidation of Proteins. *Anal. Chem.* **2010,** *82* (18), 7821-7827.
15. Hambly, D.; Gross, M., Laser flash photochemical oxidation to locate heme binding and conformational changes in myoglobin. *Int. J. Mass Spectrom.* **2007,** *259* (1-3), 124-129.
16. Hambly, D. M.; Gross, M. L., Laser Flash Photolysis of Hydrogen Peroxide to Oxidize Protein Solvent-Accessible Residues on the Microsecond Timescale. *J. Am. Soc. Mass Spectrom.* **2005,** *16* (12), 2057-2063.
17. Eng, J.; McCormack, A.; Yates, J., An approach to correlate tandem mass spectral data of peptides with amino acid sequences in a protein database. *J. Am. Soc. Mass Spectrom.* **1994,** *5* (11), 976-989.
18. Geer, L. Y.; Markey, S. P.; Kowalak, J. A.; Wagner, L.; Xu, M.; Maynard, D. M.; Yang, X.; Shi, W.; Bryant, S. H., Open Mass Spectrometry Search Algorithm. *Journal of Proteome Research* **2004,** *3* (5), 958-964.

19. Hartley, R. W., Barnase and barstar : Expression of its cloned inhibitor permits expression of a cloned ribonuclease. *Journal of Molecular Biology* **1988,** *202* (4), 913-915.
20. Hartley, R. W., Barnase and barstar: two small proteins to fold and fit together. *Trends Biochem. Sci* **1989,** *14* (11), 450-454.
21. Nölting, B.; Golbik, R.; Neira, J. L.; Soler-Gonzalez, A. S.; Schreiber, G.; Fersht, A. R., The folding pathway of a protein at high resolution from microseconds to seconds. *Proc. Natl. Acad. Sci. U.S.A.* **1997,** *94* (3), 826-830.
22. Nölting, B.; Golbik, R.; Fersht, A. R., Submillisecond events in protein folding. *Proc. Natl. Acad. Sci. U.S.A.* **1995,** *92* (23), 10668-10672.
23. Aye, T. T.; Low, T. Y.; Sze, S. K., Nanosecond Laser-Induced Photochemical Oxidation Method for Protein Surface Mapping with Mass Spectrometry. *Anal. Chem.* **2005,** *77* (18), 5814-5822.
24. Gau, B. C.; Sharp, J. S.; Rempel, D. L.; Gross, M. L., Fast Photochemical Oxidation of Protein Footprints Faster than Protein Unfolding. *Anal. Chem.* **2009,** *81* (16), 6563-6571.
25. Slebos, R. J. C.; Brock, J. W. C.; Winters, N. F.; Stuart, S. R.; Martinez, M. A.; Li, M.; Chambers, M. C.; Zimmerman, L. J.; Ham, A. J.; Tabb, D. L.; Liebler, D. C., Evaluation of Strong Cation Exchange versus Isoelectric Focusing of Peptides for Multidimensional Liquid Chromatography-Tandem Mass Spectrometry. *Journal of Proteome Research* **2008,** *7* (12), 5286-5294.
26. Durr, E.; Yu, J.; Krasinska, K. M.; Carver, L. A.; Yates, J. R.; Testa, J. E.; Oh, P.; Schnitzer, J. E., Direct proteomic mapping of the lung microvascular endothelial cell surface in vivo and in cell culture. *Nat Biotech* **2004,** *22* (8), 985-992.
27. Zhu, W.; Smith, J. W.; Huang, C.-M., Mass Spectrometry-Based Label-Free Quantitative Proteomics. *Journal of Biomedicine and Biotechnology* **2010,** *2010*, 1-6.
28. David M. Creasy, J. S. C., Error tolerant searching of uninterpreted tandem mass spectrometry data. *PROTEOMICS* **2002,** *2* (10), 1426-1434.
29. Vidavsky, I.; Rempel, D. L.; Gross, M. L., 2D Mass Spectra Correlation – Semi Automatic Tool for Modified Peptide Discovery. In *Proceedings of the 54th ASMS Conference on Mass Spectrometry and Allied Topics*, Seattle, WA, 2006.
30. Finley, E. L.; Dillon, J.; Crouch, R. K.; Schey, K. L., Identification of tryptophan oxidation products in bovine α-crystallin. *Protein Sci.* **1998,** *7* (11), 2391-2397.
31. Maleknia, S. D.; Wong, J. W. H.; Downard, K. M., Photochemical and electrophysical production of radicals on millisecond timescales to probe the structure, dynamics and interactions of proteins. *Photochem. & Photobiol. Sci.* **2004,** *3*, 741-748.
32. Wong, J. W. H.; Maleknia, S. D.; Downard, K. M., Study of the Ribonuclease-S-Protein-Peptide Complex Using a Radical Probe and Electrospray Ionization Mass Spectrometry. *Anal. Chem.* **2003,** *75* (7), 1557-1563.
33. Maleknia, S. D.; Brenowitz, M.; Chance, M. R., Millisecond Radiolytic Modification of Peptides by Synchrotron X-rays Identified by Mass Spectrometry. *Anal. Chem.* **1999,** *71* (18), 3965-3973.
34. Xu, G.; Takamoto, K.; Chance, M. R., Radiolytic Modification of Basic Amino Acid Residues in Peptides: Probes for Examining Protein−Protein Interactions. *Anal. Chem.* **2003,** *75* (24), 6995-7007.
35. Privalov, P. L., Cold Denaturation of Protein. *Critical Reviews in Biochemistry and Molecular Biology* **1990,** *25* (5), 281-306.

36. Lubienski, M. J.; Bycroft, M.; Freund, S. M. V.; Fersht, A. R., Three-dimensional solution structure and 13C assignments of barstar using nuclear magnetic resonance spectroscopy. *Biochemistry* **1994,** *33* (30), 8866-8877.
37. Kaur, P.; Kiselar, J. G.; Chance, M. R., Integrated Algorithms for High-Throughput Examination of Covalently Labeled Biomolecules by Structural Mass Spectrometry. *Anal. Chem.* **2009,** *81* (19), 8141-8149.

4 Fast photochemical oxidation of proteins (FPOP) by the sulfate radical anion probes solvent accessibility

4.1 Introduction

Chemical footprinting[1-3] of proteins is becoming an efficient alternative and augmentative method to X-ray crystallography and NMR spectroscopy for the elucidation of protein structure and interactions. By mass spectrometric analysis of the protein-footprint products in the presence and absence of ligand, the binding site(s) and induced changes in protein conformation can be determined, provided that the labeling reactions in these regions are attenuated in the holo state. The most general and, thus, informative chemical reactions currently used for protein footprinting are hydrogen/deuterium exchange (HDX)[4] and hydroxyl radical oxidation.[5] The methods are complementary in revealing features of protein structure. Predominantly side chain accessibility is sampled by properly controlled •OH reaction[6], whereas HDX samples backbone amide hydrogen accessibility and secondary structure.[7-8]

Hydroxyl radicals probe solvent accessibility because they have both comparable size to solvent water molecules and high reactivity with a significant fraction of amino-acid side chains. One of the advantages of •OH footprinting is that the stability (irreversibility) of modifications enables a "bottom-up" proteomics methodology of proteolysis and online LC-MS/MS for their detection and quantification. Interest in other chemical probes that engender similarly stable modifications, including the highly reactive methylene carbene[9-11], continues to increase, driven by the possibility that complementary structural information of protein complexes might be obtained with different chemical selectivity of accessible protein residues.

We demonstrated that FPOP occurs on the microsecond timescale for •OH labeling reactions,[12] affording near millimolar levels of •OH from the homolytic cleavage of H_2O_2 upon irradiation by a 17 ns flash of 248 nM KrF excimer laser. Constituent Gln acts as a radical scavenger, ensuring the quenching of labeling on this timescale. The strength of this approach to footprinting is the high yield of protein modification by •OH from a profoundly short exposure. A microsecond labeling timescale avoids the sampling of protein conformation that are altered by the modification, as ultimately will be the case for timescales that are longer.[13]

Herein we report a new footprinting agent for the FPOP method, an ionic sulfate radical anion, SO_4^{-}•. The primary reason for choosing SO_4^{-}• is that its reduction potential at 2430 mV is higher than that of •OH (1900 mV),[14] making it a potentially useful oxidant for proteins. For example, the formation of protein cross-links can be triggered by SO_4^{-}•[15-16], and protein oxidation using SO_4^{-}• can occur in the metal-catalyzed oxidation reactions.[17] It is a reasonable expectation that SO_4^{-}•, like •OH, oxidizes proteins very rapidly, which is an advantage of FPOP using •OH. Reactions of SO_4^{-}• with amino acids and some dipeptides in aqueous solution are known albeit on a continuous timescale rather than pulsed as we demonstrate here. This chemistry of SO_4^{-}• is determined by its very high electron affinity and its capability to oxidize aromatic and Met side chains to the corresponding radical cations, which subsequently undergo either fragmentation or hydration.[18-19] The sulfate radical anion can also oxidize carboxyl anions including zwitterionic amino acids in aqueous solution to acyloxyl radicals (RCO_2•), which rapidly decarboxylate to give carbon-centered radicals.[14, 20] Radicals

formed by SO_4^{-}• hydrogen abstraction also occur for some amino acids such as Leu and Ser.[20]

The precursor compound used for the generation of SO_4^{-}• is the relatively stable and water-soluble inorganic salt $Na_2S_2O_8$. The $S_2O_8^{2-}$ aqueous ion has a UV band maximum at 215 nm; we measured the extinction coefficient at 248 nm in PBS as 24 M^{-1} cm^{-1}. The photolysis of $S_2O_8^{2-}$ in water gives SO_4^{-}• radical anions with a quantum yield of 0.55 at 308 nm.[21]

In the present study, we compared the amino-acid residue reactions of laser-initiated sulfate radical anion with those of hydroxyl radicals after tuning the oxidation levels so that they nearly match. The tests were two proteins, apomyoglobin (aMb) and Ca^{2+}-free calmodulin (CaM), and a mixture of peptides, bradykinin and angiontensin II, which were subjected to both peroxide and persulfate FPOP. We focused the proteolysis/LC-MS/MS analysis (1) to identify the types of residue modifications and their frequency and ascertain whether any subset of residues SO_4^{-}• may better sample than •OH and (2) to determine whether persulfate FPOP exclusively modifies solvent accessible residues, and on a timescale fast enough to sample native conformation only.

More than any other oxidative-modification protein footprinting method, FPOP is highly tunable both in yield (by altering starting material levels of quencher and labeling precursor), timescale, and targeted chemistry. Besides hydroxyl radicals and sulfate radical anions, there are several potential peroxy-[22] and diazirine[23] species capable of UV photolysis to generate either other radicals or carbenes, which may be selected for their physical properties or residue specificity. These opportunities make clear another

purpose of this study; that is, to illustrate a method for validating such starting materials for developing new methods of protein footprinting by FPOP.

4.2 Experimental Procedures

4.2.1 Reagents.

Bovine β-Lactoglobulin A (BLG), 30% hydrogen peroxide, sodium persulfate, angiotensin II, bradykinin, *L*-glutamine, *L*-methionine, catalase, urea, ethylene glycol-bis(2-aminoethylether)-*N*,*N*,*N*′,*N*′-tetraacetic acid (EGTA), acetonitrile, formic acid, proteomics grade trypsin, and phosphate buffered saline (PBS) were purchased from the Sigma Aldrich Chemical Company (St. Louis, MO). Bovine CaM was purchased from Oceanbiologics (Corvallis, OR). The proteins were used without further purification. Purified water (18 MΩ) was obtained from an in-house Milli-Q Synthesis system (Millipore, Billerica, MA).

4.2.1 Oxidative-modification labeling.

Each 50 μL sample was prepared in PBS (10 mM phosphate buffer, 138 mM NaCl, 2.7 mM KCl, pH 7.4 at 25 °C), with a final protein concentration of 10 μM. The bradykinin and angiotensin II components of peptide mixture samples were also prepared at these concentrations. Apo-CaM samples included 100 μM EGTA for the chelation of adventitious calcium. Glutamine was added to a final concentration of 20 mM in normal FPOP samples. Hydrogen peroxide or $Na_2S_2O_8$ was added to a final concentration of 15 mM or 3 mM, respectively, just before FPOP infusion except for BLG, where $Na_2S_2O_8$ was added to 5 mM. The experimental apparatus and procedure for laser flash photolysis of samples was detailed previously.[12] The laser power was adjusted to 44 mJ/pulse. The

fraction of sample masked from irradiation was set to 20% by adjusting the infusion flow rate and laser pulse frequency; this ensured that no protein was double-shot.[12-13]

Sample was collected in a microcentrifuge tube containing 20 μL of 70 mM Met, and immediately purified from excess H_2O_2 or $Na_2S_2O_8$ by Millipore Ziptip (Billerica, MA) 0.6 μL bed solid-phase extraction. C4 tips were used for BLG, aMb, and CaM samples; C18 tips were used for samples containing peptide mixtures. Each 10 μL Ziptip accommodates up to 45 μL in aspirate with careful pipette action. One slow aspiration/dispense cycle was sufficient to load the Ziptip with good recovery; this precaution minimized post-FPOP oxidation (data not shown).

Except for BLG, four treatments per protein or peptide mixture were applied in triplicate. "Native" samples were solutions of analyte, buffer, and Gln, and were not laser irradiated. "Peroxide" sample solutions included H_2O_2 and were subjected to flash photolysis. "Persulfate" sample solutions included $Na_2S_2O_8$ and were subjected to flash photolysis. "Persulfate control" sample solutions were prepared identically to "Persulfate" but were not laser irradiated. Their persulfate exposure was limited to 5 min prior to desalting. BLG samples were processed similarly but at two persulfate levels and in duplicate.

4.2.2 Global mass spectrometry of FPOP-labeled β-lactoglobulin.

For BLG samples, $Ziptip_{C4}$ eluent was diluted 5-fold in 50% acetonitrile and immediately infused onto a Waters Ultima Global quadrupole time-of-flight (Milford, MA), operating in V mode at 12,000 FWHM resolving power at 838.8 m/z ($(CF_3COONa)_6Na^+$ calibrant ion).

4.2.3 Proteolysis and LC-MS/MS

Apomyoglobin samples were trypsin-digested for 18 h at 37 °C; CaM samples were trypsin-digested 6 h at 37 °C; each was digested at a 1:10 trypsin:protein weight ratio. The peptides were desalted using $Ziptip_{C18}$ (Millipore), and the 10 μL eluent was diluted 20-fold with purified water. A small sample (2 μL) was loaded by autosampler (Eksigent nanoLC, Dublin, CA) onto a capillary column with a laser-pulled tip (Sutter Instruments, Novato, CA), bomb-packed with C18 reverse phase material (Magic, 0.075mm × 200mm, 5μm, 300Å, Michrom, Auburn, Ca). The gradient was from 1% solvent B (97% acetonitrile, 3% water, 0.1% formic acid) to 60% solvent B over 60 min at an eluent flow of 260 nL/min. The LC was coupled to the nanospray source of an LTQ-Orbitrap mass spectrometer (Thermo Fisher, Waltham, MA), for aMb and peptide mixture samples, or an LTQ-FT mass spectrometry (Thermo Fisher), for CaM. Mass spectra of eluting peptides were obtained at high mass resolving power (100,000 for ions of *m/z* 400) with the FT mass spectrometer component, while MS/MS experiments on the six most abundant eluting ions per high resolution scan were performed in the LTQ at a normalized collision energy of 35% of maximum, using a 2 Da isolation width and wide-band activation. Ions submitted to MS/MS were placed in a dynamic exclusion list for 8 s. A blank run followed every sample acquisition.

4.2.4 Data Analysis

The peak alignment algorithm of the Rosetta Elucidator data management system (Rosetta Biosoftware) was used to generate tables of extracted ion chromatogram features. Manually validated Mascot error-tolerant search results were paired to their tabulated mass spectral features by a custom Excel VBA program, which also augmented

the search results with a 5 ppm threshold mass list of anticipated peroxide and persulfate FPOP products not found by Mascot. Augmented hits were included only if a product-ion spectrum verified the accurate mass match. A third modification discovery method utilized a correlation algorithm to compare unidentified product-ion spectra to exemplary CID fragment spectra of unmodified tryptic peptides of aMb, CaM, and of bradykinin and angiontensin II.[24]

4.3 Results and Discussion

4.3.1 Optimal Sodium Persulfate FPOP Conditions.

The mass spectrum bounding the 15th charge state of β-lactoglobulin (BLG) obtained when 15 mM $Na_2S_2O_8$ was mixed with PBS-buffered 10 μM BLG and incubated 5 min at room temperature (Figure 4.1a) shows an insignificant amount of protein oxidation. The base peak corresponds to unmodified BLG; the very low levels of modified and/or ESI adducts of BLG are superimposable with the mass spectrum of a stock solution BLG (data not shown). Thus, short-time exposure to low levels of $Na_2S_2O_8$ does not oxidize BLG. Apomyoglobin, CaM, bradykinin, and angiontensin II also do not show $Na_2S_2O_8$ oxidation over short-time exposures, although ESI MS revealed that CaM in its starting state was already oxidized to show +16 and +32 Da adducts.

Irradiating the flowing solution containing the same level of $Na_2S_2O_8$ with the KrF excimer laser, however, gives rise to a high yield of modified BLG (Figure 4.1b). Two aspects are readily apparent. First, the dominant persulfate radical modification products correspond to successive +16 Da additions (or +1.07 *m/z* addition for the 15th charge state). This is also the dominant product of •OH reactions in other protein

footprinting chemistry[5] and is what we observed with 15 mM H_2O_2 FPOP (Figure 4.1d). Second, 15 mM $Na_2S_2O_8$ FPOP gives a much higher yield of modified protein than the standard 15 mM H_2O_2 FPOP treatment. Solely by reducing the concentration of $Na_2S_2O_8$ to 5 mM, the modification distribution seen in Figure 4.1c is moderated to nearly the same global protein outcome as with standard H_2O_2 FPOP. A more rigorous analysis of this product distribution, presented in the Supporting Information section, shows it is well modeled by a Poisson distribution of 0, +16, +32, … Da states, indicating the labeling has sampled a single (native) conformation. β-lactoglobulin is known to be conformationally sensitive to oxidation.[25] It follows that 5 mM $Na_2S_2O_8$ FPOP labeling, like 15 mM H_2O_2 FPOP, labels faster than most secondary and tertiary protein motions[26-27] and corroborates the theoretical prediction of sub-μs-to-μs labeling.

4.3.2 Residue-Resolved Modification Measurement by LC-MS/MS.

Owing to the stable covalent label imparted by •OH and the high percentage of solvent-accessible residues that may be labeled, a "bottom-up" proteomics approach in data acquisition for modification identification and quantitation can be employed in protein footprinting, typically using trypsin proteolysis and online LC-MS/MS.[5] We used this strategy because the global pattern of persulfate modification

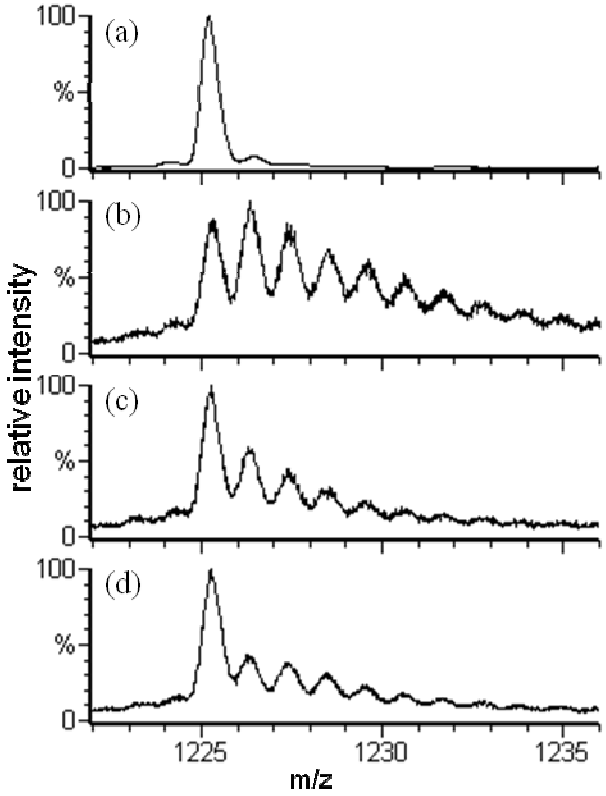

Figure 4.1: The ESI-QTOF mass spectra of the 15th charge state of β-lactoglobulin subjected to different labeling conditions. Spectrum (a) is of the 15 mM $Na_2S_2O_8$ control, absent only laser irradiation; (b) is of 15 mM $Na_2S_2O_8$ FPOP; (c) is of 5 mM $Na_2S_2O_8$ FPOP; (d) is of 15 mM H_2O_2 FPOP.

indicates a similar promiscuity in residue reaction as with •OH labeling.

Site-specific labeling was established by LC-MS/MS analysis. The aggregate of all modifications at each site was determined (Tables 4.1, Supporting Information Tables 4.1 and 4.2) as a "fraction-modified" metric, and comparisons for amino-acid types using the data from persulfate and peroxide treatments are plotted in Figure 4.2. The fraction-modified metric is calculated, per residue, by summing, in the numerator, signals for all detected peptides having a modification at that residue and by summing, in the denominator, signals for all peptides, modified and unmodified, having the same 1° sequences as the numerator set of peptides. The fraction-modified metric is implicitly

normalized across samples because all variations in post-FPOP sample handling, proteolysis, de-salting, on-line chromatography, and mass spectrometry that affect a modified peptide's signal will likely influence signals for its unmodified and modified siblings in the same proportion, with the exception of ionization efficiency.[28]

We observed no detectable modifications of proteins in their mass spectra following control experiments for which no laser irradiation was used, consistent with global observations (e.g. Figure 4.1a). Furthermore, we found that the fraction modified levels of persulfate control residues are statistically identical to the "native" control (absent peroxo- starting material) fraction modified levels, and with the exception of Met test the limit of detection. These results follow from examination of Tables 4.1 and Supporting Information Tables 4.1 and 4.2, and they show one general trend necessary for validating persulfate FPOP as a viable labeling strategy.

4.3.3 Selectivity of $Na_2S_2O_8$ FPOP.

From these tables and Figure 4.2, it is clear that $Na_2S_2O_8$ FPOP is a non-specific labeling method that samples many of the same residues with comparable reactivity to H_2O_2 FPOP. Both methods reliably label over one half of the 20 common amino acids. Comparing reactivity on a residue-by-residue basis (Figure 4.2a) shows that peroxide FPOP more readily labels aliphatic residues as well as Phe, Thr, Gln, and Lys. If equivalent levels of labeling are expected for 5 mM persulfate vs. 15 mM hydrogen peroxide, as witnessed at the protein global level, it seems unlikely that the large-difference contributors underlying this trend (for example, aMb I21 in Table 4.1) are explained solely by the use of 3 mM $Na_2S_2O_8$ starting material instead of 15 mM.

Table 4.1: Apomyoglobin Fraction Modified per Residue[a]

residue	SASA ($Å^2$)[b]	$k_{\cdot OH}$ (M^{-1} sec^{-1})[c]	native	peroxide	persulfate	persulfate control
E6	56.1	2.3×10^8	0	0.13 +/- 0.04%	0.069 +/- 0.007%	0.0003 +/- 0.0002%
W7	15.3	1.3×10^{10}	1.41 +/- 0.09%	13.9 +/- 0.9%	15.3 +/- 0.6%	2.2 +/- 0.2%
W14	6.8	1.3×10^{10}	0.84 +/- 0.06%	12.5 +/- 0.6%	4.6 +/- 0.5%	1.57 +/- 0.07%
E18	65.5	2.3×10^8	0	2.07 +/- 0.06%	2.4 +/- 0.2%	0.004 +/- 0.002%
D20	65.8	7.5×10^7	0	0.20 +/- 0.01%	0.247 +/- 0.009%	0
I21	62.1	1.8×10^9	0	0.45 +/- 0.03%	0.0573 +/- 0.0001%	0
H24	7.7	4.8×10^9	0.0047 +/- 0.0003%	0.70 +/- 0.05%	0.32 +/- 0.02%	0.0060 +/- 0.0004%
Q26	22.5	5.4×10^8	0	0.07 +/- 0.01%	0.07 +/- 0.01%	0.0001 +/- 0.0001%
E27	49.0	2.3×10^8	0	0.71 +/- 0.03%	0.24 +/- 0.01%	0.0001 +/- 0.0001%
I30	7.9	1.8×10^9	0	0.054 +/- 0.006%	0.002 +/- 0.002%	0
T34	48.8	5.1×10^8	0.0042 +/- 0.0009%	0.43 +/- 0.04%	0.08 +/- 0.03%	0.008 +/- 0.001%
H36	54.5	4.8×10^9	0.0023 +/- 0.0007%	2.4 +/- 0.2%	1.7 +/- 0.8%	0.009 +/- 0.004%
P37	81.9	6.5×10^8	0	0.38 +/- 0.04%	0.06 +/- 0.01%	0.0002 +/- 0.0002%
E41	93.5	2.3×10^8	0	0.105 +/- 0.005%	0.14 +/- 0.04%	0
H64	41.8	4.8×10^9	0.0022 +/- 0.0003%	0.81 +/- 0.01%	4.5 +/- 0.6%	0.042 +/- 0.009%
V67	86.1	8.5×10^8	0.00034 +/- 0.0001%	0.41 +/- 0.02%	0.071 +/- 0.009%	0.0003 +/- 0.0001%
T70	79.3	5.1×10^8	0.016 +/- 0.006%	0.09 +/- 0.02%	0.03 +/- 0.02%	0.009 +/- 0.003%
H81	129.3	4.8×10^9	0.029 +/- 0.003%	3.9 +/- 0.1%	7 +/- 1%	0.49 +/- 0.03%
H82	5.1	4.8×10^9	0.0052 +/- 0.0005%	0.61 +/- 0.04%	0.69 +/- 0.06%	0.011 +/- 0.001%
E83	112.0	2.3×10^8	0.018 +/- 0.002%	0.36 +/- 0.06%	0.73 +/- 0.02%	0.026 +/- 0.004%
L86	1.9	1.7×10^9	0	0.37 +/- 0.03%	0.0004 +/- 0.0003%	0
L89	43.1	1.7×10^9	0.010 +/- 0.002%	1.06 +/- 0.08%	0.08 +/- 0.02%	0.0077 +/- 0.0005%
Q91	72.9	5.4×10^8	0	0.29 +/- 0.02%	0.14 +/- 0.02%	0.04 +/- 0.03%
H93	52.0	4.8×10^9	0.0023 +/- 0.0004%	1.9 +/- 0.1%	1.63 +/- 0.07%	0.004 +/- 0.002%
H113	80.6	4.8×10^9	0	1.9 +/- 0.1%	2.0 +/- 0.4%	0.009 +/- 0.004%
H116	63.9	4.8×10^9	0	0.2 +/- 0.1%	1.7 +/- 0.5%	0
H119	30.9	4.8×10^9	0	0.95 +/- 0.07%	0.55 +/- 0.06%	0
Q128	66.5	5.4×10^8	0	0.34 +/- 0.03%	0.018 +/- 0.002%	0
M131	0.9	8.5×10^9	3.7 +/- 0.3%	25 +/- 1%	24 +/- 3%	5.9 +/- 0.4%
K133	67.6	3.5×10^8	0	0.09 +/- 0.01%	0.0001 +/- 0.0001%	0
E136	76.3	2.3×10^8	0	0.083 +/- 0.007%	0.137 +/- 0.006%	0
L137	40.4	1.7×10^9	0	0.27 +/- 0.03%	0.003 +/- 0.001%	0
F138	19.8	6.9×10^9	0	0.70 +/- 0.03%	0.141 +/- 0.007%	0.0009 +/- 0.0006%
F151	26.7	6.9×10^9	0	36 +/- 2%	7.9 +/- 0.4%	0

[a] The numerator is the sum all signal of peptides modified at a residue. The denominator is the sum of all signal of peptides, modified and unmodified, having the same sequences as the numerator set of peptides.

[b] Solvent accessible surface area (SASA) was calculated as the sum of non-hydrogen side chain and α-carbon areas using the online calculator at http://molbio.info.nih.gov/structbio/basic.html , using a 1.4 Å probe [29]. The myoglobin crystal structure 1WLA.pdb was used with heme atoms omitted [30].

[c] http://allen.rad.nd.edu/browse compil.html.

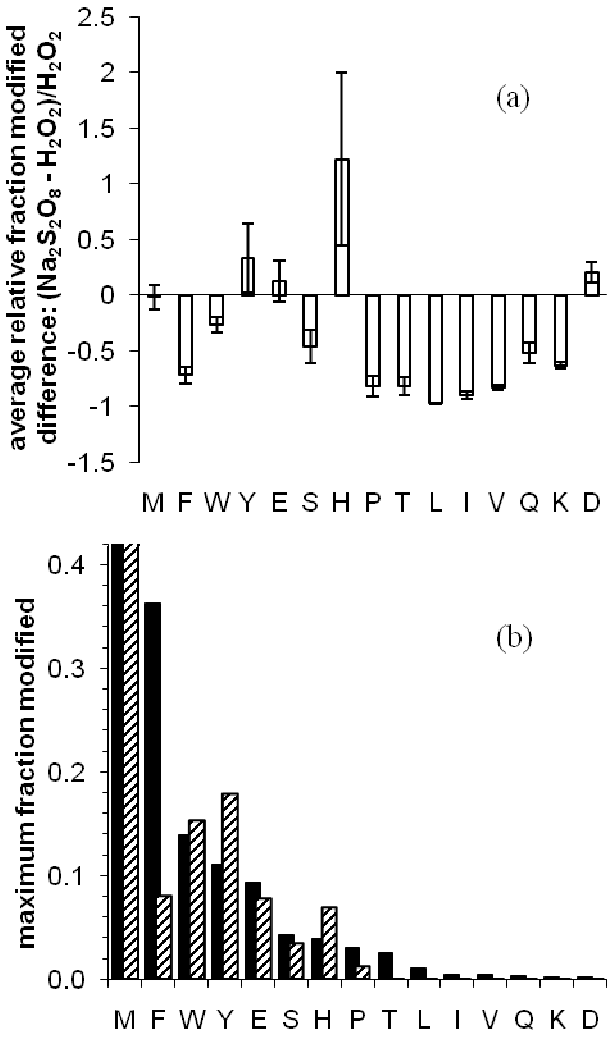

Figure 4.2: With (a), the relative difference between persulfate and peroxide fraction modified, of CaM, aMb, bradykinin, and angiotensin II residues, are determined per residue; these values are averaged per amino-acid type. The error bars denote the average pairwise-comparison standard error. In (b) the maximum fraction modified among all same-amino acid residues is plotted. Black bars denote H_2O_2 FPOP labeling; diagonal-pattern bars denote $Na_2S_2O_8$ FPOP labeling.

These differences must also arise from the differences in the inherent reactivities of •OH and SO_4^{-}•, and from the difference in their size. In particular, Trp is exceptionally sensitive to both labeling methods; aMb W7 and W14 are equivalently labeled by H_2O_2 FPOP, butW7 is 3-fold more oxidized than W14 with $Na_2S_2O_8$ FPOP. The solvent-accessible surface area values are small but non-zero, 15 and 7 $Å^2$, respectively, for W7

and W14, so that the difference between labeling methods for this residue type may be a function exclusively of size differences in the reactant probes.

The amino acid labeling levels are listed from left-to-right in both graphs of Figure 4.2 in order of decreasing observable peroxide reactivity per amino-acid group, as established by the maximum observed fraction modified per residue of each group (Figure 4.2b). These maximum fraction values should pertain to the most fully solvent-exposed sidechain residues of each amino acid group, and thus allow for a comparison of the inherent reactivity of SO_4^{-}• vs. •OH. The order of SO_4^{-}• reactivity is slightly different: M > Y = W > F = E = H > S > P > D = T > K = Q > L = V = I. In either case, the most reactive residues are consistent with amino acid rate data and with the •OH labeling products from water radiolysis[31], with the exception of Glu. Persulfate FPOP is more reactive to His, and Tyr and equally reactive to Met, Trp, Glu, and Ser. Despite the negative charge of SO_4^{-}• and its precursor, no increased affinity for basic residues is observed except for His. This is probably due to attenuation of electrostatic interaction by the phosphate-buffered saline solution, but trypsin digestion may bias against detecting modified Lys and Arg.

4.3.4 Chemistry of $Na_2S_2O_8$ FPOP.

With the exception of the +34 Da His modification (Supporting Information) many modifications discernable for peroxide FPOP were also found among persulfate FPOP replicates (Table 4.2). Furthermore, these modifications comprise the "usual suspects" in •OH labeling by peroxide-initiated and water radiolysis experiments.[5] The commonality of the sets of modifications produced by each FPOP method suggests that the dominant chemical pathways of SO_4^{-}• labeling are analogous to the better understood

•OH mechanisms.[32] A likely explanation for these similar outcomes is that both processes begin with an initial hydrogen abstraction reaction at aliphatic sites. Additionally, the transfer of radical to water (equation 1) may be a competing pathway, giving rise to the common •OH footprinting products.

$$SO_4^{-}\bullet + H_2O \rightarrow SO_4^{2-} + H^+ + \bullet OH \quad (1)$$

There may be other novel products of $SO_4^{-}\bullet$ not detected in these experiments; that 85% of all +2 and higher charge state species of significant abundance were identified as aMb modified and unmodified peptides suggests that these putative products are from low-yield pathways.

4.3.5 Solvent Accessibility.

In comparing equilibrium states, as is typical for footprinting experiments[5], changes in the fraction modified at a residue between states should solely reflect a change in solvent accessibility—all other biases are inherently normalized. The sensitivity of persulfate FPOP labeling to solvent accessibility can be assayed by comparing the solvent accessible surface area (SASA) calculated from X-ray and NMR structures to the per-residue fraction modified for any same-amino-acid set of residues of a protein. The restriction to same residue types stems from the inherent •OH (and presumably with $SO_4^{-}\bullet$) reactivity difference between free amino acids.[5] An analysis of the aMb His modification levels is illustrative of the promise of this approach (Figure 4.3). We find that its inherent reactivity is not too low to limit detection of the modifications and that a large range of SASA values are spanned by 11 myoglobin His residues. The reactivity of His in $Na_2S_2O_8$ FPOP correlates reasonably well with the calculated SASA (the Figure 4.3b straight-line fit R^2 is 0.83). Although the R^2 does not indicate perfect correlation,

one should bear in mind that part and perhaps most of the uncertainty is in the calculated SASA. When H64, an outlier, is excluded, an even better correlation is obtained. The motivation for omitting this residue (Figure 4.4) is that it is an axial ligand of the heme iron. The H_2O_2 FPOP correlation of aMb His labeling with SASA is better still, even with H64 inclusion (plot not shown). We propose that $S_2O_8^{2-}$ or SO_4^{-}• has an affinity for the heme binding pocket that H_2O_2 or •OH does not share, such that the local concentration of labeling agent is higher than that at the bulk. That H64 and H93, the second heme-ligating residue, are not equally labeled suggests a preferred orientation, such as a chelate bridge, which in turn suggests an affinity model for persulfate.

Table 4.2: Observed Residue Modifications of Persulfate and Peroxide FPOP

Amino Acid	Net Modifications (Da)						
Asp	-44						
Gln	+16						
Glu	-44	-30	-28	-18			
Gly[a]	-44						
His	-23	-22	-10	+5	+16	+32	+34[b]
Ile	+14	+16					
Leu	-2	+16					
Lys	+14	+16					
Met	+16						
Phe	+16	+30	+46				
Pro	+14	+16					
Ser	-2	+16					
Thr	-2						
Trp	-14	+4	+16	+32	+48		
Tyr	+16	+32	+34[b]				
Val	+14	+16					

[a] Only C-terminus G153 of myoglobin exhibited carbon dioxide loss.
[b] Only observed among persulfate FPOP replicates.

With the exception of Glu, all same-amino-acid residues of a protein show increasing labeling yield with increasing SASA, though the data sets for Trp, Phe, Leu,

Ile, and Thr are too small for proper correlation analysis. Their sampling may be improved with a different proteolysis methodology, to give shorter or longer peptides in regions of too few or too many trypsin cleavage sites, thus enabling informative product-ion (MS/MS) spectra in these regions. Nevertheless the most compelling correlation is binary: never is a non-Met residue labeled that shouldn't be. Although Met is extremely sensitive to oxidative labeling, it does not serve as the ideal residue for probing changes in solvent accessibility without careful controls[5] because its inherent reactivity is high even with mild oxidizing agents[33] and because it may serve as an oxidation sink for persistent protein hydroperoxides that can arise as intermediates in the

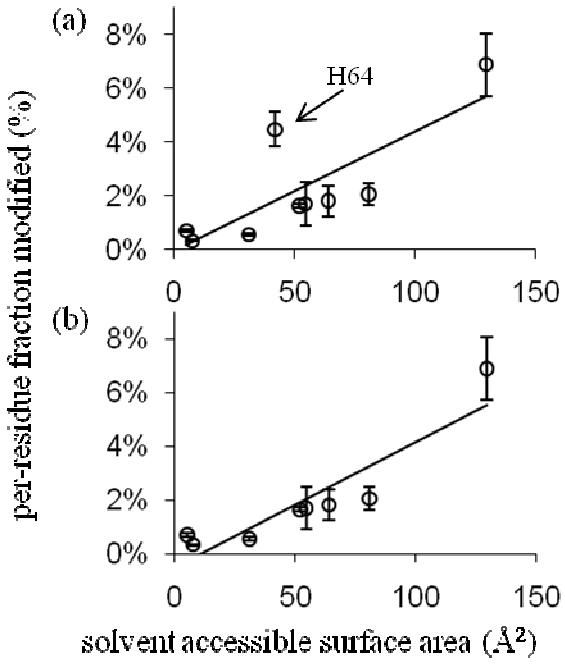

Figure 4.3: The modification yields of aMb His residues are plotted against their calculated solvent accessible surface area (SASA), with least-squares straight-line fits shown. In plot (b) the myoglobin His64 was omitted; this improved the R^2 fit from 0.63 in (a) to 0.83. The SASA values were calculated from the 1WLA.pdb crystal structure of myoglobin with its heme ignored by the calculator at http://molbio.info.nih.gov/structbio/basic.html, using a 1.4 Å probe.

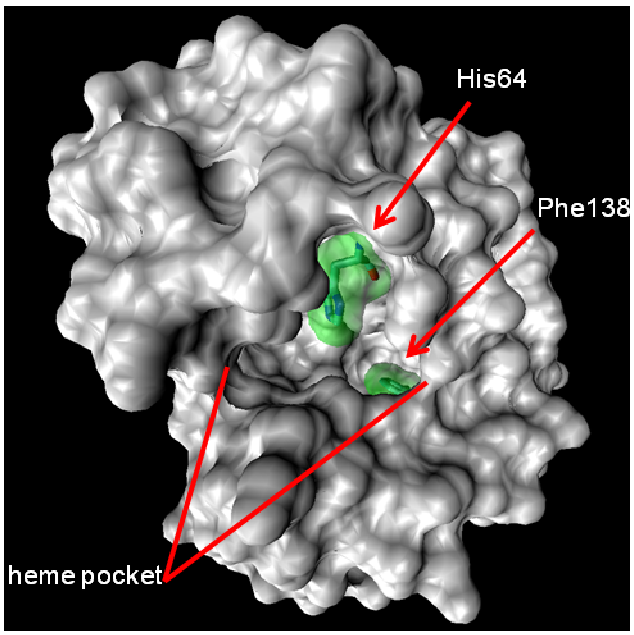

Figure 4.4: The 1.4 Å probe surface rendering of the myoglobin 1WLA.pdb crystal structure, showing the heme binding pocket, His64, and Phe138.

formation of common oxidative-modification products initiated by fast •OR chemistry.[34] Furthermore, many proteins are isolated with endogenous Met oxidation; we found, for example, that CaM samples exhibited significant Met oxidation "out of the box" (Supporting Information Table 4.1, "native" column).

Apomyoglobin F138 labeling signal is 50-fold lower than that of F151, although the calculated SASA is but 25% less. This calculation is based on the myoglobin crystal structure 1WLA[30] with the heme removed. This result quantitatively reproduces the Hambly and Gross finding that H-helix moves to close the pocket in the apo state, burying F138. This also underscores the potential biases of using static high resolution solid-state structures to determine dilute aqueous phase protein residue SASAs. Finally, the myoglobin E18 is dominated by significant CO_2 loss (- 44 Da) signal in both peroxide and persulfate FPOP. Other acidic residues also exhibit this pathway, but their yields are significantly lower. This may be a consequence of local $S_2O_8^{2-}$ and H_2O_2 affinity but

probably not a consequence of error in SASA estimation as the magnitude of yield change is so large.

4.3.6 Sodium persulfate vs. hydrogen peroxide FPOP: physical considerations and future prospects.

Although protein footprinting at physiologic levels of analyte, ionic activity, and pH are possible with FPOP, the requirement of peroxy starting material begs the definition of "physiologic". It is, therefore, advantageous that persulfate FPOP requires 3-5 fold less starting material than peroxide FPOP to deliver the same levels of modification (Figure 4.1). On the other hand, excess $Na_2S_2O_8$ must be removed non-enzymatically after labeling, and this may introduce another source of unbiased error. One application of the FPOP method that we would like to pursue is the study of membrane proteins in micelles, liposomes, lipoprotein particles, and synthetic protein-wrapped phospholipid bilayer discs.[35] The lipid bilayer permeability of $S_2O_8^{2-}$ is in all likelihood dramatically smaller than that of H_2O_2, commonly known to be membrane-permeable [36]. Marla and coworkers [37] showed that $ONOO^-$ readily permeates large unilamellar vesicles composed of *L*-α-phosphatidylcholine , stearyl amine, and cholesterol, but that SO_4^{2-} is membrane-impermeable. They argued the high peroxynitrate permeability may be due to its relatively high basicity (pK_a = 6.8 [38-39]), whereas sulfate is the conjugate base of a strong acid. Persulfate retains its anionic character in PBS-buffered solution and, thus, should be membrane-impermeable. It is possible that by using H_2O_2 and $Na_2S_2O_8^{2-}$ in tandem FPOP experiments, a footprint may be acquired of extracellular-accessible and cytoplasmic-accessible residues in aqueous-stable membrane particles imbedded with analyte protein. Finally, the thermal stability

of $S_2O_8^{2-}$ relative to H_2O_2 is advantageous for any temperature-varied FPOP experiment up to 50°C [40-41].

4.4 Conclusions

The H_2O_2 and $Na_2S_2O_8$ FPOP results presented here demonstrate the viability of persulfate FPOP protein footprinting. The ideal footprinting experiment is of state comparisons whereby one seeks differences in labeling yield at identical sites for two treatments (e.g., apo vs. holo, native vs. unfolded) to reflect residue protection (or exposure with signal increase) owing to direct inter- or intramolecular interaction or allosteric change from distal binding. If a detailed footprinting picture is required in which the "fraction modified" ascribes a solvent accessibility value, a thorough search and replicate quantitation for all FPOP modifications in addition to calibration with proteins of known structure will be required. The kinds of modifications with persulfate and peroxide, with one exception, are identical, and the promiscuity of SO_4^{-}• is similar and tunable like •OH. The choice for utilizing persulfate FPOP for non-residue-specific stable modification footprinting is best made considering its physical, rather than chemical properties. Most importantly, this study demonstrates the utility of the general FPOP method. That persulfate FPOP works serves as an invitation to try other UV-sensitive precursor molecules, such as L-photoleucine[23], or to use the sulfate radical anion to produce other radicals and radical anions (e.g., CO_3^{-}• from HCO_3^{-} or •NO_2 from NO_2^{-}). These approaches may give controllable radical species capable of very fast labeling, not only sampling native conformations is a non-specific or targeted way but also expanding the scope of FPOP.

4.5 Supporting Information

4.5.1 Global mass spectrometry of FPOP-labeled β-lactoglobulin.

The capacity of the 0.6 μL bed Ziptip$_{C4}$ was approximately 3.3 μg, so that 180-230 pmol samples of BLG were infused at a flow rate adjusted to ensure accuracy in the time-to-digital conversion of the QTOF multi-channel plate detector, requiring 80-180 ion counts/scan base peak. Scans spanning the entire chromatogram were summed to improve the signal to noise, typically 60-150 scans depending on the flow rate.

4.5.2 *β*-lactoglobulin FPOP global product distribution analysis.

A 1216-1245 *m/z* spectrum window centered about the 15th charge state of BLG was fit with a model FPOP product distribution described previously[13] for each BLG duplicate. The window range encompassed all detected product peaks, and a 10 *m/z* region lower than the unmodified peak average *m/z* was used for baseline estimation. A Mathcad 14 Minimize algorithm was used to fit a Poisson distribution to the resulting set of 0, +16, +32… state abundances.

4.5.3 Optimal Sodium Persulfate FPOP Conditions.

Tuning the level of radical exposure controls the kind and extent of modifications. Early footprinting work used Fenton-generated •OH radicals to cleave DNA and protein backbones; absence of a cleavage product was indicative of protection due to biomolecular interaction.[42] The ESI mass spectrum of BLG labeled by FPOP with 15 mM $Na_2S_2O_8$ and without Gln radical scavenger shows a background in each BLG charge state m/z region ≥ 20% the charge state's base peak (data not shown). We attribute this high baseline to the mass-spectral convolution of many protein fragments generated by radical-induced cleavage along the protein backbone. Under these

conditions, too much radical labeling agent has persisted for too long an exposure. The reactivity of protein side chains is, in general, not high at α-carbons because steric hindrance is protective under typical low-exposure conditions.[43-44] Thus, the identification and quantitation of side chain-modified residues for *scavenger-free* $Na_2S_2O_8$ FPOP-labeled protein would not measure the solvent accessibility at these sites in the protein's native state.

A more difficult problem is that this excessive labeling may also be the case with insufficient scavenger or too high a concentration of the radical precursor; that is, the quenching is not fast enough to stop labeling before side chain modifications cause protein conformational change leading to misleading labeling. Therefore, we undertook an analysis on the underlying protein product distributions of the Figure 4.1 spectra to support the hypothesis that 5 mM $Na_2S_2O_8$, 20 mM Gln (Figure 4.1c) is sufficient to label the native protein state without sampling partially unfolded products.

In a previous study, we provided empirical evidence that FPOP with H_2O_2 labels proteins faster than any conformational response to •OH modifications.[13] This result was based on the analysis of the mass spectra of the modified proteins, where a model was used to digitize signals for FPOP-labeled proteins into bins of primary modification of 0, +16, +32, … Da. Simplification of the modification spectrum to a 0, +16, +32, … distribution allowed for a comparison to a Poisson distribution. For BLG, CaM, and lysozyme, a good match occurred only when radical scavenger was present. Testing for a Poisson distribution, which should apply for proteins having an invariant single conformation during labeling and for which there are many sites available to •OH modification, is an appropriate means of establishing the "snapshot" nature of a

footprinting method . We employed the same analysis here, using BLG as the test protein because it is highly sensitive to conformational changes due to oxidation.[25] At 5 mM $Na_2S_2O_8$, the modification distribution is approximately Poisson (Supporting Information Figure 4.1), but when a larger number of sulfate anion radicals are produced with 15 mM $Na_2S_2O_8$, FPOP labeling gives a distribution that clearly fails this test. Moreover, modeling the latter spectrum failed to meet a requirement that at least 20% of protein signal should contribute to the unmodified, 0^{th} state. This requirement stems from matching the laser pulse frequency, irradiation volume, and sample flow rate to ensure that all labeled protein, and an un-reacted volume that is 20% of the irradiation volume, vacates the flow cell before the next laser shot. At 5 mM $Na_2S_2O_8$, the 20% exclusion fraction can be properly accounted for by the modeling, and the 0, +16, +32, … distribution is consistent with a single BLG conformation during labeling. Thus, the appropriate persulfate level for FPOP labeling is ≤ 5 mM $Na_2S_2O_8$, with 20 mM constituent Gln and laser and optics parameters set as described in the Experimental Procedures section.

4.5.4 Chemistry of $Na_2S_2O_8$ FPOP.

Comparing the product-formation reactivities of SO_4^{-}• and •OH requires quantitation with good precision of every detectable modification. Supporting Information Figure 4.2 shows the product-ion mass spectra for two unusual modifications. Kynurenination (Supporting Information Figure 4.2a, +3.9949) of tryptophan is not a major oxidation product in water radiolysis labeling of Trp-NH_2[31], but it is a common metal-catalyzed protein oxidation product.[45-47] This modification pathway significantly contributes to the total Trp modification with both H_2O_2 and persulfate

FPOP methods. A novel His and Tyr modification only seen with persulfate FPOP, however, is of +33.974 Da (Supporting Information Figure 4.2b), which comprises 50-90% of the total modification reactions of His but is of trivial abundance for Tyr. The nature of this modification has not yet been determined.

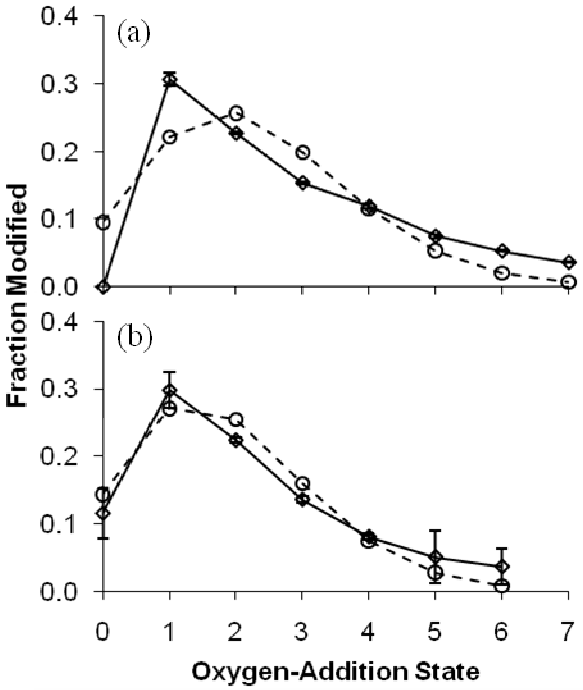

Supporting Information Figure 4.1: The 0, +16, +32, ... Da ion counts are modeled for the 15th charge state QTOF *m/z* spectrum of β-lactoglobulin. Solid line-connected diamonds with standard error bars plot the average of the normalized ion counts for duplicate FPOP treatments. Dashed line-connected circles show the non-linear regression, best-fitting Poisson distribution. (a) is for FPOP with 15 mM $Na_2S_2O_8$. (b) is for FPOP with 5 mM $Na_2S_2O_8$. The modeling was constrained to subtract 20% of total protein signal from the 0th state because this signal is attributed to the irradiation-masked FPOP volume. In case (a), all 0th state signal is attributed to this non-reaction fraction but is modeled as only 7.4% of total protein signal. The number of states per sample distribution fit to a Poisson was chosen to account for at least 98% of protein signal.

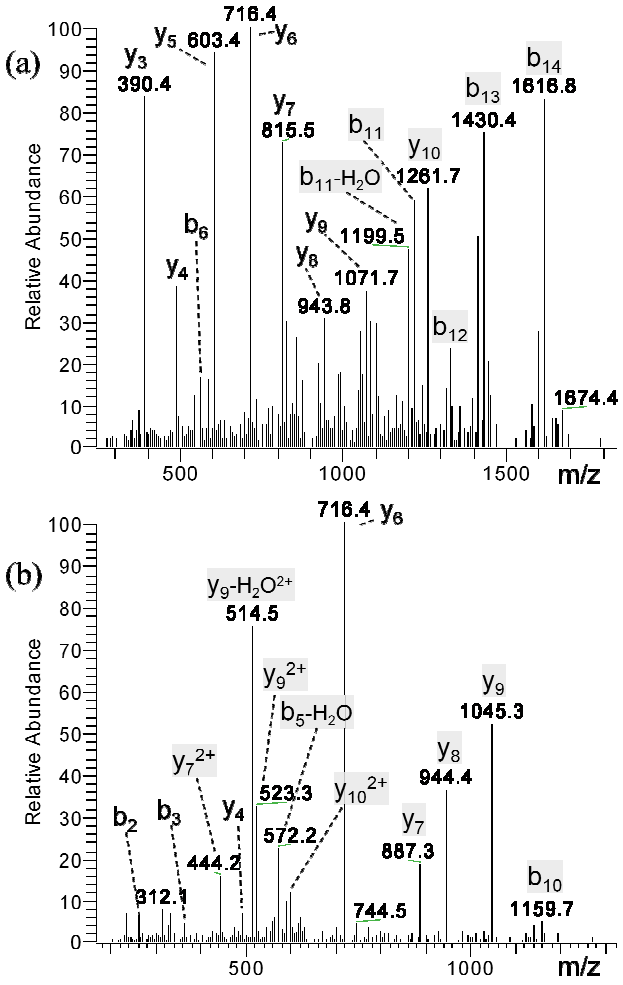

Supporting Information Figure 4.2: The LTQ product-ion spectra of myoglobin peptides showing uncommon •OH modifications. (a): $[M + 2H]^{2+}$ of *m/z* 910.4569. The annotation is for peaks matching the theoretical y- and b- fragment ions of GLSDGEW*QQVLNVWGK, with W7 modified by a net +4 Da (kynurenine) mass shift. Ions labeled in gray boxes carry this modification. These spectra were produced in both peroxide and persulfate FPOP replicates. (b): $[M +2 H]^{2+}$ of *m/z* 653.3199. The annotation is for LFTGH*PETLEK with H36 modified by a net +34 Da mass shift. Ions labeled in gray boxes carry this modification. This spectrum was only observed for persulfate FPOP replicates.

Supporting Information Table 4.1: Calcium-free Calmodulin Fraction Modified per Residue[a]

residue	SASA ($Å^2$)[a]	$k_{\cdot OH}$ (M^{-1} sec^{-1})[b]	native	peroxide	persulfate	persulfate control
T5	55.63	5.1×10^8	0.16 +/- 0.01%	1.25 +/- 0.05%	0.22 +/- 0.01%	0.15 +/- 0.02%
I9	58.52	1.8×10^9	0.026 +/- 0.005%	0.159 +/- 0.008%	0.022 +/- 0.007%	0.016 +/- 0.004%
F12	7.58	6.9×10^9	0.76 +/- 0.03%	2.9 +/- 0.2%	1.19 +/- 0.04%	0.67 +/- 0.01%
K13	112.84	3.5×10^8	0.20 +/- 0.01%	0.224 +/- 0.004%	0.17 +/- 0.01%	0.17 +/- 0.02%
T28	47.02	5.1×10^8	0.5 +/- 0.2%	2.6 +/- 0.4%	0.13 +/- 0.08%	0.06 +/- 0.04%
E31	46.21	2.3×10^8	2.6 +/- 0.4%	9.4 +/- 0.8%	7.8 +/- 0.4%	4 +/- 1%
M36	2.44	8.5×10^9	13 +/- 2%	35 +/- 2%	33 +/- 1%	15 +/- 4%
M76	39.87	8.5×10^9	24 +/- 1%	49 +/- 3%	62 +/- 2%	26 +/- 2%
S81	46.75	3.2×10^8	1.5 +/- 0.2%	4.3 +/- 0.3%	3.4 +/- 0.4%	2.3 +/- 0.5%
Y99	101.55	1.3×10^{10}	0.33 +/- 0.02%	2.0 +/- 0.2%	2.2 +/- 0.1%	0.22 +/- 0.02%
M109	0	8.5×10^9	17 +/- 2%	46 +/- 5%	45 +/- 3%	25 +/- 5%
M124	15.55	8.5×10^9	43 +/- 4%	79 +/- 9%	64 +/- 4%	46 +/- 6%
M144	43.19	8.5×10^9	37 +/- 2%	59 +/- 2%	58 +/- 3%	44 +/- 4%
M145	10.97	8.5×10^9	11 +/- 1%	49 +/- 7%	48 +/- 4%	19 +/- 2%

[a]All Table 4.1 footnotes apply except that 1CFC.pdb was used for the calmodulin SASA calculation (51).

Supporting Information Table 4.2: Peptide Mixture Fraction Modified per Residue

residue	$k_{\cdot OH}$ (M^{-1} sec^{-1})[a]	native	peroxide	persulfate	persulfate control
Y4_Angiotensin II	1.3×10^{10}	0.027 +/- 0.006%	11 +/- 4%	17.8 +/- 0.9%	0.8 +/- 0.1%
P7_Angiotensin II	6.5×10^8	0	1.7 +/- 0.4%	0.020 +/- 0.008%	0
F8_Angiotensin II	6.9×10^9	0.0010 +/- 0.0005%	6 +/- 1%	1.1 +/- 0.2%	0.0011 +/- 0.0002%
P2_Bradykinin	6.5×10^8	0.00015 +/- 0.00001%	0.4 +/- 0.2%	0.07 +/- 0.01%	0.00007 +/- 0.00003%
F5_Bradykinin	6.9×10^9	0.0016 +/- 0.0004%	7 +/- 2%	1.66 +/- 0.05%	0.05 +/- 0.04%
S6_Bradykinin	3.2×10^8	0.013 +/- 0.002%	1.9 +/- 0.7%	0.6 +/- 0.3%	0.3 +/- 0.1%
P7_Bradykinin	6.5×10^8	0.0008 +/- 0.0003%	3 +/- 2%	1.2 +/- 0.3%	0.00040 +/- 0.00001%
F8_Bradykinin	6.9×10^9	0.0008 +/- 0.0004%	3 +/- 1%	1.11 +/- 0.03%	0.0007 +/- 0.0004%

[a] http://allen.rad.nd.edu/browse compil.html.

4.6 References

1. Hambly, D. M.; Gross, M. L., In *The Encyclopedia of Mass Spectrometry: Ionization Methods*, Gross, M. L.; Caprioli, R. M., Eds. 2006; Vol. 6.
2. Guan, J.-Q.; Chance, M. R., Structural proteomics of macromolecular assemblies using oxidative footprinting and mass spectrometry. *Trends Biochem. Sci* **2005,** *10*, 583-592.
3. Galas, D. J.; Schmitz, A., DNAase footprinting a simple method for the detection of protein-DNA binding specificity. *Nucl. Acids Res.* **1978,** *5* (9), 3157-3170.
4. Chen, S.; Engen, J. R., Isotope Exchange and Covalent Modification Strategies for Studying Protein Structure and Function. *Cur. Anal. Chem.* **2009,** *5*, 205-212.
5. Xu, G.; Chance, M. R., Hydroxyl Radical-Mediated Modification of Proteins as Probes for Structural Proteomics. *Chem. Rev.* **2007,** *107* (8), 3514-3543.
6. Maleknia, S. D.; Brenowitz, M.; Chance, M. R., Millisecond Radiolytic Modification of Peptides by Synchrotron X-rays Identified by Mass Spectrometry. *Anal. Chem.* **1999,** *71* (18), 3965-3973.
7. Zhang, Z.; Smith, D. L., Determination of amide hydrogen exchange by mass spectrometry: A new tool for protein structure elucidation. *Protein Sci.* **1993,** *2* (4), 522-531.
8. Katta, V.; Chait, B. T., Hydrogen/deuterium exchange electrospray ionization mass spectrometry: a method for probing protein conformational changes in solution. *J. Am. Chem. Soc.* **1993,** *115* (14), 6317-6321.
9. Gabriela, E. G.; Ana, C.; Patricio, O. C.; Fernando, A. G.; José, M. D., Exploring protein interfaces with a general photochemical reagent. *Protein Sci.* **2006,** *15* (4), 744-752.
10. Patricio, O. C.; Daniela, B. U.; José, M. D., Probing protein conformation with a minimal photochemical reagent. *Protein Sci.* **2002,** *11* (6), 1353-1366.
11. Frederic, M. R.; Raphael, L.; Richard, W.; Darshan, P.; Gerard, O., Methylene as a possible universal footprinting reagent that will include hydrophobic surface areas: Overview and feasibility: Properties of diazirine as a precursor. *Protein Sci.* **2000,** *9* (12), 2506-2517.
12. Hambly, D. M.; Gross, M. L., Laser Flash Photolysis of Hydrogen Peroxide to Oxidize Protein Solvent-Accessible Residues on the Microsecond Timescale. *J. Am. Soc. Mass Spectrom.* **2005,** *16* (12), 2057-2063.
13. Gau, B. C.; Sharp, J. S.; Rempel, D. L.; Gross, M. L., Fast Photochemical Oxidation of Protein Footprints Faster than Protein Unfolding. *Anal. Chem.* **2009,** *81* (16), 6563-6571.
14. Davies, M. J.; Dean, R. T., *Radical-Mediated Protein Oxidation: From Chemistry to Medicine*. Oxford University Press: 1997.
15. Fancy, D. A.; Kodadek, T., Chemistry for the analysis of protein-protein interactions: Rapid and efficient cross-linking triggered by long wavelength light. *Proc. Natl. Acad. Sci. U.S.A.* **1999,** *96* (11), 6020-6024.
16. Rayshell, M.; Ross, J.; Werbin, H., Evidence that N-acetoxy-N-acetyl-2-aminofluorene crosslinks DNA to protein by a free radical mechanism. *Carcinogenesis* **1983,** *4* (5), 501-507.
17. Bridgewater, J. D.; Lim, J.; Vachet, R. W., Transition Metal-Peptide Binding Studied by Metal-Catalyzed Oxidation Reactions and Mass Spectrometry. *Anal. Chem.* **2006,** *78* (7), 2432-2438.
18. Davies, M. J.; Gilbert, B. C.; Norman, R. O. C., Electron spin resonance. Part 67. Oxidation of aliphatic sulphides and sulphoxides by the sulphate radical anion (SO_4^-) and of aliphatic radicals by the peroxydisulphate anion ($S_2O_8^{2-}$). *J. Chem. Soc., Perkin Trans. 2* **1984**, 503-509.

19. Davies, M. J.; Gilbert, B. C.; McCleland, C. W.; Thomas, C. B.; Young, J., E.s.r. evidence for the multiplicity of side-chain oxidation pathways in the acid-catalysed decomposition of substituted hydroxycyclohexadienyl radicals. *J. Chem. Soc., Chem. Commun.* **1984,** (15), 966-967.
20. Rustgi, S. N.; Riesz, P., An e.s.r. and spin-trapping study of the reactions of the SO4 radical with protein and nucleic acid constituents. *Int. J. Radiat. Biol.* **1978,** *34*, 301-316.
21. Ivanov, K. L.; Glebov, E. M.; Plyusnin, V. F.; Ivanov, Y. V.; Grivin, V. P.; Bazhin, N. M., Laser flash photolysis of sodium persulfate in aqueous solution with additions of dimethylformamide. *J. Photochem. Photobiol., A* **2000,** *133* (1-2), 99-104.
22. Chatgilialoglu, C.; Lunazzi, L.; Macciantelli, D.; Placucci, G., Absolute rate constants for hydrogen abstraction from aldehydes and conformational studies of the corresponding aromatic acyl radicals. *J. Am. Chem. Soc.* **1984,** *106* (18), 5252-5256.
23. Jumper, C. C.; Schriemer, D., Carbene-Labeling Strategy for Interface Mapping of Protein Complexes. In *58th ASMS Conference on Mass Spectrometry and Allied Topics*, Salt Lake City, UT, 2010.
24. Vidavsky, I.; Rempel, D. L.; Gross, M. L., 2D Mass Spectra Correlation – Semi Automatic Tool for Modified Peptide Discovery. In *Proceedings of the 54th ASMS Conference on Mass Spectrometry and Allied Topics*, Seattle, WA, 2006.
25. Venkatesh, S.; Tomer, K. B.; Sharp, J. S., Rapid identification of oxidation-induced conformational changes by kinetic analysis. *Rapid Commun. Mass Spectrom.* **2007,** *21* (23), 3927-3936.
26. Chung, H. S.; Ganim, Z.; Jones, K. C.; Tokmakoff, A., Transient 2D IR spectroscopy of ubiquitin unfolding dynamics. *Proc. Natl. Acad. Sci. U.S.A.* **2007,** *104* (36), 14237-14242.
27. Chung, H. S.; Khalil, M.; Smith, A. W.; Ganim, Z.; Tokmakoff, A., Conformational changes during the nanosecond-to-millisecond unfolding of ubiquitin. *Proc. Natl. Acad. Sci. U.S.A.* **2005,** *102* (3), 612-617.
28. Fenn, J. B., Ion formation from charged droplets: roles of geometry, energy, and time. *J. Am. Soc. Mass Spectrom.* **1993,** *4* (7), 524-535.
29. Gerstein, M., A resolution-sensitive procedure for comparing protein surfaces and its application to the comparison of antigen-combining sites. *Acta Crystallographica Section A* **1992,** *48* (3), 271-276.
30. Maurus, R.; Overall, C. M.; Bogumil, R.; Luo, Y.; Mauk, A. G.; Smith, M.; Brayer, G. D., A myoglobin variant with a polar substitution in a conserved hydrophobic cluster in the heme binding pocket. *Biochim. Biophys. Acta Prot. Struct. Mol. Enzym.* **1997,** *1341* (1), 1-13.
31. Xu, G.; Chance, M. R., Radiolytic Modification and Reactivity of Amino Acid Residues Serving as Structural Probes for Protein Footprinting. *Anal. Chem.* **2005,** *77* (14), 4549-4555.
32. Garrison, W. M., Reaction mechanisms in the radiolysis of peptides, polypeptides, and proteins. *Chem. Rev.* **1987,** *87* (2), 381-398.
33. Shechter, Y.; Burstein, Y.; Patchornik, A., Selective oxidation of methionine residues in proteins. *Biochemistry* **1975,** *14* (20), 4497-4503.
34. Saladino, J.; Liu, M.; Live, D.; Sharp, J. S., Aliphatic Peptidyl Hydroperoxides as a Source of Secondary Oxidation in Hydroxyl Radical Protein Footprinting. *J. Am. Soc. Mass Spectrom.* **2009,** *20* (6), 1123-1126.
35. Nath, A.; Atkins, W. M.; Sligar, S. G., Applications of Phospholipid Bilayer Nanodiscs in the Study of Membranes and Membrane Proteins *Biochemistry* **2007,** *46* (8), 2059-2069.
36. Rozga, M.; Bal, W., The Cu(II)/Ab/Human Serum Albumin Model of Control Mechanism for Copper-Related Amyloid Neurotoxicity. *Chemical Research in Toxicology* **2009**.

37. Marla, S. S.; Lee, J.; Groves, J. T., Peroxynitrite rapidly permeates phospholipid membranes. *Proc. Natl. Acad. Sci. U.S.A.* **1997,** *94* (26), 14243-14248.
38. Pryor, W. A.; Jin, X.; Squadrito, G. L., One- and two-electron oxidations of methionine by peroxynitrite. *Proc. Natl. Acad. Sci. U.S.A.* **1994,** *91* (23), 11173-11177.
39. Radi, R.; Beckman, J. S.; Bush, K. M.; Freeman, B. A., Peroxynitrite oxidation of sulfhydryls. The cytotoxic potential of superoxide and nitric oxide. *J. Biol. Chem.* **1991,** *266* (7), 4244-4250.
40. Santos, A. M.; Ph, V.; Graillat, C.; Guyot, A.; Guillot, J., Study of the thermal decomposition of potassium persulfate by potentiometry and capillary electrophoresis. *J. Polymer Sci. Polymer Chem.* **1996,** *34* (7), 1271-1281.
41. Rice, F. O.; Reiff, O. M., The Thermal Decomposition of Hydrogen Peroxide. *J. Phys. Chem.* **1927,** *31* (9), 1352-1356.
42. Heyduk, E.; Heyduk, T., Mapping Protein Domains Involved in Macromolecular Interactions: A Novel Protein Footprinting Approach. *Biochemistry* **1994,** *33* (32), 9643-9650.
43. Hawkins, C. L.; Davies, M. J., Generation and propagation of radical reactions on proteins. *Biochim. Biophys. Acta Bioenergetics* **2001,** *1504* (2-3), 196-219.
44. Hawkins, C. L.; Davies, M. J., EPR studies on the selectivity of hydroxyl radical attack on amino acids and peptides. *J. Chem. Soc., Perkin Trans.* **1998,** *2*, 2617-2622.
45. Stadtman, E. R.; Judith, P. K., Role of oxidized amino acids in protein breakdown and stability. In *Methods in Enzymology*, Academic Press: 1995; Vol. Volume 258, pp 379-393.
46. Finley, E. L.; Dillon, J.; Crouch, R. K.; Schey, K. L., Identification of tryptophan oxidation products in bovine alpha-crystallin. *Protein Sci.* **1998,** *7*, 2391-2397.
47. Sofia, G.; Rui, V.; Rosário, D.; Francisco, A.; Pedro, D., Oxidation of bovine serum albumin: identification of oxidation products and structural modifications. *Rapid Commun. Mass Spectrom.* **2009,** *23* (15), 2307-2315.

5 Mass Spectrometry-based Protein Footprinting Characterizes the Structures of Oligomeric Apolipoprotein E2, E3, and E4

5.1 Introduction

Apolipoprotein E is a 34 kDa protein, whose function is to regulate lipid metabolism and control lipid redistribution in tissue and cells, especially in the brain [1]. The three most common isoforms differ at two residues; apolipoprotein E2 (ApoE2) has cysteines at sites 112 and 158 whereas apolipoprotein E4 (ApoE4) has arginines at these residue sites. The most common isoform, apolipoprotein E3 (ApoE3), has C112 and R158. The ApoE4 isoform is strongly associated with Alzheimer's disease [2-3], and is a risk factor for several other diseases [4]. These risk associations, which ultimately stem from the single mutation C112R, differentiate ApoE4 from ApoE2 and ApoE3 in the preferred lipoprotein particle structure [5]. Structural determinations by X-ray crystallography and solution NMR of the lipid-free N-terminal domain showed it to be an elongated four-helix bundle[6-7]. Since then, no high resolution structures have been reported for the wild type isoforms or their C-terminal domains in the lipid-free state owing to the propensity of apoE isoforms to oligomerize.

The three ApoE isoforms each self-associate in a lipid-free solution, forming predominantly tetramers at μM concentration [8-12]. The rate constants for the association-dissociation process of monomer-dimer-tetramer have been determined by Garai and Frieden (8). Based on the most recent high resolution structure determination of the N-terminal domain, Sivashanmugam and Wang [7] proposed a scheme whereby lipid binding

to the C-terminal-domain induces the N-terminal four-helix bundle to open, thus allowing further lipid interaction. Potentially affecting this mechanism in a isoform-specific manner are the lipid-free domain interaction and kinetics of oligomerization. Clearly high resolution structures of the full-length isoforms would inform these inferences, but no structures of the oligomers are known at the atomic level. Thus, we undertook an implicit analysis of the full-length WT isoform structures at "residue resolution" by using mass spectrometry (MS)-based protein footprinting. The overarching question we pose is whether the amino acid accessibility of full-length ApoE2, ApoE3, and ApoE4 isoforms differ in their oligomeric states at μM concentrations. We also seek to identify those regions responsible for oligomeric interactions by comparing the protein footprints of WT ApoE3 with those of a monomeric mutant of ApoE3.

MS-based protein footprinting provides peptide and residue-resolved structural information in the primary sequence dimension [13-14]. The general strategy provides insight about the difference between the structure of a protein or a protein complex in two or more states rather than resolve their structures in three dimensions. The expectation is that labeling at solvent-accessible residues is attenuated at protein-ligand or protein-protein interfaces in the complex compared to those residues in the apo state. The approach is effective and efficient because, if the labeling is stable, identification of the modification sites can be done by using a proteomics-based "bottom-up" mass spectrometry methodology. In this methodology, proteolytic peptides are chromatographically resolved and detected in a hybrid mass spectrometer capable of monitoring their accurate mass-to-charge ratios at high resolving power. The

instrument's other spectrometer acquires the characteristic product ion spectra of peptide ions subjected to collisional activation in an elution-dependent manner. The high-resolution LC-MS intensities provide a quantitative measure of each peptide, and their product ion spectra, acquired in this tandem MS mode (MS^2), can indicate their identity and modification site(s).

An informative chemical footprinting method is hydroxyl radical-mediated modification of solvent accessible sidechains (for a comprehensive review detailing several methodologies for •OH generation, expected product chemistry, and MS analysis, see ref. [15]). Hydroxyl-radical labeling is advantageous because it effectively samples solvent accessibility, given that •OH has the same size as water, and it imparts stable (irreversible) modifications to solvent-accessible sidechains of over half of the common amino acids [16]. Here we used the method of fast photochemical oxidation of proteins (FPOP), as developed by Hambly and Gross with an approach is similar to that of Aye and coworkers [17-18]. In the FPOP method, low millimolar levels of H_2O_2 are homolytically cleaved by a 17 ns flash of 248 nm light from a KrF excimer laser source. The resultant •OH reacts with the side chains of constituent proteins. An important feature of FPOP is the reaction time scale can be controlled and in the presence of the scavenger glutamine, the lifetime of the radical is approximately 1 μs. The use of a radical scavenger ensures that only equilibrium conformations are sampled by •OH; any modification-induced changes to conformation would evolve on a longer timescale [17, 19]. To corroborate the FPOP results, we also employed a method of acidic-side-chain footprinting, using glycine ethyl ester (GEE) and a zero-length cross-linker [20-22].

5.2 Experimental Procedures

5.2.1 Reagents.

Acetonitrile, acetic acid, formic acid, 30% hydrogen peroxide, *L*-glutamine, *L*-methionine, *tris*(2-carboxyethyl)phosphine hydrochloride (TCEP), catalase, guanidinium hydrochloride, glycine ethyl ester (GEE), 1-ethyl-3-(3-dimethylaminopropyl)carbodiimide (EDC), 2-amino-2-hydroxymethyl-propane-1,3-diol (Tris base), and phosphate buffered saline (PBS) were purchased from Sigma Aldrich Chemical Co. (St. Louis, MO). Trypsin, sequencing grade, was purchased from Roche Diagnostics Corp. (Indianapolis, IN). Purified water (18 MΩ) was obtained from a Milli-Q Synthesis system (Millipore, Billerica, MA).

5.2.2 Protein Expression, Mutagenesis, Purification, and Solubilization.

ApoE2, ApoE3, ApoE4, and ApoE3MM, each expressed in *E. coli*, were kindly provided by Drs. K. Garai and C. Frieden. All proteins was dissolved in 6 M guanidinium chloride and dialyzed overnight into phosphate buffered saline (PBS) solution containing 100 μM TCEP disulfide reductant. Protein concentrations were determined by measuring their 280 nm absorbance using $\varepsilon_{280} = 44950\ M^{-1}\ cm^{-1}$. The resultant solutions were stored as aliquots at -80 °C after $N_2(l)$ freezing.

5.2.3 FPOP labeling.

The FPOP labeling of ApoE3MM and ApoE3 in the monomer/oligomer experiment was performed on the same days under the same conditions for both proteins. Each started with a 3 h, 22 °C equilibration of 4 μM protein containing 20 mM Gln and

100 μM TCEP in PBS. Three replicates were drawn from each of these solutions for FPOP labeling. Just prior to FPOP, H_2O_2 was added to each replicate by 10-fold dilution from a concentrated solution, to give a final concentration of 40 mM. The FPOP apparatus was essentially the same as originally described [17]. The KrF excimer laser power (GAM Laser Inc., Orlando, FL) was adjusted to 39 mJ/pulse and its pulse frequency set to 5 Hz. The flow rate was adjusted to ensure a 25% exclusion volume to avoid repeat •OH exposure[19]. Each replicate was collected in a microcentrifuge tube containing 10 μL of 200 fM catalase and Met to give a final concentration of 20 mM in the total sample volume. The addition of Met was to mitigate post-FPOP oxidation of protein [23]. Catalase was allowed to oxidize H_2O_2 to $O_2(g)$ for 10 min at room temperature with pipette mixing; $O_2(g)$ was removed by three centrifugation steps during the incubation. After 10 min, samples were frozen by immersion in $N_2(l)$ and stored at -80 °C prior to proteolysis. Control samples were handled in the same manner as those submitted to FPOP, but they were not laser irradiated; instead, they were incubated for 5 min with H_2O_2, after which the solution was added to the catalase-methionine collection volume. The FPOP labeling of WT-ApoE2, ApoE3, and ApoE4 was performed as described above with the following exceptions: the final H_2O_2 concentration was 20 mM, and the excimer laser power was measured to be 47 mJ/pulse.

5.2.4 Carboxylic Acid labeling with GEE.

For the monomer/oligomer experiment, samples were drawn from the same ApoE3 and ApoE3MM equilibrated solution as was used for FPOP labeling, at approximately the same time. GEE was added to a final concentration of 50 mM to a

portion of each equilibrated solution. Samples were drawn from this solution, and EDC was added to each to give a final concentration of 5 mM. One molar acetic acid was added to a final concentration of 0.5 M to quench the reaction after a certain incubation period starting after the addition of EDC. Instead of running standard control samples for the GEE labeling, time-dependent data were obtained for GEE/EDC exposures times of 1, 3, 6, and 12 min for labeled ApoE3 and ApoE3MM samples, in duplicate, to provide a data trend. Samples were frozen in $N_2(l)$ and stored at -80 °C prior to proteolysis.

5.2.5 Proteolysis.

GEE-labeled samples were thawed and concentrated with Millipore Ziptip$_{C4}$ prior to proteolysis; the eluent, 5 μL 50% acetonitrile acid-free, was diluted to 45 μL with 250 mM Tris buffer, pH 7.3. FPOP-labeled and control samples were thawed and used as such for proteolysis. All samples were proteolyzed with 8:1 protein:trypsin (by weight) at 37 °C for 3 h. ESI MS of several control replicates on a Bruker Maxis Q-TOF verified that the digestion was complete. The samples were concentrated 3-fold by SpeedVac drying at 30 °C, then immobilized on Millipore Ziptip$_{C18}$, de-salted with elution into 10 μL of 50% acetonitrile 1% formic acid solution. A portion of this was diluted 25-fold with water and 0.1% formic acid for autosampler loading and subsequent analysis.

5.2.6 LC-MS/MS acquisition.

The experiments were not analyzed by LC-MS/MS contiguously; a new column was packed for each, and the nanospray source conditions varied slightly for each analysis. Five microliters of each replicate was loaded by autosampler onto a 20 cm column with a PicoFrit tip (New Objective, Inc, Woburn, MA), bomb-packed with C18

reverse phase material (Magic, 0.075 mm × 200 mm, 5 μm, 300 Å, Michrom, Auburn, CA). Peptides were eluted by a 70 min, 260 nL/min gradient coupled to the nanospray source of an LTQ-Orbitrap mass spectrometer (Thermo Fisher, Waltham, MA). Mass spectra were obtained at high mass resolving power (100,000 for ions of *m*/*z* 400) on the Orbitrap component, and the six most abundant ions eluting per scan were each subjected to CID MS^2 experiment in the LTQ component, using a collision energy 35% of the maximum, a 2 Da isolation width, and wideband activation. Precursor ions were added to a dynamic exclusion list for 8 s to ensure good sampling of the apex of their elution peaks. Blanks were run between every sample acquisition.

5.2.7 Data analysis.

The Rosetta Elucidator data management system (Rosetta Biosoftware) was used to generate tables of all LC-MS features eluting in time at high *m/z* resolution (± 5 ppm); all quantitation was based on ion abundances from extracted ion chromatograms. Usually more than one high resolution feature mapped to a single eluting peptide, owing to the splitting of its ion signal among multiple charge states and isotopomers. All such features contributed to the measure of total peptide abundance. Most modified and unmodified peptide features were annotated by error-tolerant Mascot database searching (Matrix Science, Boston, MA), with the common •OH outcomes added to its variable modification database [15]. An Excel visual basic-assisted strategy was employed to validate questionable Mascot-error tolerant calls. Ultimately the CID product-ion spectra of over two thirds of all calls were checked manually. Additional features having no Mascot annotations were included if their ions' m/z matched those of putative tryptic

ApoE modified or unmodified peptides within 8 ppm, and they had product-ion spectra that were consistent (manual interpretation) with these calls. This manual validation was assisted by using a custom correlation algorithm that compared these spectra to exemplary CID fragment spectra of unmodified tryptic peptides of the WT isoforms and ApoE3MM[24].

The labeling yield per residue is determined according to equation 1.

$$i^{th}\ residue\ yield = \frac{\sum peptide\ abundances\ modified\ at\ residue\ i}{\sum peptide\ abundances\ with\ same\ 1°\ sequence\ as\ numerator\ peptides} \quad (1)$$

Equation 1 avoids a potential underestimation bias by excluding the measured abundances for large peptides in the denominator, whose modified siblings did not give CID MS^2 spectra definitively locating their modification sites. Typically these large peptides are those which were not completely cleaved by trypsin. . Comparing FPOP and control yields shows that, with one exception, there is no evidence that FPOP introduces a proteolytic bias, which could undermine eq 1. We do observe a low abundance of the •OH-mediated loss of 43 u as a portion of the guanidino-group of Arg[15]; we have not included these low-abundant data because of their clear influence on trypsin proteolysis.

5.3 Results

5.3.1 Data Acquisition and Processing.

We determined the FPOP footprints of the WT isoforms existing as oligomers, as they do at low μM concentrations [8, 10-11, 25-26] (Supporting Information Table 5.1 presents the per-residue FPOP yields determined from all validated LC-MS features). In this residue-resolved analysis, we tracked 266 unmodified and modified tryptic peptides of

the isoforms, from 1,457 extracted ion LC-MS chromatographic (EIC) ions comprising 67.8% of all eluting ions. We were able to find peptides from all regions of the protein after FPOP labeling and trypsin proteolysis except for the region 39-61. Although peptide 39-61 is detectable as unmodified, it was not well sampled upon FPOP owing to its low abundance or response. Nevertheless, approximately one in five residues was FPOP-modified at 0.1% or greater yield. One of FPOP's virtues is that, though the reaction window is short, protein labeling is high yield. Consequently many solvent exposed residues of marginal reactivity can still be assayed as compared to the same kind of residues in synchrotron radiolysis •OH footprinting [27-29]. Same-day labeling, same-column separation in LC/MS, and the Rosetta Elucidator peak alignment software ensured that the same modified and unmodified-peptide features were used in determining the residue yields for all WT samples. We, therefore, attribute any significant differences in residue yields to differences in solvent-accessible surface areas (SASA) of the isoforms, as all other sources of bias are shared identically.

The average residue labeling yield per amino-acid type is similar but not identical to the known reaction rates of •OH with free amino acids [30], and to the MS analysis of •OH –amino amide reaction products [16]. We observe Cys > Met > Trp > His > Gln > Tyr > Phe > Asp > Pro > Glu > Leu > Val > Arg > Lys. Differences between inherent and observed reactivity are due to the structural context of residues, as their inherent amino acid-reactivity with •OH is mitigated by solvent accessibility in a properly controlled footprinting experiment. For example, Gln is less reactive with •OH than is Tyr or Phe as a free amino acid or amide. Being more hydrophilic than these residues, however, Gln is

likely to be more solvent-exposed in a protein and so may suffer experience a higher level of modification than a more reactive amino acid that is protected in some way (Supporting Information Table 5.1, Q21 yield > Y162 yield).

The results are presented as a difference in labeling yield per residue as normalized to the average labeling yield for all residues of the same amino-acid type (Figures 5.1, 5.2, and 5.3). A value above the x axis indicates more labeling in the comparison protein than at the same site in ApoE3. Values below convey the opposite trend. The extent of labeling is a function of the SASA of a site, and its inherent fully-solvent-exposed reactivity with •OH. We observe a linear correlation between the SASA of residues of the same amino acid type and their FPOP yield (data not shown). Thus, by normalizing each residue's yield by the maximum FPOP yield among all same-amino acid residues, the inherent reactivity dependence is eliminated, and we may compare the yields of dissimilar-amino acid residues. Furthermore, the normalization of the yield difference between isoforms ensures that a departure from near zero labeling at a residue is not misinterpreted as complete exposure of the residue in one protein state, and complete concealment in its comparison state.

5.3.2 WT-ApoE2 vs. ApoE3 vs. ApoE4.

The extent of modification per residue for WT-ApoE2, ApoE3, and ApoE4 are very similar, although ApoE4 exhibits more differences with ApoE3 than does ApoE2. In Figure1A, all detected residues shared by ApoE3 and ApoE4 are shown. Only M108, Y162, P183, V185, and E266 are significantly different at a 95% confidence by a Student's t-test. In Figure 5.2A, all detected residues shared by ApoE3 and ApoE2 are

shown. Tyrosine 162, E255, and E266 are significantly different. If the uncertainties in yield measurements were zero, the differences in labeling, and therefore in solvent accessibility change, are small for the majority of the residues. Comparing ApoE4 to ApoE3, 43 of 56 residues exhibit a change of less than 15% relative to the maximum SASA of each kind of amino acid in the proteins. Comparing ApoE2 to ApoE3, 49 of 56 residues also exhibit a maximum-amino acid-area-relative change of less than 15%.

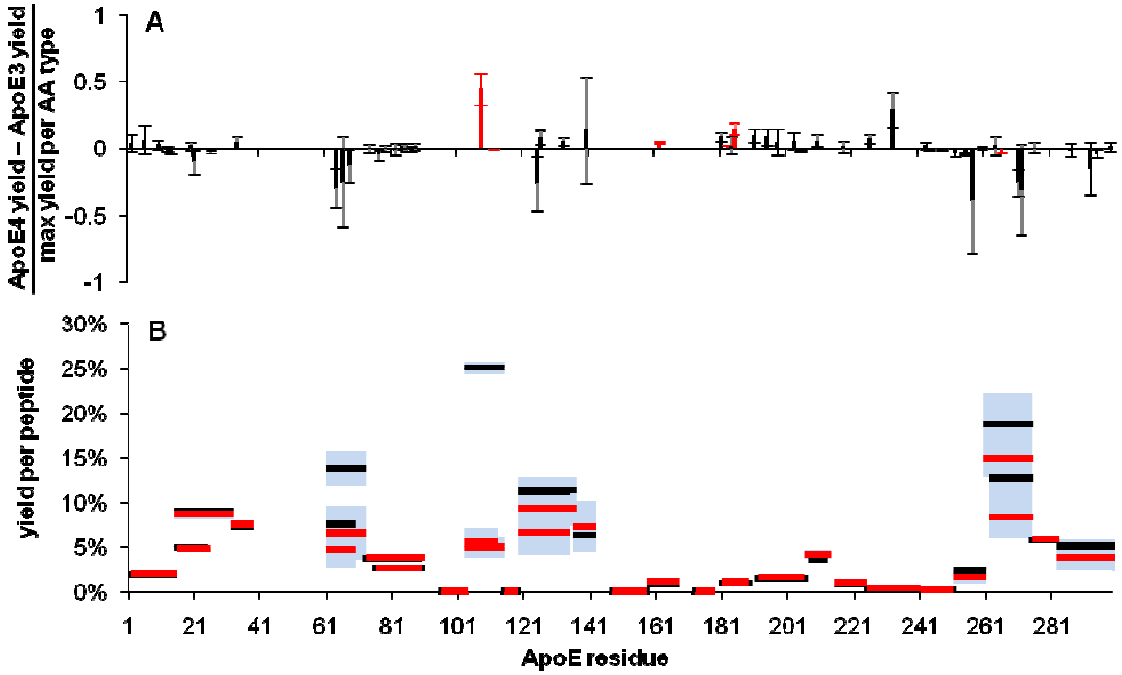

Figure 5.1: Comparison of the tryptic-peptide-resolved and residue-resolved FPOP labeling yields for ApoE3 and ApoE4. Panel **A** plots the difference in yield per residue between isoforms, relative to the maximum yield per residue for all residues of the same amino-acid type. Background modification yields observed in the control experiments are subtracted from their corresponding FPOP yields before the relative value is determined. Error bars are propagated from the standard errors of the per-residue average labeling yields for ApoE3 FPOP, ApoE3 control, ApoE4 FPOP, and ApoE4 control treatments. Residues M108, Y162, P183, V185, and E266, shown in red, are significantly different between isoforms at 95% confidence by the Student's t-test. Panel **B** plots the FPOP labeling yield/tryptic peptide of ApoE3 in black and ApoE4 in red. The background modification fraction per peptide has been subtracted. The light-blue areas convey the standard error of each labeling measurement. Where peptides exhibit very similar labeling levels, the red ApoE4 may bars obscure the ApoE3 bars.

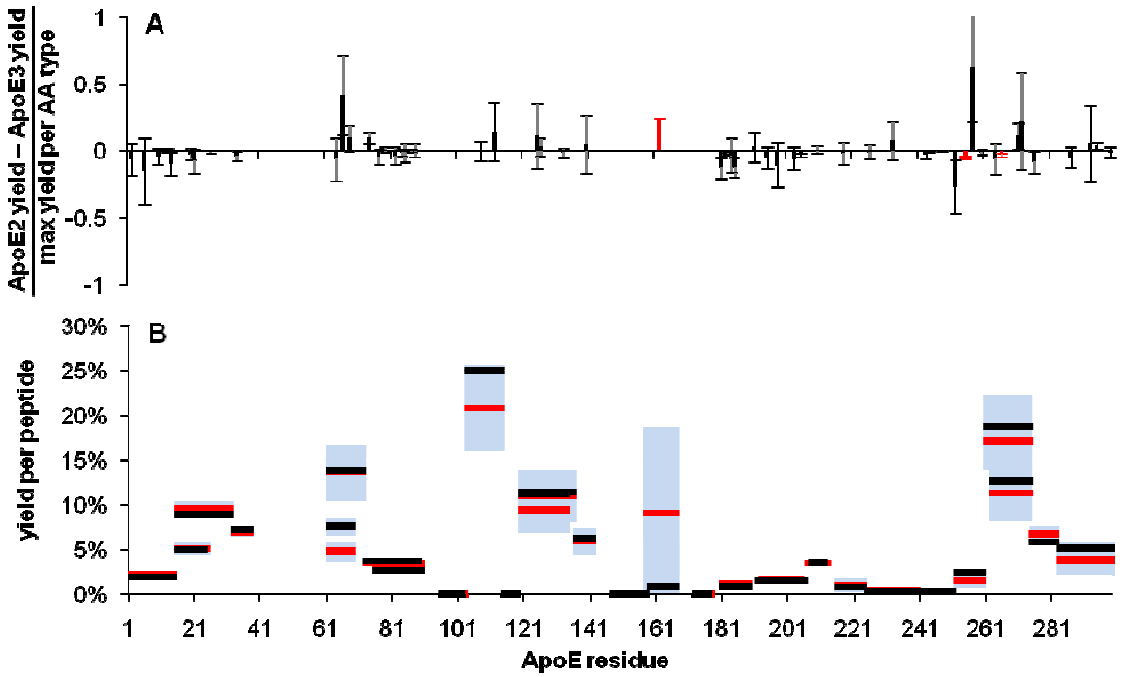

Figure 5.2: Comparison of the tryptic-peptide-resolved and residue-resolved FPOP labeling yields for ApoE2 and ApoE3. Panel **A** plots the difference in yield per residue between isoforms, relative to the maximum yield per residue for all residues of the same amino-acid type. Background modification yields observed in the control experiments are subtracted from their corresponding FPOP yields before the relative value is determined. Error bars are determined as described in Figure 5.1. The asterisked residues Y162, E255, and E266, shown in red, are significantly different between isoforms at 95% confidence by the Student's t-test. Panel **B** plots the FPOP labeling yield/tryptic peptide of ApoE3 in black and ApoE2 in red. The background modification fraction per peptide has been subtracted. The light-blue areas convey the standard error of each labeling measurement. Where peptides exhibit very similar labeling levels, the red ApoE2 may bars obscure the ApoE3 bars.

We contend that a 15% change in SASA relative to the maximum SASA for the same kind of residues is small. In absolute square ångstroms, a 15% change could be less than 5 or more than 30, depending on the type of residue—but relative to fully-exposed sidechain surface areas, this is a small area. For example, W20 in the truncated protein ApoE3 1-183 has a SASA value of 199 $Å^2$, determined by the GETAREA algorithm[31] for the 1kc3.pdb NMR structure[7]. The relative SASA change is due to at least two different protein oligomer conformations. In the simplest scenario one conformation would exclusively describe 4 μM ApoE3, and the other would exclusively belong to the other ApoE isoform at 4 μM. In this case a statistically-significant amino acid-relative labeling change is directly attributed to a change in the surface areas of each conformation. If the change were less than 15% we would conclude the isoform is only slightly more exposed or protected than ApoE3. This is the case for three of the five residues in ApoE4 significantly different from their ApoE3 analogs: Y162 and P183 are slightly more exposed, with same-amino acid-relative changes of 7% and 5%, respectively, while E266 is slightly protected, with a relative change of -10%. Two of the three significantly different residues in ApoE2 compared to ApoE3, are not substantially so: relative to the average of all glutamic acid yields, E255 shows a -17% and E266 a -10% change in labeling.

The extent of modification per peptide between the isoforms is also similar (Figures 1B and 2B). The analysis at the peptide level affords the inclusion of 88 more features than the analysis at the residue level. Each added feature's precursor mass is within 5 ppm of a theoretical ApoE peptide mass, and each had an MS^2 spectrum that

confirmed the identity of the root peptide sequence; however, each added feature's modification could not be localized to a single residue by its MS^2 spectrum. The inclusion of these features provides for the most accurate measure of the peptide FPOP-labeling yield. Comparing ApoE4 to ApoE3 (Figure 5.1B), 22 of 29 peptides exhibited statistically identical labeling yields. Peptides spanning 62-72, 120-134, and 261-274 each exhibit slightly more labeling in ApoE4 than ApoE3, while 104-112 is significantly more labeled in ApoE3. Comparing ApoE2 to ApoE3 (Figure 5.2B), only peptide 62-68 is significantly different, with less labeling in ApoE2.

The wild-type isoforms are similar in their response to FPOP labeling and the residue-resolved differences are small compared to the average level of labeling measured per amino-acid type. The one exception to this trend is M108. Its modification level (5 ± 1%) is high for ApoE4,whereas M108 undergoes negligible modification for ApoE2 and ApoE3. This effect cannot be confirmed with peptide-level analysis because signals corresponding to modified C112 are included in the consideration of ApoE3 104-114 but cannot be for ApoE4 104-112 and ApoE4 104-114 tryptic peptides. This difference suggests a structural difference in the region of ApoE4 with respect to the other isoforms. It is also possible that C112, which is missing in E4, outcompetes M108 in ApoE3 or that the MS detection of M108 modification may have been obscured by the multiple C112 modification fates[32].

The modification extent for 158-167 of ApoE2 (Figure2B) is also high because its primary modification is of C158, an amino-acid that is not present in ApoE3 and ApoE4. The modification extent of Met also distinguishes ApoE 62-72 from the corresponding

peptides of ApoE4 and ApoE3; in this case, ApoE4 is appreciably less labeled than that in ApoE3. A pair-wise residue comparison does not resolve this difference at 95% confidence (M64 $p = 0.11$), but the modification levels of M64, E66, and M68 together give rise to peptide signals that are significantly different. This underscores the need to examine footprinting data at several levels of sequence context. The variance in Met and Cys modification yields, although large, is not unusual, owing to the high sensitivity of sulfur-containing residues to endogenous reactive oxygen species and to oxidation during handling before and after the labeling experiment [15, 33-34].

5.3.3 ApoE3 vs. ApoE3 Monomeric Mutant.

It is clear that in the C-terminal and linker domains the FPOP yields at the residue level of ApoE3MM are higher than those of WT-ApoE3 (Figure 5.3A). This conclusion is based on analysis of 323 unmodified and modified tryptic peptides of ApoE3 and ApoE3MM, from 1,182 EIC features comprising 67.2% of all detected features (Supporting Information Table 5.2). The criteria for inclusion are identical to those applied to the WT isoform experiment. One in four residues is detected as modified. The order of reactivity is nearly identical to that observed for •OH footprinting of the WT protein. Figure 5.3A plots only the residues which are significantly different between ApoE3 and ApoE3MM, at 95% confidence. A total of 26 residues spanning residues 167 to 299 show significantly greater labeling for ApoE3MM, indicating these sites are more solvent-protected in the WT protein than the MM. Clearly the C-terminal domain is involved in WT oligomerization, as was inferred from previous studies [10, 35]. The high density of protected sites in regions 183-205 and 232-251 may indicate localized regions

of oligomeric interaction in the WT. Other sites in the C-terminal domain can't fairly be compared. Sites 257, 264, and 287 were detected as modified in both proteins. These are three of the four mutation sites (F257A, W264R, L279Q, and V287E) that together engender monomericity[36]. We do not compare their signals because each residue's inherent •OH reactivity is different from its analog, no matter their possible difference in SASA.

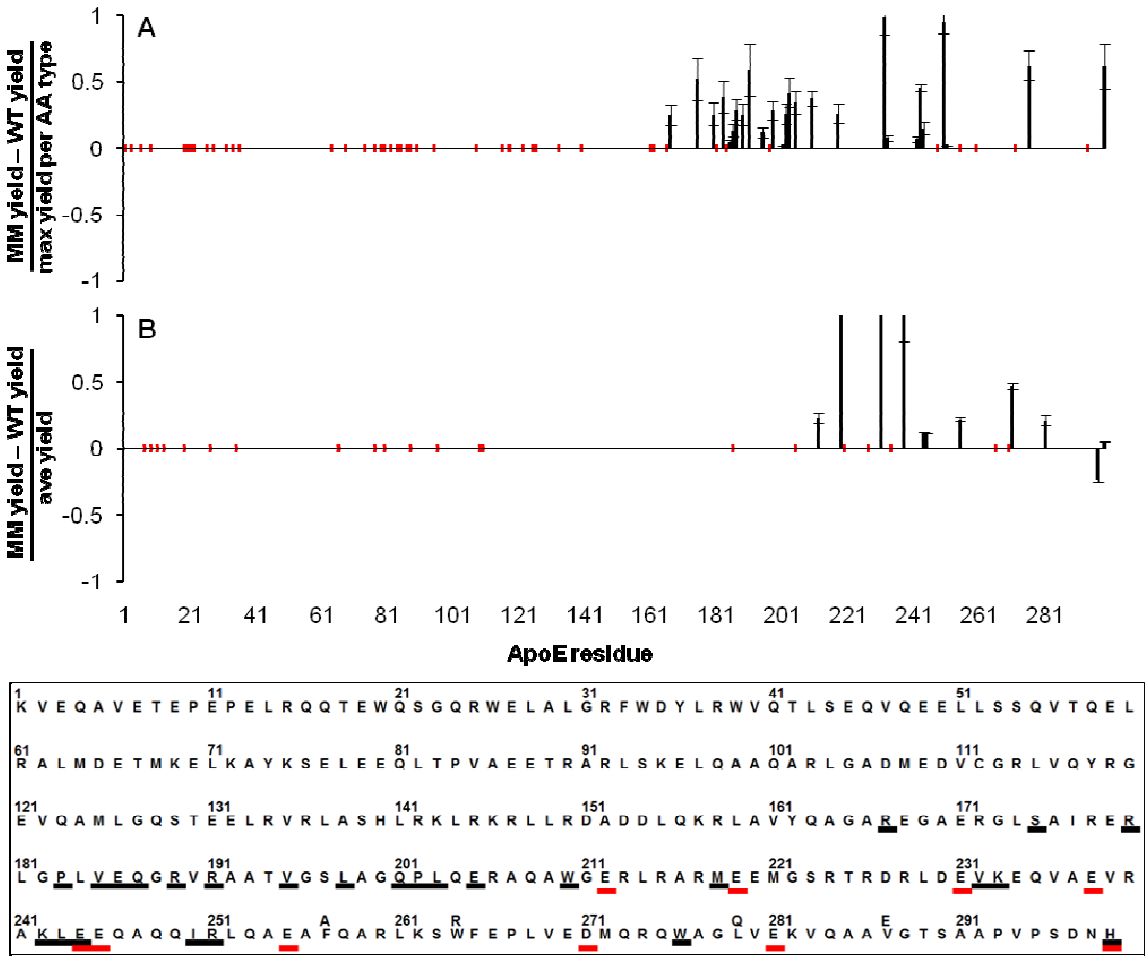

Figure 5.3: Comparison of the tryptic-peptide-resolved and residue-resolved FPOP and GEE labeling yields for ApoE3 and ApoE3MM. Panel **A** plots the residue-resolved significant differences in FPOP yields between the proteins. Each yield difference is normalized to the maximum yield per residue for all residues of the same amino-acid type, averaged from all FPOP experiments. Background modification yields observed in the control experiments are subtracted from their corresponding FPOP yields before the relative value is determined. Error bars are determined as described in Figure 5.1. Significance was determined at 95% confidence by the Student's t-test. Panel **B** plots the residue-resolved significant differences in 3 min GEE yields between the proteins. Each yield difference is normalized to the average yield per residue for all acidic residues, averaged from all 3 min GEE experiments. Error bars are the normalized standard errors for the 3 min measurement. Significant difference was defined as at least 2 GEE labeling time points exhibiting a difference at 95% confidence by the Student's t-test, and having the same sign. The bottom panel shows the residues along the ApoE3

primary sequence exhibiting more labeling in the monomeric mutant. Black-underlined residues convey the significant FPOP labeling difference; red-underlined residues the significant GEE labeling difference.

5.3.4 Glycyl Ethyl Ether (GEE) Footprinting.

To corroborate the findings in the FPOP monomer/oligomer experiment, we employed a second footprinting approach whereby carboxyl side chains were submitted to a GEE modification. As with the FPOP data, quantitation was based on unmodified and modified LC-MS EIC features, with annotation accepted if the precursor ion is within 5 ppm mass tolerance of theory and the product-ion spectra (MS^2) is acceptable. A control whereby the protein is not submitted to modification is unnecessary for this kind of labeling because exogenous background modifications at +85.0528 D are highly unlikely in the protein prior to modification and do not occur during peptide workup. In the absence of GEE-induced unfolding, the time-dependence for the modification level should be monotonic; consequently, we used four GEE exposure times to more reliably differentiate the labeling yields of the acidic residues (Supporting Information Table 5.3). Two exemplary kinetic plots show that E212 is consistently more modified in ApoE3MM (Figure4a) whereas E109 is labeled nearly identically and at a lower level for both proteins (Figure4b). This analysis informs a conservative criterion for assigning difference per acidic residue: by 3 min the pair-wise Student's t-test should show a significant difference at 95% confidence, and this trend should also pertain at 6 and 12 min. By this criterion the significantly different residues are plotted in Figure 5.3B, showing their 3 min labeling yields.

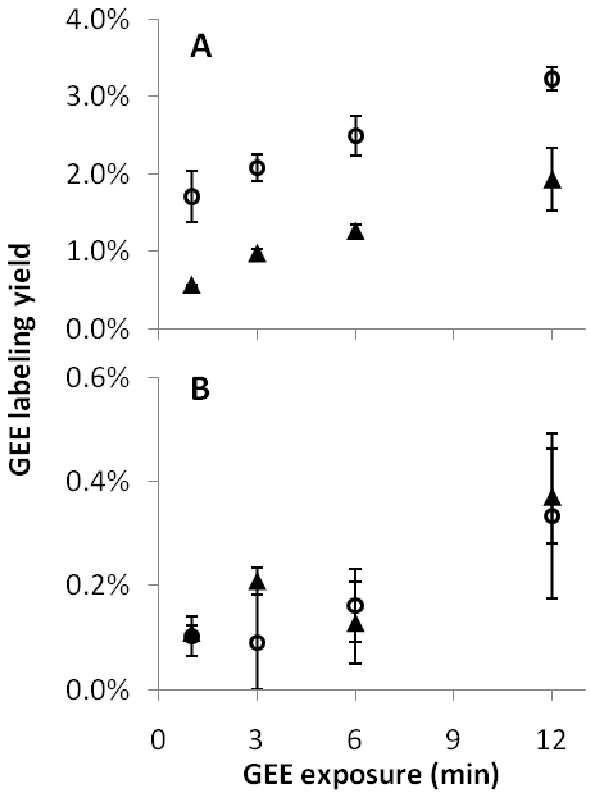

Figure 5.4: Exemplary plots of GEE labeling for 2 residues. Open circles denote ApoE3MM GEE-modified yields at 4 time points; solid triangles denote the ApoE3 yields. Residue E212 data is shown in plot **A**. Residue E109 data is shown in plot **B**.

The results from GEE labeling corroborate the findings of the per-residue FPOP results. Figure 5.3D shows those residues that are more significantly labeled by FPOP (black) or GEE (blue) in the monomeric mutant. Analysis of FPOP data at the peptide level conveys the same C-terminal domain trend and also shows that ApoE3MM 16-25 and 33-38 are slightly though significantly more labeled than the same regions of ApoE3. The magnitudes of change in FPOP labeling for ApoE3 vs. ApoE3MM at the residue level are, in general, more than three times greater than the changes seen comparing the three WT isoforms, and are more numerous. By virtue of the normalization discussed

above, the magnitude of change measured in the monomer/oligomer experiment is indicative of a larger SASA change between monomer and oligomer, than is seen between WT isoforms explored in the 1st experiment.

5.4 Discussion

5.4.1 Structures of the ApoE isoforms.

We conclude that the overall structures (mixtures of structures) are nearly the same for the three ApoE isoforms by invoking a syllogism. (1) FPOP snapshot –labels an ensemble of conformations and complexes at equilibrium[17, 19]. (2) Of the 56 residues detected as modified among the isoforms, 95% were modified at statistically equivalent levels for ApoE2 and ApoE3, and 91% were so modified for ApoE3 and ApoE4. (3) Therefore, the overall structures of the ApoE isoforms as measured by this technique are similar with one exception, to be discussed later.

Garai and Frieden[8] have modeled the isoform monomer, dimer, and tetramer concentrations as a function of the total monomer concentration, based on self-association rate constants for a monomer-dimer-tetramer model determined from FRET kinetics measurements. At 4 μM total protein, their model shows that 84% of proteins are bound as tetramers, irrespective of the ApoE isoform. A reasonable conclusion from the similarity in FPOP response among the ApoE isoforms, given the high prevalence of the tetrameric component in the oligomer state studied here, is that the ApoE2, ApoE3, and ApoE4 tetrameric structures are highly similar.

Despite the strong similarities in overall structure, the region of ApoE4 around M108 is different from that of ApoE2 and E3. The extensive modification of M108 in

ApoE4 shows that it is somewhat solvent-accessible, whereas the near lack of modification in ApoE3 and E2 indicates that M108 is buried, consistent with the high resolution structures of the N-terminal ApoE3 domain [6, 37]. The exposure of M108 in E4 can occur by an intra or intermolecular interaction pulling on the 50-79 α helix (Figure 5.5). Supporting this model are the M64 and M68 FPOP yields, which are slightly diminished in ApoE4 relative to those for ApoE3. On the other hand, the sensitivity of methionine to •OH-mediated modification the overall change in SASA may not require a substantially different oligomeric structural model.

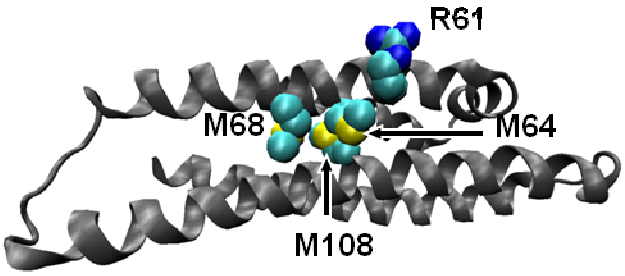

Figure 5.5: ApoE4 24-162 X-ray crystal structure[38] with R61, M64, M68, and M108 sidechains depicted by element type and van der Waals radius.

5.4.2 Solvent Accessibility of N- vs. C-terminal Regions.

A comparison of the FPOP modification extents for the Trp residues shows that the carboxyl-terminal Trp residues are more solvent exposed than the N-terminal Trp residues for each isoform (Supporting Information Table 5.1). For example, W264 is the most efficiently modified Trp, followed by W276, W210, and then the N-terminus Trp residues. W39 cannot be detected as modified, although this may be due to the low abundance of tryptic peptide 39-61. A similar conclusion was reached by Garai et al. [39] using apoE labeled with ^{19}F tryptophan . Our conclusion arises from a comparison of the

FPOP yields for same-amino-acid-type residues from the same protein. These comparisons may allow more insightful conclusions about protein structure than yield comparisons of same residue in two different protein isoforms. Essentially, residues of the same type may be ranked in order of their yield; those at the top of the list should have the highest SASA.

5.4.3 Regions of oligomeric interaction.

This is the first study of only full-length ApoE that shows that the C-terminal domain is the primary region of self-association in the tetrameric form, which has long been the hypothesis[5, 10-11].Westerlund and Weisgraber [10] showed in sedimentation experiments of C-terminal-truncated ApoE3 isoforms that region 267-299 is essential to association. This conclusion was reinforced by using several biophysical techniques for similar truncated ApoE isoforms [9, 25]. Furthermore, the 10 kDa C-terminal domain itself oligomerizes [11]. The choice of ApoE3MM used in our study was determined by the observation that mutations at F257, W264, V269, L179, and V287 resulted in a monomeric form in both the C-terminal domain alone [35] and the full-length apoE3 protein [36]. A substantial number of residues in the C-terminal and hinge domains are more solvent-accessible in the monomeric mutant than in the ApoE3 WT isoform, whereas modifications of their N-terminal domains are statistically identical. Moreover, this result is demonstrated by two independent footprinting methods, FPOP and GEE labeling (Figure 5.3), with a high degree of consistency. The FPOP data indicate that, although these substitutions demonstrably prevent oligomerization, a larger region of self-association interaction is at play, involving the hinge region (ApoE 192-215) as well.

That the formation of oligomers requires at least two patches for self-association is consistent with our results identifying multiple regions of oligomerization.

5.4.4 Comparison of GEE and FPOP footprinting.

In general, there is good qualitative agreement between the results from FPOP and those from GEE footprinting. An apparent discrepancy is seen for ApoE 181-205. Although several residues undergo some increased oxidative modification by FPOP in ApoE3MM, the levels of labeling by GEE are the same (Supporting Information Table 5.3). This region contains only two modifiable residues, E186 and E205. Aside from this low resolution sampling by GEE, there are several other aspects of GEE and FPOP footprinting germane to discrepancies in their outcomes. Maybe the following discussion should come earlier. First, the secondary structure of a protein dictates that intermolecular or inter-domain interactions are not shared equally by neighboring residues, as the backbone torsion angles enforce different side-chain β–carbons orientations along a sequence. Therefore, one should not expect neighboring residues to exhibit the same response when probing the "on" and "off" states of the interaction. Second, the sampling of acidic residues, by their "priming" by EDC and subsequent reaction with GEE, requires interaction volumes that are larger than that of the water molecule, whereas •OH is a probe much the same size as water. Additionally, the sites of reaction on acidic residues are different. Whereas the e^- pair of the oxygen conjugate base attack carbodiimide carbon as a first step [40], •OH preferentially abstracts hydrogen from the Glu β and γ carbons [15, 41]. Thus the relevant solvent accessibilities are different for the same

residue. Finally, the timescale of labeling is dramatically different; the much longer exposure to GEE labeling may sample conformations induced by initial labeling events.

5.4.5 Comparison of the N-terminal domains of ApoE2, ApoE3, ApoE4, and ApoE3MM.

We find little difference between the labeling footprints of the N-terminal domains for the WT isoforms and between ApoE3 and its monomeric mutant isoform (Figures 1, 2, and 4). Thus, the WT isoforms must adopt similar N-terminal structures as that of the monomeric mutant. In a separate manuscript examining the ApoE3MM data, we propose that it adopts an N-terminal domain structure much like the most recent NMR ApoE3 1-183 structure [7]. With few exceptions, the rank order of yields of ApoE3 residues detected as modified in the first and second experiment are the same, although the levels of modification are higher in the ApoE3 monomer/oligomer study owing to the doubling of H_2O_2 starting material. Some of the detected oxidations in the latter case may be due to secondary protein-peroxy reactions that do not sample the equilibrium structure [42], but such signal cannot account for the overwhelming differences seen between ApoE3 and ApoE3MM.

5.5 Conclusions

At 4 μM, WT-ApoE2, ApoE3, and ApoE4 exist in solution as similar structures, primarily as tetramers, and that our data is consistent with the assignment of a four-helix bundle structure in the N-terminal domain of the 299 amino acid monomeric mutant of ApoE3. Although the overall structures are similar, that of region M108 in E4 is

significantly different, though its overall change in SASA may be small. By virtue of the per-residue trends drawn from two independent MS-based footprinting data sets of ApoE3 and ApoE3MM, we conclude that residues spanning 183-205 and 232-251 in the hinge and C-terminal domains are involved in inter and intramolecular interactions concomitant with tetrameric self-association in ApoE3. Owing to their sequence invariance in this region, we suggest that the same oligomerization interaction occurs for ApoE2 and ApoE4.

One advantage of MS-based protein footprinting is that it can sample physiologic mixtures. Thus, future studies will characterize ApoE in the presence of Aβ proteins both with and without the context of lipoproteins. This should be possible at high sequence resolution and may reveal interactions implied in the genetic association of ApoE4 with Alzheimer's disease [43].

5.6 Supporting Information

Supporting Information Table 5.1: FPOP labeling yield per ApoE residue, WT experiment

residue	ApoE2	ApoE3	ApoE4	residue	ApoE2	ApoE3	ApoE4
V2	0.30 ± 0.05%	0.269 +/- 0.005%	0.29 +/- 0.03%	P183	0.13 +/- 0.02%	0.091 +/- 0.003%	0.13 +/- 0.01%
V6	0.4 +/- 0.1%	0.38 +/- 0.01%	0.41 +/- 0.05%	L184	0.43 +/- 0.07%	0.42 +/- 0.01%	0.43 +/- 0.03%
P10	0.8 +/- 0.1%	0.74 +/- 0.02%	0.81 +/- 0.07%	V185	0.20 +/- 0.03%	0.142 +/- 0.003%	0.21 +/- 0.02%
E13	0.31 +/- 0.02%	0.32 +/- 0.01%	0.32 +/- 0.02%	R191	0.27 +/- 0.03%	0.283 +/- 0.009%	0.31 +/- 0.01%
L14	0.24 +/- 0.04%	0.192 +/- 0.008%	0.18 +/- 0.01%	V195	0.23 +/- 0.04%	0.208 +/- 0.005%	0.25 +/- 0.03%
W20	3.9 +/- 0.5%	3.6 +/- 0.2%	3.9 +/- 0.3%	L198	0.45 +/- 0.08%	0.40 +/- 0.02%	0.42 +/- 0.05%
Q21	4.1 +/- 0.2%	3.8 +/- 0.3%	3.4 +/- 0.2%	L203	0.28 +/- 0.04%	0.249 +/- 0.006%	0.28 +/- 0.03%
W26	1.08 +/- 0.07%	1.0 +/- 0.1%	0.74 +/- 0.08%	E205	0.26 +/- 0.02%	0.215 +/- 0.007%	0.198 +/- 0.007%
W34	3.3 +/- 0.4%	2.9 +/- 0.2%	3.4 +/- 0.4%	W210	3.4 +/- 0.3%	3.5 +/- 0.1%	4.2 +/- 0.5%
M64	10 +/- 2%	9.4 +/- 0.9%	6 +/- 1%	M218	1.0 +/- 0.8%	0.8 +/- 0.4%	1.0 +/- 0.2%
E66	0.0 +/- 0.4%	0.6 +/- 0.2%	0.2 +/- 0.5%	R226	0.12 +/- 0.02%	0.121 +/- 0.003%	0.144 +/- 0.009%
M68	2.5 +/- 0.9%	3.6 +/- 0.6%	2 +/- 1%	K233	0.042 +/- 0.007%	0.047 +/- 0.006%	0.066 +/- 0.006%
Y74	2.8 +/- 0.1%	3.07 +/- 0.04%	3.08 +/- 0.08%	L243	0.09 +/- 0.02%	0.079 +/- 0.006%	0.09 +/- 0.01%
E77	1.47 +/- 0.07%	1.41 +/- 0.04%	1.34 +/- 0.04%	E244	0.067 +/- 0.009%	0.067 +/- 0.005%	0.061 +/- 0.003%
E79	0.18 +/- 0.02%	0.20 +/- 0.02%	0.20 +/- 0.02%	Q248	0.14 +/- 0.02%	0.15 +/- 0.01%	0.15 +/- 0.02%
L82	0.15 +/- 0.03%	0.13 +/- 0.01%	0.13 +/- 0.02%	L252	0.5 +/- 0.1%	0.38 +/- 0.01%	0.37 +/- 0.01%
P84	0.29 +/- 0.05%	0.279 +/- 0.009%	0.31 +/- 0.03%	E255	0.37 +/- 0.01%	0.30 +/- 0.02%	0.250 +/- 0.002%
V85	0.11 +/- 0.03%	0.108 +/- 0.008%	0.113 +/- 0.009%	F257	0.5 +/- 0.6%	1.5 +/- 0.2%	0.9 +/- 0.6%
E87	0.12 +/- 0.02%	0.12 +/- 0.01%	0.12 +/- 0.02%	R260	0.034 +/- 0.006%	0.033 +/- 0.001%	0.036 +/- 0.003%
E88	0.30 +/- 0.07%	0.31 +/- 0.02%	0.33 +/- 0.03%	W264	11 +/- 1%	10.4 +/- 0.4%	10.6 +/- 0.6%
M108	0.0 +/- 0.7%	0.0 +/- 0.5%	5 +/- 1%	E266	0.38 +/- 0.01%	0.340 +/- 0.005%	0.299 +/- 0.006%
C112	22 +/- 5%	26 +/- 1%		D271	0.91 +/- 0.06%	1.03 +/- 0.09%	0.77 +/- 0.05%
M125	10 +/- 3%	12 +/- 1%	9 +/- 2%	M272	6 +/- 3%	9 +/- 3%	5 +/- 2%
L126	0.14 +/- 0.03%	0.16 +/- 0.01%	0.20 +/- 0.02%	W276	6.7 +/- 0.9%	5.8 +/- 0.2%	5.9 +/- 0.3%
L133	0.11 +/- 0.02%	0.102 +/- 0.005%	0.13 +/- 0.01%	V287	0.15 +/- 0.03%	0.134 +/- 0.005%	0.13 +/- 0.02%
H140	6 +/- 2%	6.2 +/- 0.5%	7 +/- 3%	P293	2.0 +/- 0.6%	2.2 +/- 0.1%	1.9 +/- 0.4%
Y162	n.d.	0.75 +/- 0.01%	0.90 +/- 0.02%	P295	0.00 +/- 0.05%	0.08 +/- 0.04%	0.02 +/- 0.06%
L181	0.21 +/- 0.04%	0.141 +/- 0.002%	0.19 +/- 0.02%	H299	1.2 +/- 0.3%	1.08 +/- 0.06%	1.2 +/- 0.3%

Supporting Information Table 5.2: FPOP labeling yield per ApoE residue, oligomer/monomer experiment

residue	ApoE3	ApoE3MM	residue	ApoE3	ApoE3MM	residue	ApoE3	ApoE3MM
K1	2.6 +/- 0.7%	3.6 +/- 0.1%	R90	0.12 +/- 0.06%	0.256 +/- 0.008%	R191	0.2 +/- 0.1%	0.60 +/- 0.04%
E3	0.4 +/- 0.1%	0.47 +/- 0.02%	K95	1.7 +/- 0.6%	2.9 +/- 0.2%	V195	0.5 +/- 0.2%	1.09 +/- 0.04%
V6	0.32 +/- 0.09%	0.36 +/- 0.01%	M108	1 +/- 3%	5. +/- 1.%	S197	0.07 +/- 0.02%	0.083 +/- 0.003%
E9	0.18 +/- 0.07%	0.24 +/- 0.02%	C112	53 +/- 12%	54 +/- 6%	L198	0.5 +/- 0.1%	1.13 +/- 0.04%
E19	0.07 +/- 0.01%	0.08 +/- 0.01%	V116	0.24 +/- 0.09%	0.37 +/- 0.02%	Q201	0.010 +/- 0.002%	0.016 +/- 0.001%
W20	11 +/- 3%	16.0 +/- 0.4%	Y118	0.24 +/- 0.09%	0.37 +/- 0.02%	P202	0.18 +/- 0.05%	0.351 +/- 0.005%
Q21	0.07 +/- 0.01%	0.08 +/- 0.01%	V122	0.2 +/- 0.1%	0.12 +/- 0.01%	L203	0.7 +/- 0.2%	1.67 +/- 0.05%
S22	0.052 +/- 0.006%	0.070 +/- 0.006%	M125	50 +/- 5%	47 +/- 5%	E205	0.4 +/- 0.1%	0.84 +/- 0.02%
W26	0.8 +/- 0.2%	1.1 +/- 0.2%	L126	2 +/- 1%	2.0 +/- 0.1%	W210	6 +/- 2%	16.4 +/- 0.4%
L28	0.4 +/- 0.1%	0.53 +/- 0.05%	L133	0.3 +/- 0.2%	0.184 +/- 0.007%	M218	9 +/- 2%	22 +/- 3%
R32	0.023 +/- 0.007%	0.042 +/- 0.004%	H140	1.3 +/- 0.4%	2.0 +/- 0.2%	V232	0.08 +/- 0.03%	4.7 +/- 0.6%
W34	11 +/- 2%	14.2 +/- 0.2%	V161	0.15 +/- 0.05%	0.20 +/- 0.03%	K233	0.10 +/- 0.08%	0.389 +/- 0.004%
Y36	1.3 +/- 0.2%	1.65 +/- 0.08%	Y162	1.6 +/- 0.4%	1.92 +/- 0.05%	K242	0.29 +/- 0.08%	0.55 +/- 0.01%
M64	3.4 +/- 0.9%	3 +/- 1%	A166	0.05 +/- 0.01%	0.076 +/- 0.006%	L243	0.05 +/- 0.02%	1.06 +/- 0.06%
M68	4 +/- 1%	2 +/- 1%	R167	0.25 +/- 0.04%	0.40 +/- 0.01%	E244	0.30 +/- 0.05%	0.49 +/- 0.02%
Y74	4. +/- 1.%	3.8 +/- 0.7%	S175	0.13 +/- 0.04%	0.27 +/- 0.02%	Q248	0.18 +/- 0.03%	0.25 +/- 0.02%
E77	0.3 +/- 0.2%	0.22 +/- 0.02%	R180	0.20 +/- 0.05%	0.36 +/- 0.02%	I250	0.03 +/- 0.01%	0.68 +/- 0.06%
E79	0.2 +/- 0.1%	0.18 +/- 0.02%	L181	0.31 +/- 0.08%	0.55 +/- 0.04%	R251	0.012 +/- 0.003%	0.027 +/- 0.001%
E80	1.2 +/- 0.8%	0.72 +/- 0.02%	P183	0.36 +/- 0.08%	0.62 +/- 0.02%	E255	0.28 +/- 0.07%	0.124 +/- 0.003%
L82	0.6 +/- 0.5%	0.187 +/- 0.006%	L184	0.4 +/- 0.1%	0.68 +/- 0.04%	R260	0.29 +/- 0.06%	0.26 +/- 0.01%
P84	0.7 +/- 0.3%	0.65 +/- 0.03%	V185	0.33 +/- 0.08%	0.58 +/- 0.01%	M272	40 +/- 6%	33 +/- 2%
V85	0.9 +/- 0.6%	0.47 +/- 0.04%	E186	0.20 +/- 0.05%	0.36 +/- 0.01%	W276	11 +/- 3%	28.7 +/- 0.8%
E87	0.8 +/- 0.3%	0.99 +/- 0.03%	Q187	0.08 +/- 0.02%	0.154 +/- 0.008%	V294	0.9 +/- 0.2%	0.24 +/- 0.03%
E88	0.7 +/- 0.3%	0.82 +/- 0.03%	R189	0.19 +/- 0.04%	0.34 +/- 0.02%	H299	0.9 +/- 0.4%	2.30 +/- 0.05%

Supporting Information Table 5.3: GEE labeling yield per ApoE residue, oligomer/monomer experiment

residue	time (min)	ApoE3	ApoE3MM	residue	time (min)	ApoE3	ApoE3MM
E7	1	5.19 +/- 0.06%	5.1 +/- 0.4%	E66	1	0.214 +/- 0.008%	0.217 +/- 0.004%
E7	3	6.3 +/- 0.3%	9.0 +/- 0.8%	E66	3	0.29 +/- 0.02%	0.34 +/- 0.09%
E7	6	8.5 +/- 0.8%	9.0 +/- 0.8%	E66	6	0.44 +/- 0.08%	0.32 +/- 0.05%
E7	12	10.6 +/- 0.3%	12.9 +/- 0.7%	E66	12	0.6 +/- 0.1%	0.59 +/- 0.04%
E9	1	4.6 +/- 0.6%	4.6 +/- 0.9%	E77	1	0.7 +/- 0.3%	0.5 +/- 0.2%
E9	3	5.91 +/- 0.08%	9.0 +/- 0.2%	E77	3	0.52 +/- 0.02%	2 +/- 1%
E9	6	9 +/- 1%	9.3 +/- 0.8%	E77	6	1.1 +/- 0.1%	0.6 +/- 0.1%
E9	12	10.9 +/- 0.3%	12.1 +/- 0.1%	E77	12	1.4 +/- 0.1%	1.03 +/- 0.03%
E11	1	0.17 +/- 0.04%	0.135 +/- 0.006%	E80	1	2.2 +/- 0.6%	2.1 +/- 0.3%
E11	3	0.16 +/- 0.01%	0.35 +/- 0.01%	E80	3	2.5 +/- 0.1%	4.2 +/- 0.8%
E11	6	0.37 +/- 0.02%	0.41 +/- 0.01%	E80	6	4.9 +/- 0.8%	4.0 +/- 0.5%
E11	12	0.9 +/- 0.6%	0.7 +/- 0.3%	E80	12	7.3 +/- 0.3%	6.3 +/- 0.1%
E13	1	1.67 +/- 0.07%	1.5 +/- 0.2%	E88	1	0.08 +/- 0.06%	0.04 +/- 0.04%
E13	3	1.98 +/- 0.04%	2.92 +/- 0.07%	E88	3	0.021 +/- 0.003%	0.2 +/- 0.2%
E13	6	3.2 +/- 0.5%	2.9 +/- 0.3%	E88	6	0.084 +/- 0.008%	0.021 +/- 0.009%
E13	12	3.63 +/- 0.06%	4.3 +/- 0.2%	E88	12	0.075 +/- 0.008%	0.041 +/- 0.002%
E19	1	2.9 +/- 0.1%	3.2 +/- 0.2%	E96	1	0.26 +/- 0.04%	0.29 +/- 0.07%
E19	3	4.18 +/- 0.08%	4.1 +/- 0.2%	E96	3	0.405 +/- 0.009%	0.35 +/- 0.07%
E19	6	5.7 +/- 0.4%	4.93 +/- 0.02%	E96	6	0.55 +/- 0.09%	0.3043 +/- 0.0003%
E19	12	10 +/- 2%	7.6 +/- 0.5%	E96	12	0.9 +/- 0.3%	0.35 +/- 0.04%
E27	1	0.3 +/- 0.1%	0.26 +/- 0.04%	E109	1	0.11 +/- 0.01%	0.10 +/- 0.04%
E27	3	0.30 +/- 0.02%	0.37 +/- 0.02%	E109	3	0.21 +/- 0.03%	0.09 +/- 0.09%
E27	6	0.51 +/- 0.02%	0.43 +/- 0.04%	E109	6	0.13 +/- 0.08%	0.16 +/- 0.07%
E27	12	0.62 +/- 0.02%	0.67 +/- 0.07%	E109	12	0.37 +/- 0.09%	0.3 +/- 0.2%
D35	1	0.07 +/- 0.02%	0.052 +/- 0.009%	D110	1	0.11 +/- 0.01%	0.10 +/- 0.04%
D35	3	0.069 +/- 0.003%	0.106 +/- 0.005%	D110	3	0.21 +/- 0.03%	0.09 +/- 0.09%
D35	6	0.16 +/- 0.04%	0.098 +/- 0.006%	D110	6	0.13 +/- 0.08%	0.16 +/- 0.07%
D35	12	0.16 +/- 0.02%	0.14 +/- 0.02%	D110	12	0.37 +/- 0.09%	0.3 +/- 0.2%
E66	1	0.214 +/- 0.008%	0.217 +/- 0.004%	E186	1	0.75 +/- 0.02%	0.75 +/- 0.02%
E66	3	0.29 +/- 0.02%	0.34 +/- 0.09%	E186	3	0.94 +/- 0.02%	0.99 +/- 0.02%
E66	6	0.44 +/- 0.08%	0.32 +/- 0.05%	E186	6	1.3 +/- 0.1%	1.22 +/- 0.02%
E66	12	0.6 +/- 0.1%	0.59 +/- 0.04%	E186	12	1.9 +/- 0.2%	1.9 +/- 0.3%
E77	1	0.7 +/- 0.3%	0.5 +/- 0.2%	E205	1	0.4 +/- 0.1%	0.5 +/- 0.2%
E77	3	0.52 +/- 0.02%	2 +/- 1%	E205	3	0.46 +/- 0.03%	1.0 +/- 0.1%
E77	6	1.1 +/- 0.1%	0.6 +/- 0.1%	E205	6	0.8 +/- 0.1%	0.93 +/- 0.02%

E77	12	1.4 +/- 0.1%	1.03 +/- 0.03%	E205	12	1.04 +/- 0.05%	1.13 +/- 0.07%
E212	1	0.56 +/- 0.01%	1.7 +/- 0.3%	E255	1	0.302 +/- 0.008%	1.3 +/- 0.3%
E212	3	0.97 +/- 0.05%	2.1 +/- 0.2%	E255	3	0.3538 +/- 0.0009%	1.41 +/- 0.07%
E212	6	1.26 +/- 0.08%	2.5 +/- 0.3%	E255	6	0.404 +/- 0.004%	1.8 +/- 0.1%
E212	12	1.9 +/- 0.4%	3.2 +/- 0.2%	E255	12	0.523 +/- 0.009%	2.4 +/- 0.3%
E219	1	2.2 +/- 0.5%	14 +/- 4%	E266	1	8 +/- 3%	3.1 +/- 0.4%
E219	3	4.4 +/- 0.4%	24 +/- 3%	E266	3	8.14 +/- 0.04%	5.5 +/- 0.8%
E219	6	4.7 +/- 0.2%	20 +/- 2%	E266	6	12 +/- 9%	6.3 +/- 0.2%
E219	12	11 +/- 5%	26.2 +/- 0.8%	E266	12	11 +/- 3%	8.23 +/- 0.08%
E220	1	5 +/- 1%	16 +/- 6%	E270	1	12 +/- 8%	1.4 +/- 0.2%
E220	3	8.4 +/- 0.9%	26 +/- 4%	E270	3	4 +/- 3%	2.4 +/- 0.2%
E220	6	9.5 +/- 0.7%	21 +/- 2%	E270	6	9 +/- 6%	2.8 +/- 0.2%
E220	12	19 +/- 8%	25. +/- 1.%	E270	12	1.9 +/- 0.9%	4.20 +/- 0.04%
D227	1	2.2 +/- 0.4%	8 +/- 2%	D271	1	0.05 +/- 0.05%	1.40 +/- 0.07%
D227	3	4.5 +/- 0.5%	17 +/- 5%	D271	3	0.02 +/- 0.02%	2.3 +/- 0.1%
D227	6	6.0 +/- 0.3%	13 +/- 2%	D271	6	0.03 +/- 0.03%	2.8 +/- 0.2%
D227	12	12 +/- 5%	17.42 +/- 0.04%	D271	12	0.2 +/- 0.2%	3.79 +/- 0.07%
E231	1	1.4 +/- 0.3%	10 +/- 3%	E281	1	0.97 +/- 0.06%	1.7 +/- 0.2%
E231	3	3.1 +/- 0.5%	19 +/- 2%	E281	3	1.28 +/- 0.02%	2.3 +/- 0.2%
E231	6	5.1 +/- 0.3%	17 +/- 2%	E281	6	1.70 +/- 0.04%	2.888 +/- 0.006%
E231	12	9 +/- 4%	21 +/- 2%	E281	12	2.3 +/- 0.2%	4.1 +/- 0.2%
E234	1	32 +/- 5%	34 +/- 10%	E287	1	0.3 +/- 0.3%	2.2 +/- 0.1%
E234	3	45.3 +/- 0.6%	45 +/- 3%	E287	3	0	2.95 +/- 0.03%
E234	6	52 +/- 3%	39 +/- 3%	E287	6	0.01 +/- 0.01%	3.9 +/- 0.1%
E234	12	64 +/- 8%	45.4 +/- 0.4%	E287	12	0	5.9 +/- 0.2%
E238	1	3.8 +/- 0.4%	9.1 +/- 0.2%	D297	1	1.4 +/- 0.2%	0.64 +/- 0.03%
E238	3	5.2 +/- 0.3%	11 +/- 2%	D297	3	2.14 +/- 0.06%	0.976 +/- 0.005%
E238	6	6.4 +/- 0.4%	14.9 +/- 0.4%	D297	6	3.49 +/- 0.03%	1.47 +/- 0.08%
E238	12	8.93 +/- 0.05%	18.2 +/- 0.2%	D297	12	5.17 +/- 0.04%	2.315 +/- 0.002%
E244	1	0.086 +/- 0.001%	0.64 +/- 0.04%	H299	1	0.011 +/- 0.008%	0.22 +/- 0.01%
E244	3	0.108 +/- 0.009%	0.72 +/- 0.02%	H299	3	0.023 +/- 0.005%	0.28 +/- 0.01%
E244	6	0.129 +/- 0.004%	0.930 +/- 0.009%	H299	6	0.042 +/- 0.008%	0.39 +/- 0.02%
E244	12	0.164 +/- 0.005%	1.39 +/- 0.08%	H299	12	0.2 +/- 0.1%	0.68 +/- 0.05%
E245	1	0.41 +/- 0.04%	0.91 +/- 0.04%				
E245	3	0.49 +/- 0.02%	1.08 +/- 0.03%				
E245	6	0.58 +/- 0.01%	1.24 +/- 0.03%				
E245	12	0.69 +/- 0.06%	1.97 +/- 0.04%				

5.7 References

1. Mahley, R. W., Apolipoprotein E: cholesterol transport protein with expanding role in cell biology. *Science* **1988,** *240*, 622-630.
2. Strittmatter, W. J.; Saunders, A. M.; Schmechel, D.; Pericak-Vance, M.; Enghild, J.; Salvesen, G. S.; Roses, A. D., Apolipoprotein E: high-avidity binding to beta-amyloid and increased frequency of type 4 allele in late-onset familial Alzheimer disease. *Proc. Natl. Acad. Sci. U.S.A.* **1993,** *90* (5), 1977-1981.
3. Corder, E. H.; Saunders, A. M.; Strittmatter, W. J.; Schmechel, D. E.; Gaskell, P. C.; Small, G. W.; Roses, A. D.; Haines, J. L.; Pericak-Vance, M. A., Gene dose of apolipoprotein E type 4 allele and the risk of Alzheimer's disease in late onset families. *Science* **1993,** *261* (5123), 921-923.
4. Bu, G., Apolipoprotein E and its receptors in Alzheimer's disease: pathways, pathogenesis and therapy. *Nat Rev Neurosci* **2009,** *10* (5), 333-344.
5. Weisgraber, K. H., Apolipoprotein E: Structure-Function Relationships. In *Advances in Protein Chemistry*, Academic Press: 1994; Vol. Volume 45, pp 249-302.
6. Wilson, C.; Wardell, M. R.; Weisgraber, K. H.; Mahley, R. W.; Agard, D. A., Three-dimensional structure of the LDL receptor-binding domain of human apolipoprotein E. *Science* **1991,** *252* (5014), 1817-1822.
7. Sivashanmugam, A.; Wang, J., A Unified Scheme for Initiation and Conformational Adaptation of Human Apolipoprotein E N-terminal Domain upon Lipoprotein Binding and for Receptor Binding Activity. *J. Biol. Chem.* **2009,** *284* (21), 14657-14666.
8. Garai, K.; Frieden, C., The Association-Dissociation Behavior of the ApoE Proteins: Kinetic and Equilibrium Studies. *Biochemistry* **2010,** *49* (44), 9533-9541.
9. Sakamoto, T.; Tanaka, M.; Vedhachalam, C.; Nickel, M.; Nguyen, D.; Dhanasekaran, P.; Phillips, M. C.; Lund-Katz, S.; Saito, H., Contributions of the Carboxyl-Terminal Helical Segment to the Self-Association and Lipoprotein Preferences of Human Apolipoprotein E3 and E4 Isoforms. *Biochemistry* **2008,** *47* (9), 2968-2977.
10. Westerlund, J. A.; Weisgraber, K. H., Discrete carboxyl-terminal segments of apolipoprotein E mediate lipoprotein association and protein oligomerization. *J. Biol. Chem.* **1993,** *268* (21), 15745-15750.
11. Aggerbeck, L. P.; Wetterau, J. R.; Weisgraber, K. H.; Wu, C. S.; Lindgren, F. T., Human apolipoprotein E3 in aqueous solution. II. Properties of the amino- and carboxyl-terminal domains. *J. Biol. Chem.* **1988,** *263* (13), 6249-6258.
12. Yokoyama, S.; Kawai, Y.; Tajima, S.; Yamamoto, A., Behavior of human apolipoprotein E in aqueous solutions and at interfaces. *J. Biol. Chem.* **1985,** *260* (30), 16375-16382.
13. Hambly, D. M.; Gross, M. L., In *The Encyclopedia of Mass Spectrometry: Ionization Methods*, Gross, M. L.; Caprioli, R. M., Eds. 2006; Vol. 6.
14. Guan, J.-Q.; Chance, M. R., Structural proteomics of macromolecular assemblies using oxidative footprinting and mass spectrometry. *Trends Biochem. Sci* **2005,** *10*, 583-592.
15. Xu, G.; Chance, M. R., Hydroxyl Radical-Mediated Modification of Proteins as Probes for Structural Proteomics. *Chem. Rev.* **2007,** *107* (8), 3514-3543.
16. Xu, G.; Chance, M. R., Radiolytic Modification and Reactivity of Amino Acid Residues Serving as Structural Probes for Protein Footprinting. *Anal. Chem.* **2005,** *77* (14), 4549-4555.

17. Hambly, D. M.; Gross, M. L., Laser Flash Photolysis of Hydrogen Peroxide to Oxidize Protein Solvent-Accessible Residues on the Microsecond Timescale. *J. Am. Soc. Mass Spectrom.* **2005,** *16* (12), 2057-2063.
18. Aye, T. T.; Low, T. Y.; Sze, S. K., Nanosecond Laser-Induced Photochemical Oxidation Method for Protein Surface Mapping with Mass Spectrometry. *Anal. Chem.* **2005,** *77* (18), 5814-5822.
19. Gau, B. C.; Sharp, J. S.; Rempel, D. L.; Gross, M. L., Fast Photochemical Oxidation of Protein Footprints Faster than Protein Unfolding. *Anal. Chem.* **2009,** *81* (16), 6563-6571.
20. Wen, J.; Zhang, H.; Gross, M. L.; Blankenship, R. E., Membrane orientation of the FMO antenna protein from Chlorobaculum tepidum as determined by mass spectrometry-based footprinting. *Proc. Natl. Acad. Sci. U.S.A.* **2009,** *106* (15), 6134-6139.
21. Swaisgood, H.; Natake, M., Effect of Carboxyl Group Modification on Some of the Enzymatic Properties of L-Glutamate Dehydrogenase. *Journal of Biochemistry* **1973,** *74* (1), 77-86.
22. Hoare, D. G.; Koshland, D. E., A Method for the Quantitative Modification and Estimation of Carboxylic Acid Groups in Proteins. *The Journal of Biological Chemistry* **1967,** *242*, 2447-2453.
23. Xu, G.; Kiselar, J.; He, Q.; Chance, M. R., Secondary Reactions and Strategies To Improve Quantitative Protein Footprinting. *Anal. Chem.* **2005,** *77* (10), 3029-3037.
24. Vidavsky, I.; Rempel, D. L.; Gross, M. L., 2D Mass Spectra Correlation – Semi Automatic Tool for Modified Peptide Discovery. In *Proceedings of the 54th ASMS Conference on Mass Spectrometry and Allied Topics*, Seattle, WA, 2006.
25. Chou, C.-Y.; Lin, Y.-L.; Huang, Y.-C.; Sheu, S.-Y.; Lin, T.-H.; Tsay, H.-J.; Chang, G.-G.; Shiao, M.-S., Structural Variation in Human Apolipoprotein E3 and E4: Secondary Structure, Tertiary Structure, and Size Distribution. *Biophysical journal* **2005,** *88* (1), 455-466.
26. Perugini, M. A.; Schuck, P.; Howlett, G. J., Self-association of Human Apolipoprotein E3 and E4 in the Presence and Absence of Phospholipid. *J. Biol. Chem.* **2000,** *275* (47), 36758-36765.
27. Guan, J. Q.; Vorobiev, S.; Almo, S. C.; Chance, M. R., Mapping the G-Actin Binding Surface of Cofilin Using Synchrotron Protein Footprinting. *Biochemistry* **2002,** *41* (18), 5765-5775.
28. Maleknia, S. D.; Ralston, C. Y.; Brenowitz, M. D.; Downard, K. M.; Chance, M. R., Determination of Macromolecular Folding and Structure by Synchrotron X-Ray Radiolysis Techniques. *Anal. Biochem.* **2001,** *289* (2), 103-115.
29. Goldsmith, S. C.; Guan, J.-Q.; Almo, S. C.; Chance, M. R., Synchrotron Protein Footprinting: A Technique to Investigate Protein-Protein Interactions. *J. Biomol. Stuc. Dyn.* **2001,** *19* (3), 405-419.
30. Buxton, G. V.; Greenstock, C. L.; Helman, W. P.; Ross, A. B., Critical Review of Rate Constants for Reactions of Hydrated Electrons, Hydrogen Atoms and Hydroxyl Radicals (*OH/*O-) in Aqueous Solution. *J. Phys. Chem. Ref. Data* **1988,** *17* (2), 513-886.
31. Gerstein, M., A resolution-sensitive procedure for comparing protein surfaces and its application to the comparison of antigen-combining sites. *Acta Crystallographica Section A* **1992,** *48* (3), 271-276.
32. Xu, G.; Chance, M. R., Radiolytic Modification of Sulfur-Containing Amino Acid Residues in Model Peptides: Fundamental Studies for Protein Footprinting. *Anal. Chem.* **2005,** *77* (8), 2437-2449.

33. Hawkins, C. L.; Morgan, P. E.; Davies, M. J., Quantification of protein modification by oxidants. *Free Radical Biology and Medicine* **2009,** *46* (8), 965-988.
34. Morand, K.; Talbo, G.; Mann, M., Oxidation of peptides during electrospray ionization. *Rapid Commun. Mass Spectrom.* **1993,** *7* (8), 738-743.
35. Fan, D.; Li, Q.; Korando, L.; Jerome, W. G.; Wang, J., A monomeric human apolipoprotein E carboxyl-terminal domain *Biochemistry* **2004,** *43* (17), 5055-5064.
36. Zhang, Y.; Vasudevan, S.; Sojitrawala, R.; Zhao, W.; Cui, C.; Xu, C.; Fan, D.; Newhouse, Y.; Balestra, R.; Jerome, W. G.; Weisgraber, K.; Li, Q.; Wang, J., A Monomeric, Biologically Active, Full-Length Human Apolipoprotein E *Biochemistry* **2007,** *46* (37), 10722-10732.
37. Sivashanmugam, A.; Wang, J., A complete receptor binding domain of human apolipoprotein E. Wayne State University School of Medicine: 2009.
38. Dong, L. M.; Wilson, C.; Wardell, M. R.; Simmons, T.; Mahley, R. W.; Weisgraber, K. H.; Agard, D. A., Human apolipoprotein E. Role of arginine 61 in mediating the lipoprotein preferences of the E3 and E4 isoforms. *J. Biol. Chem.* **1994,** *269* (35), 22358-22365.
39. Garai, K.; Mustafi, S. M.; Baban, B.; Frieden, C., Structural differences between apolipoprotein E3 and E4 as measured by 19F NMR. *Protein Sci.* **2009,** *19* (1), 66-74.
40. Hermanson, G. T., *Bioconjugate Techniques (Second Edition)*. Elsevier: 2008.
41. Garrison, W. M., Reaction mechanisms in the radiolysis of peptides, polypeptides, and proteins. *Chem. Rev.* **1987,** *87* (2), 381-398.
42. Saladino, J.; Liu, M.; Live, D.; Sharp, J. S., Aliphatic Peptidyl Hydroperoxides as a Source of Secondary Oxidation in Hydroxyl Radical Protein Footprinting. *J. Am. Soc. Mass Spectrom.* **2009,** *20* (6), 1123-1126.
43. Zhong, N.; Weisgraber, K. H., Understanding the Association of Apolipoprotein E4 with Alzheimer Disease: Clues from Its Structure. *J. Biol. Chem.* **2009,** *284* (10), 6027-6031.

6 Characterization of the Apolipoprotein E3 Monomer Structure by Mass Spectrometry-based Protein Footprinting.

6.1 Introduction

Apolipoprotein E (ApoE) has three common variants among humans, differing at two residues in the 299-residue protein. Variant ApoE2 has cysteines at residues 112 and 158; ApoE3 has a cysteine at 112 and an arginine at 158; and ApoE4 has arginines at both residues. No high resolution structure of any variant has been determined, owing to the propensities of the full proteins to oligomerize. ApoE is comprised of two domains connected by a protease-sensitive hinge region[1]; the N-terminal domain and C-terminal domain span residues 1-191 and 216-299, respectively. The first X-ray crystal structure of $ApoE_{23-164}$ revealed a four-helix-bundle structure of the N-terminal domain[2]; the most recent NMR structure of $ApoE_{1-183}$ expands the high-resolution coverage of this domain[3]. Conversely, no high-resolution structure of the isolated C-terminal domain has been determined, although it is thought that this domain is the primary region for oligomeric interactions [1, 4-5].

ApoE4 carries the highest risk of any genetic factor for Alzheimer's disease (AD)[6-8]. This high genetic risk ultimately is owed to the single amino-acid difference between ApoE4 and the most common ApoE variant, ApoE3. There is evidence for several mechanisms of ApoE4-associated AD risk, although there is no consensus on a single theory[9-12]. Significantly, ApoE4 has a higher preference of forming VLDL lipoproteins than do the other common ApoE variants, and this has been attributed to a conformation involving an N-terminal:C-terminal domain interaction enhanced in ApoE4 possibly by a salt bridge between R61 and E255[13-15]. Garai and Frieden [16] showed that

the oligomerization of lipid-free ApoE is not diffusion-controlled, and that the variants exhibit different rates of association and dissociation. These differences may impact the lipoprotein dynamic equilibrium in the brain. Such studies highlight the need for a fundamental understanding of the lipid-free ApoE structure, to help unravel the physiological consequence of mutation C158R.

The central problem inhibiting the structural characterization of ApoE is oligomerization. Zhang and colleagues [17] recently engineered two mutants of ApoE3, existing as monomers to 20 mg/mL and possessing lipid-binding and LDL receptor-binding properties that are similar to those of ApoE3. The two mutants share four substitutions in the C-terminal domain; one of the mutants has an additional substitution in this domain. Its NMR ^{1}H-^{15}N HSQC spectrum in the lipid-free state shows many of the same spectral features as the spectrum of truncated ApoE3 1-183, suggesting that the four-helix bundle structure is present in the N-terminal domain of the full length monomeric mutant[17]. This has been a common presumption in the modeling of ApoE domain interactions and lipid-binding reorganization[3, 9]. We report here the testing of this hypothesis with a different method of structural characterization.

Protein footprinting by covalent labeling of solvent-exposed sidechains, with detection and quantitation by mass spectrometry, is a method of analyzing structure by comparison[18-19]. Usually two states of a protein or protein complex are modified under identical conditions. By virtue of the irreversibility of the modification, the proteins can be proteolyzed in any appropriate manner, and the resulting peptides analyzed by chromatography and mass spectrometry to reveal modification sites. In a proper footprinting experiment, the labeling modification yield at a site will depend on the

inherent reactivity of the residue to the labeling agent and on the site's average solvent accessibility in the equilibrium state of interest. Comparing the yields of labeling at identical residues between two states allows for an accurate assessment of the relative change in solvent accessible surface area (SASA) at the residue. The state with attenuated labeling has lower SASA; such a result for the holo state in a ligand-binding experiment reveals the site of direct ligand interaction or of distal allosteric change upon binding.

One class of protein footprinting utilizes hydroxyl-radical-mediated modification. This method has several advantages. The •OH probes aqueous accessibility because its size is comparable to that of water molecules, and its high reactivity allows for reliable sampling of over half of the 20 common amino acids[20-22]. Additionally, in oxygenated solutions, an abundant product of •OH-sidechain modification that is common to most amino acids is the net incorporation of oxygen [23], a stable +16 Da modification easily detected by mass spectrometry. While indiscriminate, •OH is not an "equal-opportunity" labeling agent: the reaction rate constant for the most reactive amino acid, Cys, is over 1000 times greater than that for the least reactive, Gly [24].

There are several ways of generating •OH for protein footprinting, including Fe(II)-reduction of H_2O_2 (Fenton chemistry)[25-28], X-ray[29-30] and γ-ray[31-32] radiolysis of water, and UV homolysis of H_2O_2 [33]. These methods and the various side-chain products they typically produce are detailed in a recent review[24]. We use here the FPOP approach developed by Hambly and Gross[34] and, independently, by Aye and colleagues[35] for •OH–mediated footprinting. We use a KrF excimer laser to provide a 17 ns flash of 248 nm light to initiate the homolysis of H_2O_2 at low millimolar levels. Twenty mM glutamine

serves as a chemical shutter, effectively scavenging all radicals within approximately 1 μs [34]. This ensures that only the equilibrium conformation(s) of the protein is sampled at high yield, avoiding potential oxidation-induced conformations that may evolve within ms of exposure [36].

The hypothesis we test, that the N-terminus of the full length ApoE monomer has the structure of truncated $ApoE3_{1-183}$, requires a different kind of comparison than is normally employed in a footprinting experiment. We segregate the extents of oxidative modification of residues among their same-amino-acid residue families, because the FPOP-yield should be proportional to the SASA among residues of the same kind. Thus an accurate determination of relative exposure is possible. The hypothesis of structural similarity in the N-terminal domain is tested by comparing FPOP-indicated buried and exposed residues to the calculated SASA of $ApoE3_{1-183}$.

6.2 Experimental Procedures

6.2.1 Reagents.

Acetonitrile, formic acid, 30% hydrogen peroxide, L-glutamine, L-methionine, *tris*(2-carboxyethyl)phosphine hydrochloride (TCEP), catalase, guanidinium hydrochloride, and phosphate buffered saline (PBS) were purchased from the Sigma Aldrich Chemical Co. (St. Louis, MO). Trypsin sequencing grade was purchased from Roche Diagnostics Corp. (Indianapolis, IN). Purified water (18 MΩ) was obtained from a Milli-Q Synthesis system (Millipore, Billerica, MA). ApoE3MM, expressed in *E. coli*, was kindly provided by Drs. K. Garai and C. Frieden. Lyophilized ApoE3MM was solubilized in 6 M guanidinium chloride and dialyzed overnight into phosphate buffered saline (PBS) solution containing 100 μM TCEP disulfide reductant; the protein

concentration was determined by 280 nm absorbance. The purity of the protein was confirmed by ESI MS on a Bruker Maxis Q-TOF (Billerica, MA) operating at 30000 resolving power for ions of *m/z* 400, using a Millipore Ziptip$_{C4}$ (Billerica, MA) de-salted aliquot of the stock solution. The stock solution was split among aliquots, frozen by immersion in N_2(I), and stored at -80°C prior to use.

6.2.2 FPOP labeling.

A solution of 4 μM ApoE3MM in PBS and 100 μM TCEP was prepared from thawed stock solutions and thermally equilibrated 2 h at room temperature (22 °C). Glutamine was solubilized to 150 mM in PBS and added to the protein solution to a final concentration of 20 mM. From this solution, 35 μL replicates were drawn. Just prior to FPOP, H_2O_2 was added to each replicate to a final concentration of 40 mM, by 10-fold dilution of a freshly prepared stock solution of H_2O_2. The FPOP apparatus was used as previously described [34] but with 150 μm i.d. fused silica (Polymicro Technologies, Phoenix, AZ). The KrF excimer laser power (GAM Laser Inc., Orlando, FL) was adjusted to 39 mJ/pulse, and its pulse frequency was set to 5 Hz. The flow rate was adjusted to ensure a 25% exclusion volume to avoid repeat •OH exposure[36]. Excess H_2O_2 was removed immediately following FPOP labeling by collecting samples in microcentrifuge tubes containing 10 μL of 200 fM catalase. This catalase solution also contained Met to give a final concentration of 20 mM following collection. $O_2(g)$ was removed from the samples by centrifugation following pipette mixing three times during a 10 minute room temperature incubation; samples were subsequently frozen in $N_2(l)$ and stored at -80°C prior to proteolysis. Control samples were drawn from the same equilibration solution and handled identically except that the laser was not used.

6.2.3 Proteolysis.

FPOP-labeled and control samples were thawed and proteolyzed at an 8:1 protein:trypsin weight ratio at 37 °C for 3 h. Digestion completion was determined by ESI MS on a Bruker Maxis Q-TOF by using an extra control replicate. The samples were concentrated 3-fold by SpeedVac drying at 30 °C, then Millipore Ziptip$_{C18}$ de-salted, with eluted into 10 uL of 50% acetonitrile 1% formic acid solution. A portion of this was diluted 25-fold with water and 0.1% formic acid for autosampler loading.

6.2.4 LC-MS/MS acquisition.

Each sample replicate was loaded by 5 μL autosampler (Eksigent nanoLC, Dublin, CA) injection onto a 20 cm x 75 μm silica capillary column with a PicoFrit tip (New Objective, Inc, Woburn, MA), bomb-packed with C18 reverse phase material (Magic, 0.075 mm × 200 mm, 5 μm, 300 Å, Michrom, Auburn, CA). The gradient was from 1% solvent B (97% acetonitrile, 3% water, 0.1% formic acid) to 60% solvent B over 70 min at an eluent flow of 260 nL/min. The LC was coupled to the nanospray source of an LTQ-Orbitrap mass spectrometer (Thermo Fisher, Waltham, MA). Mass spectra of eluting peptides were obtained at high mass resolving power (100,000 for ions of *m*/*z* 400) by using the Orbitrap spectrometer component. The six most abundant ions eluting per high- resolving-power scan were each subjected to CID MS^2 experiment in the LTQ component, using a collision energy 35% of the maximum, a 2 Da isolation width, and wideband activation. Precursor ions submitted to an MS^2 experiment were rejected for repeat experiment within 6 s of their original MS^2 scan; this dynamic exclusion setting enabled good sampling of the apex of most chromatogram peaks, which were typically 12-18 s wide at half maximum. Blanks were run between every sample acquisition.

6.2.5 Data analysis.

A measure of the abundance of a peptide is the sum of the integrated areas of its extracted ion chromatogram (EIC) features from the Orbitrap MS data, determined at ± 5 ppm about the theoretical *m/z* values of the isotopomer ions. The Rosetta Elucidator data management system (Rosetta Biosoftware) was used to determine all EIC features aligned in time across all FPOP and control samples. These EIC features were annotated by Mascot (Matrix Science, Boston, MA) error-tolerant searching with the variable modification list updated for known •OH sidechain modifications[24]. The feature annotations were corrected for, or rejected by, errors in mass tolerance, unusual modifications, and discrepant annotations, using custom VBA software for efficient manual MS^2 inspection. The custom processing also augmented the Mascot results by identifying peaks not Mascot-annotated but within 8 ppm of a putative FPOP-modified or unmodified tryptic peptide of ApoE3MM. These features were included if they had an associated product-ion spectra that were consistent with their accurate-mass match. The interpretation of such spectra was assisted by a custom-developed correlation algorithm that compared these spectra to exemplary CID fragment spectra of unmodified tryptic peptides of ApoE3MM[37].

The yield per residue was determined as the sum of all peptide features modified at a residue divided by all peptide features having the same sequences as the peptide contributors modified at that residue. This definition avoids potential yield underestimations that occurred, for example, when a tryptic peptide was detected as modified at a residue but a missed-cleavage peptide spanning this residue was only detected as unmodified. Here is the argument: The protein modification yield at a

residue should be recapitulated at the peptide level. Unless there is a modification bias with trypsin proteolysis, the missed-cleavage peptide will also be modified at the residue in the same yield. The lack of detection of the modified missed-cleavage peptide does not mean the missed-cleavage peptide isn't modified; rather it is an analytic failure usually owing to a low frequency of trypsin missed cleavages. Therefore the unmodified missed-cleavage peptide should not be included in the yield denominator in this instance. Except for modifications at lysine and arginine, our data shows trypsin is not influenced by residue modifications.

6.3 Results

6.3.1 LC-MS/MS analysis.

When subjected to LC-MS peak-alignment analysis, the proteolytic digests of the three samples submitted to FPOP and of the three control samples had 10,122 unique ion features of known charge state eluting during their 70 min LC-MS acquisitions. An LC-MS feature is a single ion isotopomer in a single charge state from a species eluting as a single peak in time. Typically a signal from an abundant tryptic peptide species was split among two or more charge states, often +2 and +3. The Orbitrap mass analyzer resolved the isotopomers, so that the measure of abundance of a tryptic peptide was determined by summing the extracted ion chromatogram (EIC) peak areas for a dozen or more co-eluting features. Owing to the precision of the Orbitrap, LC-MS features were included for integration as a single species if their ^{12}C monoisotopic de-charged masses were within 5 ppm of the average of all such features co-eluting in time. Thus, the 10,122 ion features were associated with 3,379 eluting species. Of these, Mascot error-tolerant database searching and accurate mass-matching software identified 1,456 species,

comprising 62.5% of all ion abundances, as ions of ApoE3MM modified and unmodified peptides. The remaining signal is predominantly associated with very low-abundance species of unknown or +1 charge state and tryptic peptides from catalase.

Reporting the extent of the characterization of LC-MS/MS protein footprinting data is important for conveying the comprehensiveness of the analysis. While we use a "bottom-up" MS-based proteomics methodology, we are not quantifying protein levels from a complex mixture with as few as two characteristic peptides, as is typically done in proteomics experiments[38]. Instead, nearly two thirds of all signal stems from a single protein made complex by the labeling experiment; our task is to accurately determine the labeling yields localized to many specific sites.

In addition to observing all standard •OH sidechain products [24], we found chemistries not commonly reported. These include the net loss of 2H at Leu and Val (-2.0157 D); loss of $HSCH_2$ and gain of OH at Met (-29.9928 D); and the net losses of CO (-27.9949 D) and CO_2 (-43.9898 D) involving both Asp and Glu residues. In all such cases, the modifications tracked exclusively with FPOP-labeled samples. Figure 6.1 shows the evidence for Glu205 -44 D modification and is exemplary of FPOP-specific signal but for one aspect. Typical •OH sidechain outcomes make the peptides more hydrophilic than are their unmodified roots; thus, they elute earlier in reverse-phase chromatography. Figure 6.1A shows that the peptide ApoE3MM(192-206) - CO_2 elutes later than unmodified ApoE3MM 192-206, consistent with the expectation that loss of an electronegative oxygen increases hydrophobicity.

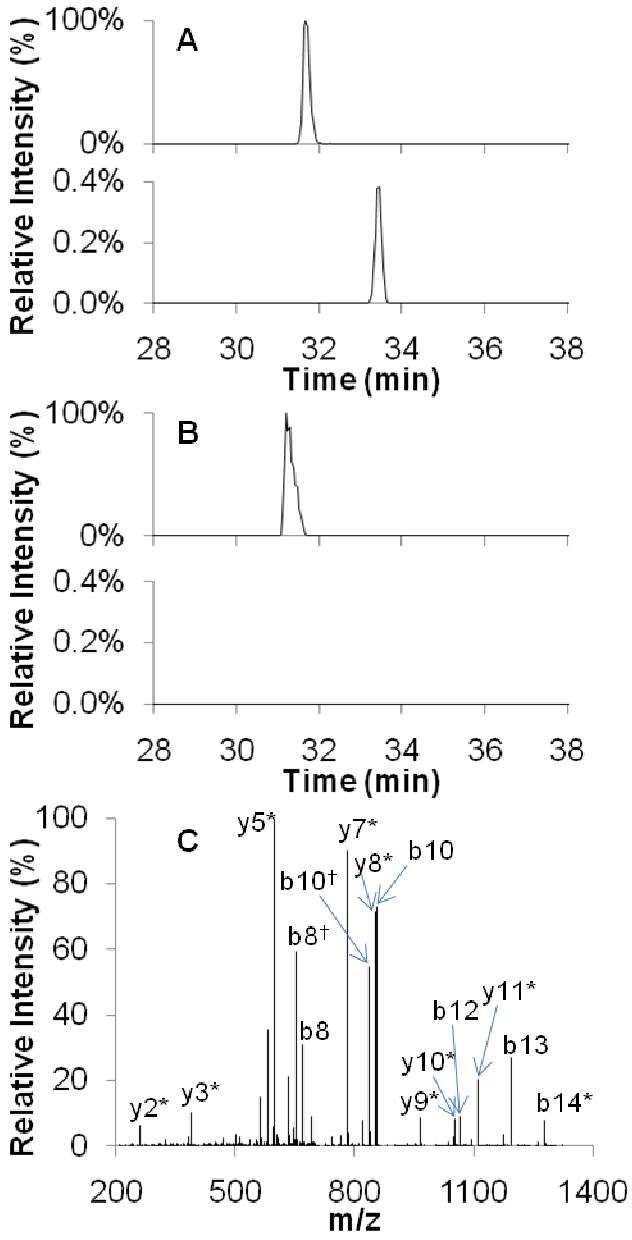

Figure 6.1: Quantitative and qualitative LC-MS/MS data for ApoE3 192-206. Panels A and B show two extracted ion chromatograms (EICs). The top is of m/z 749.4046±0.0037, the 5 ppm window about the doubly protonated unmodified peptide. The bottom is of m/z 727.4097±0.0036, the 5 ppm window about the doubly protonated peptide minus CO_2. Panel A is from FPOP-labeled sample; panel B is from control sample. Panel C shows the MS^2 scan of the CID fragmentation of the modified precursor from the FPOP-labeled sample. The labeled ions are consistent with the characteristic b- and y- CID fragment ions of the ApoE3 192-206 sequence, AATVGSLAGQPLQER, with the CO_2 loss at E205. Ions with an asterisk carry this -44 D loss; ions with a dagger carry a -18 D water loss.

6.3.2 Per-residue labeling.

Of ApoE3MM's 299 residues, 69 were quantifiably detected as modified (Table 6.1). The uncertainties are determined by the propagation of the standard errors for the triplicate-averaged FPOP and control levels. The modifications are of those reported for •OH-mediated labeling: +16 Da for most residues; +14 Da for aliphatic residues; +32 and +48 Da for cysteine, methionine, and tryptophan; +4 for tryptophan; +5, -10, and -23 Da for histidine; -2 Da for serine and threonine ; -30 Da for aspartic acid and glutamic acid; and -43 Da for arginine. Seventeen other residues (V2, E7, T8, P10, E11, P12, E13, L14, E27, D35, L174, I177, L179, A192, E212, L262, and E281) were detected as modified but were of very low abundance and were either not well chromatographically resolved, or were of new OH products described above, or both. These residue signals have not been included for the ApoE3MM self-analysis reported here.

The same-amino acid residue averages for all detected-as-modified residues show a trend similar to the reported free amino acid reaction rate with •OH[39] and to the MS analysis of •OH–amino amide reaction products[21] (Table 6.2). Sulfur-containing residues and aromatic residues are the most sensitive towards FPOP labeling, with hydrophobic residues next. Free cysteine is the most •OH-reactive amino acid[39], but trails methionine and tryptophan in Table 6.2. This is probably due to the only cysteine residue, C112, being significantly buried.

Table 6.1: ApoE3MM FPOP labeling yield

residue	FPOP yield[a]	exposure[b]	residue	FPOP yield[a]	exposure[b]
K1	3.6 +/- 0.1%	exposed	R180	0.37 +/- 0.02%	NA
V6	0.36 +/- 0.01%		L181	0.55 +/- 0.04%	
E19	0.08 +/- 0.01%	buried	P183	0.63 +/- 0.02%	exposed
W20	16.0 +/- 0.4%		L184	0.68 +/- 0.04%	
Q21	0.08 +/- 0.01%		V185	0.58 +/- 0.01%	
S22	0.070 +/- 0.006%	buried	E186	0.25 +/- 0.01%	
W26	1.1 +/- 0.2%	buried	Q187	0.154 +/- 0.008%	
L28	0.53 +/- 0.05%		R189	0.154 +/- 0.008%	NA
R32	0.042 +/- 0.004%	NA	V195	1.09 +/- 0.04%	exposed
W34	14.2 +/- 0.2%		S197	0.083 +/- 0.003%	
Y36	1.65 +/- 0.08%		L198	1.13 +/- 0.04%	
M64	1 +/- 1%	buried	Q201	0.0160 +/- 0.0006%	buried
M68	4 +/- 1%	buried	P202	0.351 +/- 0.005%	
Y74	3.8 +/- 0.7%	exposed	L203	1.67 +/- 0.05%	exposed
E80	0.25 +/- 0.02%		E205	0.84 +/- 0.02%	exposed
L82	0.190 +/- 0.006%	buried	W210	16.4 +/- 0.4%	
P84	0.72 +/- 0.04%	exposed	M218	22 +/- 3%	
V85	0.48 +/- 0.04%		K233	0.389 +/- 0.004%	buried
E87	0.76 +/- 0.02%	exposed	K242	0.55 +/- 0.01%	buried
E88	0.59 +/- 0.03%		L243	1.03 +/- 0.06%	
M108	5. +/- 1.%	buried	E244	0.49 +/- 0.02%	
C112	7 +/- 2%	NA	Q248	0.25 +/- 0.02%	exposed
V116	0.37 +/- 0.02%		I250	0.70 +/- 0.06%	NA
Y118	0.37 +/- 0.02%	buried	R251	0.027 +/- 0.001%	NA
V122	0.12 +/- 0.01%	buried	E255	0.124 +/- 0.003%	buried
M125	47 +/- 5%	exposed	R260	0.124 +/- 0.003%	NA
L126	2.0 +/- 0.1%	exposed	F265	1.88 +/- 0.04%	NA
T130	0.39 +/- 0.02%		P267	0.124 +/- 0.002%	buried
L133	0.45 +/- 0.02%	buried	M272	33 +/- 2%	exposed
H140	2.0 +/- 0.2%		W276	28.7 +/- 0.8%	exposed
V161	0.20 +/- 0.03%	buried	T289	0.85 +/- 0.03%	
Y162	1.92 +/- 0.05%		V294	0.24 +/- 0.03%	
A166	0.076 +/- 0.006%	NA	P295	0.24 +/- 0.03%	
R167	0.150 +/- 0.006%	NA	H299	2.31 +/- 0.05%	
S175	0.27 +/- 0.02%	exposed			

[a] Each per-residue yield was determined by subtracting the average yield of the residue from triplicate control samples from the average yield of the residue from triplicate FPOP samples.
[b] Residues marked as "buried" are less than 50% labeled compared to the average labeling of all modification-detected residues of the same type. Residues marked as "exposed" are more than 50% labeled compared to the average labeling of all modification-detected residues of the same type. Arginine residues are marked as NA because the yield determinations for some Arg residues are biased, due to their FPOP-mediated loss of the Trypsin-substrate guanidinium group. Other residues marked as

NA were the only of their kind detected as modified.

Table 6.2: Average reactivity per amino acid

amino acid	average yield
M	18.61%
W	15.27%
C	6.55%
K	2.18%
H	2.17%
Y	1.93%
F	1.88%
L	0.92%
I	0.70%
T	0.62%
V	0.43%
E	0.42%
P	0.41%
R	0.15%
S	0.14%
Q	0.12%
A	0.08%

6.3.3 Basic residue yields.

The average lysine labeling (Table 6.2) is higher than expected from its free-amino acid reaction rate[39]. This may be due to a bias imparted by using trypsin for proteolysis, as seven of eight peptides having a modified lysine are also trypsin-missed-cleavage peptides at that lysine (data not shown). Their yield calculations are each relative to the measure of the analogous unmodified trypsin-missed-cleavage peptide, whose occurrence is less prevalent due to absence of modification at the interior cleavage site. A more dramatic example of this bias is R180, whose only detected modified signal was the loss of its trypsin-substrate guanidinium group (-43 Da) in peptide

E_{179}RLGPLVEQGR$_{189}$; in this case the R180 yield was also re-calculated to include all fates of L_{181}GPLVEQGR$_{189}$ as an approximate measure of the total amount of peptide detected at R180. It is likely that some other arginines have also undergone this modification, giving rise to peptides that are too large to validate by MS^2. Owing to these uncertainties in yield calculation and modification detection, we will not rely on the arginine data for self-comparison analysis presented here. We note that in a more typical state vs. state experiment, the changes in labeling yield for the same arginine between states is still a valid, informative comparison.

6.3.4 Normalized labeling yields and relative solvent accessibility.

Of the 69 detected-as-modified residues in Table 6.1, sixteen are significantly less, and fourteen are significantly more labeled than the average labeling of the same kind of residue for each outlier. There is an approximately linear response to fast oxidative-labeling and SASA, incumbent on careful LC-MS/MS analysis[40-41]. Without a full structure for ApoE3MM, the structure cannot be tested by looking for a correlation of residue yield with calculated SASA. Instead, we have digitized the residue yields to indicate whether each is buried, exposed, or neither. Residues with a high level of labeling relative to others of the same-amino acid kind are solvent exposed, whereas residues with a low level of labeling are buried. The exposure annotation in Table 6.1 was determined by normalizing each residue's yield with the appropriate average amino acid yield in Table 6.2, then employing a > 50% or <-50% threshold relative to the average yield to signify relative exposure. The relative levels for all residues is conveyed in Figure 6.2. If we instead compare each residue to the maximum per-residue modification yield in the appropriate set of same-amino acid residues, thresholds of

>80% and <26% of the maximum exactly reproduce the average yield-determined exposed and buried classifications.

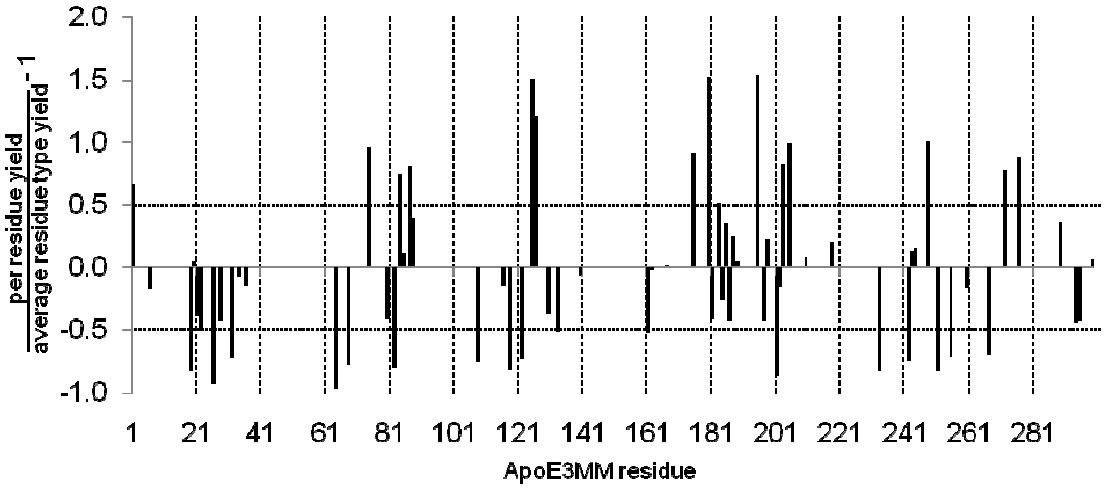

Figure 6.2: Residue-type-specific normalization of per-residue yields plotted vs. the ApoE3MM primary sequence. The average labeling for each kind of residue (Table 6.2) has been used to normalize the residue control-subtracted FPOP yields. This fraction is shifted by -1 to put residues exhibiting yields close to their same-amino acid residue average near zero. Residues with less labeling than their like average are thus below the x axis; residues with more labeling than their like average are above the x axis. Buried and exposed cutoff thresholds are shown as horizontal dashed lines at -0.5 and 0.5, respectively.

Note that the y-axis of Figure 6.2 does not convey a measure of the absolute SASA at each site. A residue sidechain SASA analysis of the $ApoE3_{1\text{-}183}$ NMR structure[3] using the GETAREA algorithm with a 1.4 Å diameter probe[42], shows that maximum non-hydrogen sidechain values vary from 64.5 $Å^2$ for alanine to 184.1 $Å^2$ for arginine and 176.58 $Å^2$ for tryptophan. Clearly a residue's SASA is determined both by its structural context and by its amino acid identity. For this reason the labeling yield was normalized to the average yield of same-amino acid residues, thus allowing the determination of exposure to be amino acid specific.

6.4 Discussion

6.4.1 LC-MS/MS analysis of protein footprint data.

This study compares each residue's labeling, relative to all other detected-as-modified residues, for a single protein state. In contrast, in most cases of chemical footprinting, two states of a protein are studied (e.g., apo vs. holo, native vs. unfolded)[29-30, 41, 43-45]. The burden of accurate detection and quantitation for the self-comparison experiment employed here is higher than that for the usual state vs. state experiment. In the latter case, it is not important if some modification fates of a residue are overlooked, as long as the proteolysis and LC-MS/MS acquisition for each state are done under identical conditions (i.e., same-day labeling, proteolysis, and contiguous MS acquisition), and the same set of ion signals from each sample's acquisition are used to calculate the yield of modification per residue. Then the difference in the measured yield at a residue between the two states reflects the difference in its solvent accessibility, no matter if some residue modification fates are missed. For example, tryptophan can be hydroxylated at several positions on its indole ring. We typically see these structural isomers resolved by reverse phase chromatography (data not shown), but sometimes one or more of the Trp-hydroxylated isomers co-elutes with the same peptide hydroxylated at a different residue. In the state vs. state experiment, this mixture EIC peak can be omitted because the same tryptophan residue is compared between states, using the same modified and unmodified peptide EIC peaks for each state—the mixture peak doesn't add any information the other well-resolved Trp-modified peaks communicate.

In this study's self-comparison analysis, all Trp-modified EIC peaks are needed, to minimize the bias of underestimation when comparing different tryptophan residues of

the single ApoE3MM state. Of course this applies to all kinds of residues. For two co-eluting peptide isomers, a fraction of the mixture peak's EIC abundance is assigned to both peptide isomers, in proportion to the number of MS^2 spectra, or spectral counts, associated with each peptide isomer. A few mixture peaks have more than two isomer components; mostly these are of the common +15.9949 hydroxylation fate. We have not included this source of signal for any residues in Table 6.1 because of the uncertainty in ascribing the appropriate EIC abundance fraction to each component. In addition, V2, E7, T8, P10, and L14 were detected-as-modified, but all of their signal resides in such isomer-mixture peaks; consequently, they have not been included in the relative SASA analysis here.

Modification fates can easily be missed in standard proteomics analysis as well. Error-tolerant searching via Mascot ensures that many more spectra looking like those of ApoE peptides are included: the error tolerant pass improved the ApoE3MM protein score to 56,907 from the initial broad database search score of 17,794. Such database matching can introduce unacceptable errors in annotation, requiring manual MS and MS^2 inspection for their correction. We have developed a generalized VBA software platform to organize and assist in the manual validation of hundreds features supporting the data reported here, and to determine which EIC peaks are comprised of isomer mixtures and provide their spectral counts.

6.4.2 Comparison of the labeling yields to the $ApoE3_{1\text{-}183}$ 3D NMR structure.

The FPOP footprint of ApoE3MM supports the hypothesis that the full structure is comprised in part by an N-terminal domain of similar fold to the $ApoE3_{1\text{-}183}$ solution phase NMR structure[3]. The primary sequences in this region of ApoE3 and ApoE3MM

are identical; this invites an analysis of the NMR structure and FPOP data to test if the full length monomeric mutant resembles the truncated protein in the 1-183 region. Residue sidechain SASA values of $ApoE3_{1-183}$ were calculated by the GETAREA algorithm[42], using a 1.4 Å diameter sphere to approximate the size of water. The expectation of exact structural concordance between the truncated and full protein is unrealistic. For this reason we have not chosen to use all labeled residues for a by-residue-type correlation analysis with the appropriate $ApoE3_{1-183}$ SASAs. Instead we reject the hypothesis of similarity if the "outlier" residues, determined by FPOP to be buried and exposed, are in fact not in the $ApoE3_{1-183}$ structure. In Figure 6.3A the ApoE3MM buried residues S22, W26, L82, Y118, V122, L133, and V161 are each significantly less exposed in $ApoE3_{1-183}$ as well, having SASAs less than 25% of the maximum SASA for either Ser, Trp, Leu, Tyr, or Val residues. Methionine SASA must be calculated differently as its product formation starts with •OH addition to its sulfur atom[23-24]; thus, the relevant SASA is of this atom only. With this correction, residues M68 and M108 are also buried in $ApoE3_{1-183}$; given the low maximum methionine sulfur SASA in $ApoE3_{1-183}$, M64 should also be considered buried. In Figure 6.3B, the ApoE3MM exposed residues K1, E87, M125, L126, S175, and P183 are also significantly more exposed in $ApoE3_{1-183}$, whereas Y74 and P84 are not. Sixteen of nineteen residues of ApoE3MM exhibit FPOP labeling in concordance with the $ApoE3_{1-183}$ structure; thus the structures may be quite similar with a slight change effecting the three discrepant residues.

The location of the FPOP-determined buried and exposed residues on the $ApoE3_{1-183}$ show a strong spatial correlation: residues along the four-helix bundle tend to be

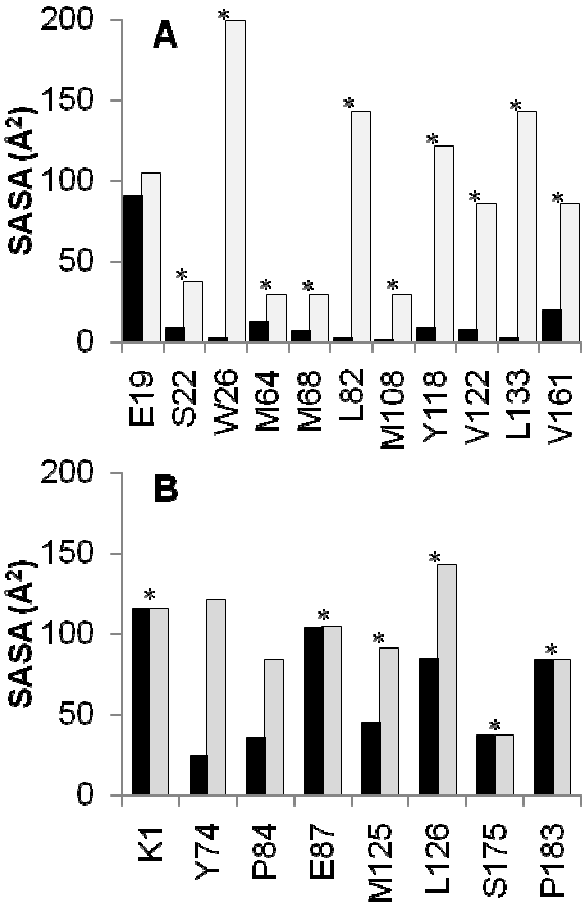

Figure 6.3: The $ApoE3_{1\text{-}183}$ protein SASA values for the set of residues determined by FPOP to be buried or exposed in $ApoE3MM_{1\text{-}299}$. SASA values are the sums of the non-hydrogen sidechain atom surface areas determined by the GETAREA algorithm of the $ApoE3_{1\text{-}183}$ NMR structure 2kc3. The black columns are the individual residue SASA values; the gray columns are the maximum SASA values per residue type, determined from the set of all such residues detected as modified. Graph A is of buried residues; graph B is of exposed residues. The asterisks mark residues exhibiting good agreement with their exposure classifications.

buried, and residues at the loop turns comprising the "end caps" of the bundle tend to be exposed (Figure 6.4). We propose that this is not coincidental, rather that the ApoE3MM adopts a similar helix-bundle structure in the 1-183 region. This suggests a reason why FPOP indicates E19, Y74, and P84 differ in ApoE3MM compared to the known structure of $ApoE3_{1\text{-}183}$. In the $ApoE3_{1\text{-}183}$ structure, these residues are resident in the same end

cap, from which the hinge and C-terminal domains are attached in ApoE3MM. This end of the putative four-helix bundle may be more allosterically-sensitive then the rest of the protein to the C-terminal domain intra- and inter-domain interactions absent in the fragment protein. There are no significant FPOP vs. SASA discrepancies between the structures that suggest a clear region of N- and C- terminal domain interaction, as the observed buried residues are turned inward or otherwise masked in the $ApoE3_{1\text{-}183}$ structure. We cannot conclude that there is no domain-domain interaction in the monomeric mutant.

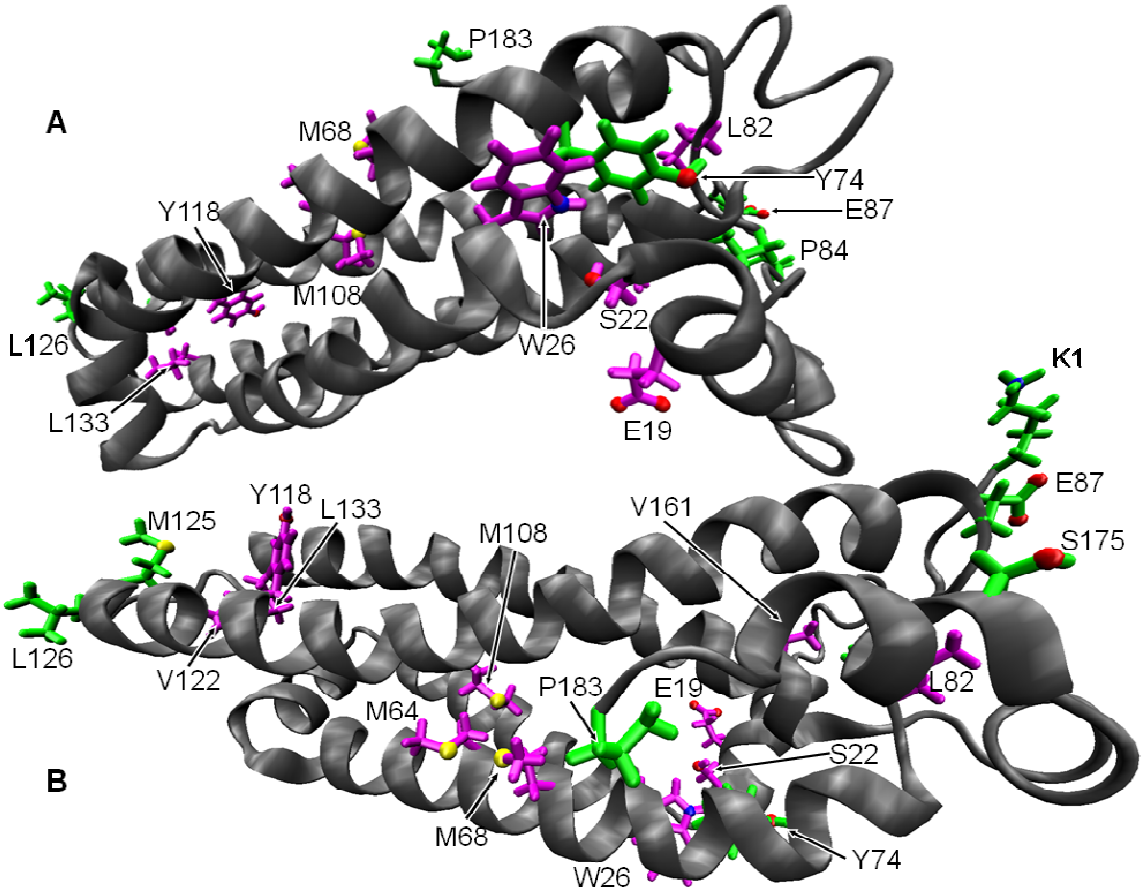

Figure 6.4: A and B are two views of the ApoE3 1-183 2kc3 NMR structure, with19 residue sidechains shown in bond and heteroatom depiction. Oxygen atoms are red, nitrogen atoms are blue, and sulfur atoms are yellow. The green residues exhibited FPOP labeling 50% greater than the average observed labeling among same-amino acid residues. The magenta residues exhibited FPOP labeling less than 50% of the average labeling among same-amino acid residues.

6.5 Conclusion

The FPOP footprinting data of ApoE3MM provide residue-resolved evidence the full monomeric structure's N-terminal-domain resembles $ApoE3_{1\text{-}183}$ structure. This is based on a subset of the observed modified residues that are significantly more labeled or less labeled than the average labeling for residues of the same kind. The thresholds for

establishing relative exposure was chosen to maximize the inclusion of residues without unduly compromising the meaning of "buried" and "exposed", relative to the size of each residue's sidechain. This tradeoff is one reason there is not enough conclusive evidence to indicate a possible N-teriminal:C-terminal domain interaction, as the subset of buried- and exposed-classified residues does not span enough of the C-terminus. Another is that observed attenuated labeling at a site cannot distinguish intra-domain packing and inter-domain interaction. We propose it is likely the ApoE3MM N-terminal domain has a structure much like $ApoE3_{1\text{-}183,}$ because the same residues buried in this domain in ApoE3MM, as determined by FPOP, are oriented away from solvent in the $ApoE3_{1\text{-}183}$ NMR structure. FPOP-observed residues buried in the ApoE3MM C-terminal domain may be so owing to the C-terminal domain's inherent structure, or may be due to an inter-domain interaction.

The utility of FPOP for prediction of structure when one is not known should be done in a digitized approach as we have employed here, to ensure that only residues that are clearly delineated are used to test hypotheses. On the other hand, with a high resolution structure of a highly homologous protein, a more rigorous analysis could be undertaken to test a hypothesis of close similarity. Evidence for corroboration is seen when the labeling yield correlates in direct proportion to the putative SASA for residues of the same amino-acid type. In either case, the analysis is based on comparing the FPOP yields of residues of the same-amino acid type. This is a more complex analysis than is typically done in protein •OH footprinting experiments, which examine the changes in protein structure between two states. Whereas tracking one modification fate of a residue can be sufficient to distinguish a SASA difference at that site between two protein states,

the experimenter must strive to quantitate all FPOP fates of the protein if a reliable judgment is to be made about the relative accessibility of each detected-as-modified residue. Were •OH footprinting not so indiscriminate in its atomic-site targeting, this task would be easier. The benefit to using •OH labeling, however, is that 1) they are so promiscuous, allowing many more sites of a protein to be probed; 2) with proper chemical control, can sample exclusively native conformations sensitive to modifications[36]; and 3) are very sensitive to SASA[40-41].

6.6 References

1. Aggerbeck, L. P.; Wetterau, J. R.; Weisgraber, K. H.; Wu, C. S.; Lindgren, F. T., Human apolipoprotein E3 in aqueous solution. II. Properties of the amino- and carboxyl-terminal domains. *J. Biol. Chem.* **1988,** *263* (13), 6249-6258.
2. Wilson, C.; Wardell, M. R.; Weisgraber, K. H.; Mahley, R. W.; Agard, D. A., Three-dimensional structure of the LDL receptor-binding domain of human apolipoprotein E. *Science* **1991,** *252* (5014), 1817-1822.
3. Sivashanmugam, A.; Wang, J., A Unified Scheme for Initiation and Conformational Adaptation of Human Apolipoprotein E N-terminal Domain upon Lipoprotein Binding and for Receptor Binding Activity. *J. Biol. Chem.* **2009,** *284* (21), 14657-14666.
4. Patel, A. B.; Khumsupan, P.; Narayanaswami, V., Pyrene Fluorescence Analysis Offers New Insights into the Conformation of the Lipoprotein-Binding Domain of Human Apolipoprotein E. *Biochemistry* **2010,** *49* (8), 1766-1775.
5. Westerlund, J. A.; Weisgraber, K. H., Discrete carboxyl-terminal segments of apolipoprotein E mediate lipoprotein association and protein oligomerization. *J. Biol. Chem.* **1993,** *268* (21), 15745-15750.
6. Farrer, L. A.; Cupples, L. A.; Haines, J. L.; Hyman, B.; Kukull, W. A.; Mayeux, R.; Myers, R. H.; Pericak-Vance, M. A.; Risch, N.; van Duijn, C. M., Effects of Age, Sex, and Ethnicity on the Association Between Apolipoprotein E Genotype and Alzheimer Disease: A Meta-analysis. *JAMA* **1997,** *278* (16), 1349-1356.
7. Strittmatter, W. J.; Saunders, A. M.; Schmechel, D.; Pericak-Vance, M.; Enghild, J.; Salvesen, G. S.; Roses, A. D., Apolipoprotein E: high-avidity binding to beta-amyloid and increased frequency of type 4 allele in late-onset familial Alzheimer disease. *Proc. Natl. Acad. Sci. U.S.A.* **1993,** *90* (5), 1977-1981.
8. Corder, E. H.; Saunders, A. M.; Strittmatter, W. J.; Schmechel, D. E.; Gaskell, P. C.; Small, G. W.; Roses, A. D.; Haines, J. L.; Pericak-Vance, M. A., Gene dose of apolipoprotein E type 4 allele and the risk of Alzheimer's disease in late onset families. *Science* **1993,** *261* (5123), 921-923.
9. Zhong, N.; Weisgraber, K. H., Understanding the Association of Apolipoprotein E4 with Alzheimer Disease: Clues from Its Structure. *J. Biol. Chem.* **2009,** *284* (10), 6027-6031.
10. Mahley, R. W.; Weisgraber, K. H.; Huang, Y., Apolipoprotein E: structure determines function, from atherosclerosis to Alzheimer's disease to AIDS. *J. Lipid Res.* **2009,** *50* (Supplement), S183-S188.
11. Bu, G., Apolipoprotein E and its receptors in Alzheimer's disease: pathways, pathogenesis and therapy. *Nat Rev Neurosci* **2009,** *10* (5), 333-344.
12. Hauser, P. S.; Narayanaswami, V.; Ryan, R. O., Apolipoprotein E: From lipid transport to neurobiology. *Progress in Lipid Research In Press, Uncorrected Proof*.
13. Xu, Q.; Brecht, W. J.; Weisgraber, K. H.; Mahley, R. W.; Huang, Y., Apolipoprotein E4 Domain Interaction Occurs in Living Neuronal Cells as Determined by Fluorescence Resonance Energy Transfer. *J. Biol. Chem.* **2004,** *279* (24), 25511-25516.
14. Dong, L.-M.; Weisgraber, K. H., Human Apolipoprotein E4 Domain Interaction. *J. Biol. Chem.* **1996,** *271* (32), 19053-19057.

15. Dong, L. M.; Wilson, C.; Wardell, M. R.; Simmons, T.; Mahley, R. W.; Weisgraber, K. H.; Agard, D. A., Human apolipoprotein E. Role of arginine 61 in mediating the lipoprotein preferences of the E3 and E4 isoforms. *J. Biol. Chem.* **1994,** *269* (35), 22358-22365.
16. Garai, K.; Frieden, C., The Association-Dissociation Behavior of the ApoE Proteins: Kinetic and Equilibrium Studies. *Biochemistry* **2010,** *49* (44), 9533-9541.
17. Zhang, Y.; Vasudevan, S.; Sojitrawala, R.; Zhao, W.; Cui, C.; Xu, C.; Fan, D.; Newhouse, Y.; Balestra, R.; Jerome, W. G.; Weisgraber, K.; Li, Q.; Wang, J., A Monomeric, Biologically Active, Full-Length Human Apolipoprotein E *Biochemistry* **2007,** *46* (37), 10722-10732.
18. Konermann, L.; Tong, X.; Pan, Y., Protein structure and dynamics studied by mass spectrometry: H/D exchange, hydroxyl radical labeling, and related approaches. *J. Mass Spectrom.* **2008,** *43* (8), 1021-1036.
19. Chance, M., *Mass Spectrometry Analysis for Protein-Protein Interactions and Dynamics*. John Wiley and Sons, Inc.: Hoboken, NJ, 2008; p 272.
20. Xu, G.; Chance, M. R., Radiolytic Modification of Sulfur-Containing Amino Acid Residues in Model Peptides: Fundamental Studies for Protein Footprinting. *Anal. Chem.* **2005,** *77* (8), 2437-2449.
21. Xu, G.; Chance, M. R., Radiolytic Modification and Reactivity of Amino Acid Residues Serving as Structural Probes for Protein Footprinting. *Anal. Chem.* **2005,** *77* (14), 4549-4555.
22. Xu, G.; Chance, M. R., Radiolytic Modification of Acidic Amino Acid Residues in Peptides: Probes for Examining Protein-Protein Interactions. *Anal. Chem.* **2004,** *76* (5), 1213-1221.
23. Garrison, W. M., Reaction mechanisms in the radiolysis of peptides, polypeptides, and proteins. *Chem. Rev.* **1987,** *87* (2), 381-398.
24. Xu, G.; Chance, M. R., Hydroxyl Radical-Mediated Modification of Proteins as Probes for Structural Proteomics. *Chem. Rev.* **2007,** *107* (8), 3514-3543.
25. Heyduk, E.; Heyduk, T., Mapping Protein Domains Involved in Macromolecular Interactions: A Novel Protein Footprinting Approach. *Biochemistry* **1994,** *33* (32), 9643-9650.
26. Shanblatt, S. H.; Revzin, A., Interactions of the catabolite activator protein (CAP) at the galactose and lactose promoters of Escherichia coli probed by hydroxyl radical footprinting. The second CAP molecule which binds at gal and the one CAP at lac may act to stimulate transcription in the same way. *J. Biol. Chem.* **1987,** *262* (24), 11422-11427.
27. Tullius, T. D.; Dombroski, B. A., Hydroxyl radical "footprinting": high-resolution information about DNA-protein contacts and application to lambda repressor and Cro protein. *Proc. Natl. Acad. Sci. U.S.A.* **1986,** *83* (15), 5469-5473.
28. Fenton, H. J. H., The oxidation of tartaric acid in presence of iron. *J. Chem. Soc. Proc.* **1894,** *10*, 157-158.
29. Maleknia, S. D.; Ralston, C. Y.; Brenowitz, M. D.; Downard, K. M.; Chance, M. R., Determination of Macromolecular Folding and Structure by Synchrotron X-Ray Radiolysis Techniques. *Anal. Biochem.* **2001,** *289* (2), 103-115.
30. Goldsmith, S. C.; Guan, J.-Q.; Almo, S. C.; Chance, M. R., Synchrotron Protein Footprinting: A Technique to Investigate Protein-Protein Interactions. *J. Biomol. Stuc. Dyn.* **2001,** *19* (3), 405-419.
31. Venkatesh, S.; Tomer, K. B.; Sharp, J. S., Rapid identification of oxidation-induced conformational changes by kinetic analysis. *Rapid Commun. Mass Spectrom.* **2007,** *21* (23), 3927-3936.
32. Sharp, J. S.; Tomer, K. B., Analysis of the Oxidative Damage-Induced Conformational Changes of Apo- and Holocalmodulin by Dose-Dependent Protein Oxidative Surface Mapping. *Biophys. J.* **2007,** *92* (5), 1682-1692.

33. Sharp, J. S.; Becker, J. M.; Hettich, R. L., Analysis of Protein Solvent Accessible Surfaces by Photochemical Oxidation and Mass Spectrometry. *Anal. Chem.* **2003,** *76* (3), 672-683.
34. Hambly, D. M.; Gross, M. L., Laser Flash Photolysis of Hydrogen Peroxide to Oxidize Protein Solvent-Accessible Residues on the Microsecond Timescale. *J. Am. Soc. Mass Spectrom.* **2005,** *16* (12), 2057-2063.
35. Aye, T. T.; Low, T. Y.; Sze, S. K., Nanosecond Laser-Induced Photochemical Oxidation Method for Protein Surface Mapping with Mass Spectrometry. *Anal. Chem.* **2005,** *77* (18), 5814-5822.
36. Gau, B. C.; Sharp, J. S.; Rempel, D. L.; Gross, M. L., Fast Photochemical Oxidation of Protein Footprints Faster than Protein Unfolding. *Anal. Chem.* **2009,** *81* (16), 6563-6571.
37. Vidavsky, I.; Rempel, D. L.; Gross, M. L., 2D Mass Spectra Correlation – Semi Automatic Tool for Modified Peptide Discovery. In *Proceedings of the 54th ASMS Conference on Mass Spectrometry and Allied Topics*, Seattle, WA, 2006.
38. Aebersold, R.; Mann, M., Mass spectrometry-based proteomics. *Nature* **2003,** *422* (6928), 198-207.
39. Buxton, G. V.; Greenstock, C. L.; Helman, W. P.; Ross, A. B., Critical Review of Rate Constants for Reactions of Hydrated Electrons, Hydrogen Atoms and Hydroxyl Radicals (*OH/*O-) in Aqueous Solution. *J. Phys. Chem. Ref. Data* **1988,** *17* (2), 513-886.
40. Gau, B. C.; Chen, H.; Zhang, Y.; Gross, M. L., Sulfate Radical Anion as a New Reagent for Fast Photochemical Oxidation of Proteins. *Anal. Chem.* **2010,** *82* (18), 7821-7827.
41. Charvátová, O.; Foley, B. L.; Bern, M. W.; Sharp, J. S.; Orlando, R.; Woods, R. J., Quantifying Protein Interface Footprinting by Hydroxyl Radical Oxidation and Molecular Dynamics Simulation: Application to Galectin-1. *J. Am. Soc. Mass Spectrom.* **2008,** *19* (11), 1692-1705.
42. Gerstein, M., A resolution-sensitive procedure for comparing protein surfaces and its application to the comparison of antigen-combining sites. *Acta Crystallographica Section A* **1992,** *48* (3), 271-276.
43. Hambly, D.; Gross, M., Laser flash photochemical oxidation to locate heme binding and conformational changes in myoglobin. *Int. J. Mass Spectrom.* **2007,** *259* (1-3), 124-129.
44. Xu, G.; Liu, R.; Zak, O.; Aisen, P.; Chance, M. R., Structural Allostery and Binding of the Transferrin{middle dot}Receptor Complex. *Mol Cell Proteomics* **2005,** *4* (12), 1959-1967.
45. Guan, J. Q.; Vorobiev, S.; Almo, S. C.; Chance, M. R., Mapping the G-Actin Binding Surface of Cofilin Using Synchrotron Protein Footprinting. *Biochemistry* **2002,** *41* (18), 5765-5775.

7 β-amyloid 1-42 Binds to the Same Region in the N-terminus Domains of Apolipoprotein E3 and Apolipoprotein E4, Determined by FPOP Footprinting and Mass Spectrometric Analysis

7.1 Introduction

Alzheimer's disease (AD) is a form of dementia, effecting more than 35 million people worldwide[1]. The consensus of research is that AD is caused by the accumulation of misfolded proteins in the brain. Certain β-amyloid (Aβ) peptides are particularly susceptible to such misfolding. Aβ peptides are 36 to 43 amino acids long and originate from the sequential proteolysis of amyloid precursor protein, a transmembrane protein of unknown function, by β and γ secretases[2]. Among these, $A\beta_{1-40}$ (Aβ40) and $A\beta_{1-42}$ (Aβ42) are the most abundant components in the insoluble fibrils comprising a central characteristic feature of advanced AD, the senile plaques found in the extracellular space of gray matter[3]. The "amyloid hypothesis" for AD development is that the dynamic equilibrium of soluble Aβ40 and Aβ42 is crucial—factors that increase Aβ peptide production or inhibit its clearance allow for their accumulation, which initiates AD and the formation of fibrillar deposits[4]. This thinking stems in part from the observation that the soluble forms of Aβ peptide, especially Aβ42, are known to be neurotoxic[5].

The highest genetic risk for AD is for homozygous carriers of the apolipoprotein E ε4 allele, who are twelve times more likely to develop late onset AD than people with two copies of the other common isoforms of apolipoprotein E (ApoE) [6-7]. ApoE is a 34 kDa protein, whose function is to regulate lipid metabolism and control lipid

redistribution in tissue and cells, especially in the brain [8]. The three most common isoforms differ at two residues; apolipoprotein E2 (ApoE2) has cysteines at positions 112 and 158; apolipoprotein E3 (ApoE3) has a cysteine at position 112 and an arginine at 158, and apolipoprotein E4 (ApoE4) has arginines at these positions. The protein has two distinct domains connected by a thrombin proteolysis-sensitive region[9]. The N-terminal (Nt) 1-191 residue domain contains the LDL receptor-binding site, and substantial fragments of the Nt domain have been characterized by X-ray crystallography and solution NMR spectroscopy as having an elongated four-helix bundle structure[10-11]. The C-terminal (Ct) 216-299 residue domain has not been characterized by high resolution methods because of its propensity to oligomerize[12]. This property is shared by all of the common isoforms of ApoE, and no high resolution structures have been reported.

There are several hypotheses that explain the association of ApoE4 with AD[13], but there is no clear consensus for a single cause. In the early study that reported this association, it was discovered that ApoE binds to Aβ in cerebrospinal fluid[6]. Since then the hypothesis that ApoE is directly involved in the deposition or clearance of Aβ is gaining widespread recognition[14]. Vital to understanding this mechanism is the characterization of the ApoE-Aβ interaction. Many studies have undertaken this goal, examining the interaction of lipoprotein and lipid-free forms of the common isoforms of ApoE and their fragment domains with soluble and insoluble preparations of Aβ40 and Aβ42 and Aβ analogs[14]. Here we focus on delipidated ApoE interactions. Several early studies showed that lipid-free ApoE binding with soluble Aβ influences fibrillogenesis[15-17]. The association of lipid-free ApoE with soluble Aβ40 can be tight, with a K_D of 10-

20 nM, but this depends on the conformation of Aβ[18-19]. Based on Nt and Ct domain fragment studies, there are at least two sites of interaction on ApoE segregated among these domains[20-23]. None of these studies provide a high resolution characterization of the sites because of the oligomeric properties of both biomolecules.

Mass spectrometry (MS)-based chemical footprinting of proteins is a method for providing peptide and residue-resolved structural information, in the primary sequence dimension[24-25]. A general strategy is to use this information to provide insight about the difference between structures of a protein or protein complex in two or more states, rather than resolve their structures in three dimensions. Labeling that well samples solvent accessible residues will be attenuated at protein-ligand or protein-protein interfaces in the complex compared to the apo state. If the labeling is stable, a proteomics-like "bottom-up" mass spectrometry methodology can be employed, in which modified proteolytic peptides from both states are quantified by LC-MS and identified by their MS^2 CID fragment spectra.

An important chemical footprinting method is hydroxyl radical-mediated modification of solvent accessible sidechains; a comprehensive review detailing several methodologies for •OH generation, expected product chemistry, and mass spectrometric analysis has recently been published[26]. The advantages of •OH-based footprinting are that (1) residue solvent accessibility surface areas (SASAs) are well sampled, because the size of •OH is comparable to water; (2) the •OH-mediated modifications are stable and thus amenable to proteolytic peptide-based LC-MS/MS analysis; and (3) •OH samples residue sidechains non-specifically, detectably reacting with over half of the common

amino acids in properly controlled experiments[27]. We use the method of fast photochemical oxidation of proteins (FPOP), developed by Hambly and Gross[28], to provide the source of •OH. This method employs a KrF excimer laser as a pulsed 248 nm source; each 17 ns flash homolytically cleaves H_2O_2, added to the sample at a low millimolar level. In the flow cell the resultant •OH reacts with protein sidechains on a microsecond timescale as added glutamine competitively scavenges radical. This ensures that only equilibrium conformations are sampled by •OH; any modification-induced changes to conformation evolve on a slower timescale[29].

By FPOP labeling and LC-MS/MS we are able to characterize the sites of interaction of Aβ42 with lipid-free ApoE3 and ApoE4. We have examined this interaction at the 4 μM protein level, at which concentration these isoforms are primarily tetramers[30], and at 100 nM for ApoE3 to probe its putative monomeric interaction with Aβ42. We also report the FPOP-characterized interaction of Aβ40 with ApoE-orangutan because of the concordance of results with the human isoforms.

7.2 Experimental Procedures

7.2.1 Reagents.

Acetonitrile, formic acid, 30% hydrogen peroxide, *L*-glutamine, *L*-methionine, *tris*(2-carboxyethyl)phosphine hydrochloride (TCEP), sodium hydroxide, hydrochloric acid, catalase, sequencing grade trypsin, and phosphate buffered saline (PBS) were purchased from Sigma Aldrich Chemical Co. (St. Louis, MO). Purified water (18 MΩ) was obtained from a Milli-Q Synthesis system (Millipore, Billerica, MA). ApoE3, ApoE4, and Aβ42, each expressed in *E. coli*, were kindly provided by Drs. K. Garai and

C. Frieden. Aβ40 was purchased from American Peptide Company (Sunnyvale, Ca). ApoE-orangutan was purchased from BioVision (Mountain View, CA).

7.2.2 Stock solution preparations.

Purified ApoE3 and ApoE4, provided as solutions in ammonium bicarbonate, were dialyzed overnight into PBS. To prevent adventitious disulfide bond formation in ApoE3, TCEP was added to 200 μM; ApoE4 also received TCEP to maintain background composition equality with ApoE3 samples. The purity of dialyzed proteins was confirmed by ESI MS on a Maxis QTOF spectrometer (Bruker Daltonics, Billerica, MA); disulfide-linked ApoE3 dimer was not observed (data not shown). ApoE3 and E4 solutions were split among aliquots, then frozen with N_2(l) and stored at -80 °C. ApoE-orangutan was solubilized in PBS and apportioned and stored by the same protocol. For all ApoE isoforms, stock concentrations were determined by their UV absorbance, with $\varepsilon_{280} = 44{,}950\ M^{-1}\ cm^{-1}$. Lyophilized Aβ40 was solubilized at 1 mg/mL in 10 mM NaOH and apportioned and stored by the same protocol. The stock Aβ42 solution was prepared from lyophilized material by solubilizing in 10 mM NaOH to 150 μM concentration; half the volume was apportioned to 16.7 μL aliquots for the nanomolar experiments. The remainder volume and aliquots were N_2(l) frozen and stored at -80 °C prior to use. Stock glutamine, methionine, catalase, and hydrogen peroxide solutions were prepared in PBS on the same days as labeling. Eppendorf Protein LoBind micro tubes (Eppendorf North America, Hauppauge, NY) were used for all protein stock and sample solutions, except for de-salting collection that used standard polypropylene microcentrifuge tubes.

7.2.3 Micromolar ApoE3 and ApoE4 experiments.

Equilibration stock solutions were prepared for ApoE3 and ApoE4 to the final concentrations of 4.0 μM protein, 22.2 mM glutamine, and for "Aβ42-present" equilibration solutions, 20 μM Aβ42. For "Aβ42-free" samples, a volume of 10 mM NaOH was added equal to the Aβ42 addition in the counterpart equilibration solutions. A volume of 100 mM HCl equal to 10% of this addition volume was added to all equilibration solutions to maintain the PBS-buffered pH of 7.4. The equilibration solutions were stored 2 hr at 22 °C with no stirring, prior to the first replicate draws for FPOP labeling. Due to the time needed to complete FPOP labeling of each set of replicates, the ApoE4 equilibration solution was prepared 1 hr after the ApoE3 solution.

7.2.4 Micromolar ApoE-orangutan experiment.

Three equilibration stock solutions were prepared. For each, the final concentrations of ApoE-orangutan and glutamine was 2.22 μM and 22.2 mM, respectively. The "1:4", "1:1", and "1:0" solutions' Aβ40 concentrations were 8.89, 2.22, and 0 μM, respectively. 10 mM NaOH was added to the 1:1 and 1:0 solutions to maintain equivalence with the 1:4 solution, and all solutions were spiked with a 1% volume of 100 mM HCl to return the pH to 7.4. These solutions were stored 4.5 hr at 22 °C with no stirring, prior to the first replicate draws for FPOP labeling.

7.2.5 NanomolarApoE3 experiments.

The replicate 100 nM samples were each prepared to final concentrations of 111 nM ApoE3, 22.2 mM glutamine, and for "Aβ42-present" samples, 5.6 μM Aβ42.

Equilibration stock solutions were not used because 25 min elapsed between each replicate's labeling. During this time the structural state of the system may change due to evolving protein-protein, protein-peptide, peptide-peptide, and biomolecule-plastic surface interactions.

Each replicate sample was processed as follows. (1) At the time of 150 μM Aβ42 stock solution preparation, 428 μL of 23.3 mM glutamine in PBS was added to 16.67 μL aliquots of either Aβ42 in 10 mM NaOH, or 10 mM NaOH for "Aβ42-free" samples. These aliquots were N_2(l) frozen and stored at -80 °C. (2) An aliquot was thawed 12 min and vortex-mixed. (3) Five μL of 10 μM ApoE3 was added to the sample with vortex-mixing. (4) The sample was stored 2 hr 5 min at 22 °C, with no stirring. (5) Hydrogen peroxide was added to the sample, and the entire volume was infused through the FPOP apparatus. The standard FPOP protocol is described below. The collection tube was the upper compartment of a 10000 MWCO Vivaspin 500 sample concentrator (GE Healthcare, Waukesha, WI), and contained 0.2 μg catalase in 36 μL 150 mM methionine. (6) The labeled sample was centrifuged at 13,500 x g for 5 min. The retentate, typically 10-20 μL, was transferred to a LoBind tube and left open for 25 min at 22 °C. (7) The labeled sample was N_2(l) frozen and stored at -80 °C prior to proteolysis.

7.2.6 FPOP labeling.

Just prior to FPOP, H_2O_2 was added to each replicate by 10-fold dilution from a concentrated solution, to give a final concentration of 20 mM. Replicate draws from the equilibrium stock solutions were 40 μL for the ApoE3 and ApoE4 μM experiments and

90 μL for the ApoE-orangutan μM experiment. The FPOP apparatus was essentially the same as originally described [28], using 150 μm ID fused silica. The KrF excimer laser (GAM Laser Inc., Orlando, FL) was focused to give a 2.54 mm irradiation window on the silica. The laser power, laser pulse frequency, and syringe pump flow rate were adjusted to the following values. For ApoE3 and ApoE4 μM experiments, these were 47.6 mJ/pulse, 5 Hz, and 17.95 μL/min. For the ApoE-orangutan μM experiment, these were 45.0 mJ/pulse, 5.5 Hz, and 18.52 μL/min. For the ApoE3 nM experiment, these were 47.0 mJ/pulse, 10 Hz, and 35.9 μL/min. These flow rate and pulse frequency settings ensured at least a 20% exclusion volume to avoid repeat •OH exposure[29]. For μM experiments, each replicate was collected in a microcentrifuge tube containing 0.2 μg of catalase in 10 μL of methionine solution, to give a final concentration of 10 mM Met in the total collected sample volume. The addition of Met was to mitigate post-FPOP oxidation of protein [31]. For μM experiments, catalase was allowed to oxidize H_2O_2 to $O_2(g)$ for 10 min at room temperature with pipette mixing; $O_2(g)$ was removed by three centrifugation steps during the incubation. After 10 min, samples were $N_2(l)$ frozen by and stored at -80 °C prior to proteolysis. For all experiments, control samples were handled in the same manner as those submitted to FPOP, but they were not laser irradiated. All experiments generated three replicates for each FPOP state and each control state, with the replicates' origin preceding the FPOP step.

7.2.7 Proteolysis.

Micromolar experiment samples were proteolyzed with 8:1 protein:trypsin (by weight) at 37 °C for 7 hr. Trypsin activity was quenched with 10% formic acid addition, and the samples were SpeedVac-concentrated 30-60 min to 30 μL. Samples were de-salted by $Ziptip_{C18}$ (Millipore, Billerica, MA), with elution into 10 μL of 50% acetonitrile/1% formic acid solution. A portion of each was diluted 33-fold with water and 0.1% formic acid for autosampler loading in its LC-MS/MS analysis. Nanomolar experiment samples were proteolyzed with 0.1 μg trypsin at 37 °C for 9 hr before quenching with formic acid. They were $Ziptip_{C18}$ de-salted without prior SpeedVac-concentration, eluted directly into autosampler vials containing 2 μL of the elution solution, and diluted with 50 μL of water.

7.2.8 LC-MS/MS acquisition.

Each replicate was loaded by autosampler onto a 20 cm column with a PicoFrit tip (New Objective, Inc, Woburn, MA), bomb-packed with C18 reverse phase material (Magic, 0.075 mm × 200 mm, 5 μm, 300 Å, Michrom, Auburn, CA). For μM samples the load volume was 5 μL; for nM samples it was 7 μL. Peptides were eluted by an 80 min, 260 nL/min gradient coupled to the nanospray source of an LTQ-Orbitrap mass spectrometer (Thermo Fisher, Waltham, MA). Mass spectra were obtained at high mass resolving power (100,000 for ions of m/z 400) on the Orbitrap component, and the six most abundant ions eluting per scan were each subjected to CID MS^2 experiment in the LTQ component, using a collision energy 35% of the maximum, a 2 Da isolation width,

and wideband activation. Precursor ions were added to a dynamic exclusion list for 8 s to ensure good sampling of the apex of their elution peaks. Blanks were run between every sample acquisition.

7.2.9 Data Analysis.

Rosetta Elucidator (Microsoft, Bellevue, WA) peak detection and alignment software was used to generate an aligned LC-MS feature tables for each sample acquisition. Briefly, a feature represents the naturally occurring isotopic ensemble of one molecule eluting in time. A feature's ion signal is split among its isotopes and sometimes among several charge states depending on its basicity and the ionization conditions at the MS source. A feature's quantitation is determined by summing the areas of all such co-eluting LC-MS extracted ion chromatogram (EIC) peaks that share the same monoisotopic mass within a high resolution tolerance (5 ppm).

All sample replicates from the same experiment were subjected to a single alignment analysis so that their shared features nearly co-eluting in time would have the same unique ID and aligned elution time in the tables. The alignment program also associated the all MS^2 spectra with their LC-MS features using the same unique ID nomenclature. Independent from the Elucidator analysis, the MS^2 spectra were searched against a restricted database containing the ApoE isoforms, Aβ peptides, catalase, and other proteins using Mascot error-tolerant searching. Common OH modification products[26] were included in the variable modification list used by Mascot. A custom Excel-based VBA program paired the Mascot calls with their LC-MS quantified features using the unique ID handles. This program augmented these LC-MS Mascot annotations

with putative matches to a theoretical FPOP-modified tryptic peptide list of the ApoE isoforms. These putative matches, and over half of the Mascot calls, were validated, corrected, or rejected by manual inspection of their associated MS^2 spectra before their use in per-peptide and per-residue yield analysis.

Per-residue yields were calculated according to equation 1.

$$residue_i\ yield = \frac{\sum peptide\ intensities\ modified\ at\ residue_i}{\sum peptide\ intensities\ with\ same\ 1^\circ\ sequence\ as\ numerator\ peptides} \quad (1)$$

Here peptide is synonymous with feature and *i* is not the index of summation. The denominator includes modified and unmodified peptides alike. The denominator excludes signal from missed-cleavage peptides spanning $residue_i$ if such peptides are not also detected as modified there, because in this case the lack of modification detection is an analytic failure and does not stem from a true absence of labeling. Per-peptide yields were determined more simply according to equation 2.

$$peptide_i\ yield = \frac{\sum modifed\ peptide_i\ intensities}{unmodified\ peptide_i\ intensity + \sum modifed\ peptide_i\ intensities} \quad (2)$$

7.2.10 Utility of per-peptide and per-residue analyses.

The peptide-level survey is warranted because it is the most inclusive of LC-MS feature data, and is easily interpreted. The per-peptide analysis uses modified peptide features whose peptide identity is certain but whose modification residue(s) cannot be determined by the associated MS^2 spectrum or spectra. Such indeterminateness is possible when an MS^2 spectrum is sparse, the modification is in a peptide region insensitive to CID fragmentation, or multiple modifications are present on the peptide. The per-peptide analysis also uses LC-MS features that are clearly comprised of modified

peptide isomers without regard to which modified peptide is the most abundant species in the mixture peak. For these reasons, the per-peptide analysis provides the most accurate measure of region-by-region footprinting yield. On the other hand, the most •OH-reactive residues, especially methionine and tryptophan [27, 32-33], dominate the signal contribution in peptides bearing them when they are solvent accessible in the protein. A per-residue level analysis rescues the SASA insight neighboring less-reactive residues may inform, as it provides a primary sequence-resolved analysis of structure for all residues detected as modified. The drawback of this analysis is that uncertain modification features and some mixture features cannot be used, though their peptide sequences are clearly identified.

7.3 Results

7.3.1 Micromolar ApoE3 and ApoE4 experiments.

A survey at the peptide level for both proteins indicates one shared region of protection, ApoE33-38, in the Aβ42-present state compared to the Aβ42-free state (Figure 7.1). This peptide yield, shown as a red bar for the Aβ42-free ApoE3 and ApoE4 states, is 50% more labeled than the Aβ42-present state for both isoforms. The same modified and unmodified peptide LC-MS features were used in the comparison yield calculations, and the modifications were created by exact adherence to the labeling protocol repeated within a two hour timeframe. These two facts mean the only explanations for the differences in FPOP-labeling between Aβ42-present and free states is due to (1) steric protection from •OH by direct interaction with Aβ42 in this region, (2)

steric protection from •OH by an allosteric response to ApoE-Aβ42 interaction, or (3) adverse radical scavenging by Aβ42. The latter explanation is not likely, given the equivalence in labeling seen for much of the rest of the protein. In particular, the C-terminal domain does not show regions of interaction at the micromolar level. The peptide 120-134 is significantly more labeled in the ApoE3 Aβ42-present state than the ApoE3 Aβ42-free state, but the opposite trend is seen for ApoE (Figure 7.1C).

At the per-residue resolved level, W34, Y36, and R167 are significantly more protected in the Aβ42-present state than the -free state for both ApoE3 and ApoE4 (Figure 7.2). P293 shows the same trend in ApoE3, while E80 and L252 are less protected in the Aβ42-present state than the -free state for ApoE4. Once again, we attribute these differences to the interaction of Aβ42 with ApoE, though the effects at E80 and L252 in ApoE4 are small. The differences plotted in Figure 7.2 are only those deemed significant by a Student's t-test at 95% confidence, and they are each normalized to the maximum yield observed in the set of same-amino acid-type of residues (all differences are calculated from the per residue yields listed in Supporting Information Table 7.1). This is done to lend a significance to the magnitude of the difference, because amino acids have inherently different reaction rates to •OH[33]. The factors affecting the protein rate of labeling in FPOP, such as laser power and protein concentration, can vary between experiments; therefore, normalization is based on experiment yields and not external standards. We interpret a normalized change of 1 to approximate full exposure of the residue in the comparison. Thus, at least half of the

potential SASA of W34, Y36, and R167 is obscured in the Aβ42-present state for both proteins.

Forty-four residues spanning the full length of both proteins show no statistical change in labeling with the addition of Aβ42, consistent with the per-peptide analysis (Figure 7.2, red marks; Supporting Information Table 7.1). For these regions we conclude there is not a strong interaction with Aβ42. Two regions are under-sampled in our analysis. Region 39-61 does not possess any intervening trypsin active sites. The analytic detection of large peptides of this kind is problematic for online chromatography optimized for smaller proteolytic peptides, and the MS^2 CID fragment spectra of modified large peptides often can't resolve the modifications' residue locations. Region 135-158 is weakly sampled because the FPOP signal can be split among dozens of small tryptic and semi-tryptic peptides by virtue of basic residues at positions 136, 142, 143, 145, 146, 147, 150, 157, and 158.

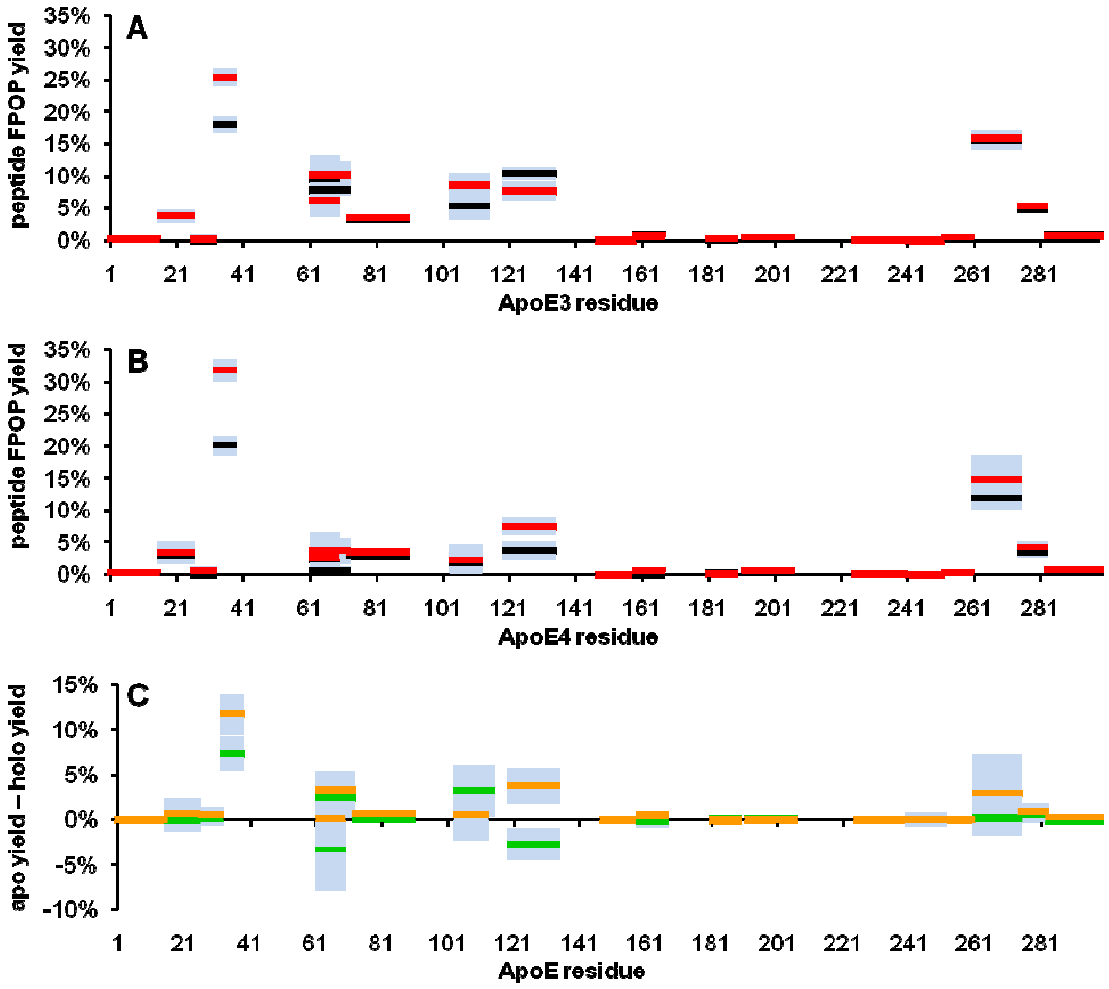

Figure 7.1: Comparison of the tryptic-peptide-resolved FPOP labeling yields for the wild type isoforms ApoE3 and ApoE4 in Aβ42-present and Aβ42-free states at 4 μM protein. The length of each bar confers the sequence length of the peptide. Peptides less than 7% of each state's maximum ApoE peptide abundance are not shown for clarity, as they typically are overlapping missed-cleavage or short peptides spanning the displayed peptides. Panel **A** plots the FPOP labeling yield for ApoE3 peptides in the Aβ42-present state in black and -free state in red. Standard errors for each yield measurement are shown in blue. The background modification fraction per peptide has been subtracted. All peptide pairs for the peptide states are shown; some black bars are obscured by red bars when the peptides have equivalent labeling yields. Panel **B** plots the per-peptide ApoE4 Aβ42-present and -free states' results, with the same color scheme. Panel **C** compares the apo/holo differential yield of ApoE3 (green) and ApoE4 (orange).

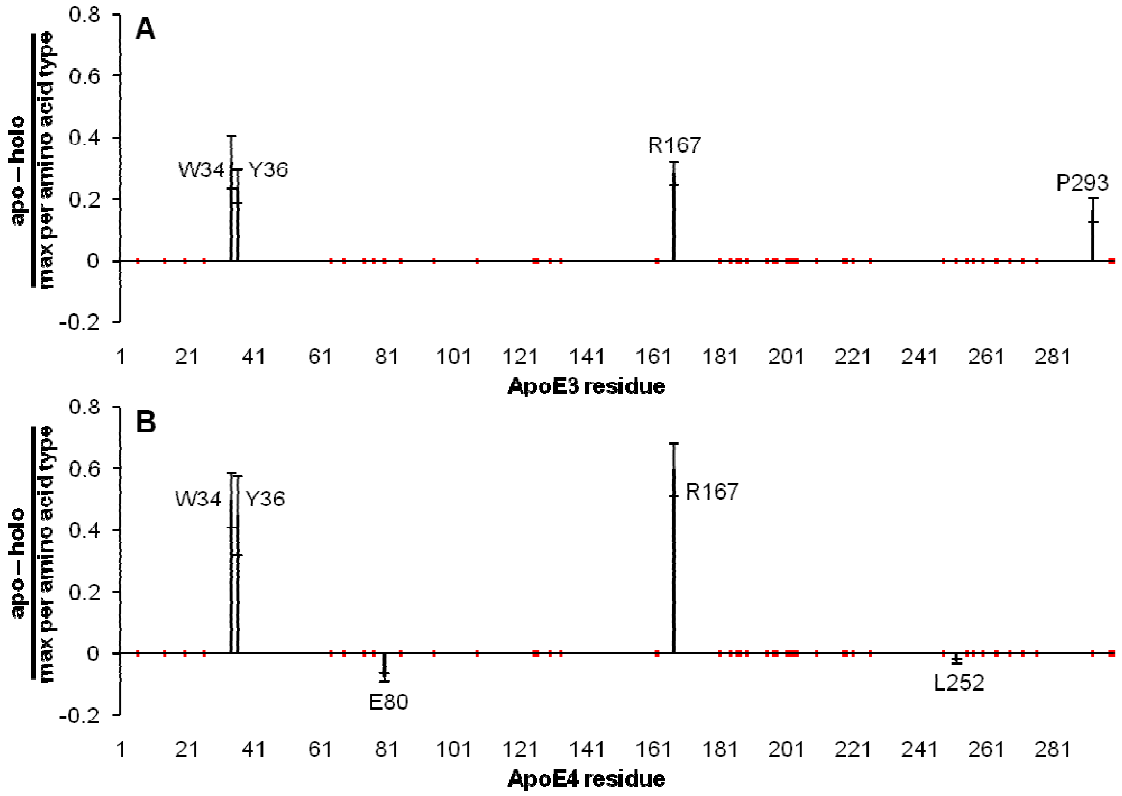

Figure 7.2: Comparison of the residue-resolved FPOP labeling yields for ApoE3 and ApoE4 in Aβ42-present and Aβ42-free states at 4 μM protein. Panel **A** plots the ApoE3 significant differences in FPOP labeling yield between each state, per residue, normalized by the maximum yields observed among all residues of the same amino acid types. Significance is determined at 95% confidence by the Student's t-test. Residues marked with red were detected as labeled in both states but their labeling difference was not significant. Panel **B** similarly plots the ApoE4 per residue data.

Both W34 and Y36 are resident in the same tryptic peptide of ApoE. One alternative explanation for the FPOP yield depression of these residues in the Aβ42-present state, is that the detection of the unmodified peptide $F_{33}WDYLR_{38}$ is attenuated in the Aβ42-free samples by an ESI bias. This unmodified peptide's signal is the major contributor to the denominator in the yield calculations for both residues. The EICs of unmodified $F_{33}WDYLR_{38}$ in sample acquisitions from each state show that the

unmodified peptide is apparently less abundant in the Aβ42-free state (Figure 7.3A, top panel), while the +15.9949 Da-modified peptide EICs exhibit the opposite trend (Figure 7.3A, bottom panel). The full MS spectra, averaged from the Orbitrap scans made during the elution of unmodified $F_{33}WDYLR_{38}$, shows that this depression is not owing to ion suppression, a major source of ESI bias[34]. This follows because the spectra are highly similar between states, and no other ions are observed at high abundance (Figure 7.3B).

7.3.2 Nanomolar ApoE3 experiment.

Only region16-25 shows a significant attenuation in labeling in the Aβ42-present state compared to the Aβ42-free in the 111 nM ApoE3 experiment (Figure 7.4). No other regions show the opposite trend, though several, including 26-38, are silent in the FPOP analysis due to the complications of working with very dilute protein solutions. At nM levels protein adsorption may have a significant effect on the system state: in a separate preliminary experiment we observed that β-lactoglobulin, an 18.3 kDa globular protein, is depleted 86% by the same sample handling steps described here (data not shown).

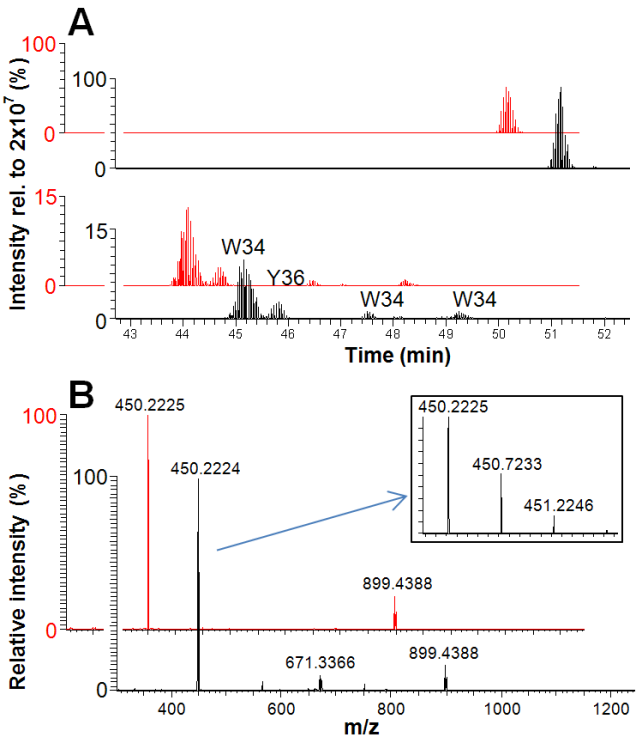

Figure 7.3: LC-MS data underlying the yield calculations for W34 and Y36 in the 4 μM ApoE3 Aβ42-present and -free states. In panel **A**, the upper two extracted ion chromatograms (EIC), at 450.2241+/- 0.0023 m/z, show LC-MS peaks eluting from 51.0 to 51.3 min in the Aβ42-present (black) and Aβ42-free (red) samples; by their accurate precursor ion m/z and MS^2 fragmentation spectra, these features are identified as the unmodified doubly protonated peptide $F_{33}WDYLR_{38}$. The lower two EIC, at 458.2216+/- 0.0023 m/z, show several features shared by each sample; these are identified as isomers of hydroxylated $F_{33}WDYLR_{38}$; their residue-resolved sites of modification are indicated. In all EIC the relative intensity is determined relative to the base peak intensity of the unmodified $F_{33}WDYLR_{38}$ Aβ42-present EIC; the modified peptide EICs are shown on a magnified scale. In panel **B**, an average mass spectrum is shown for the 10 high resolution Orbitrap spectra acquired from 51.0 to 51.3 min. The black trace is for the Aβ42-present sample; the red trace is for the Aβ42-free sample. Peaks at 450.224 and 899.439 correspond to doubly and singly protonated unmodified $F_{33}WDYLR_{38}$, respectively. The zoomed inset of the spectrum about 450.224 shows the characteristic half-m/z ^{13}C spacing for doubly-charged ions.

Figure 7.4 presents per-peptide data in a different way than Figure 7.1 and Figure 7.2, due to an additional limitation imposed by chromatographic variance. Each plotted value is the average of yield differences, not difference in average yields, between states,

normalized by the standard deviation and with control yield levels subtracted. The LC-MS/MS acquisitions of the triplicate samples from the two treatments (FPOP and control) of the two states (Ab42-present and –free, for a total of 12 samples) were segregated into three replicate groups by virtue of their acquisition time. The same column was used for each sample's LC-MS/MS acquisition, though not consecutively, and significant shifts in elution times were observed between the sets of replicates. Consequently LC-MS peak alignment and subsequent analysis was employed three times. Normally, averaging yields for their comparison between states requires using the same EIC features for both states to avoid potential state bias. We can't ensure this requirement with three independent analyses, and thus plot the average of their independent results at the peptide level. This limits the confidence with which we may make conclusions; nevertheless, the ApoE 16-25 peptide shows a very compelling increase in labeling in Aβ42-free samples.

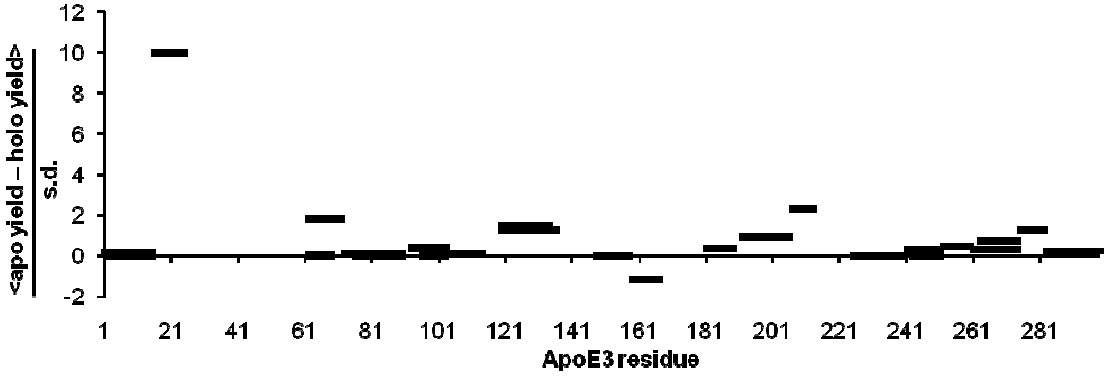

Figure 7.4: Significance plot comparing the tryptic peptide FPOP labeling yields of 100 nM ApoE3 in Aβ42-present and Aβ42-free states. The average state vs. state peptide yield difference was calculated from three singlicate state vs. state comparisons; the quotient of this average with the standard deviation is plotted. The length of each bar confers the sequence length of the peptide.

7.3.3 Micromolar ApoE-orangutan experiment.

Eight μM Aβ40 inhibits the FPOP labeling of 2 μM ApoE-orangutan in several of the same sites as seen for Aβ42 in nM ApoE3 and μM ApoE3 and ApoE4 experiments (Figure 7.5). In this preliminary experiment with a homolog of human ApoE, two levels of Aβ40 were tested together with an Aβ40 absent state. Residues L14, W20, W26, W34, Y74, L82, and W264 were most protected in the 1:4 ApoE:Aβ40 state; except for W264, the same residues showed intermediate protection in the 1:1 ApoE:Aβ40 state.

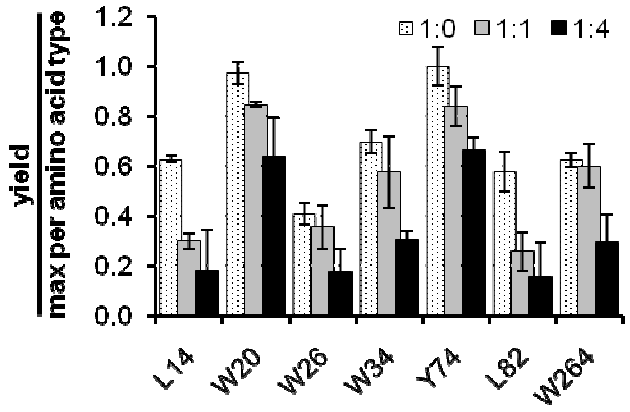

Figure 7.5: Residue-resolved FPOP labeling yields of the subset of residues that exhibit a significant attenuation trend between three ApoE-orangutan:Aβ40 states. 2μM ApoE-orangutan in its Aβ40-free is shown as white specked columns, 2μM Aβ40 as gray columns, and 8 μM Aβ40 as black columns.

7.4 Discussion

7.4.1 ApoE N-terminus domain-Aβ interaction.

The data from the four experiments presented here suggest that there is an interaction between the ApoE variants and Aβ (Figures 7.1, 7.2, 7.4, 7.5). All show significantly lower levels of labeling in the Aβ-present state in the Nt domain.

Importantly, various residues in the 16-36 region are protected by Aβ in all experiments. Though the full lipid-free structure of ApoE is unknown, it is instructive to map the Aβ-present state-protected sites in the Nt domains from the ApoE3, E4, and orangutan isoforms onto a single structure that models these domains; we have chosen the NMR solution phase structure of the ApoE3 1-183[10] (Figure 7.6). This choice is warranted for ApoE3 and ApoE4 because their X-ray crystal structures of their Nt domain fragments are highly similar[11, 35]. Moreover, the full length proteins have a similar FPOP footprint in this region (Figure 7.1), which we've reported in a recent study (supplementary manuscript). In the Nt domain, the 97% sequence homology between ApoE3 and ApoE-orangutan suggests close structural homology as well.

Sites of protection are located along helix 1 and at its turn towards the N-terminus, as well as at other sites residing in the loops connecting the four helices at the same end of their four-helix bundle (Figure 7.6). Residues W26 and Y74 form a surface-accessible patch on the Nt NMR structure; in the ApoE-orangutan structure these residues are clearly protected in the Aβ40-present state (Figure 7.6, green residues). That this finding is for residues non-contiguous in sequence lends credence to the structural interpretation of these footprinting results. Furthermore, the fact that three proteins in four experiments exhibit a similar response reinforces the conclusion that ApoE 16-36 is central to the Nt interaction with Aβ peptide.

Evidence for this interaction is not unprecedented. Evans and colleagues[23] showed that the Nt fragment of ApoE3 inhibits the amyloid fibril formation, and Chan and colleagues[22] observed the ApoE3 Nt-Aβ complex by dot blot analysis of gel filtration

fractions. Golabek and colleagues[21] determined the separate affinities of the ApoE3 Nt domain and Ct domain for Aβ40, with K_Ds of ~11 nM and 45 nM, respectively. A recent MD study suggests that Aβ40 monomer will form a stable complex with the Nt domains of ApoE3 and ApoE4, with the interaction region comprising the adjacent 1st and 4th helices [36]. In this study, Luo and colleagues used the X-ray crystal structures of ApoE2, ApoE3 and ApoE4 Nt domain fragments, and the SDS-induced α-helical structure of Aβ40 determined by NMR spectroscopy[37], as a starting point in the subsequent energy minimization, rigid-body docking, and MD simulations. Germaine to our finding is their conclusion of the interaction region, which clearly involves a direct interaction with W34 for both isoforms. Y36 may also experience a change, though it is oriented more towards the 2nd helix of the four-helix bundle in the variant structures. Due to the high number of

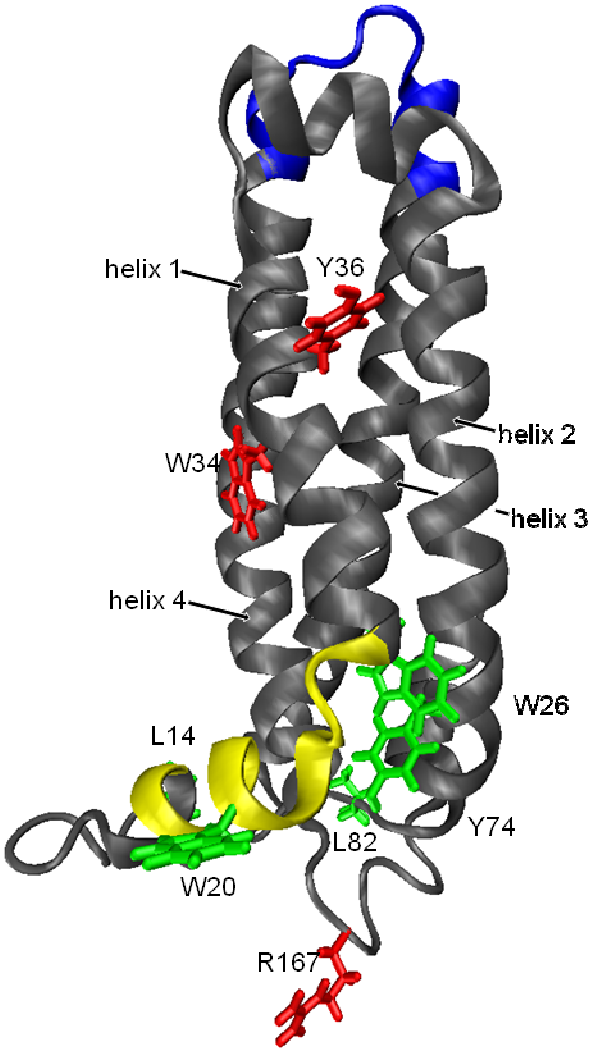

Figure 7.6: Mapping of various per-residue and per-peptide FPOP footprinting results onto the ApoE3$_{1\text{-}183}$ 2kc3 NMR structure[10]. This NMR structure is of the truncated variant of ApoE3 absent Aβ and is monomeric. The red residues exhibited significant protection for both ApoE isoforms in the 4 μM ApoE:20 μM Aβ42 state compared to the Aβ42-free state. The green residues exhibited significant protection in the 2 μM ApoE-orangutan, 8 μM Aβ40 state, compared to the Aβ40-free state. Region 16-25, colored yellow, shows significant protection for the 100 nM ApoE3:5 μM Aβ42 state, compared to its Aβ42-free state. Relative to the Aβ42-free states, region 120-134, colored blue, shows more labeling in the 4 μM ApoE3:20 μM Aβ42 state, and less labeling in the 4 μM ApoE4:20 μM Aβ42 state.

basic sites spanning 135-158, there is no residue-resolved FPOP data to confirm the interaction with the 4th helix. A striking result from their study is that in the simulations

the ApoE4 Nt domain reorganizes its conformation to accommodate Aβ40, whose orientation is flipped head-to-tail from the ApoE3 Nt domain-Aβ40 complex. Such reorganization, an indirect consequence of the C112R mutation, may explain the difference in the Aβ42-induced response we observe at E80 and region 120-134 for ApoE3 compared to ApoE4.

7.4.2 ApoE C-terminus domain-Aβ interaction.

While ApoE3 P293 is protected in the micromolar ApoE3 Aβ42-present state (Figure 7.2A), most of the modified fates of ApoE3 283-299 show no such trend (Figure 7.1A). Furthermore, the remaining regions of the Ct domain for both ApoE3 and ApoE4 appear to be only slightly affected by the presence of Aβ42 in the 4μM experiments if at all (Supporting Information Table 7.1). In particular, W264 and W276 show a concerted negative change in their modification levels in the Aβ42-present state relative to the –free state. Taken together these may convey significance, but individually they are not statistically different. Phu and colleagues[20] have characterized the interaction of ApoE3 201-299 (encompassing part of the thrombin-active hinge region as well as the Ct domain) and Aβ42 by monitoring the FRET between an Aβ42-attached fluorophore and ApoE Trp, and suggested that binding occurs in the vicinity of W264 and W276. In their study of the Nt and Ct domains of ApoE3, Golabek and colleagues also observed Aβ40 complexation, but with 4-10 fold weaker affinity than with the Nt domain[21]. These studies were conducted in the same protein concentration regime (2-12 μM) as our micromolar experiments. This allows comparison with our FPOP state change results for

the ApoE3 and ApoE4 μM experiments, and we find corroboration: (1) that a strong interaction region is localized to a region on the Nt domain; (2) a weaker interaction may be present in the Ct domain.

7.4.3 Implications of the ApoE oligomeric state.

At μM levels, both ApoE3 and ApoE4 are mostly tetramers[9, 12, 30, 38-39]. In an FPOP comparison study of a monomeric mutant of ApoE3 and WT ApoE3, we observed a significant change in the solvent accessibility of regions 181-221 and 242-290 (supplementary manuscript). Whatever interaction may be favored with Aβ in this region, we do not observe the kind of changes characteristic of the disruption of oligomeric structure witnessed in the monomeric mutant. The fact that the 1-191 Nt domain is mostly not involved in oligomerization implies that the tetramer may take up four Aβ peptides independently, and it motivates our use of the monomeric Nt domain structure for mapping interaction sites (Figure 7.6). This also predicts that the ApoE3 monomer should show the same Aβ interactions in the Nt domain. The 111 nM ApoE3 experiment was conducted to footprint the WT monomer-Aβ42 interaction, because at this concentration ApoE3 is primarily monomeric[30]. While peptide 33-38 is not well sampled in the experiment owing to post-labeling adsorption, the neighboring peptide 16-25 shows significant protection. If the underlying interaction with Aβ42 is proximal to both peptides, our prediction is validated.

7.4.4 Heterogeneity of participants.

The characterization of the insoluble aggregate or fibrillar content of Aβ42 and Aβ40 was not undertaken in the experiments, though a common starting point established for all replicates. The introduction of Aβ42 from a thawed high pH stock solution to a final concentration of 0.09 mg/mL in PBS at 22 °C will initiate self associations that ultimately produce the spectrum of soluble oligomer and insoluble amyloid species[40]. Moreover, the 4 μM state of ApoE3 and ApoE4 cannot be describe exclusively as tetrameric, as higher order oligomers are present as well [9, 12, 30, 38-39]. Probing the complicated evolving state of the mixture of these biomolecules without employing an artificial simplification—such as using domain fragments, denaturants, or fluorophore labeling—risks missing important interactions whose characteristic change in signal is only presented by a subset of the molecules. We have nevertheless undertaken such experiments, enabled by the sensitivity of FPOP and LC-MS/MS analysis to physiologic SASA. The finding of significant results is more compelling in light of the inherent complexity of the system.

7.5 Conclusion

ApoE 16-36, and W34 in particular, comprises a region in both ApoE3 and ApoE4 that is a site of direct Aβ42 interaction. It may instead be a site of allosteric protection, induced by Aβ42 interaction elsewhere, but in the same domain only R167 shows a similarly significant protection. We propose that its protection is rather induced by the interaction of Aβ42 with ApoE16-36, based on a recent MD study of the Nt

fragment and Aβ40[36]. This study has focused on the regions of interaction on ApoE3 and ApoE4 with Aβ peptide. Owing to the use of excess levels Aβ42 as ligand, we cannot yet conclude which regions of Aβ42 peptide interact with ApoE3 or ApoE4. Mass spectrometry-based FPOP footprinting is equally amenable to addressing this question, and is where we turn next in understanding this important interaction.

7.6 Supporting Information

Supporting Information Table 7.1: FPOP labeling yields[1] for the 4 μM experiments

residue	ApoE3:Ab	ApoE3	ApoE4:Ab	ApoE4
V6	0.20 +/- 0.01%	0.207 +/- 0.006%	0.210 +/- 0.007%	0.19 +/- 0.02%
L14	0.097 +/- 0.005%	0.098 +/- 0.005%	0.095 +/- 0.005%	0.098 +/- 0.004%
W20	3.8 +/- 0.4%	4 +/- 1%	2.8 +/- 0.9%	3 +/- 2%
W26	0.4 +/- 0.2%	0.4 +/- 0.7%	0.2 +/- 0.6%	0.7 +/- 0.6%
W34	15 +/- 1%	22 +/- 1%	17 +/- 1%	27 +/- 1%
Y36	2.9 +/- 0.2%	3.81 +/- 0.08%	3.2 +/- 0.3%	4.9 +/- 0.4%
M64	9 +/- 2%	9 +/- 2%	6 +/- 1%	6 +/- 3%
M68	7 +/- 2%	7 +/- 2%	4 +/- 1%	4 +/- 2%
Y74	3.28 +/- 0.03%	3.4 +/- 0.2%	2.8 +/- 0.2%	3.3 +/- 0.1%
E77	0.094 +/- 0.007%	0.075 +/- 0.002%	0.09 +/- 0.01%	0.078 +/- 0.002%
E80	0.09 +/- 0.01%	0.075 +/- 0.003%	0.093 +/- 0.002%	0.072 +/- 0.003%
V85	0.085 +/- 0.008%	0.091 +/- 0.003%	0.083 +/- 0.004%	0.08 +/- 0.01%
K95	1.93 +/- 0.03%	1.8 +/- 0.2%	2.9 +/- 0.2%	3.6 +/- 0.7%
M108	3.4 +/- 0.9%	1 +/- 2%	2 +/- 1%	3 +/- 2%
M125	10.5 +/- 0.9%	8 +/- 2%	4 +/- 1%	7 +/- 1%
L126	0.043 +/- 0.007%	0.055 +/- 0.004%	0.050 +/- 0.003%	0.066 +/- 0.005%
T130	0.0187 +/- 0.0005%	0.017 +/- 0.001%	0.015 +/- 0.001%	0.0177 +/- 0.0006%
L133	0.037 +/- 0.001%	0.035 +/- 0.003%	0.031 +/- 0.002%	0.035 +/- 0.001%
Y162	0.7 +/- 0.5%	0.5 +/- 0.5%	0.0 +/- 0.3%	0.4 +/- 0.3%
R167	0.1149 +/- 0.0009%	0.156 +/- 0.005%	0.111 +/- 0.008%	0.20 +/- 0.01%
L181	0.0114 +/- 0.0003%	0.0114 +/- 0.0008%	0.011 +/- 0.001%	0.0097 +/- 0.0005%
L184	0.12 +/- 0.02%	0.16 +/- 0.03%	0.17 +/- 0.03%	0.132 +/- 0.007%
E186	0.00 +/- 0.02%	0.04 +/- 0.03%	0.01 +/- 0.03%	0.00 +/- 0.02%
Q187	0.038 +/- 0.003%	0.033 +/- 0.002%	0.046 +/- 0.004%	0.042 +/- 0.003%
R189	0.074 +/- 0.004%	0.079 +/- 0.006%	0.073 +/- 0.004%	0.09 +/- 0.01%
V195	0.050 +/- 0.007%	0.056 +/- 0.002%	0.055 +/- 0.005%	0.060 +/- 0.006%
S197	0.11 +/- 0.01%	0.111 +/- 0.005%	0.118 +/- 0.005%	0.127 +/- 0.003%
L198	0.12 +/- 0.02%	0.134 +/- 0.008%	0.135 +/- 0.005%	0.14 +/- 0.01%
Q201	0.023 +/- 0.001%	0.029 +/- 0.003%	0.033 +/- 0.003%	0.031 +/- 0.005%
P202	0.049 +/- 0.008%	0.057 +/- 0.008%	0.063 +/- 0.007%	0.06 +/- 0.01%
L203	0.06 +/- 0.01%	0.063 +/- 0.004%	0.060 +/- 0.004%	0.059 +/- 0.002%
Q204	0.021 +/- 0.003%	0.022 +/- 0.006%	0.025 +/- 0.004%	0.026 +/- 0.005%
W210	0.7 +/- 0.3%	1 +/- 1%	0 +/- 1%	0 +/- 2%
M218	0 +/- 2%	2 +/- 1%	0.0 +/- 0.3%	1 +/- 1%

E219	0.0 +/- 0.9%	0.6 +/- 0.3%	0.0 +/- 0.7%	0.5 +/- 0.6%
M221	2 +/- 2%	1 +/- 1%	0.6 +/- 0.6%	0 +/- 1%
R226	0.044 +/- 0.006%	0.049 +/- 0.002%	0.052 +/- 0.003%	0.05 +/- 0.01%
Q248	0.052 +/- 0.002%	0.052 +/- 0.002%	0.048 +/- 0.002%	0.046 +/- 0.004%
L252	0.048 +/- 0.004%	0.043 +/- 0.004%	0.048 +/- 0.002%	0.031 +/- 0.005%
E255	0.054 +/- 0.003%	0.051 +/- 0.002%	0.060 +/- 0.003%	0.055 +/- 0.002%
F257	0.24 +/- 0.07%	0.3 +/- 0.1%	0.16 +/- 0.04%	0.22 +/- 0.06%
R260	0.107 +/- 0.002%	0.118 +/- 0.006%	0.102 +/- 0.003%	0.116 +/- 0.009%
W264	12.5 +/- 0.6%	14.1 +/- 0.9%	9.0 +/- 0.4%	10.0 +/- 0.6%
L268	0.9 +/- 0.1%	0.9 +/- 0.2%	0.5 +/- 0.1%	0.5 +/- 0.1%
M272	14 +/- 2%	14 +/- 2%	10 +/- 1%	11 +/- 3%
W276	4.8 +/- 0.2%	5.3 +/- 0.6%	3.4 +/- 0.7%	4.2 +/- 0.8%
P293	0.200 +/- 0.002%	0.238 +/- 0.009%	0.23 +/- 0.02%	0.25 +/- 0.02%
N298	0.12 +/- 0.01%	0.11 +/- 0.03%	0.17 +/- 0.03%	0.04 +/- 0.04%
H299	0.26 +/- 0.04%	0.22 +/- 0.02%	0.22 +/- 0.02%	0.19 +/- 0.02%

[1]Each residue's yield was determined by subtracting the average yield among control replicates from the average yield among FPOP replicates.

7.7 References

1. Querfurth, H. W.; LaFerla, F. M., Alzheimer's Disease. *New England Journal of Medicine* **2010,** *362* (4), 329-344.
2. Hartmann, T.; Bieger, S. C.; Bruhl, B.; Tienari, P. J.; Ida, N.; Allsop, D.; Roberts, G. W.; Masters, C. L.; Dotti, C. G.; Unsicker, K.; Beyreuther, K., Distinct sites of intracellular production for Alzheimer's disease Aβ40/42 amyloid peptides. *Nat Med* **1997,** *3* (9), 1016-1020.
3. Hashimoto, M.; Rockenstein, E.; Crews, L.; Masliah, E., Role of protein aggregation in mitochondrial dysfunction and neurodegeneration in Alzheimer's and Parkinson's diseases. *NeuroMolecular Medicine* **2003,** *4* (1), 21-35.
4. Hardy, J.; Selkoe, D. J., The amyloid hypothesis of Alzheimer's disease: progress and problems on the road to therapeutics. *Science (New York, N.Y.)* **2002,** *297* (5580), 353-6.
5. Walsh, D. M.; Klyubin, I.; Fadeeva, J. V.; Cullen, W. K.; Anwyl, R.; Wolfe, M. S.; Rowan, M. J.; Selkoe, D. J., Naturally secreted oligomers of amyloid β protein potently inhibit hippocampal long-term potentiation *in vivo*. *Nature* **2002,** *416* (6880), 535-539.
6. Strittmatter, W. J.; Saunders, A. M.; Schmechel, D.; Pericak-Vance, M.; Enghild, J.; Salvesen, G. S.; Roses, A. D., Apolipoprotein E: high-avidity binding to beta-amyloid and increased frequency of type 4 allele in late-onset familial Alzheimer disease. *Proc. Natl. Acad. Sci. U.S.A.* **1993,** *90* (5), 1977-1981.
7. Corder, E. H.; Saunders, A. M.; Strittmatter, W. J.; Schmechel, D. E.; Gaskell, P. C.; Small, G. W.; Roses, A. D.; Haines, J. L.; Pericak-Vance, M. A., Gene dose of apolipoprotein E type 4 allele and the risk of Alzheimer's disease in late onset families. *Science* **1993,** *261* (5123), 921-923.
8. Mahley, R. W., Apolipoprotein E: cholesterol transport protein with expanding role in cell biology. *Science* **1988,** *240*, 622-630.

9. Aggerbeck, L. P.; Wetterau, J. R.; Weisgraber, K. H.; Wu, C. S.; Lindgren, F. T., Human apolipoprotein E3 in aqueous solution. II. Properties of the amino- and carboxyl-terminal domains. *J. Biol. Chem.* **1988,** *263* (13), 6249-6258.
10. Sivashanmugam, A.; Wang, J., A Unified Scheme for Initiation and Conformational Adaptation of Human Apolipoprotein E N-terminal Domain upon Lipoprotein Binding and for Receptor Binding Activity. *J. Biol. Chem.* **2009,** *284* (21), 14657-14666.
11. Wilson, C.; Wardell, M. R.; Weisgraber, K. H.; Mahley, R. W.; Agard, D. A., Three-dimensional structure of the LDL receptor-binding domain of human apolipoprotein E. *Science* **1991,** *252* (5014), 1817-1822.
12. Westerlund, J. A.; Weisgraber, K. H., Discrete carboxyl-terminal segments of apolipoprotein E mediate lipoprotein association and protein oligomerization. *J. Biol. Chem.* **1993,** *268* (21), 15745-15750.
13. Bu, G., Apolipoprotein E and its receptors in Alzheimer's disease: pathways, pathogenesis and therapy. *Nat Rev Neurosci* **2009,** *10* (5), 333-344.
14. Carter, D. B., The Interaction of Amyloid-β with ApoE. In *Alzheimer's Disease*, Harris, J. R.; Fahrenholz, F., Eds. Springer US: 2005; Vol. 38, pp 255-272.
15. Soto, C.; Golabek, A.; Wisniewski, T.; Castaño, E. M., Alzheimer's β-amyloid peptide is conformationally modified by apolipoprotein E in vitro. *NeuroReport* **1996,** *7* (3), 721-725.
16. Wisniewski, T.; Castaño, E. M.; Golabek, A.; Vogel, T.; Frangione, B., Acceleration of Alzheimer's fibril formation by apolipoprotein E in vitro. *Am J Pathol.* **1994,** *145* (5), 1030-1035.
17. Ma, J.; Yee, A.; Brewer, H. B.; Das, S.; Potter, H., Amyloid-associated proteins α1-antichymotrypsin and apolipoprotein E promote assembly of Alzheimer β-protein into filaments. *Nature* **1994,** *372* (6501), 92-94.
18. Shuvaev, V. V.; Siest, G., Interaction between human amphipathic apolipoproteins and amyloid β-peptide: surface plasmon resonance studies. *FEBS Letters* **1996,** *383* (1-2), 9-12.
19. Golabek, A. A.; Soto, C.; Vogel, T.; Wisniewski, T., The Interaction between Apolipoprotein E and Alzheimers Amyloid -Peptide Is Dependent on -Peptide Conformation. *J. Biol. Chem.* **1996,** *271* (18), 10602-10606.
20. Phu, M.-J.; Hawbecker, S. K.; Narayanaswami, V., Fluorescence resonance energy transfer analysis of apolipoprotein E C-terminal domain and amyloid β peptide (1–42) interaction. *Journal of Neuroscience Research* **2005,** *80* (6), 877-886.
21. Golabek, A. A.; Kida, E.; Walus, M.; Perez, C.; Wisniewski, T.; Soto, C., Sodium Dodecyl Sulfate-Resistant Complexes of Alzheimer's Amyloid β-Peptide with the N-Terminal, Receptor Binding Domain of Apolipoprotein E. *Biophysical journal* **2000,** *79* (2), 1008-1015.
22. Chan, W.; Fornwald, J.; Brawner, M.; Wetzel, R., Native Complex Formation between Apolipoprotein E Isoforms and the Alzheimer's Disease Peptide Aβ. *Biochemistry* **1996,** *35* (22), 7123-7130.
23. Evans, K. C.; Berger, E. P.; Cho, C. G.; Weisgraber, K. H.; Lansbury, P. T., Apolipoprotein E is a kinetic but not a thermodynamic inhibitor of amyloid formation: implications for the pathogenesis and treatment of Alzheimer disease. *Proc. Natl. Acad. Sci. U.S.A.* **1995,** *92* (3), 763-767.
24. Hambly, D. M.; Gross, M. L., In *The Encyclopedia of Mass Spectrometry: Ionization Methods*, Gross, M. L.; Caprioli, R. M., Eds. 2006; Vol. 6.

25. Guan, J.-Q.; Chance, M. R., Structural proteomics of macromolecular assemblies using oxidative footprinting and mass spectrometry. *Trends Biochem. Sci* **2005,** *10*, 583-592.
26. Xu, G.; Chance, M. R., Hydroxyl Radical-Mediated Modification of Proteins as Probes for Structural Proteomics. *Chem. Rev.* **2007,** *107* (8), 3514-3543.
27. Xu, G.; Chance, M. R., Radiolytic Modification and Reactivity of Amino Acid Residues Serving as Structural Probes for Protein Footprinting. *Anal. Chem.* **2005,** *77* (14), 4549-4555.
28. Hambly, D. M.; Gross, M. L., Laser Flash Photolysis of Hydrogen Peroxide to Oxidize Protein Solvent-Accessible Residues on the Microsecond Timescale. *J. Am. Soc. Mass Spectrom.* **2005,** *16* (12), 2057-2063.
29. Gau, B. C.; Sharp, J. S.; Rempel, D. L.; Gross, M. L., Fast Photochemical Oxidation of Protein Footprints Faster than Protein Unfolding. *Anal. Chem.* **2009,** *81* (16), 6563-6571.
30. Garai, K.; Frieden, C., The Association-Dissociation Behavior of the ApoE Proteins: Kinetic and Equilibrium Studies. *Biochemistry* **2010,** *49* (44), 9533-9541.
31. Xu, G.; Kiselar, J.; He, Q.; Chance, M. R., Secondary Reactions and Strategies To Improve Quantitative Protein Footprinting. *Anal. Chem.* **2005,** *77* (10), 3029-3037.
32. Xu, G.; Chance, M. R., Radiolytic Modification of Sulfur-Containing Amino Acid Residues in Model Peptides: Fundamental Studies for Protein Footprinting. *Anal. Chem.* **2005,** *77* (8), 2437-2449.
33. Buxton, G. V.; Greenstock, C. L.; Helman, W. P.; Ross, A. B., Critical Review of Rate Constants for Reactions of Hydrated Electrons, Hydrogen Atoms and Hydroxyl Radicals (*OH/*O-) in Aqueous Solution. *J. Phys. Chem. Ref. Data* **1988,** *17* (2), 513-886.
34. Kebarle, P.; Tang, L., From ions in solution to ions in the gas phase - the mechanism of electrospray mass spectrometry. *Anal. Chem.* **1993,** *65* (22), 972A-986A.
35. Dong, L. M.; Wilson, C.; Wardell, M. R.; Simmons, T.; Mahley, R. W.; Weisgraber, K. H.; Agard, D. A., Human apolipoprotein E. Role of arginine 61 in mediating the lipoprotein preferences of the E3 and E4 isoforms. *J. Biol. Chem.* **1994,** *269* (35), 22358-22365.
36. Luo, J.; Maréchal, J.-D.; Wärmländer, S.; Gräslund, A.; Perálvarez-Marín, A., *In Silico* Analysis of the Apolipoprotein E and the Amyloid *β* Peptide Interaction: Misfolding Induced by Frustration of the Salt Bridge Network. *PLoS Comput Biol* **2010,** *6* (2), e1000663.
37. Coles, M.; Bicknell, W.; Watson, A. A.; Fairlie, D. P.; Craik, D. J., Solution Structure of Amyloid β-Peptide(1−40) in a Water−Micelle Environment. Is the Membrane-Spanning Domain Where We Think It Is?†,‡. *Biochemistry* **1998,** *37* (31), 11064-11077.
38. Sakamoto, T.; Tanaka, M.; Vedhachalam, C.; Nickel, M.; Nguyen, D.; Dhanasekaran, P.; Phillips, M. C.; Lund-Katz, S.; Saito, H., Contributions of the Carboxyl-Terminal Helical Segment to the Self-Association and Lipoprotein Preferences of Human Apolipoprotein E3 and E4 Isoforms. *Biochemistry* **2008,** *47* (9), 2968-2977.
39. Yokoyama, S.; Kawai, Y.; Tajima, S.; Yamamoto, A., Behavior of human apolipoprotein E in aqueous solutions and at interfaces. *J. Biol. Chem.* **1985,** *260* (30), 16375-16382.
40. Hilbich, C.; Kisters-Woike, B.; Reed, J.; Masters, C. L.; Beyreuther, K., Aggregation and secondary structure of synthetic amyloid [beta]A4 peptides of Alzheimer's disease. *Journal of Molecular Biology* **1991,** *218* (1), 149-163.